UNIVERSITY OF CAPE TOWN
IYUNIVESITHI YASEKAPA • UNIVERSITEIT VAN KAAPSTAD

Formulation, analysis and solution algorithms for a model of gradient plasticity within a discontinuous Galerkin framework

by

Andrew Trevor McBride

Thesis Presented for the Degree of
DOCTOR OF PHILOSOPHY
in the Department of Civil Engineering
UNIVERSITY OF CAPE TOWN
August 2008

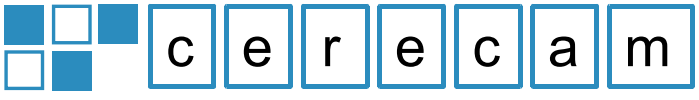

Centre for Research in Computational and Applied Mechanics

Formulation, analysis and solution algorithms for a model of gradient plasticity within a discontinuous Galerkin framework

Andrew Trevor McBride
University of Cape Town

Abstract

An investigation of a model of gradient plasticity in which the classical von Mises yield function is augmented by a term involving the Laplacian of the equivalent plastic strain is presented. The theory is developed within the framework of nonsmooth convex analysis by exploiting the equivalence between the primal and dual expressions of the plastic deformation evolution relations. The nonlocal plastic evolution relations for the case of gradient plasticity are approximated using a discontinuous Galerkin finite element formulation. Both the small- and finite-strain theories are investigated.

Considerable attention is focused on developing a firm mathematical foundation for the model of gradient plasticity restricted to the infinitesimal-strain regime. The key contributions arising from the analysis of the classical plasticity problem and the model of gradient plasticity include demonstrating the consistency of the variational formulation, and analyses of both the continuous-in-time and fully-discrete approximations; the error estimates obtained correspond to those for the conventional Galerkin approximations of the classical problem. The focus of the analysis is on those properties of the problem that would ensure existence of a unique solution for both hardening and softening problems. It is well known that classical finite element method simulations of softening problems are pathologically dependent on the discretisation. The ability of the gradient model to accommodate a degree of softening and the role of the internal length scale are made clear.

The development of well-understood solution algorithms is essential for efficient implementation within a finite element framework, especially given the nonstandard nature of the gradient plasticity model. Conditions for the convergence of the solution algorithms are established, first for the abstract problem, and then, as particular cases, for various predictors. The convergence proof does not assume symmetry of the underlying bilinear form and is therefore valid for a broad class of symmetric and nonsymmetric discontinuous Galerkin formulations. Details of the consistent tangent predictor for the case of gradient plasticity are presented. Various features and the performance of the algorithms are illustrated through a number of numerical examples. These examples address issues such as the role of softening and size-dependence.

The extension of the model of gradient plasticity to the finite-deformation regime is facilitated by adopting an exponential approximation of the evolution of plastic deformation. This approximation allows many of the key features of the small-strain theory to be retained. A low-order locking-free finite element formulation is developed using the method of enhanced assumed strains. This is validated against various benchmark problems. As in the small-strain theory, a series of numerical examples demonstrate the effectiveness and features of the finite-strain model of gradient plasticity.

The work concludes with a discussion of a range of potential extensions, for example, to problems of crystal plasticity and microstructure formation.

Acknowledgements

First and foremost I wish to express my most sincere gratitude to my supervisor, Prof. B. Daya Reddy, for his guidance, patience and encouragement throughout this work.

I am also highly indebted to Francois Ebobisse and Jules Djoko for their significant input.

To my colleagues in CERECAM, thank you for making this an interesting and exciting time. A special thanks to all those I have shared offices with at one time or another; Victor Balden and Indresan Govender deserve special mention.

A special thanks to my friends and family who I have seen far too little of over the last couple of years.

Lastly, I want to thank Diane Scott for her patience and support during this period. I truly appreciate it.

Contents

List of Figures

List of Tables

Nomenclature

$\mathcal{P}_{\text{int}}$	internal power
$(\cdot)^\star$	a trial state
A	finite element assembly operator
$\boldsymbol{\alpha}$	back-stress due to kinematic hardening
$\bar{\boldsymbol{C}}^e$	elastic right Cauchy–Green tensor
$\bar{\boldsymbol{E}}^e$	elastic Green strain in the intermediate configuration
$\bar{\boldsymbol{L}}^p$	plastic velocity gradient in the intermediate configuration
$\bar{\boldsymbol{S}}$	symmetric second Piola–Kirchhoff stress tensor in the intermediate configuration
$\bar{g}$	internal stress conjugate to ξ
$\bar{M}$	function space of hardening variables for classical plasticity
$\boldsymbol{B}$	body force per unit reference volume
$\boldsymbol{b}$	left Cauchy–Green tensor
$\boldsymbol{b}^e$	elastic left Cauchy–Green tensor
$\boldsymbol{B}_\varphi$	matrix composed of gradients of the displacement interpolation functions N_φ
$\boldsymbol{C}$	right Cauchy–Green tensor
$\boldsymbol{\chi}$	set of internal variables conjugate to the internal plastic variable $\boldsymbol{\xi}$
$\boldsymbol{d}$	rate of deformation tensor
$\boldsymbol{d}^p$	plastic part of the rate of deformation tensor
$\boldsymbol{d}_{\text{A}}$	nodal displacement associated with node A
$\boldsymbol{E}$	Green strain tensor
$\boldsymbol{F}$	deformation gradient

$\boldsymbol{F}^e$	elastic part of the deformation gradient
$\boldsymbol{F}^p$	plastic part of the deformation gradient
$\boldsymbol{F}_{\text{ext}}$	external force vector
$\boldsymbol{F}_{\text{int}}$	internal force vector
$\boldsymbol{g}$	linearised enhanced strain operator
$\boldsymbol{J}$	Jacobian between the reference configuration and the reference element
$\boldsymbol{J}_0$	Jacobian between the reference configuration and the reference element evaluated at the centroid
$\boldsymbol{K}$	stiffness matrix
$\boldsymbol{k}^e$	stiffness matrix of the e^{th} element
$\boldsymbol{l}$	spatial velocity gradient
$\boldsymbol{l}^e$	elastic velocity gradient
$\boldsymbol{l}^p$	plastic velocity gradient
$\boldsymbol{m}$	conjugate quantity to $\nabla\xi$
$\boldsymbol{N}$	outward normal to the boundary of the domain in the reference configuration
$\boldsymbol{P}$	nonsymmetric nominal stress tensor
$\boldsymbol{\psi}^e$	isoparametric map from the reference element to the reference configuration
$\boldsymbol{R}$	residual vector
$\boldsymbol{S}$	second Piola–Kirchhoff stress tensor
$\boldsymbol{\sigma}$	Cauchy stress tensor
$\boldsymbol{\tau}$	Kirchhoff stress tensor
$\boldsymbol{U}$	left stretching tensor
$\boldsymbol{u}$	displacement field
C^{con}	algorithmic consistent tangent modulus
$\boldsymbol{V}$	material velocity field
$\boldsymbol{v}$	spatial velocity field
$\boldsymbol{\varepsilon}$	infinitesimal-strain tensor
$\boldsymbol{\varepsilon}^e$	elastic part of the infinitesimal-strain tensor
$\boldsymbol{\varepsilon}^p$	plastic part of the infinitesimal-strain tensor
$\boldsymbol{\varphi}$	motion of the reference configuration
$\boldsymbol{w}$	axial vector associated with the skew-symmetric spin tensor

$\boldsymbol{w}^p$	plastic part of the spin tensor
$\boldsymbol{X}$	material point in the reference placement
$\boldsymbol{x}$	point in the current placement
$\boldsymbol{\xi}$	set of internal plastic variables
$\mathcal{C}$	elasticity tensor
$\mathcal{E}$	elastic domain containing admissible stress states
$\mathcal{E}_h^o$	set of all interior edges
$\mathcal{E}_h$	set of all edges
$\mathcal{L}$	Lie derivative
$\mathcal{P}_k$	space of polynomials of degree at most $k \geq 0$
$\mathcal{S}$	current placement of a continuum body
$\mathcal{T}_h$	subdivision of a domain into elements
$\delta(\cdot)$	increment in $(\cdot)$
γ	equivalent plastic strain
Γ_{A}	the A^{th} enhanced assumed parameter
Γ_φ	part of the boundary $\partial\Omega$ where Dirichlet conditions are specified
Γ_T	part of the boundary $\partial\Omega$ where Neumann conditions are specified
$\Gamma_{\overline{\mathcal{AE}}}$	set of all element edges in $\overline{\mathcal{AE}}$
$\hat{\boldsymbol{w}}$	spin tensor
κ	initial yield stress
Λ	first Lamé modulus
λ	plastic consistency parameter
λ_A	A^{th} eigenvalue of $\boldsymbol{C}$ or $\boldsymbol{b}$
$\{\!\{(\cdot)\}\!\}$	the average of $(\cdot)$ on an edge
$[\![(\cdot)]\!]$	the jump in $(\cdot)$ across an edge
$\mathbb{F}$	enhanced part of the deformation gradient defined on the reference element
$\mathcal{AE}$	set of elements containing active quadrature points
$\mathcal{AP}$	set of active quadrature points
μ	second Lamé modulus
n_{dim}	number of space dimensions

$n^{\mathrm{e}}_{\gamma\mathrm{node}}$ number of nonconforming nodes per element associated with the hardening parameter

n_{node} number of nodes in the triangulation of the domain

$n^{\mathrm{e}}_{\mathrm{node}}$ number of nodes per element

ν Poisson's ratio

Ω reference placement of a continuum body

Ω^p active subdomain of the body Ω in the reference placement

$\partial\mathcal{E}$ yield surface

$\partial\Omega$ boundary of the reference placement Ω

$\partial\Omega_F$ part of the boundary $\partial\Omega$ where which Neumann conditions for ξ are prescribed

$\partial\Omega_H$ part of the boundary $\partial\Omega$ where Dirichlet conditions for ξ are prescribed

$\partial f(\boldsymbol{x})$ subdifferential of a convex function f at the point $\boldsymbol{x}$

ψ Helmholtz free energy

ψ^e elastic part of the Helmholtz free energy

ψ^p plastic part of the Helmholtz free energy

ρ_K radius of the largest circle contained in element K

n_{int} number of internal variables describing plastic deformation

$\tilde{\boldsymbol{F}}_h$ enhanced part of the deformation gradient

$\tilde{\boldsymbol{R}}$ rotation tensor

$\tilde{\boldsymbol{V}}$ right stretching tensor

$\tilde{\mathbb{F}}$ enhanced part of the deformation gradient in the reference domain

$\Delta(\cdot)$ total increment in $(\cdot)$

ε^e_A A^{th} principal component of the logarithmic elastic stretch

ξ isotropic hardening parameter

$\{\boldsymbol{N}^{(1)}, \boldsymbol{N}^{(2)}, \boldsymbol{N}^{(3)}\}$ Eulerian basis vectors

$\{\boldsymbol{n}^{(1)}, \boldsymbol{n}^{(2)}, \boldsymbol{n}^{(3)}\}$ Lagrangian basis vectors

D dissipation function

E Young's modulus

e an edge of an element K

f yield criterion

g conjugate force in the gradient plasticity formulation

h	maximum element diameter
h_e	length of an edge e
h_K	diameter of element K
I_A	A^{th} principal invariant of $\boldsymbol{C}$ or $\boldsymbol{b}$
ID	array relating local node numbering to the global node numbering
j	determinant of the Jacobian between the reference configuration and the reference element
j_0	determinant of the Jacobian between the reference configuration and the reference element evaluated at the centroid
j_{xX}	determinant of the deformation gradient between the current and reference configuration
K	generic finite element
k_1	kinematic hardening constant
k_2	isotropic hardening constant
k_3	positive gradient hardening constant
l	length scale
M	function space of scalar hardening parameters for the gradient problem
N_γ	local hardening parameter polynomial basis function defined on the reference element
N_φ	local displacement polynomial basis function defined on the reference element
$N_Y(\boldsymbol{x})$	normal cone to a convex set Y evaluated at a point $\boldsymbol{x}$
Q	function space of plastic strains
V	function space of displacements
W	stored energy function
Z	product space $V \times Q \times \bar{M}$
$\mathfrak{b}$	linearised strain operator in the enhanced assumed strain formulation

Summary of extensively used definitions and standard results

The following is a summary of extensively used definitions, theorems, and standard results. For further details see, for example, Reddy [152] from which many of these definitions are taken.

Multi-index notation

Let each component of the set $\alpha = (\alpha_1, \alpha_2, \ldots, \alpha_n)$ be a nonnegative integer. We denote by $|\alpha|$ the sum $|\alpha| = \sum_{i=1}^{n} \alpha_n$. The partial derivative $D^\alpha u$ is defined by

$$D^\alpha u = \frac{\partial D^{|\alpha|} u}{\partial x_1^{\alpha_1} \partial x_2^{\alpha_2} \cdots \partial x_n^{\alpha_n}} .$$

The spaces $L^p(\Omega)$ and the Sobolev spaces $H^m(\Omega)$

Let p be a real number with $p \geq 1$. A function u defined on a subset Ω of $\mathbb{R}^n$ belongs to $L^p(\Omega)$ if u is measurable and

$$\int_\Omega |u(\boldsymbol{x})|^p dx < \infty .$$

The norm on the space $L^p(\Omega)$ is defined by

$$\|u\|_{L^p} = \left[\int_\Omega |u(\boldsymbol{x})|^p \, dx \right]^{1/p} .$$

The Sobolev space of order m, denoted $H^m(\Omega)$, is defined to be the space of functions in $L^2(\Omega)$ that, together with their weak partial derivatives up to and including

those of order m, belong to $L^2(\Omega)$:

$$H^m(\Omega) = \left\{u \ : \ D^\alpha u \in L^2(\Omega) \text{ for all } \alpha \text{ such that } |\alpha| \leq m\right\} \ .$$

The norm on the space $H^m(\Omega)$ is defined by

$$\|u\|_{H^m} = \left[\int_\Omega \sum_{|\alpha|\leq m} \left(D^\alpha u\right)^2 \ dx\right]^{1/2} \ .$$

The spaces $L^\infty(\Omega)$

The space $L^\infty(\Omega)$ contains all measurable functions on Ω that are bounded almost everywhere on Ω:

$$L^\infty(\Omega) = \left\{u \ : \ |u(\boldsymbol{x})| \leq k \text{ a.e. on } \Omega \text{ for some } k \in \mathbb{R}^+\right\} .$$

The Young inequality

$$ab \leq \frac{\epsilon}{2}a^2 + \frac{1}{2\epsilon}b^2 \qquad \text{for } a, b \in \mathbb{R}^+ \text{ and } \epsilon > 0 \ .$$

The Cauchy–Schwarz inequality

If u and v are members of an inner product space X with inner product $(\cdot, \cdot)$ then

$$|(u, v)| \leq (u, u)^{1/2}(v, v)^{1/2} \ .$$

The Hölder inequality

For $1 \leq p, q \leq \infty$ with $1/p + 1/q = 1$,

$$\int_\Omega |uv| \ dx \leq \left[\int_\Omega |u|^p \ dx\right]^{1/p} \left[\int_\Omega |v|^q \ dx\right]^{1/q} \ .$$

The Minkowski inequality for integrals

For $1 \leq p < \infty$

$$\left[\int_\Omega |u \pm v|^p \, dx\right]^{1/p} \leq \left[\int_\Omega |u|^p\right]^{1/p} + \left[\int_\Omega |v|^p\right]^{1/p} .$$

The triangle inequality

If u and v are members of a normed space X then

$$\|u + v\| \leq \|u\| + \|v\| .$$

The Poincaré–Friedrichs inequality

Let Ω be a domain in $\mathbb{R}^n$. Then there exists a constant $C > 0$ such that

$$\int_\Omega |u|^2 \, dx \leq C \int_\Omega |\nabla u|^2 \, dx \qquad \text{for all } u \in H_0^1(\Omega) .$$

Gronwall's Lemma

Let $u : [0, \alpha] \to \mathbb{R}$ be continuous and nonnegative. Suppose $C \geq 0$ and $K \geq 0$ are such that

$$u(t) \leq C + \int_0^t Ku(s) \, ds \qquad \text{for all } t \in [0, \alpha].$$

Then

$$u(t) \leq C \exp[Kt] \qquad \text{for all } t \in [0, \alpha].$$

Cauchy sequence

A sequence $\{u_\mathrm{n}\}$ in a subset Y of a normed space X is called a Cauchy sequence if

$$\lim_{\mathrm{m,n}\to\infty} \|u_\mathrm{m} - u_\mathrm{n}\| = 0 .$$

More formally, the sequence is a Cauchy sequence if for any given $\epsilon > 0$ there exists a number N such that

$$\|u_{\mathrm{m}} - u_{\mathrm{n}}\| < \epsilon \quad \text{whenever } \mathrm{m}, \mathrm{n} > N\,.$$

Lipschitz continuous functions

A function f defined on a set Ω in $\mathbb{R}^n$ is Lipschitz continuous if there exists a constant $L > 0$ such that

$$|f(\boldsymbol{x}) - f(\boldsymbol{y})| \leq L|\boldsymbol{x} - \boldsymbol{y}|\,.$$

Continuous, convex, positively homogeneous, proper and lower semicontinuous functions

A function $f(\boldsymbol{x})$ defined on a subset of Ω of $\mathbb{R}^n$ is continuous at a point $\boldsymbol{x}_0$ on Ω if for all positive ϵ it is possible to find a positive number δ such that

$$|f(\boldsymbol{x}) - f(\boldsymbol{x}_0)| < \epsilon \quad \text{whenever} \quad |\boldsymbol{x} - \boldsymbol{x}_0| < \delta \text{ and } \boldsymbol{x} \in \Omega\,.$$

The function $f(\boldsymbol{x})$ is termed convex if, for $0 < \theta < 1$,

$$f(\theta\boldsymbol{x} + (1-\theta)\boldsymbol{y}) \leq \theta f(\boldsymbol{x}) + (1-\theta) f(\boldsymbol{y})\,.$$

The function $f(\boldsymbol{x})$ is said to be strictly convex if the strict inequality above holds whenever $\boldsymbol{x} \neq \boldsymbol{y}$. Furthermore, the function $f(\boldsymbol{x})$ is said to be positively homogeneous if

$$f(\alpha\boldsymbol{x}) = \alpha f(\boldsymbol{x}) \quad \forall \boldsymbol{x} \in \Omega, \qquad \text{for all } \alpha > 0\,,$$

proper if

$$f(\boldsymbol{x}) < +\infty \quad \text{for at least one } \boldsymbol{x} \in \Omega \text{ and } f(\boldsymbol{x}) > -\infty \qquad \text{for all } \boldsymbol{x} \in \Omega\,,$$

and lower semicontinuous if

$$\lim_{\mathrm{n}\to\infty} \inf f(\boldsymbol{x}_{\mathrm{n}}) \geq f(\boldsymbol{x})\,,$$

for any sequence $\{\boldsymbol{x}_{\mathrm{n}}\}$ converging to $\boldsymbol{x}$.

The Sobolev Embedding Theorem

Let Ω be a bounded domain in $\mathbb{R}^n$ with a Lipschitz boundary Γ. If $m - k > n/2$, then every function in $H^m(\Omega)$ belongs to $C^k(\overline{\Omega})$. Furthermore, the embedding

$$H^m(\Omega) \subseteq C^k(\overline{\Omega})$$

is continuous.

1

Introduction

The theoretical underpinnings of the classical theory of elastoplasticity have been vigorously developed during the last half-century, and constitutive models for infinitesimal and large strains, and for a range of material types that include both ductile and brittle behaviour, are now firmly established. Computational methods for the solution of complex problems involving inelastic behaviour have undergone a parallel development, and there is now a good understanding of the associated algorithms and, particularly for small strains, of the convergence theory.

Motivated in large part by the inability of classical theories to model material behaviour at the mesoscale level, various plasticity theories that incorporate size-dependence via the inclusion of strain gradients have been developed. These theories include in a natural way a length scale, and permit phenomena such as shear banding to be captured. For example, in the early works of Dillon and Kratochvil [66], Aifantis [2, 3], and Coleman and Hodgdon [56] the von Mises yield function is augmented by a term involving the Laplacian of the equivalent plastic strain, and possibly further higher-order terms. The relation of theories of gradient plasticity to the underlying interpretation of plastic deformation arising due to the flow of dislocations in the crystal lattice structure was established by Aifantis [2, 3].

The terms involving higher-order derivatives of quantities such as the equivalent plastic strain in gradient plasticity models require careful attention in the development of computational approximations. In classical theories the plastic strain and other internal variables may be approximated by piecewise discontinuous functions since there is no requirement of continuity. Furthermore, in finite element approximations these

quantities may be condensed out at the element level, or computations may be carried out locally at quadrature points, in either case with the consequence that the predictor part of the solution algorithm involves only the displacement degrees of freedom. Such approaches have either to be modified in gradient theories, or it becomes essential to assume continuity of the relevant internal variables and possibly their gradients, with a consequent significant increase in the size of the discrete problem to be solved. The need to develop a computational procedure for gradient plasticity that retains the simplicity of the classical algorithms is therefore self-evident.

A candidate approach is the class of discontinuous Galerkin methods, in which interelement continuity is relaxed in a framework in which the discrete problem remains consistent. Discontinuous Galerkin methods were developed in the 1970s and 1980s [139, 11], but it is only in recent years that they have been exploited in a wide range of problems. The collection [53] provides an excellent overview of many of the key approaches for elliptic and hyperbolic problems.

Within the context of linear elasticity there have been important contributions by Rivière and Wheeler [159] and Wihler [190], the latter considering the case of nonconvex domains and vanishing compressibility. Ten Eyck and Lew [180] demonstrated the effectiveness of the discontinuous Galerkin formulation in circumventing locking-related problems arising due to vanishing compressibility within the context of nonlinear elasticity. A key contribution of their work was to show that the discontinuous Galerkin formulation produced results of similar accuracy to those obtained using a conforming approximation with a comparable, and often lower, computational cost. The effective treatment of the incompressibility constraint is of significant importance in many models of plasticity in which plastic deformation is assumed incompressible.

A discontinuous Galerkin formulation has recently been developed for strain gradient dependent damage models [188, 135], while the work by Engel et al. [74] treats continuous/discontinuous Galerkin methods for fourth-order problems by reducing the classical requirement of C^1 continuity of the unknown variable to one of continuity (see also [29, 14]). This approach has recently been applied by Wells et al. [189] to solve the Cahn–Hilliard equation, a fourth-order nonlinear parabolic partial differential equation, and to develop finite element solutions to plate [187] and

shell [142, 72] problems involving only discretisations of the displacement field. The continuous/discontinuous Galerkin method is an ideal candidate for those models of gradient plasticity in which it is essential to impose C^1 continuity on the equivalent plastic strain variable; one such model is that proposed by Mülhaus and Aifantis [136] in which both the Laplacian and the biharmonic of the effective plastic strain enter the yield condition. Furthermore, discontinuous Galerkin methods in both time and space appear to be ideally suited to evolving interface problems such as arise in elastoplasticity [6, 69].

Another attractive property of discontinuous Galerkin schemes is the design of more flexible finite element spaces. Within a discontinuous Galerkin approach non-matching grids containing hanging nodes and nonuniform interpolations can be handled easily. The flexibility offered by the discontinuous Galerkin method renders it well suited for implementation on large-scale, parallel computing platforms [104, 24].

One of the potential drawbacks of discontinuous Galerkin methods is the proliferation of the number of degrees of freedom relative to conventional Galerkin methods. The computational overhead can be reduced considerably by interpreting the discontinuous Galerkin formulation within a multi-scale framework [28, 103]. The multi-scale framework could potentially be extended to include various models of gradient plasticity as the gradient effects are generally related to scale-dependent phenomena. The additional computational overhead must also be seen in perspective, as noted previously in reference to the work on incompressible media by ten Eyck and Lew [180]. A further example concerns the application of discontinuous Galerkin methods to fourth-order problems in which C^1 continuous interpolants are required. The construction of such interpolants is problematic and computationally expensive within a conforming approximation for space dimensions higher than one.

Motivated in large part by the success of discontinuous Galerkin methods to provide elegant and effective solutions to the challenging problems in computational mechanics mentioned previously, the focus of the work presented here is on the use of discontinuous Galerkin methods for the solution of problems in elastoplasticity. Both classical plasticity and a model of gradient plasticity [66, 2, 3, 56] are considered,

though the emphasis is on the latter, for which case discontinuous Galerkin methods carry several significant advantages.

A discontinuous Galerkin formulation of the displacement field in plasticity problems elegantly circumvents locking-related complications that occur when using low-order finite element formulations. The use of low-order finite elements is attractive for reasons of computational efficiency and for their robustness in large deformation problems, provided that they are suitably stabilised.

Furthermore, discontinuous Galerkin formulations provide an elegant and effective framework in which to deal with the higher-order derivatives arising in gradient plasticity formulations.

The model of gradient plasticity considered here serves as a basis for more complex models involving additional higher-order terms and possibly multiple length scales [81]; indeed, the model of gradient plasticity investigated here can be treated using a conforming finite element approximation [115]. The imposition of the internal plastic boundary is, however, problematic in conforming approximations and the extension of the formulation to other models of gradient plasticity is by no means straightforward. The classical plasticity formulation can be recovered easily from the gradient model considered here within the context of the discontinuous Galerkin method by simply not imposing continuity of the internal hardening parameter. Thus, the influence of the gradient effects can be varied spatially.

In addition, the computational procedures for the discontinuous Galerkin model of gradient plasticity considered retain much of the simplicity associated with the classical algorithms. Indeed, the solution algorithms developed here are extensions of those developed by Martin and coworkers for the classical problem [26, 27, 79].

The application of the discontinuous Galerkin formulation to problems in classical plasticity and the model of gradient plasticity considered here is largely novel. A key aspect of this work involves the careful construction of an appropriate mathematical framework, and the development, analysis and implementation of solution algorithms. Features and the performance of the algorithms are illustrated through a series of example problems performed using a finite element code developed for this work.

The context of the analysis and the subsequent algorithm development is initially that of the infinitesimal-strain problem. The finite-strain implementation is considered in Part II. The analysis of the finite-strain problem is a delicate matter even for the classical problem (see, for example, [132]), and is not considered in this work.

The discontinuous Galerkin formulation of both the classical and the gradient plasticity models considered here are presented as variational inequalities within a convex analytic framework. The adoption of the convex analytic framework is motivated by the analysis of the primal and dual forms of the classical plasticity problem presented by Han and Reddy [151, 93, 95, 94], and the work of Carstensen and coworkers who have made significant contributions to the numerical analysis of the primal problem [8, 34, 37, 47, 44].

The focus here is on the primal formulation of plasticity in which the kinematic quantities such as displacement, plastic strain, and equivalent plastic strain are the unknown variables. The primal formulation is less popular than the dual form as a basis for computational treatments of the problem, which uses the flow law in its traditional form of the normality law with the Kuhn–Tucker conditions. Nevertheless, as will be seen, the primal formulation is particularly well suited to problems such as gradient plasticity in which higher-order derivatives of the kinematic quantities appear. Furthermore, various authors, for example, de Borst and Mülhaus [62] and Fleck and Hutchinson [81], have commented on the suitability of what are essentially primal formulations as a basis for carrying out finite element approximations.

The key contributions arising from the analysis of the classical plasticity problem and the model of gradient plasticity include demonstrating the consistency of the variational formulation and analyses of both the continuous-in-time and fully-discrete approximations. The error estimates obtained correspond to those for the conventional Galerkin approximations of the classical problem. The focus of the analysis is on those properties of the problem that would ensure existence of a unique solution for both hardening and softening problems. The ability of the gradient model to accommodate softening, as has been alluded to by Aifantis [3] in the context of ellipticity of the equilibrium equations, is made clear.

The development of well-understood solution algorithms is essential for the efficient numerical realisation of the problem within the finite element method, especially given the nonstandard nature of the gradient plasticity model. The construction of solution algorithms for the model of gradient plasticity is initially presented within the general context of an abstract problem. Conditions for the convergence of the algorithms are established first for the abstract problem, and then, as particular cases, for the elastic, secant and consistent tangent predictors. In the last case it is known [94] that it is not possible to establish conditions for unconditional convergence. This problem is overcome here by introducing a perturbation of the approximation of the tangent involving a positive multiple of the identity.

A feature of the convergence analysis worth emphasising is its applicability to problems in which the underlying bilinear form may not be symmetric; this is the case for many discontinuous Galerkin formulations. A further key contribution is the construction of the consistent tangent predictor for the case of gradient plasticity, the use of which is essential for the efficient numerical implementation. The approach taken in the derivation of the consistent tangent predictor borrows from the classical theory (see, for example, Simo and Hughes [166]), though the derivation is more complex given the nonlocal nature of the problem.

The extension of the discontinuous Galerkin formulation for the model of gradient plasticity to the finite deformation regime is another key aspect of the work. The extension is greatly facilitated by adopting on exponential approximation for the evolution of plastic deformation [163] that preserves the general structure of the algorithms developed for the infinitesimal problem.

As mentioned previously, discontinuous Galerkin methods have been recently applied to problems in nonlinear elasticity [180, 141, 181, 182]. The effectiveness of the method to overcome locking-related problems arising due to vanishing compressibility in nonlinear elasticity was demonstrated by ten Eyck and Lew [180]. The issue of vanishing compressibility arises in models of plasticity where plastic deformation is assumed incompressible, as it is here. We choose, however, not to adopt a discontinuous Galerkin approach for the approximation of the displacement field in the nonlinear theory, but instead use the more mature enhanced assumed strain formu-

lation proposed by Simo and Armero [165] to circumvent locking related problems at finite strains. While the discontinuous Galerkin approach is extremely attractive, the focus of this work and the key contributions concern the model of gradient plasticity. Thus, only the nonlocal plastic evolution equations are solved using the discontinuous Galerkin method.

The structure of the rest of this work is as follows. Part I is dedicated to the problem of gradient elastoplasticity restricted to the infinitesimal-strain regime. In Chapter 2 the governing equations and inequalities for the classical and gradient problems are presented, and the well-posedness of the variational formulation is discussed. A simple symmetric interior penalty discontinuous Galerkin method is introduced in Chapter 3, and the consistency of the discrete formulation is shown. Chapter 3 concludes with an analysis of the fully-discrete discontinuous Galerkin approximation.

The remainder of Part I focuses on algorithmic and computational aspects of the problem. In Chapter 4 the predictor–corrector solution algorithm for this class of problems is formulated, and conditions for the convergence of the algorithm given. In Chapter 5, various features and the performance of the algorithm are illustrated through a number of numerical examples. These address issues such as the role of softening and size-dependence, and the performance of the algorithm using different moduli in the predictor step.

The second part of this work concerns the extension of the gradient plasticity model considered in Part I to the finite-strain regime. The first half of Chapter 6 summarises standard results in classical nonlinear continuum mechanics. The remainder of the chapter describes the multiplicative hyperelastic model of plasticity adopted here. Both the conventional dual and less widely adopted primal form of the classical plastic evolution equations are given. The enhanced assumed strain formulation is presented in Chapter 7. The performance of the technique is assessed via a series of numerical examples. The discontinuous Galerkin formulation of gradient plasticity at finite strains is the focus of Chapter 8. In Chapter 9 various features and the performance of the algorithm are illustrated through a series of numerical example problems. As in the small-strain case the role of material softening and scale, and the performance of the algorithm using different moduli in the predictor step are assessed.

The conclusions arising from this work and suggested areas for further research are presented in Chapter 10.

Substantial portions of the work presented here are contained in the following publications [67, 68, 125, 126]:

- J. K. Djoko, F. Ebobisse, A. T. McBride, B. D. Reddy, A discontinuous Galerkin formulation for classical and gradient plasticity. Part 1 – Formulation and analysis, Comput. Methods Appl. Mech. Eng., 196 (2007) 3881–3897.
- J. K. Djoko, F. Ebobisse, A. T. McBride, B. D. Reddy, A discontinuous Galerkin formulation for classical and gradient plasticity. Part 2: Algorithms and numerical analysis, Comput. Methods Appl. Mech. Eng., 197 (2007) 1–21.
- A. T. McBride and B. D. Reddy, Some aspects of a discontinuous Galerkin formulation for gradient plasticity at finite strains, Proceedings of the IUTAM Symposium on Theoretical, Modelling and Computational Aspects of Inelastic Media, Cape Town, South Africa, (in press).
- A. T. McBride and B. D. Reddy, A Discontinuous Galerkin formulation for gradient plasticity at finite strains, Comput. Methods Appl. Mech. Eng., (in press).

Part I

The infinitesimal-strain theory

Summary: The infinitesimal-strain theory

In Part I the structure, analysis and implementation of a model of strain gradient plasticity under the assumption of infinitesimal strains are presented. The model is extended to the finite-strain regime in Part II.

The formulation of the classical and gradient plasticity models is presented in Chapter 2. The emphasis of the presentation is on the primal formulation of plasticity. The classical and gradient plasticity models are presented as variational inequalities within a convex analytic framework and their well-posedness discussed.

A symmetric interior penalty discontinuous Galerkin formulation of the classical and gradient plasticity models is presented in Chapter 3, and the consistency of the discrete formulation shown. Both the continuous-in-time and the fully-discrete approximations are analysed.

The predictor–corrector solution strategy is introduced in Chapter 4. The convergence analysis of an abstract problem, whose general structure allows results for particular predictors to be deduced as special cases, is presented. An error estimate for the convergence rate of the discrete problem is obtained without assuming symmetry of the bilinear form. The chapter concludes with a detailed account of the solution algorithm for the gradient plasticity model.

Finally, in Chapter 5 the gradient plasticity formulation is used to analyse two illustrative example problems.

2

The formulation of classical plasticity and a model of gradient plasticity at infinitesimal strains

The objective of this chapter is to present the governing equations and inequalities for classical plasticity and a model of gradient plasticity due to Dillon and Kratochvil [66], Aifantis [2, 3], and Coleman and Hodgdon [56].

The emphasis here is on the primal formulation of plasticity in which the kinematic quantities such as displacement, plastic strain, and equivalent plastic strain, are the unknown variables. The primal formulation, which has received a detailed treatment in Han and Reddy [94], is less popular as a basis for computational treatments of problems in plasticity than the dual formulation, which uses the flow law in its traditional form of the normality law and the Kuhn–Tucker conditions. Nevertheless, as will be seen, the primal formulation is particularly well suited to problems in gradient plasticity in which higher-order derivatives of the kinematic quantities appear; for example, the recent work of Reddy et al. [154] uses the primal formulation to analyse a model of gradient plasticity due to Gurtin and Anand [92]. Furthermore, various authors, for example, de Borst and Mülhaus [62] and Fleck and Hutchinson [81], have commented on the suitability of what are essentially primal formulations as a basis for carrying out finite element approximations.

Careful attention is paid to constructing the appropriate variational form of the plasticity problem. Both the classical plasticity problem and the model of gradient plasticity considered here are presented as variational inequalities within a convex analytic framework, thereby facilitating the subsequent analysis. The adoption of the convex analytic framework is motivated by the analysis of the primal and dual forms of the classical plasticity problem presented by Han and Reddy [151, 93, 95, 94], and

the work of Carstensen and coworkers who have made significant contributions to the numerical analysis of the primal problem [8, 34, 37, 47, 44].

The structure of the rest of this chapter is as follows. In Section 2.1 the governing equations and inequalities for the classical and gradient problems are presented. The conventional dual representation of the plastic flow law is given. A detailed exposition of the primal formulation follows. Several results from convex analysis are presented to facilitate the exposition. The linkage between the various forms of the flow law is then made. Finally, in Section 2.2 the classical and gradient plasticity problems are formulated as variational inequalities of the second kind and their well-posedness discussed.

2.1 The governing equations for the problem

Let Ω be a bounded convex Lipschitz domain in $\mathbb{R}^{n_{\text{dim}}}$, where n_{dim} refers to the number of space dimensions. The domain Ω is occupied by an elastoplastic body in its undeformed configuration as shown in Fig. 2.1. A material point in Ω is denoted by $\boldsymbol{X}$ and the time domain under consideration is the interval $[0, T]$. The boundary of Ω is denoted by $\partial\Omega$ with an outward normal $\boldsymbol{N}$. Dirichlet and Neumann boundary conditions are prescribed on Γ_φ and Γ_T respectively, where $\Gamma_\varphi \cap \Gamma_T = \varnothing$ and $\overline{\Gamma_\varphi \cup \Gamma_T} = \overline{\partial\Omega}$.

The body is assumed to undergo a quasi-static infinitesimal motion. Its behaviour is governed by the equation of equilibrium

$$\text{DIV}[\boldsymbol{\sigma}] + \boldsymbol{B} = \boldsymbol{0}\,, \tag{2.1}$$

where $\boldsymbol{\sigma}$ is the symmetric stress tensor, $\text{DIV}[(\cdot)]_I := \partial(\cdot)_{IJ}/\partial X_J$ denotes the divergence of an arbitrary second-order tensor, and $\boldsymbol{B}$ is the body force per unit volume.

The theory of elastoplasticity subject to the infinitesimal-strain assumption is completed by specifying, in addition to the equilibrium equation (2.1), the relationship between the strain tensor and the displacement, the elastic constitutive relation, and a set of evolution equations for the plastic variables.

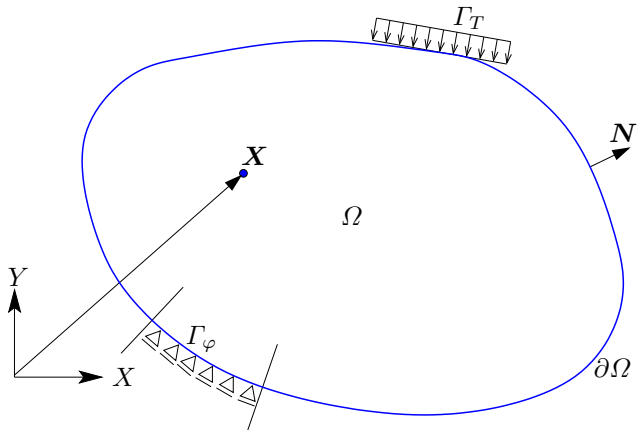

Fig. 2.1. Schematic of an elastoplastic body in the reference configuration subject to loading and boundary conditions

2.1.1 Elastic behaviour

The elastic part of the constitutive relation is given by

$$\boldsymbol{\sigma} = \mathcal{C}\boldsymbol{\varepsilon}^e = \mathcal{C}\left(\boldsymbol{\varepsilon} - \boldsymbol{\varepsilon}^p\right) \qquad \text{or} \qquad \sigma_{IJ} = \mathcal{C}_{IJKL}\varepsilon^e_{KL} = \mathcal{C}_{IJKL}\left(\varepsilon_{KL} - \varepsilon^p_{KL}\right) , \tag{2.2}$$

in which $\boldsymbol{\varepsilon}^e$ is the elastic strain, defined to be the difference between the total strain $\boldsymbol{\varepsilon}$ and the plastic strain $\boldsymbol{\varepsilon}^p$; that is,

$$\boldsymbol{\varepsilon}^e = \boldsymbol{\varepsilon} - \boldsymbol{\varepsilon}^p \ .$$

The summation convention has been used in $(2.2)_2$; the appearance of an index twice implies the sum of all terms obtained by replacing the letter with each of the values in the range of the index. We adopt this convention throughout unless an indication to the contrary is given. All strain quantities are symmetric. In addition, the total strain is given in terms of the displacement $\boldsymbol{u}$ as

$$\boldsymbol{\varepsilon} = \tfrac{1}{2}\left(\nabla[\boldsymbol{u}] + (\nabla[\boldsymbol{u}])^T\right) \ ,$$

where $\nabla[(\cdot)] := \partial(\cdot)/\partial\boldsymbol{X}$ is the gradient operator with respect to the reference configuration. The plastic response is assumed incompressible, so that

$$\mathrm{tr}[\boldsymbol{\varepsilon}^p] = \varepsilon^p_{11} + \varepsilon^p_{22} + \varepsilon^p_{33} = 0 \ .$$

Elastic behaviour is assumed to be isotropic and homogeneous, so that the fourth-order elasticity tensor $\mathcal{C}$ is given in component form by

$$\mathcal{C}_{IJKL} = \Lambda\delta_{IJ}\delta_{KL} + \mu\left(\delta_{IK}\delta_{JL} + \delta_{IL}\delta_{JK}\right) \ ;$$

that is,

$$\mathcal{C}\boldsymbol{\varepsilon}^e = \Lambda\,\mathrm{tr}[\boldsymbol{\varepsilon}^e]\boldsymbol{I} + 2\mu\boldsymbol{\varepsilon}^e$$

for any symmetric tensor $\boldsymbol{\varepsilon}^e$. The quantity δ_{IJ} denotes the Kronecker delta. Here $\Lambda > 0$ and $\mu > 0$ are the Lamé moduli which are related to the Young's modulus E and the Poisson's ratio ν by

$$\Lambda = \frac{E}{(1+\nu)\,(1-2\nu)} \qquad \text{and} \qquad \mu = \frac{2}{1+\nu}.$$

The assumption of material homogeneity implies that Λ and μ are constant. It follows from the positivity of the Lamé moduli that

$$\boldsymbol{\eta} : \mathcal{C}\boldsymbol{\eta} \geq 2\mu|\boldsymbol{\eta}|^2 \qquad \text{for any second-order tensor } \boldsymbol{\eta} \ .$$

We also define

$$|\mathcal{C}|_\infty := \max_{I,J,K,L}[\mathcal{C}_{IJKL}] = \Lambda + 2\mu \, .$$

2.1.2 Plastic flow relations

The relations governing the evolution of plastic deformation are now given. We initially consider the more familiar dual form of the plastic evolution relations which uses the flow law in the form of the normality law with the Kuhn–Tucker conditions. We shall make extensive use of the flow law in the alternative, but equivalent, primal form [93, 95, 94]. Prior to deriving the primal form of the plastic flow relations, how-

ever, we recast the constitutive relations for elastoplasticity within a thermodynamic framework. As will be seen, the thermodynamic framework facilitates the extension of the classical plasticity model to the gradient regime in a manner that makes clear the various conjugate quantities.

Dual representation of the classical plastic flow relations

The classical model of plasticity considered assumes, pointwise a.e., a convex elastic domain $\mathcal{E}$ with boundary $\partial\mathcal{E}$, the yield surface, and a generalised normality law, as depicted in Fig. 2.2. For definiteness $\mathcal{E}$ is assumed to be defined by the von Mises condition, and both linear kinematic and isotropic hardening are initially adopted, so that the region of admissible generalised stresses becomes the set $\boldsymbol{\Sigma} = (\boldsymbol{\sigma}, \boldsymbol{\alpha}, \bar{g})$ that satisfies the von Mises yield criterion

$$f(\boldsymbol{\sigma}, \boldsymbol{\alpha}, \bar{g}) = |\operatorname{dev}[\boldsymbol{\sigma}] + \boldsymbol{\alpha}| - (\kappa - \bar{g}) \leq 0 \ . \tag{2.3}$$

Here $\operatorname{dev}[(\cdot)] := (\cdot) - \operatorname{tr}[(\cdot)]\boldsymbol{I}$ denotes the deviatoric part of an arbitrary second-order tensor $(\cdot)$, κ is related to the initial yield stress of the material in uniaxial tension, and

$$\boldsymbol{\alpha} = -k_1 \boldsymbol{\varepsilon}^p \qquad \text{(the back-stress)}, \tag{2.4}$$

$$\bar{g} = -k_2 \xi \qquad \text{(the internal stress conjugate to the isotropic hardening parameter } \xi) \ , \tag{2.5}$$

where k_1 and k_2 are the kinematic and isotropic hardening constants respectively.

The flow law for the evolution of the set of generalised kinematic plastic strain quantities $\boldsymbol{P} := (\boldsymbol{\varepsilon}^p, \xi)$ takes the form

$$\dot{\boldsymbol{\varepsilon}}^p = \lambda \frac{\partial f(\boldsymbol{\sigma}, \boldsymbol{\alpha}, \bar{g})}{\partial \boldsymbol{\sigma}} = \lambda \frac{\operatorname{dev}[\boldsymbol{\sigma}] + \boldsymbol{\alpha}}{|\operatorname{dev}[\boldsymbol{\sigma}] + \boldsymbol{\alpha}|} \ , \tag{2.6a}$$

$$\dot{\xi} = \lambda \frac{\partial f(\boldsymbol{\sigma}, \boldsymbol{\alpha}, \bar{g})}{\partial \bar{g}} = \lambda \, , \tag{2.6b}$$

$$\lambda \geq 0, \quad f \leq 0, \quad \text{and} \quad \lambda f = 0 \ , \tag{2.6c}$$

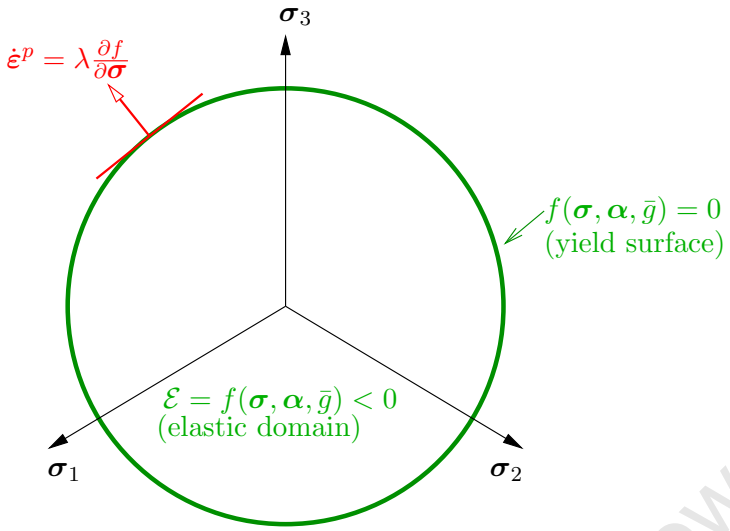

Fig. 2.2. Schematic of the yield surface in stress space for classical plasticity at infinitesimal strains

where (2.6c) are the Kuhn–Tucker conditions and λ is the plastic consistency parameter. The equivalent plastic strain $\gamma(t)$ is related to the plastic consistency parameter by $\dot{\gamma} = \lambda$. It follows that

$$\dot{\xi} = \lambda = |\dot{\boldsymbol{\varepsilon}}^p| \,.$$

Equations (2.6a)–(2.6c) collectively denote the flow law in its most widely presented dual form.

Example 2.1. The following example serves to make clear various features of the dual form of the plastic evolution relations for the special case of plane stress, for which $\sigma_{i3} = 0$, $i = 1, 2, 3$. Furthermore, we consider a perfectly plastic material, for which $k_1 = k_2 = 0$. This example problem will be revisited shortly when we consider the primal expression of the flow law.

If the global axes are chosen to be aligned locally with the principal axes of $\boldsymbol{\sigma}$, then the von Mises yield function (2.3) takes the form

$$f = f(\sigma_1, \sigma_2) = \left(\sigma_1^2 - \sigma_1\sigma_2 + \sigma_2^2\right) - \sigma_0^2 \leq 0 \,,$$

where σ_1 and σ_2 are the principal components of the stress and σ_0 is the yield stress in uniaxial tension. The yield surface $f = 0$ and the elastic region $f < 0$ are shown in Fig. 2.3. The yield surface is an ellipsoid relative to the axes (σ_1, σ_2).

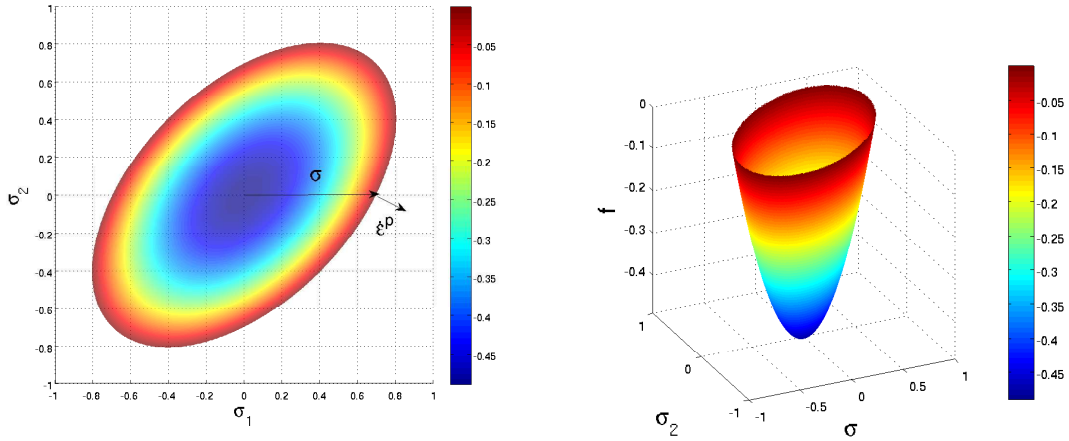

Fig. 2.3. The von Mises yield function in principal stress space for the case of plane stress

Consider now a point on the yield surface at a stress state of $\sigma_1 = \sigma_0$ and $\sigma_2 = 0$ as indicated in Fig. 2.3. The direction of evolution of the plastic strain is the normal to the yield surface at $(\sigma_0, 0)$.

A thermodynamic framework for elastoplasticity

The adoption of a thermodynamic framework for elasticity is advantageous as it is conveniently extended to account for plastic behaviour using the concept of internal variables [55]. The thermodynamic framework will be exploited in this work to ensure that, amongst other things, the model of gradient plasticity developed is thermodynamically consistent. A thermodynamic framework has been used in [176, 148, 115], amongst others, as a basis for gradient plasticity formulations.

We assume from the outset that all processes take place under isothermal conditions. We denote by ψ the Helmholtz free energy. Following standard thermodynamic arguments [55], we arrive at the local statement of the dissipation inequality in the form

$$\dot{\psi} - \boldsymbol{\sigma} : \dot{\boldsymbol{\varepsilon}} \leq 0 \,. \tag{2.7}$$

A homogeneous elastic material is defined such that the free energy and the stress are functions of the strain only; that is,

$$\psi = \hat{\psi}(\boldsymbol{\varepsilon}) \,, \tag{2.8}$$

$$\boldsymbol{\sigma} = \hat{\boldsymbol{\sigma}}(\boldsymbol{\varepsilon}) \,. \tag{2.9}$$

Substitution of (2.8) into the local dissipation inequality (2.7) yields the following

$$\begin{aligned} 0 &\geq \frac{\partial \psi}{\partial \boldsymbol{\varepsilon}} : \dot{\boldsymbol{\varepsilon}} - \boldsymbol{\sigma} : \dot{\boldsymbol{\varepsilon}} \\ &\geq \left(\frac{\partial \psi}{\partial \boldsymbol{\varepsilon}} - \boldsymbol{\sigma} \right) : \dot{\boldsymbol{\varepsilon}} \,, \end{aligned}$$

from which we obtain the relationship between the stress and the free energy as

$$\boldsymbol{\sigma} = \frac{\partial \psi}{\partial \boldsymbol{\varepsilon}} \,.$$

The linear isotropic material presented in Section 2.1.1 is recovered by assuming a free energy that is a quadratic function of the strain; that is,

$$\psi = \hat{\psi}(\boldsymbol{\varepsilon}) = \tfrac{1}{2} \boldsymbol{\varepsilon} : \mathcal{C} \boldsymbol{\varepsilon} \qquad \text{or} \qquad \psi = \hat{\psi}(\boldsymbol{\varepsilon}) = \tfrac{1}{2} \mathcal{C}_{IJKL} \varepsilon_{IJ} \varepsilon_{KL} \,. \tag{2.10}$$

The extension of the thermodynamic framework to account for plastic deformation is accomplished as follows. The additive decomposition of the strain tensor into an elastic and a plastic part can be deduced from thermodynamic considerations [117]. Thus, the free energy may be additively composed of an elastic and a plastic part, denoted ψ^e and ψ^p respectively. The elastic part of the free energy is dependent upon the elastic strain $\boldsymbol{\varepsilon}^e$. The plastic part is dependent upon a set of internal variables, denoted $\boldsymbol{\xi}$, which characterise the plastic deformation; that is,

$$\psi = \hat{\psi}(\boldsymbol{\varepsilon}, \boldsymbol{\xi}) = \hat{\psi}^e(\boldsymbol{\varepsilon}^e) + \hat{\psi}^p(\boldsymbol{\xi}) \,.$$

The number of internal variables describing the plastic deformation is denoted n_{int}. Substitution of the above relation into the local dissipation inequality (2.7) yields

$$\begin{aligned} 0 &\geq \dot{\psi} - \boldsymbol{\sigma} : \dot{\boldsymbol{\varepsilon}} \\ &\geq \frac{\partial \psi^e}{\partial \boldsymbol{\varepsilon}^e} : \dot{\boldsymbol{\varepsilon}}^e + \sum_{\mathrm{A}}^{\mathrm{n}_{int}} \frac{\partial \psi^p}{\partial \boldsymbol{\xi}_{\mathrm{A}}} : \dot{\boldsymbol{\xi}}_{\mathrm{A}} - \boldsymbol{\sigma} : (\dot{\boldsymbol{\varepsilon}}^e + \dot{\boldsymbol{\varepsilon}}^p) \\ &\geq \left(\frac{\partial \psi^e}{\partial \boldsymbol{\varepsilon}^e} - \boldsymbol{\sigma} \right) : \dot{\boldsymbol{\varepsilon}}^e - \boldsymbol{\sigma} : \dot{\boldsymbol{\varepsilon}}^p + \sum_{\mathrm{A}=1}^{\mathrm{n}_{int}} \frac{\partial \psi^p}{\partial \boldsymbol{\xi}_{\mathrm{A}}} : \dot{\boldsymbol{\xi}}_{\mathrm{A}} \,. \end{aligned} \tag{2.11}$$

Following the standard thermodynamic arguments used previously, we obtain the constitutive relationship for the stress as

$$\boldsymbol{\sigma} = \frac{\partial \psi^e}{\partial \boldsymbol{\varepsilon}^e} \,,$$

and the reduced dissipation inequality as

$$\boldsymbol{\sigma} : \dot{\boldsymbol{\varepsilon}}^p - \sum_{\mathrm{A}=1}^{\mathrm{n}_{int}} \frac{\partial \psi^p}{\partial \boldsymbol{\xi}_{\mathrm{A}}} : \dot{\boldsymbol{\xi}}_{\mathrm{A}} \geq 0 \,.$$

We denote by $\boldsymbol{\chi}$ the set of internal variables conjugate to $\boldsymbol{\xi}$ and defined by

$$\boldsymbol{\chi}_{\mathrm{A}} := -\frac{\partial \psi^p}{\partial \boldsymbol{\xi}_{\mathrm{A}}} \qquad \mathrm{A} = 1, \ldots, \mathrm{n}_{int} \,.$$

The reduced local dissipation inequality may thus be restated as

$$\boldsymbol{\sigma} : \dot{\boldsymbol{\varepsilon}}^p + \sum_{\mathrm{A}=1}^{\mathrm{n}_{int}} \boldsymbol{\chi}_{\mathrm{A}} : \dot{\boldsymbol{\xi}}_{\mathrm{A}} \geq 0 \,. \tag{2.12}$$

The assumption of linear isotropic and kinematic hardening corresponds to choosing a plastic free energy of the following quadratic form

$$\psi^p = \hat{\psi}^p(\boldsymbol{\alpha}, \xi) = \tfrac{1}{2} k_1 |\boldsymbol{\alpha}|^2 + \tfrac{1}{2} k_2 \xi^2 \,, \tag{2.13}$$

for which case (2.12) becomes

$$\boldsymbol{\sigma} : \dot{\boldsymbol{\varepsilon}}^p + \bar{g}\dot{\xi} + \boldsymbol{\alpha} : \dot{\boldsymbol{\varepsilon}}^p \geq 0\,. \tag{2.14}$$

Primal representation of the classical plastic flow relations

We will make extensive use of the expression of the plastic flow law in its alternative, but equivalent, primal form [151, 93, 95, 94]. The primal framework is adopted here to facilitate the analysis of the classical and gradient plasticity formulations presented in subsequent chapters. In addition, as mentioned previously, the primal framework is particularly well suited to gradient plasticity problems [62, 81]. Carstensen and coworkers have made significant contributions to the numerical analysis [34, 37] and the development of effective adaptive finite element procedures [8, 47] for the primal problem. Prior to stating the primal form of the flow law, it is convenient to define certain terminology.

Let X be a normed vector space with a topological dual $X^{'}$, the space of continuous linear functionals on X. The action of $\boldsymbol{x} \in X^{'}$ on $\boldsymbol{x} \in X$ is denoted by $\langle \boldsymbol{x}^*, \boldsymbol{x} \rangle$ where the result is in $\mathbb{R}$.

The normal cone to a convex set $Y \subset X$ at $\boldsymbol{x}$, denoted by $N_Y(\boldsymbol{x})$ and depicted in Fig. 2.4(a), is the set of functionals in the dual space $X^{'}$ defined by

$$N_Y(\boldsymbol{x}) = \left\{ \boldsymbol{x}^* \in X^{'} \;:\; < \boldsymbol{x}^*, \boldsymbol{y} - \boldsymbol{x} > \;\leq 0 \quad \forall \boldsymbol{y} \in Y \right\}.$$

The subdifferential of a convex function $f(\boldsymbol{x})$ on X, where $\boldsymbol{x} \in X$, is the, possibly empty, set of subgradients to f in $X^{'}$ defined by (see Fig. 2.4(b))

$$\partial f(\boldsymbol{x}) = \left\{ \boldsymbol{x}^* \in X^{'} \;:\; f(\boldsymbol{y}) \geq f(\boldsymbol{x}) + < \boldsymbol{x}^*, \boldsymbol{y} - \boldsymbol{x} > \quad \forall \boldsymbol{y} \in X \right\}.$$

If the function is differentiable then $\partial f(\boldsymbol{x}) = \{\nabla f(\boldsymbol{x})\}$.

Consider the function in $\mathbb{R}$ shown in Fig. 2.5 taken from Han and Reddy [94]. A function f defined on a subset Ω of $\mathbb{R}^n$ is continuous at a point $\boldsymbol{x}_0$ on Ω if for all positive ϵ it is possible to find a positive number δ such that

$$|f(\boldsymbol{x}) - f(\boldsymbol{x}_0)| < \epsilon \quad \text{whenever} \quad |\boldsymbol{x} - \boldsymbol{x}_0| < \delta \quad \text{and } \boldsymbol{x} \in \Omega\,.$$

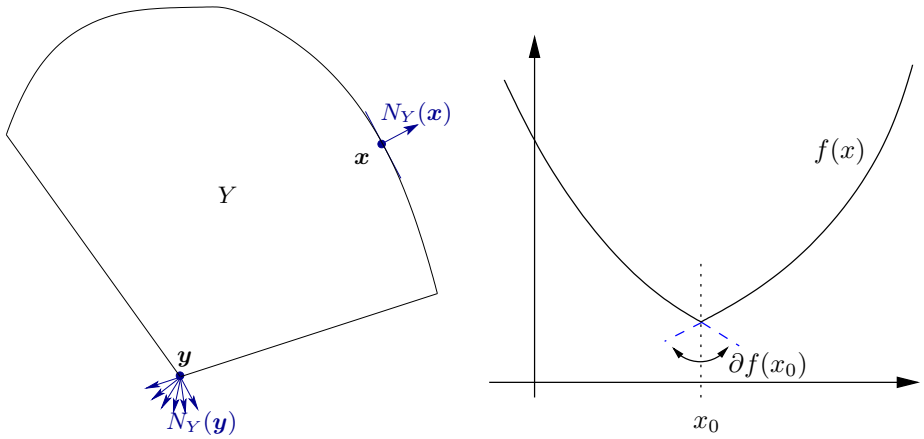

(a) Normal cone to the convex set Y

(b) Subdifferential of a nonsmooth convex function of a single variable

Fig. 2.4. Schematic of the normal cone to a convex set and the subdifferential to a convex function

The function $f(\boldsymbol{x})$ is termed convex if, for $0 < \theta < 1$,

$$f(\theta\boldsymbol{x} + (1-\theta)\boldsymbol{y}) \leq \theta f(\boldsymbol{x}) + (1-\theta) f(\boldsymbol{y})\,. \tag{2.15}$$

The function $f(\boldsymbol{x})$ is said to be strictly convex if the strict inequality in (2.15) holds whenever $\boldsymbol{x} \neq \boldsymbol{y}$. Furthermore, the function $f(\boldsymbol{x})$ is said to be positively homogeneous if

$$f(\alpha\boldsymbol{x}) = \alpha f(\boldsymbol{x}) \quad \forall \boldsymbol{x} \in \Omega, \qquad \forall \alpha > 0\,,$$

proper if

$$f(\boldsymbol{x}) < +\infty \quad \text{for at least one } \boldsymbol{x} \in \Omega \text{ and } f(\boldsymbol{x}) > -\infty \quad \forall \boldsymbol{x} \in \Omega\,,$$

and lower semicontinuous if

$$\liminf_{\mathrm{n}\to\infty} f(\boldsymbol{x}_\mathrm{n}) \geq f(\boldsymbol{x})\,,$$

for any sequence $\{\boldsymbol{x}_\mathrm{n}\}$ converging to $\boldsymbol{x}$.

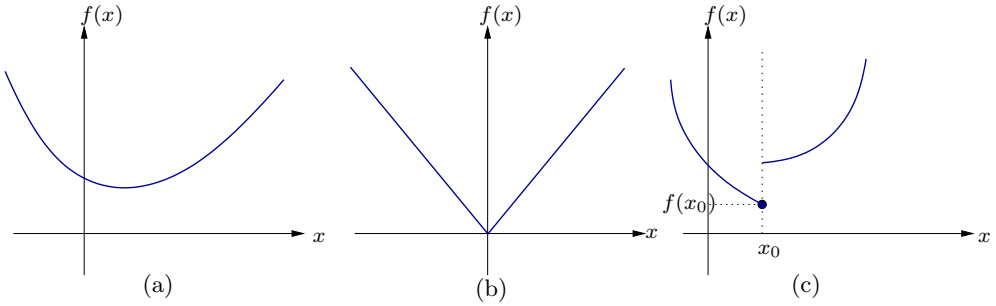

Fig. 2.5. Illustration in one dimension of (a) a convex function; (b) a positively homogeneous function; and (c) a lower semicontinuous function (from [94])

Derivation of the primal form of the plastic flow law

With the necessary terminology defined, we now proceed to derive the primal form of the flow law.

As stated previously, the standard dual form of the flow rule with the loading and unloading conditions formulated in the Kuhn–Tucker form implies the normality law

$$\dot{\boldsymbol{P}} \in N_{\mathcal{E}}(\boldsymbol{\Sigma}) \ , \tag{2.16}$$

where $\dot{\boldsymbol{P}} = \{\dot{\boldsymbol{\varepsilon}}^p, \dot{\boldsymbol{\xi}}\}$ are the generalised plastic strain rates conjugate to the generalised plastic stress $\boldsymbol{\Sigma} = \{\boldsymbol{\sigma}, \boldsymbol{\chi}\}$. The generalised normality law states that the plastic strain evolves in the normal cone to the convex elastic set $\mathcal{E}$.

An alternative primal formulation for the plastic flow law can be derived by recognising that the support function on $\mathcal{E}$ is the dissipation function $D \ : \ \dot{\boldsymbol{P}} \rightarrow \mathbb{R}_+$ in the context of plasticity, defined by

$$D(\dot{\boldsymbol{P}}) = \sup \Big\{ (\boldsymbol{T} : \dot{\boldsymbol{P}}) \text{ where } \boldsymbol{T} \in \mathcal{E} \Big\} = \boldsymbol{\Sigma} : \dot{\boldsymbol{P}} \ . \tag{2.17}$$

The function D is convex, homogeneous of degree one in $\dot{\boldsymbol{P}}$, and lower semicontinuous. It follows from the properties of D that (2.16) is equivalent to stating that the generalised stress state lies in the subdifferential to the generalised plastic strain rate [94], that is,

$$\boldsymbol{\Sigma} \in \partial D(\dot{\boldsymbol{P}}) \, . \tag{2.18}$$

The following two equivalent formulations of the plastic flow law are therefore permitted [94]:

(I)	Primal formulation,	D is convex, homogeneous and lower semicontinuous, $D(\dot{\boldsymbol{P}}) \geq 0$, $\boldsymbol{\Sigma} \in \partial D(\dot{\boldsymbol{P}})$, $\Updownarrow$
(II)	Dual formulation,	K is closed, convex, contains $\mathbf{0}$, $\dot{\boldsymbol{P}} \in N_K(\boldsymbol{\Sigma})$.

The relationship between the primal and dual forms of the flow law is explored further using two examples.

Example 2.2. Consider the convex set $\mathcal{E}$ and yield surface shown in Fig. 2.6 with two generalised stress states, denoted $\boldsymbol{\Sigma}'$ and $\boldsymbol{\Sigma}''$ respectively, indicated. The dual form of the flow law states that the direction of plastic flow $\dot{\boldsymbol{E}}'^p$ at the stress state $\boldsymbol{\Sigma}'$ lies in the normal cone to the yield surface. For the stress state $\boldsymbol{\Sigma}'$ the normal cone is simply the normal to the yield surface. The normal cone to the yield surface at $\boldsymbol{\Sigma}''$ contains the fan of possible directions for the evolution of plastic flow.

The level set of the dissipation function corresponding to the yield surface $\mathcal{E}$ is also shown in Fig. 2.6. The plastic strain rate $\dot{\boldsymbol{E}}'^p$ is in the direction parallel to the normal to the yield surface at $\boldsymbol{\Sigma}'$. The stress state $\boldsymbol{\Sigma}'$ lies in the gradient to the level set of D at $\dot{\boldsymbol{E}}'^p$. The plastic strain rates $\dot{\boldsymbol{E}}''^p$ are parallel to the normal fan to the yield surface at $\boldsymbol{\Sigma}''$ with a corresponding stress state $\boldsymbol{\Sigma}''$.

Example 2.3. We revisit Example 2.1 in which the dual form of the flow law for a problem in plane stress with a von Mises yield condition was described. The corresponding dissipation function, the form of which will be given shortly, is shown in Fig. 2.7. The dissipation function is a nonnegative elliptical cone in the space of plastic strain rates.

The plastic strain rate corresponding to the state of stress $(\sigma_0, 0)$ lies parallel, in the space of plastic strain rates, to the normal to the yield surface. The corresponding stress state on the surface of the dissipation function is also shown.

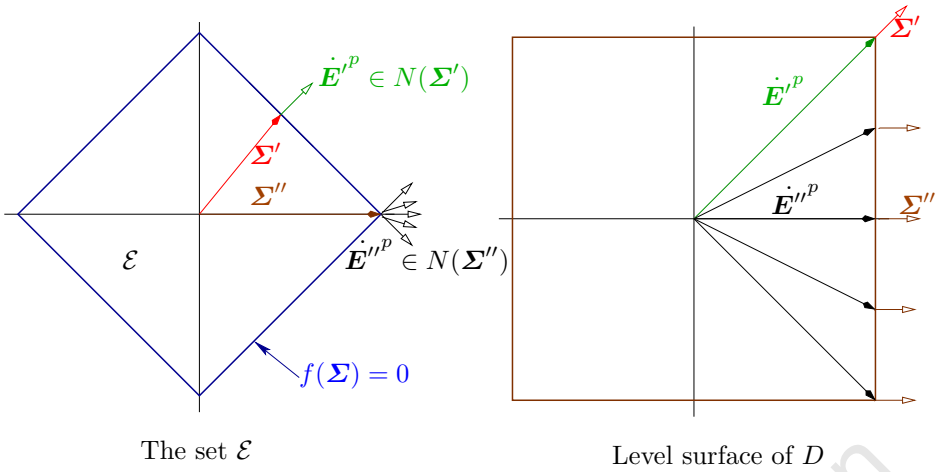

Fig. 2.6. Relationship between the level surface of the dissipation function D and the set $\mathcal{E}$

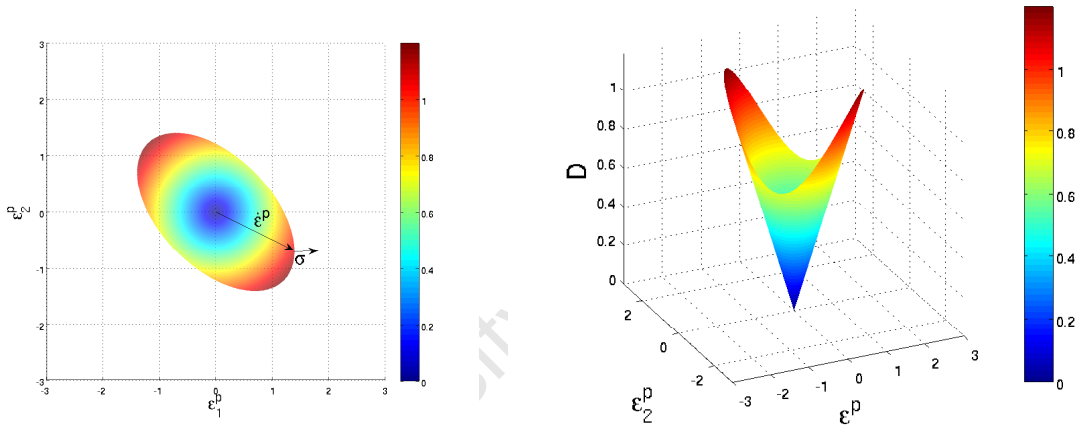

Fig. 2.7. The dissipation function in the space of plastic strain rates for the case of plane stress

Expression of the classical flow law using the primal formulation with the von Mises condition and both kinematic and isotropic hardening

For the model of plastic flow governed by the von Mises yield criterion with both kinematic and isotropic hardening, it can be shown [94] that the dissipation function defined in (2.17) takes the form

$$D(\boldsymbol{q}, \eta) = \begin{cases} \kappa|\boldsymbol{q}| & \text{if } |\boldsymbol{q}| < \eta \ , \\ +\infty & \text{otherwise,} \end{cases}$$

where $\boldsymbol{q}$ and η are arbitrary plastic strain and hardening parameter rates respectively. Using (2.18), we obtain the flow rule in its primal form as

$$\begin{aligned} D(\boldsymbol{q},\eta) &\geq D(\dot{\boldsymbol{\varepsilon}}^p,\dot{\xi}) + (\boldsymbol{\sigma}+\boldsymbol{\alpha}) : (\boldsymbol{q}-\dot{\boldsymbol{\varepsilon}}^p) + \bar{g}(\eta-\dot{\xi}) \\ &= D(\dot{\boldsymbol{\varepsilon}}^p,\dot{\xi}) + (\boldsymbol{\sigma}-k_1\boldsymbol{\varepsilon}^p) : (\boldsymbol{q}-\dot{\boldsymbol{\varepsilon}}^p) - k_2\xi(\eta-\dot{\xi}) \qquad \forall\,(\boldsymbol{q},\eta)\ . \end{aligned} \tag{2.19}$$

2.2 The variational problem

The derivation of the variational problems governing the classical and gradient models of plasticity is now presented.

For the sake of convenience homogeneous Dirichlet boundary conditions are assumed for the analysis; that is,

$$\boldsymbol{u} = \boldsymbol{0} \qquad \text{on } \partial\Omega\ ,$$

where $\boldsymbol{u}$ is the displacement field. In addition, the body is assumed initially undeformed and unstressed with the initial conditions

$$\boldsymbol{u}(\boldsymbol{X},0) = \boldsymbol{0} \qquad \text{and} \qquad \boldsymbol{\varepsilon}^p(\boldsymbol{X},0) = \boldsymbol{0}\ , \qquad \boldsymbol{X}\in\Omega\ .$$

2.2.1 Classical plasticity

We proceed with the derivation of the variational problem governing the classical plasticity problem restricted to the case of linear isotropic and kinematic hardening.

We define the function spaces of displacements V, plastic strains Q, and hardening variables $\bar{M}$ by

$$\begin{aligned} &V = H_0^1(\Omega)^2\ , \\ &Q = \left\{\boldsymbol{q} = (q)_{IJ}\ \middle|\ q_{IJ} = q_{JI},\ q_{IJ}\in L^2(\Omega),\ \mathrm{tr}[\boldsymbol{q}] = 0 \text{ a.e. in } \Omega\right\}\ , \\ &\bar{M} = L^2(\Omega)\,, \end{aligned}$$

and the product space $\bar{Z}$ and the convex set $\bar{W}$ by

$$\bar{Z} = V \times Q \times \bar{M} \ ,$$
$$\bar{W} = \left\{ (\boldsymbol{v}, \boldsymbol{q}, \eta) \in \bar{Z} \ : \ |\boldsymbol{q}| \leq \eta \text{ a.e. in } \Omega \right\} \ .$$

For any function $\phi \ : \ \Omega \times [0,T] \to \mathbb{R}$, we adopt the notation $\phi(t)$ for the function $\boldsymbol{X} \in \Omega \to \phi(\boldsymbol{X}, t)$.

Let $1 \leq p \leq \infty$. For any Banach space X we define the spaces

$$L^p(0,T;X) = \left\{ v \ : \ [0,T] \to X \text{ measurable} : \ \int_0^T \|v(t)\|_X^p \ dt \leq \infty \right\} \ ,$$
$$L^\infty(0,T;X) = \Bigg\{ v \ : \ [0,T] \to X \text{ measurable} : \ \exists C > 0 \ \|v(t)\|_X \leq C \quad \text{a.e.} \quad t \in [0,T] \Bigg\} \ .$$

These are Banach spaces equipped respectively with the norms

$$\|v\|_{L^p(0,T;X)} = \left(\int_0^T \|v(t)\|_X^p \ dt \right)^{1/p} \ ,$$
$$\|v\|_{L^\infty(0,T;X)} = \operatorname*{ess\,sup}_{0 \leq t \leq T} \|v(t)\|_X \ .$$

We also define the space

$$H^1(0,T;X) = \left\{ v \in L^2(0,T;X) \mid \dot{v} \in L^2(0,T;X) \right\} \ ,$$

in which the time derivative is defined in a weak sense. This is a Hilbert space with inner product and norm

$$(u,v)_{H^1(0,T;X)} = \int_0^T \left[(u(t), v(t))_X + (\dot{u}(t), \dot{v}(t))_X \right] \ dX \ ,$$
$$\|v\|_{H^1(0,T;X)} = (v,v)_{H^1(0,T;X)}^{1/2} \ .$$

The weak form of the equilibrium equation is obtained by taking the scalar product of (2.1) with $(\boldsymbol{v}-\dot{\boldsymbol{u}})$ for arbitrary $\boldsymbol{v} \in V$, integrating the product over the domain Ω, performing an integration by parts, and using the constitutive expression (2.2) for $\boldsymbol{\sigma}$ to obtain

$$\int_{\Omega} \mathcal{C}\left(\boldsymbol{\varepsilon}(\boldsymbol{u})-\boldsymbol{\varepsilon}^{p}\right):\left(\boldsymbol{\varepsilon}(\boldsymbol{v})-\boldsymbol{\varepsilon}(\dot{\boldsymbol{u}})\right)\ dX=\int_{\Omega} \boldsymbol{B}\cdot(\boldsymbol{v}-\dot{\boldsymbol{u}})\ dX\,. \tag{2.20}$$

The classical weak formulation corresponding to the boundary value problem governing linear elasticity is obtained by setting $\boldsymbol{\varepsilon}^{p}=\mathbf{0}$ and $\xi=0$ to obtain

$$\int_{\Omega} \mathcal{C}\boldsymbol{\varepsilon}(\boldsymbol{u}):\boldsymbol{\varepsilon}(\boldsymbol{v})\ dX=\int_{\Omega} \boldsymbol{B}\cdot\boldsymbol{v}\ dX\,.$$

The weak form of the dissipation inequality is obtained by integrating the relation (2.19) to obtain

$$\begin{aligned}\int_{\Omega} D(\boldsymbol{q},\eta)\ dX \geq \int_{\Omega} D(\dot{\boldsymbol{\varepsilon}}^{p},\dot{\xi})\ dX+\int_{\Omega}(\boldsymbol{\sigma}+\boldsymbol{\alpha}):(\boldsymbol{q}-\dot{\boldsymbol{\varepsilon}}^{p})\ dX\\ +\int_{\Omega}\bar{g}(\eta-\dot{\xi})\ dX \qquad \forall\,(\boldsymbol{q},\eta)\in\bar{W}\,.\end{aligned} \tag{2.21}$$

The variational inequality corresponding to the primal formulation of classical plasticity is obtained by adding (2.20) and (2.21). The primal variational problem for classical plasticity is that of finding $\boldsymbol{w}=(\boldsymbol{u},\boldsymbol{\varepsilon}^{p},\xi)\ :\ [0,T]\rightarrow\bar{Z}$ such that $\boldsymbol{w}(0)=\mathbf{0},\ \dot{\boldsymbol{w}}\in\bar{W}$ for almost every $t\in[0,T]$ and

$$\bar{a}\left(\boldsymbol{w}(t),\boldsymbol{z}-\dot{\boldsymbol{w}}(t)\right)+j(\boldsymbol{z})-j(\dot{\boldsymbol{w}})\geq\langle l(t),\boldsymbol{z}-\dot{\boldsymbol{w}}\rangle\ , \tag{2.22}$$

in which the bilinear form and functionals are given by

$$
\begin{aligned}
&\bar{a} : \bar{Z} \times \bar{Z} \to \mathbb{R} \ , \\
&\bar{a}(\boldsymbol{w}, \boldsymbol{z}) = \int_\Omega \left(\mathcal{C} \left(\boldsymbol{\varepsilon}(\boldsymbol{u}) - \boldsymbol{\varepsilon}^p \right) : \left(\boldsymbol{\varepsilon}(\boldsymbol{v}) - \boldsymbol{q} \right) + k_1 \boldsymbol{\varepsilon}^p : \boldsymbol{q} + k_2 \xi \eta \right) \, dX \\
&\qquad\qquad \forall \boldsymbol{w} = (\boldsymbol{u}, \boldsymbol{\varepsilon}^p, \xi), \ \boldsymbol{z} = (\boldsymbol{v}, \boldsymbol{q}, \eta) \in \bar{Z} \ ,
\end{aligned} \tag{2.23}
$$

$$
j : \bar{Z} \to \mathbb{R}, \ j(\boldsymbol{z}) \ = \begin{cases} \displaystyle\int_\Omega \kappa |\boldsymbol{q}| \, dX & \text{if } \boldsymbol{z} \in \bar{W} \quad \forall \boldsymbol{z} = (\boldsymbol{v}, \boldsymbol{q}, \eta) \in \bar{Z} \, , \\ \infty & \text{otherwise} \ , \end{cases} \tag{2.24}
$$

$$
\ell : \bar{Z} \to \mathbb{R}, \ \langle \ell, \boldsymbol{z} \rangle = \int_\Omega \boldsymbol{B} \cdot \boldsymbol{v} \, dX \qquad \forall \boldsymbol{z} = (\boldsymbol{v}, \boldsymbol{q}, \eta) \in \bar{Z} \ . \tag{2.25}
$$

Note that by simple integration, the condition $\dot{\boldsymbol{w}}(t) \in \bar{W}$ implies also that $\boldsymbol{w}(t) \in \bar{W}$.

The following result is proved in Han and Reddy [94].

Theorem 2.4. *Assume that* $\boldsymbol{B} \in H^1(0, T; H^1(\Omega)^2)$ *and* $\boldsymbol{B}(0) = \boldsymbol{0}$. *Then the variational inequality (2.22) has a unique solution* $(\boldsymbol{u}, \boldsymbol{\varepsilon}^p, \xi) \in H^1(0, T; V) \times H^1(0, T; Q) \times H^1(0, T; \overline{M})$.

Remark 2.5. The proof makes use of the continuity of the bilinear form and functionals, the coercivity of $\bar{a}(\cdot, \cdot)$, and the weak lower semicontinuity of $j(\cdot)$, which follows from its convexity and its strong lower semicontinuity (the latter follows from the closedness of the set $\bar{W}$ and Fatou's Lemma). Coercivity of $\bar{a}(\cdot, \cdot)$ is subject to either k_1 or k_2 nonnegative and one of k_1 or k_2 positive. This follows from

$$
\begin{aligned}
\bar{a}(\boldsymbol{z}, \boldsymbol{z}) &= \int_\Omega \left(\mathcal{C} \left(\boldsymbol{\varepsilon}(\boldsymbol{v}) - \boldsymbol{q} \right) : \left(\boldsymbol{\varepsilon}(\boldsymbol{v}) - \boldsymbol{q} \right) + k_1 \boldsymbol{q} : \boldsymbol{q} + k_2 \eta \eta \right) \, dX \\
&\geq \int_\Omega \left(2\mu \left[|\boldsymbol{\varepsilon}(\boldsymbol{v})|^2 - 2\boldsymbol{\varepsilon}(\boldsymbol{v}) : \boldsymbol{q} + |\boldsymbol{q}|^2 \right] + k_1 |\boldsymbol{q}|^2 + k_2 |\eta|^2 \right) \, dX \\
&\geq \int_\Omega \left(2\mu \left[|\boldsymbol{\varepsilon}(\boldsymbol{v})|^2 - \theta |\boldsymbol{\varepsilon}(\boldsymbol{v})|^2 - \tfrac{1}{\theta} |\boldsymbol{q}|^2 + |\boldsymbol{q}|^2 \right] + k_1 |\boldsymbol{q}|^2 + k_2 |\eta|^2 \right) \, dX \\
&\quad \text{(using Young's inequality)} \\
&= \int_\Omega 2\mu \left(1 - \theta \right) |\boldsymbol{\varepsilon}(\boldsymbol{v})|^2 \, dX + \int_\Omega \left(2\mu \left(1 - \tfrac{1}{\theta} \right) + k_1 \right) |\boldsymbol{q}|^2 \, dX \\
&\quad + \int_\Omega k_2 |\eta|^2 \, dX \, ,
\end{aligned}
$$

where $\theta > 0$. It follows that the bilinear form is guaranteed to be coercive provided that

$$1 > \theta > \frac{2\mu}{2\mu + k_1} \quad \text{and} \quad k_2 > 0\,.$$

The coercivity of the bilinear form holds for either k_1 or k_2 zero provided that the nonzero constant is positive. Thus, coercivity is guaranteed for hardening but this is not the case for perfect plasticity or softening. The loss of coercivity leads in turn to the well-documented pathological dependence of the resulting finite element approximation upon the discretisation of the domain.

Remark 2.6. The problem is posed on the whole space $\bar{Z}$ rather than on $\bar{W}$. This is legitimate since $\dot{\boldsymbol{w}}(t)$ is sought in $\bar{W}$, and this implies by integration that $\boldsymbol{w}(t) \in \bar{W}$. The functional j is extended by $+\infty$ to all $\bar{Z}\backslash\bar{W}$, consistent with the definition (2.24), while it is also clear (set $\boldsymbol{z} = \boldsymbol{0}$ in (2.22)) that $j(\dot{\boldsymbol{w}})$ is bounded (see also Han and Reddy [94] for further details).

2.2.2 Gradient plasticity

We consider next a simple strain gradient plasticity model due to Dillon and Kratochvil [66], Coleman and Hodgdon [56], Aifantis [2] and Mülhaus and Aifantis [136] and studied computationally by de Borst and Mülhaus [62] and Liebe and Steinmann [115], in which the classical yield condition (2.3) is replaced by one in which the yield condition depends also on the Laplacian of the scalar hardening parameter or equivalent plastic strain. That is, we still have (2.3), but the conjugate force g ($\bar{g}$ in (2.5)) is now given by

$$g = -k_2\xi + k_3\nabla^2\xi\,, \tag{2.26}$$

in which k_3 is a positive constant that effectively introduces a length scale $l := \sqrt{\text{abs}[k_3/k_2]}$ into the formulation and ∇^2 is the Laplacian operator. The classical plasticity formulation is recovered by setting $k_3 = 0$.

The classical free energy function for combined isotropic and kinematic hardening given in (2.13) is extended to the gradient regime by setting

$$\psi = \hat{\psi}\,(\boldsymbol{\varepsilon}, \xi, \nabla\xi) = \hat{\psi}^e(\boldsymbol{\varepsilon}^e) + \underbrace{\left(\tfrac{1}{2}k_1|\boldsymbol{\alpha}|^2 + \tfrac{1}{2}k_2\xi^2 + \tfrac{1}{2}k_3|\nabla\xi|^2\right)}_{\hat{\psi}^p(\xi,\nabla\xi)}\,.$$

Following the classical thermodynamic arguments used in Section 2.1.2 for the classical plasticity problem, the dissipation inequality takes the form

$$\begin{aligned} 0 &\leq \boldsymbol{\sigma} : \dot{\boldsymbol{\varepsilon}} - \dot{\psi} \\ &\leq \boldsymbol{\sigma} : (\dot{\boldsymbol{\varepsilon}}^e + \dot{\boldsymbol{\varepsilon}}^p) - \frac{\partial\hat{\psi}^e(\boldsymbol{\varepsilon}^e)}{\partial\boldsymbol{\varepsilon}^e} : \dot{\boldsymbol{\varepsilon}}^e + \boldsymbol{\alpha} : \dot{\boldsymbol{\varepsilon}}^p + \bar{g}\dot{\xi} + \boldsymbol{m}\cdot\nabla\dot{\xi} \\ &\leq \left(\boldsymbol{\sigma} - \frac{\partial\hat{\psi}^e}{\partial\boldsymbol{\varepsilon}^e}\right) : \dot{\boldsymbol{\varepsilon}}^e + \boldsymbol{\sigma} : \dot{\boldsymbol{\varepsilon}}^p + \boldsymbol{\alpha} : \dot{\boldsymbol{\varepsilon}}^p + \bar{g}\dot{\xi} + \boldsymbol{m}\cdot\nabla\dot{\xi}\,, \end{aligned} \tag{2.27}$$

where $\boldsymbol{\alpha} := -\partial\psi/\partial\boldsymbol{\varepsilon}^p$, $\bar{g} := -\partial\psi/\partial\xi$ and $\boldsymbol{m} := -\partial\psi/\partial\nabla\xi$.

From the dissipation inequality (2.27) we obtain the elastic relation

$$\boldsymbol{\sigma} = \frac{\partial\hat{\psi}^e(\boldsymbol{\varepsilon}^e)}{\partial\boldsymbol{\varepsilon}^e}$$

and the reduced dissipation inequality

$$\boldsymbol{\sigma} : \dot{\boldsymbol{\varepsilon}}^p + \boldsymbol{\alpha} : \dot{\boldsymbol{\varepsilon}}^p + \bar{g}\dot{\xi} + \boldsymbol{m}\cdot\nabla\dot{\xi} \geq 0\,. \tag{2.28}$$

The dissipation inequality for the gradient plasticity problem is formally given by

$$\begin{aligned} D(\boldsymbol{q},\eta) \geq\; & D(\dot{\boldsymbol{\varepsilon}}^p,\dot{\xi}) + (\boldsymbol{\sigma}+\boldsymbol{\alpha}) : (\boldsymbol{q} - \dot{\boldsymbol{\varepsilon}}^p) \\ & + g(\eta - \dot{\xi}) + \boldsymbol{m}\cdot\nabla(\eta - \dot{\xi}) \qquad \forall(\boldsymbol{q},\eta)\,. \end{aligned} \tag{2.29}$$

In order to construct the weak formulation of the problem corresponding to gradient plasticity we define the space M of scalar hardening parameters by

$$M = H_0^1(\Omega)\,, \tag{2.30}$$

and we set

$$Z = V \times Q \times M \ , \tag{2.31}$$

$$W = \{(\boldsymbol{v}, \boldsymbol{q}, \eta) \in Z : \ |\boldsymbol{q}| \leq \eta \text{ a.e. in } \Omega\} \ . \tag{2.32}$$

We proceed in the construction of the weak form by integrating (2.29) over Ω and performing integration by parts on the term involving $\boldsymbol{m}$. It is necessary at this point to specify the additional nonstandard boundary contributions that arise. We consider here the possibility of either homogeneous Dirichlet boundary conditions, homogeneous Neumann boundary conditions, or combinations thereof on the exterior of the reference configuration $\partial\Omega$. We denote by $\partial\Omega_H$ and $\partial\Omega_F$ complementary subsets of $\partial\Omega$, that is, $\partial\Omega_H \cup \Omega_F = \partial\Omega$ and $\partial\Omega_H \cap \Omega_F = \varnothing$. The additional boundary conditions arising due to the presence of the gradient terms are

$$\xi = 0 \text{ on } \partial\Omega_H \qquad \text{and} \qquad -\boldsymbol{m} \cdot \boldsymbol{N} = k_2 \frac{\partial \xi}{\partial \boldsymbol{N}} = 0 \text{ on } \partial\Omega_F \, ,$$

where $\boldsymbol{m} = -k_3 \nabla \xi$. Further discussion on the physical implications of the additional boundary conditions that arise in gradient plasticity formulations can be found in Gurtin [89, 90] and Peerlings [146], amongst others.

After application of the relevant boundary conditions, we then obtain the dissipation inequality in weak form as

$$\begin{aligned} j(\boldsymbol{z}) \geq j(\dot{\boldsymbol{w}}) + \int_\Omega (\boldsymbol{\sigma} - k_1 \boldsymbol{\varepsilon}^p) : (\boldsymbol{q} - \dot{\boldsymbol{\varepsilon}}^p) \ dX - \int_\Omega k_2 \xi (\eta - \dot{\xi}) \ dX \\ - \int_\Omega k_3 \nabla \xi \cdot \nabla (\eta - \dot{\xi}) \ dX \qquad \forall \boldsymbol{z} \in Z \ , \end{aligned} \tag{2.33}$$

in which the definition of $j(\cdot)$ is unchanged from (2.24).

Following the approach for the classical problem and combining the dissipation inequality (2.33) with the weak form of the equilibrium equation (2.20) we arrive at the problem of finding $\boldsymbol{w} := (\boldsymbol{u}, \boldsymbol{\varepsilon}^p, \xi) : [0, T] \to Z$ which satisfies: $\boldsymbol{w}(0) = \boldsymbol{0}$, $\dot{\boldsymbol{w}}(t) \in W$ for almost every $t \in [0, T]$ and

$$a\left(\boldsymbol{w}(t), \boldsymbol{z} - \dot{\boldsymbol{w}}(t)\right) + j(\boldsymbol{z}) - j(\dot{\boldsymbol{w}}) \geq \langle \ell(t), \boldsymbol{z} - \dot{\boldsymbol{w}} \rangle \qquad \forall \boldsymbol{z} \in Z \ , \tag{2.34}$$

in which the bilinear form $a(\cdot, \cdot)$ is given by

$$a : Z \times Z \to \mathbb{R}, \quad a(\boldsymbol{w}, \boldsymbol{z}) = \overline{a}(\boldsymbol{w}, \boldsymbol{z}) + \int_\Omega k_3 \nabla \xi \cdot \nabla \eta \, dX \ , \tag{2.35}$$

with $\overline{a}$ defined in (2.23).

Remark 2.7. In contrast to the classical problem, the presence in the yield condition of a term involving a Laplacian leads to the requirement that ξ be sought in the space $H^1(\Omega)$ rather than $L^2(\Omega)$. Again, following the corresponding proof for the classical problem in [94], it can be shown that for $\boldsymbol{B} \in H^1(0, T; L^2(\Omega)^2)$, the variational inequality (2.34) has a unique solution

$$\boldsymbol{w} = (\boldsymbol{u}, \boldsymbol{\varepsilon}^p, \xi) \in H^1(0, T; V) \times H^1(0, T; Q) \times H^1(0, T; M) \, .$$

The coercivity of the bilinear form $a(\cdot, \cdot)$ is established as follows:

$$\begin{aligned}
a(\boldsymbol{z}, \boldsymbol{z}) &= \bar{a}(\boldsymbol{z}, \boldsymbol{z}) + \int_\Omega k_3 \nabla \eta \cdot \nabla \eta \, dX \\
&= \int_\Omega \left(\mathcal{C} \left(\boldsymbol{\varepsilon}(\boldsymbol{v}) - \boldsymbol{q} \right) : \left(\boldsymbol{\varepsilon}(\boldsymbol{v}) - \boldsymbol{q} \right) + k_1 \boldsymbol{q} : \boldsymbol{q} + k_2 \eta \eta \right) dX + \int_\Omega k_3 \nabla \eta \cdot \nabla \eta \, dX \\
&\geq \int_\Omega 2\mu \left(1 - \theta\right) |\boldsymbol{\varepsilon}(\boldsymbol{v})|^2 \, dX + \int_\Omega \left(2\mu \left(1 - \tfrac{1}{\theta}\right) + k_1 \right) |\boldsymbol{q}|^2 \, dX \\
&\quad + \int_\Omega \left(k_2 |\eta|^2 + k_3 |\nabla \eta|^2 \right) dX \\
&\geq \int_\Omega 2\mu \left(1 - \theta\right) |\boldsymbol{\varepsilon}(\boldsymbol{v})|^2 \, dX + \int_\Omega \left(2\mu \left(1 - \tfrac{1}{\theta}\right) + k_1 \right) |\boldsymbol{q}|^2 \, dX \\
&\quad + \int_\Omega \left(k_2 + \frac{c_p k_3}{2} \right) |\eta|^2 \, dX + \int_\Omega \frac{k_3}{2} |\nabla \eta|^2 \, dX \\
&\geq \int_\Omega 2\mu \left(1 - \theta\right) |\boldsymbol{\varepsilon}(\boldsymbol{v})|^2 \, dX + \int_\Omega \left(2\mu \left(1 - \tfrac{1}{\theta}\right) + k_1 + \frac{c_p k_3}{4} \right) |\boldsymbol{q}|^2 \, dX \\
&\quad + \int_\Omega \left(k_2 + \frac{c_p k_3}{4} \right) |\eta|^2 \, dX + \int_\Omega \frac{k_3}{2} |\nabla \eta|^2 \, dX \, ,
\end{aligned}$$

where we have made use of the Poincaré–Friedrichs inequality

$$\int_\Omega \eta^2 \, dX \leq c_p \int_\Omega |\nabla \eta|^2 \, dX \,, \tag{2.36}$$

and the definition of W. It follows that the bilinear form is guaranteed coercive provided that

$$1 > \theta > \frac{8\mu}{8\mu + 4k_1 + c_p k_3} \quad \text{and} \quad k_2 > \frac{-c_p k_3}{4} \,.$$

Thus the model is able to accommodate a degree of softening, both kinematic and isotropic, which, unsurprisingly, depends on the magnitude of the parameter associated with the gradient term.

2.2.3 Regularity of solutions

It is important, both when dealing with finite element interpolation error estimates and when determining the consistency of discontinuous Galerkin formulations, to set out in clear terms the regularity of the exact solution to the problem. The question of the regularity of solutions to problems in plasticity is a much more subtle matter than the corresponding question for linear elasticity, say, and complete results are not available. We summarise some key regularity results for classical hardening plasticity, and indicate the assumptions that need to be made for the case of gradient plasticity.

First, we assume that

$$\boldsymbol{B} \in H^1(0, T; [H^1(\Omega)]^2) \,. \tag{2.37}$$

Then it has been shown by Repin [156] for the Hencky problem (essentially one step in a family of incremental problems arrived at by discretisation in time), that for a Lipschitz domain Ω and hardening plasticity,

$$\boldsymbol{u} \in [H^2_{loc}(\Omega)]^2 \qquad \text{and} \qquad \boldsymbol{\sigma} \in [H^1_{loc}(\Omega)]^{2\times 2} \,. \tag{2.38}$$

Additional smoothness of the domain leads to greater regularity. In particular, as shown in Repin, if the boundary of Ω is C^3, then

$$\boldsymbol{u} \in [H^2(\Omega)]^2 \qquad \text{and} \qquad \boldsymbol{\sigma} \in [H^1(\Omega)]^{2\times 2}\,. \tag{2.39}$$

There are no corresponding results for the case of gradient plasticity.

We will assume in all cases that

$$\begin{aligned}
&\boldsymbol{u} \in H^1(0,T;[H^2(\Omega)]^2)\,,\\
&\boldsymbol{\varepsilon}^p \in H^1(0,T;[H^1(\Omega)]^{2\times 2})\,,\\
&\xi \in H^1(0,T;H^2(\Omega))\,.
\end{aligned} \tag{2.40}$$

These assumptions are somewhat stronger than what is known for the case of classical plasticity, at least for Lipschitz domains, while in the case of gradient plasticity it is not unreasonable to assume that the regularising effect of the gradient terms impart a greater degree of regularity to the solution, when compared with the classical case.

3

A discontinuous Galerkin formulation of classical and gradient plasticity under the assumption of infinitesimal strains

A feature of gradient plasticity formulations that requires careful attention in the development of computational solution procedures is the introduction of terms involving higher-order derivatives of quantities such as the equivalent plastic strain. In classical theories these and other internal variables may be approximated by piecewise discontinuous functions since they are merely required to be square integrable. Furthermore, in finite element approximations these quantities may be condensed out at element level, or computations may be carried out locally at integration points, in either case with the consequence that the predictor part of the solution algorithm involves only the displacement degrees of freedom. Such approaches have either to be modified in gradient theories, or it becomes essential to assume continuity of the relevant internal variables, with a consequently significant increase in the size of the discrete problem to be solved. The need to develop a computational procedure for gradient plasticity that retains the simplicity of the classical algorithms is therefore self-evident.

A candidate approach is the class of discontinuous Galerkin methods, in which interelement continuity is relaxed in a framework in which the discrete problem remains consistent. Discontinuous Galerkin methods were developed in the 1970s and 1980s [139, 11], but it is only in recent years that they have been exploited in a wide range of problems. The collection [53] provides an excellent overview of the key approaches for elliptic and hyperbolic problems. Within the context of linear elasticity there have been important contributions by Rivière and Wheeler [159] and Wihler [190], the latter considering the case of nonconvex domains and vanishing com-

pressibility. A discontinuous Galerkin method has been developed for strain gradient dependent damage models [188, 135], while the work by Engel et al. [74] treats continuous/discontinuous Galerkin methods for fourth-order problems by reducing the classical requirement of C^1 continuity of the unknown variable to one of continuity. This approach for fourth-order problems has recently been applied by Wells et al. [189] to solve the Cahn–Hilliard equation, a fourth-order nonlinear parabolic partial differential equation, and to develop finite element solutions to plate [187] and shell [142, 72] problems involving only discretisations of the displacement field. Furthermore, discontinuous Galerkin time integration schemes appear to be ideally suited to evolving interface problems, as demonstrated by Alberty and Carstensen [6].

A discontinuous Galerkin approximation of the displacement field for the problems of incompressible elasticity (see, for example, [190]) and plasticity elegantly circumvents locking-related problems that occur when using low-order finite elements formulations. The use of low-order finite elements is attractive for reasons of computational efficiency and their robustness in large deformation problems.

Another attractive property of discontinuous Galerkin schemes is the design of more flexible finite element spaces. Within a discontinuous Galerkin approach nonmatching grids containing hanging nodes and nonuniform interpolations can be handled easily. The flexibility offered by the discontinuous Galerkin method renders it well suited for implementation on large-scale, parallel computing platforms [104, 24].

One of the potential drawbacks of discontinuous Galerkin methods is the proliferation of the number of degrees of freedom relative to conventional Galerkin methods. This additional computational overhead can be mitigated by interpreting the discontinuous Galerkin formulation within a multi-scale framework [28, 103]. This framework could potentially be extended to include various models of gradient plasticity as the gradient effects are generally related to scale-dependent phenomena. The additional computational overhead must also be seen in perspective, as emphasised by ten Eyck and Lew [180] in their work on incompressible elastic media. A further example concerns the application of discontinuous Galerkin methods to fourth-order problems for which C^1 continuous interpolants are required. The construction of C^1 continu-

ous interpolants is problematic and computationally expensive within a conforming approximation for space dimensions higher than one.

Motivated in large part by the ability of discontinuous Galerkin methods to provide elegant and effective solutions to the challenging problems in computational mechanics mentioned previously, the focus of the work presented here is on the use of discontinuous Galerkin methods for the solution of problems in elastoplasticity. Both classical plasticity and a model of gradient plasticity [66, 2, 3, 56] are considered, though the emphasis is on the latter, for which case discontinuous Galerkin methods carry several significant advantages.

Discontinuous Galerkin formulations provide an elegant and effective framework in which to deal with the higher-order derivatives arising in gradient plasticity formulations. The model of gradient plasticity considered serves as a foundation for more complex models possibly involving additional higher-order terms and multiple length scales [81]; indeed the model of gradient plasticity can be treated using a conforming finite element approximation [115]. The imposition of the internal plastic boundary is, however, problematic in conforming approximations and the extension of the formulation to other models of gradient plasticity is by no means straightforward. The classical plasticity formulation can also be recovered easily from the gradient model considered here within the context of the discontinuous Galerkin method by simply not imposing the continuity of the internal hardening parameter. Thus, the influence of the gradient effects can be varied spatially. Furthermore, we do not assume continuity of the effective plastic strain field but impose this in a weak sense where needed.

The objective of this chapter is to explore the use of discontinuous Galerkin methods for the solution of problems in elastoplasticity under the assumption of small strains. Both the classical and gradient plasticity formulations are considered, though the emphasis is on the latter, for which case discontinuous Galerkin methods carry significant advantages, as discussed earlier.

A symmetric interior penalty method is introduced in Section 3.1, and the consistency of the discrete formulation is shown. Section 3.2 is devoted to an analysis of the continuous-in-time approximations, and here it is shown that the displacement ap-

proximation satisfies the same error estimate as the conventional Galerkin approximations of the classical problem [94]. Finally, in Section 3.3 fully-discrete discontinuous Galerkin approximations are analysed. Here too the same estimate associated with the classical approach, at least in the absence of greater regularity of the solution, is obtained.

3.1 A discontinuous Galerkin formulation

Consider the subdivision of an arbitrary domain Ω into n_{elem} triangular elements as depicted in Fig. 3.1. An individual element is denoted K with $\mathcal{T}_h = \{K\}$ the set of all elements in the subdivision. The number of nodes per element is denoted $n^{\text{e}}_{\text{node}}$ while the total number of unique nodes in the triangulation $\mathcal{T}_h$ is denoted n_{node}.

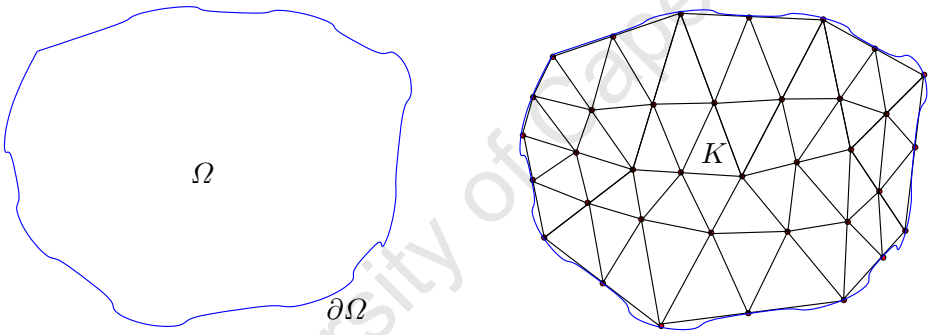

Fig. 3.1. Decomposition of an arbitrary domain Ω into triangular elements

We denote by $\mathcal{P}_k(K)$ the space of polynomials of degree at most $k \geq 0$ on K. For example, the 3-noded linear and the 6-noded quadratic triangular elements shown in Fig. 3.2 correspond to setting $k = 1$ and $k = 2$ respectively.

We denote by $h_K = \text{diam}(K)$ a measure of the element size, taken here to be the diameter of the smallest circle that contains the element K, as shown in Fig. 3.3. The mesh size $h = \max\{h_K, K \in \mathcal{T}_h\}$ is the diameter of the smallest circle that encloses the largest element. We denote by ρ_K the radius of the largest circle contained in K. A family of triangulations $\mathcal{T}_h$ is called shape-regular if there exists a positive constant C independent of h, such that

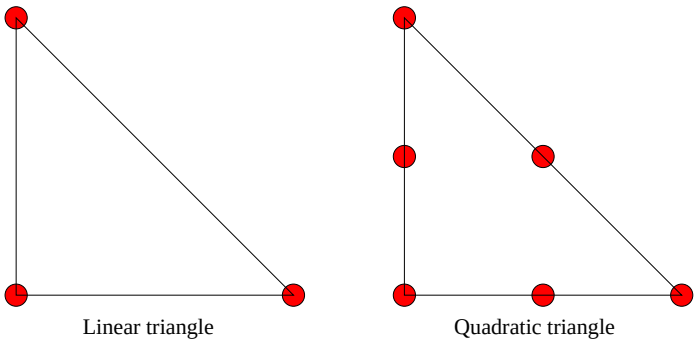

Fig. 3.2. Linear and quadratic triangular elements

$$h_K \leq C\rho_K \,.$$

For further details on triangulations the reader is referred to Toselli and Widlund [185] amongst others.

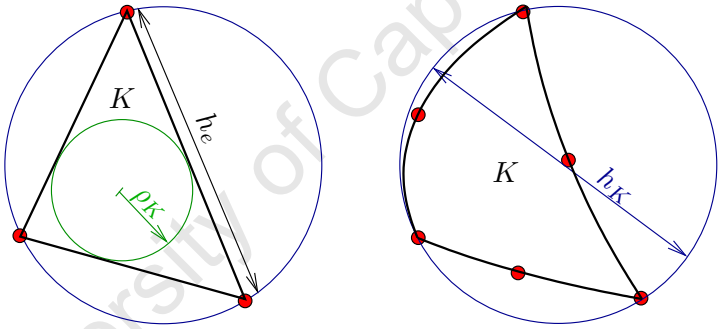

Fig. 3.3. Schematic of the mesh parameters h_K, ρ_K and h_e

Consider the pair of elements shown in Fig. 3.4 that share a common edge. Let $\mathcal{E}_h = \{e\}$ denote the set of the edges e of $\mathcal{T}_h$, and $\mathcal{E}_h^o = \mathcal{E}_h \setminus \partial\Omega$ the set of all interior edges. We associate with each edge of an element K_i the outward unit normal vector $\boldsymbol{N}_i$. For an edge that lies on the boundary, $\boldsymbol{N}_i$ is defined to be the outward normal to $\partial\Omega$. The length of an edge $e \in \mathcal{E}_h$ is denoted h_e.

For a positive integer m, we define

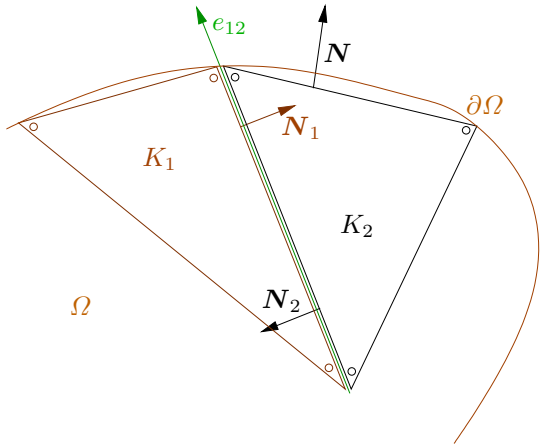

Fig. 3.4. A portion of the decomposition of an arbitrary domain Ω into a collection of triangular elements and edges

$$H^m(\mathcal{T}_h) = \left\{ v \in L^2(\Omega),\ v|_K \in H^m(K) \qquad \forall K \in \mathcal{T}_h \right\} ,$$
$$T(\mathcal{E}_h) = \prod_{K \in \mathcal{T}_h} L^2(\partial K) .$$

The jumps $[\![\cdot]\!]$ and the averages $\{\!\{\cdot\}\!\}$ of $\eta \in L^2(\mathcal{E}_h)$, $\boldsymbol{v} \in L^2(\mathcal{E}_h)^2$ and $\boldsymbol{\tau} \in L^2(\mathcal{E}_h)^{2\times 2}$ across an edge e that is common to elements K_1 and K_2 are defined by

$$\begin{aligned} [\![\eta]\!] &= \eta_1 \boldsymbol{N}_1 + \eta_2 \boldsymbol{N}_2 , & \{\!\{\eta\}\!\} &= \tfrac{1}{2}(\eta_1 + \eta_2) , \\ [\![\boldsymbol{v}]\!] &= \boldsymbol{v}_1 \otimes \boldsymbol{N}_1 + \boldsymbol{v}_2 \otimes \boldsymbol{N}_2 , & \{\!\{\boldsymbol{v}\}\!\} &= \tfrac{1}{2}(\boldsymbol{v}_1 + \boldsymbol{v}_2) , \\ [\![\boldsymbol{\tau}]\!] &= \boldsymbol{\tau}_1 \boldsymbol{N}_1 + \boldsymbol{\tau}_2 \boldsymbol{N}_2 , & \{\!\{\boldsymbol{\tau}\}\!\} &= \tfrac{1}{2}(\boldsymbol{\tau}_1 + \boldsymbol{\tau}_2) , \end{aligned} \tag{3.1}$$

in which η_i, $\boldsymbol{v}_i$ and $\boldsymbol{\tau}_i$ are the one-sided values of the quantities concerned along an edge $e \in \partial K_i$, while $\boldsymbol{N}_i$ is the outward unit normal vector to edge e of element K_i. Fig. 3.5 shows the jump in and average of a scalar field u on the boundary between two elements in one dimension.

If e is an edge of element K_1 that lies on the boundary of the domain $\partial\Omega$, then the jumps and averages are defined by

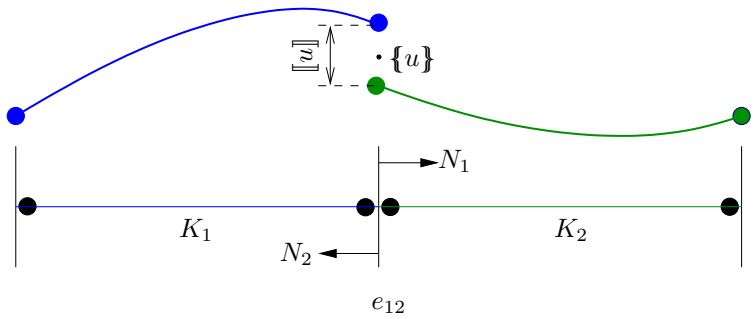

Fig. 3.5. Schematic of the jump in and average of a scalar field on the boundary between two elements in one dimension

$$
\begin{aligned}
[\![\eta]\!] &= \eta_1 \boldsymbol{N}_1 \,, & \{\!\{\eta\}\!\} &= \eta_1 \,, \\
[\![\boldsymbol{v}]\!] &= \boldsymbol{v}_1 \otimes \boldsymbol{N}_1 \,, & \{\!\{\boldsymbol{v}\}\!\} &= \boldsymbol{v}_1 \,, \\
[\![\boldsymbol{\tau}]\!] &= \boldsymbol{\tau}_1 \boldsymbol{N}_1 \,, & \{\!\{\boldsymbol{\tau}\}\!\} &= \boldsymbol{\tau}_1 \,.
\end{aligned}
\tag{3.2}
$$

The following identity relates the scalar product of two quantities to the products of their jumps and averages [13]:

$$
\sum_{K \in \mathcal{T}_h} \int_{\partial K} \boldsymbol{v} \cdot \boldsymbol{\tau} \boldsymbol{N} \, dS = \sum_{e \in \mathcal{E}_h} \int_e [\![\boldsymbol{v}]\!] : \{\!\{\boldsymbol{\tau}\}\!\} \, dS + \sum_{e \in \mathcal{E}_h^o} \int_e \{\!\{\boldsymbol{v}\}\!\} : [\![\boldsymbol{\tau}]\!] \, dS \,. \tag{3.3}
$$

Furthermore, we will also make use of the inequalities [see 11]

$$
\begin{aligned}
&\|v_h\|_e^2 \le c_1 h_K^{-1} \|v_h\|_K^2 \qquad \text{for } v_h \in \mathcal{P}_k(K) \,, \\
&\|v\|_e^2 \le c_2 (h_K^{-1} \|v\|_K^2 + h_K \|\nabla v\|_K^2) \qquad \text{for } v \in H^1(\mathcal{T}_h) \,,
\end{aligned}
\tag{3.4}
$$

where c_1 and c_2 are positive constants independent of h_K and e denotes an edge of K. Thus, from $(3.4)_1$ and using $0 < h_e/h_K \le 1$ (see Fig. 3.3) we obtain

$$
\begin{aligned}
h_e \|\{\!\{\mathcal{C}\boldsymbol{\varepsilon}(\boldsymbol{v}_h)\}\!\}\|_e^2 &\le c_1 h_e h_K^{-1} \|\mathcal{C}\boldsymbol{\varepsilon}(\boldsymbol{v}_h)\|_K^2 \\
&\le c_1 \|\mathcal{C}\boldsymbol{\varepsilon}(\boldsymbol{v}_h)\|_K^2 \,, \qquad (3.5) \\
h_e \|\{\!\{\nabla \xi_h\}\!\}\|_e^2 &\le c_1 h_e h_K^{-1} \|\nabla \xi_h\|_K^2 \\
&\le c_1 \|\nabla \xi_h\|_K^2 \,. \qquad (3.6)
\end{aligned}
$$

Here and henceforth $\|\cdot\|_K$ and $\|\cdot\|_e$ will denote respectively the L^2-norms on an element K and edge e.

The definition of continuity and coercivity of a bilinear form is as follows. A bilinear form $b : V \times W \to \mathbb{R}$ is continuous if

$$|b(v,w)| \le \alpha \|v\|_V \|w\|_W \qquad \forall v \in V,\ w \in W\,,$$

and coercive if there exists a positive constant c such that

$$|b(v,v)| \ge c\|v\|_V^2\,.$$

The following finite-dimensional spaces and subsets will be required:

$$\begin{aligned}
&V_h = \left\{\boldsymbol{v}_h \in L^2(\Omega)^2;\ \boldsymbol{v}_h|_K \in \mathcal{P}_1(K)^2 \qquad \forall K \in \mathcal{T}_h\right\}\,,\\
&Q_h = \left\{\boldsymbol{q}_h \in L^2(\Omega)^{2\times 2};\ q_h|_K \in \mathcal{P}_0(K)^{2\times 2} \qquad \forall K \in \mathcal{T}_h\right\}\,,\\
&\overline{M}_h = \left\{\eta_h \in L^2(\Omega);\ \eta_h|_K \in \mathcal{P}_0(K) \qquad \forall K \in \mathcal{T}_h\right\}\,,\\
&\overline{Z}_h = V_h \times Q_h \times \overline{M}_h\,,\\
&\overline{W}_h = \left\{\boldsymbol{z}_h = (\boldsymbol{v}_h, \boldsymbol{q}_h, \eta_h) \in \overline{Z}_h;\ \ |\boldsymbol{q}_h| \le \eta_h \text{ in each } K \in \mathcal{T}_h\right\}\,,\\
&M_h = \left\{\eta_h \in L^2(\Omega);\ \eta_h|_K \in \mathcal{P}_1(K) \qquad \forall K \in \mathcal{T}_h\right\}\,,\\
&Z_h = V_h \times Q_h \times M_h\,,\\
&W_h = \{\boldsymbol{z}_h = (\boldsymbol{v}_h, \boldsymbol{q}_h, \eta_h) \in Z_h;\ |\boldsymbol{q}_h| \le \eta_h \text{ in each } K \in \mathcal{T}_h\}\,.
\end{aligned} \tag{3.7}$$

We introduce on $\overline{Z}_h$ and Z_h the norms $\|\cdot\|_{\overline{h}}$ and $\|\cdot\|_h$, defined for $\boldsymbol{z}_h = (\boldsymbol{v}_h, \boldsymbol{q}_h, \eta_h)$ by

$$\|\boldsymbol{z}_h\|_{\overline{h}}^2 = \sum_K \left(\|\boldsymbol{\varepsilon}(\boldsymbol{v}_h)\|_K^2 + \|\boldsymbol{q}_h\|_K^2 + \|\eta_h\|_K^2\right) + \sum_e \frac{1}{h_e}\|[\![\boldsymbol{v}_h]\!]\|_e^2\,, \tag{3.8}$$

$$\|\boldsymbol{z}_h\|_h^2 = \|\boldsymbol{z}_h\|_{\overline{h}}^2 + \sum_K \|\nabla\eta_h\|_K^2 + \sum_e \frac{1}{h_e}\|[\![\eta_h]\!]\|_e^2\,. \tag{3.9}$$

To verify the positive definiteness of $\|\cdot\|_{\overline{h}}$ we note that for $\boldsymbol{z} = (\boldsymbol{v}, \boldsymbol{q}, \eta) \in Z_h$ and $\|\boldsymbol{z}\|_{\overline{h}} = 0$, $\boldsymbol{q} = \boldsymbol{0}$, $\eta = 0$ and $\|\boldsymbol{\varepsilon}(\boldsymbol{v})\|_K = 0$. Thus $\boldsymbol{v}|_K$ is a rigid body motion on K,

that is $\boldsymbol{v} = \boldsymbol{a}_K + \boldsymbol{b}_K \times \boldsymbol{x}$, where $\boldsymbol{a}_K$ and $\boldsymbol{b}_K$ are constant in each element K. But $\|[\![\boldsymbol{v}]\!]\|_e = 0$ for each interior edge e, so that $\boldsymbol{a}$ and $\boldsymbol{b}$ are independent of K. Finally, on the boundary edges $\|[\![\boldsymbol{v}]\!]\|_e = \|\boldsymbol{v}\|_e = 0$, so that $\boldsymbol{a} = \boldsymbol{b} = \boldsymbol{0}$. Thus $\|\boldsymbol{z}\|_{\overline{h}} = 0$ implies $\boldsymbol{v} = \boldsymbol{0}$, $\boldsymbol{q} = \boldsymbol{0}$ and $\eta = 0$. The positive definiteness of $\|\cdot\|_h$ then follows from (3.9).

We consider a symmetric interior penalty discontinuous Galerkin formulation (see, for example, Arnold et al. [13] for a unified analysis of various discontinuous Galerkin schemes, and Brezzi et al. [30] where a general framework for the construction and the analysis of discontinuous Galerkin schemes is presented) and introduce the bilinear forms and functionals

$$\begin{aligned}
&\overline{a}_h((\boldsymbol{u}_h,\boldsymbol{\varepsilon}_h^p,\xi_h),(\boldsymbol{v}_h,\boldsymbol{q}_h,\eta_h)) \\
&\quad = \sum_K \int_K \Big(\mathcal{C}(\boldsymbol{\varepsilon}(\boldsymbol{u}_h) - \boldsymbol{\varepsilon}_h^p) : (\boldsymbol{\varepsilon}(\boldsymbol{v}_h) - \boldsymbol{q}_h) + k_1 \boldsymbol{\varepsilon}_h^p : \boldsymbol{q}_h + k_2 \xi_h \eta_h \Big)\, dX \\
&\qquad - \sum_e \int_e \Big(\{\!\{ \mathcal{C}(\boldsymbol{\varepsilon}(\boldsymbol{u}_h) - \boldsymbol{\varepsilon}_h^p) \}\!\} : [\![\boldsymbol{v}_h]\!] + \{\!\{ \mathcal{C}(\boldsymbol{\varepsilon}(\boldsymbol{v}_h) - \boldsymbol{q}_h) \}\!\} : [\![\boldsymbol{u}_h]\!] \Big)\, dS \\
&\qquad + \sum_e \frac{\beta_1}{h_e} \int_e [\![\boldsymbol{u}_h]\!] : [\![\boldsymbol{v}_h]\!]\, dS \,, \qquad (3.10) \\
&a_h((\boldsymbol{u}_h,\boldsymbol{\varepsilon}_h^p,\xi_h),(\boldsymbol{v}_h,\boldsymbol{q}_h,\eta_h)) \\
&\quad = \overline{a}_h((\boldsymbol{u}_h,\boldsymbol{\varepsilon}_h^p,\xi_h),(\boldsymbol{v}_h,\boldsymbol{q}_h,\eta_h)) + \sum_K \int_K k_3 \nabla \xi_h \cdot \nabla \eta_h\, dX \\
&\qquad - \sum_e \int_e k_3 \Big(\{\!\{ \nabla \xi_h \}\!\} \cdot [\![\eta_h]\!] + \{\!\{ \nabla \eta_h \}\!\} \cdot [\![\xi_h]\!] \Big)\, dS \\
&\qquad + \sum_e \frac{\beta_2}{h_e} \int_e [\![\xi_h]\!] \cdot [\![\eta_h]\!]\, dS \,, \qquad (3.11) \\
&j(\boldsymbol{v}_h,\boldsymbol{q}_h,\xi_h) = \begin{cases} \displaystyle\sum_K \int_K \kappa |\boldsymbol{q}_h|\, dX & \text{if } \boldsymbol{w}_h \in W_h \,, \\ +\infty & \text{otherwise,} \end{cases} \qquad (3.12)
\end{aligned}$$

where β_1 and β_2 are positive penalty parameters.

The semi-discrete discontinuous Galerkin approximations corresponding to the classical (2.22) and gradient (2.34) plasticity problems are then as follows:

given that $\boldsymbol{w}_h(0) = \boldsymbol{0}$, find $\boldsymbol{w}_h : [0,T] \to \overline{Z}_h$ such that for almost all $t \in (0,T)$,

$\dot{\boldsymbol{w}}_h(t) \in \overline{W}_h$ and

$$\overline{a}_h(\boldsymbol{w}_h(t), \boldsymbol{z}_h - \dot{\boldsymbol{w}}_h(t)) + j(\boldsymbol{z}_h) - j(\dot{\boldsymbol{w}}_h(t)) \geq \langle \ell(t), \boldsymbol{z}_h - \dot{\boldsymbol{w}}_h(t) \rangle \qquad \forall \boldsymbol{z}_h \in \overline{Z}_h \,, \tag{3.13}$$

and

given that $\boldsymbol{w}_h(0) = \boldsymbol{0}$, find $\boldsymbol{w}_h : [0, T] \to Z_h$ such that for almost all $t \in (0, T)$, $\dot{\boldsymbol{w}}_h(t) \in W_h$ and

$$a_h(\boldsymbol{w}_h(t), \boldsymbol{z}_h - \dot{\boldsymbol{w}}_h(t)) + j(\boldsymbol{z}_h) - j(\dot{\boldsymbol{w}}_h(t)) \geq \langle \ell(t), \boldsymbol{z}_h - \dot{\boldsymbol{w}}_h(t) \rangle \qquad \forall \boldsymbol{z}_h \in Z_h \,. \tag{3.14}$$

We now proceed to show the consistency of the classical and gradient plasticity problems. The discrete discontinuous Galerkin approximation of the classical and gradient plasticity problems, governed by the variational inequalities (2.22) and (2.34) respectively, are consistent if the exact solution to the boundary value problem solves the discrete problem.

Lemma 3.1 (Consistency). *Let $\overline{\boldsymbol{w}}$ and $\boldsymbol{w}$ be the solutions of (2.22) and (2.34) respectively. Then*

$$\begin{aligned} &\overline{a}_h(\overline{\boldsymbol{w}}(t), \boldsymbol{z} - \dot{\overline{\boldsymbol{w}}}(t)) + j(\boldsymbol{z}) - j(\dot{\overline{\boldsymbol{w}}}(t)) \geq \langle \ell(t), \boldsymbol{z} - \dot{\overline{\boldsymbol{w}}}(t) \rangle \,, \qquad \forall \boldsymbol{z} \in \overline{Z}_h \,, \\ &a_h(\boldsymbol{w}(t), \boldsymbol{z} - \dot{\boldsymbol{w}}(t)) + j(\boldsymbol{z}) - j(\dot{\boldsymbol{w}}(t)) \geq \langle \ell(t), \boldsymbol{z} - \dot{\boldsymbol{w}}(t) \rangle \,, \qquad \forall \boldsymbol{z} \in Z_h \,. \end{aligned} \tag{3.15}$$

Proof. We present the proof for gradient plasticity only; the proof for classical plasticity follows along similar lines. Let $\boldsymbol{z}_h = (\boldsymbol{v}_h, \boldsymbol{q}_h, \eta_h) \in Z_h$. From the regularity assumption (2.40) the equilibrium equation holds pointwise. Multiplying the equilibrium equation by $(\boldsymbol{v}_h - \dot{\boldsymbol{u}}(t))$, integrating by parts on $K \in \mathcal{T}_h$, summing over $K \in \mathcal{T}_h$, and using (3.3), we obtain

$$
\begin{aligned}
\mathbf{0} &= \operatorname{div}[\boldsymbol{\sigma}(t)] + \boldsymbol{B} \\
&= \int_\Omega \operatorname{div}[\boldsymbol{\sigma}(t)]\ dX + \int_\Omega \boldsymbol{B}\ dX\,, \qquad (3.16)\\
0 &= \sum_K \int_K \operatorname{div}[\boldsymbol{\sigma}(t)] \cdot (\boldsymbol{v}_h - \dot{\boldsymbol{u}}(t))\ dX + \sum_K \int_K \boldsymbol{B} \cdot (\boldsymbol{v}_h - \dot{\boldsymbol{u}}(t))\ dX \\
&= \sum_K \int_K \boldsymbol{\sigma}(t) : \boldsymbol{\varepsilon}(\boldsymbol{v}_h - \dot{\boldsymbol{u}}(t))\ dX - \sum_K \int_{\partial K} \boldsymbol{\sigma}(t)\boldsymbol{N} \cdot (\boldsymbol{v}_h - \dot{\boldsymbol{u}}(t))\ dS \\
&\qquad - \sum_K \int_K \boldsymbol{B} \cdot (\boldsymbol{v}_h - \dot{\boldsymbol{u}}(t))\ dX\,, \\
&\sum_K \int_K \boldsymbol{\sigma}(t) : \boldsymbol{\varepsilon}(\boldsymbol{v}_h(t) - \dot{\boldsymbol{u}}(t))\ dX - \sum_{e \in \mathcal{E}_h^0} \int_e [\![\boldsymbol{\sigma}(t)]\!] : \{\!\{\boldsymbol{v}_h(t) - \dot{\boldsymbol{u}}(t)\}\!\}\ dS \\
&- \sum_{e \in \mathcal{E}_h} \int_e \{\!\{\boldsymbol{\sigma}(t)\}\!\} : [\![\boldsymbol{v}_h(t) - \dot{\boldsymbol{u}}(t)]\!]\ dS = \sum_K \int_K \boldsymbol{B} \cdot (\boldsymbol{v}_h(t) - \dot{\boldsymbol{u}}(t))\ dX\ . \qquad (3.17)
\end{aligned}
$$

Similarly, from the dissipation inequality (2.29), we obtain

$$
\begin{aligned}
D(\boldsymbol{z}_h) - D(\dot{\boldsymbol{w}}(t)) &\geq (\boldsymbol{\sigma}(t) - k_1\boldsymbol{\epsilon}^p(t)) : (\boldsymbol{q}_h - \dot{\boldsymbol{\epsilon}}^p(t)) - k_2\xi(\eta_h - \dot{\xi}) \\
&\quad + \boldsymbol{m} \cdot \nabla(\eta_h - \dot{\xi})\,, \qquad (3.18)\\
\int_\Omega D(\boldsymbol{z}_h)\; dX - \int_\Omega D(\dot{\boldsymbol{w}}(t))\; dX &= \int_\Omega \boldsymbol{\sigma}(t) : (\boldsymbol{q}_h - \dot{\boldsymbol{\epsilon}}^p(t))\; dX \\
&\quad - k_1 \int_\Omega \boldsymbol{\epsilon}^p(t) : (\boldsymbol{q}_h - \dot{\boldsymbol{\epsilon}}^p(t))\; dX - k_2 \int_\Omega \xi(t)(\eta_h - \dot{\xi}(t))\; dX \\
&\quad + k_3 \int_\Omega \boldsymbol{m}(t) \cdot \nabla(\eta_h - \dot{\xi}(t))\; dX\,, \\
j(\boldsymbol{z}_h) - j(\dot{\boldsymbol{w}}(t)) \;&\geq\; \sum_K \int_K \boldsymbol{\sigma}(t) : (\boldsymbol{q}_h - \dot{\boldsymbol{\varepsilon}}^p(t))\; dX \\
&\quad - k_1 \sum_K \int_K \boldsymbol{\varepsilon}^p(t) : (\boldsymbol{q}_h - \dot{\boldsymbol{\varepsilon}}^p(t))\; dX - k_2 \sum_K \int_K \xi(t)(\eta_h - \dot{\xi}(t))\; dX \\
&\quad - k_3 \sum_K \int_K \nabla\xi(t) \cdot \nabla(\eta_h - \dot{\xi}(t))\; dX \\
&\quad + k_3 \sum_{e \in \mathcal{E}_h^0} \int_e \operatorname{tr}\big([\![\nabla\xi(t)]\!]\big) \cdot \{\!\{\eta_h - \dot{\xi}(t)\}\!\}\; dS \\
&\quad + k_3 \sum_{e \in \mathcal{E}_h} \int_e \{\!\{\nabla\xi(t)\}\!\} \cdot [\![\eta_h - \dot{\xi}(t)]\!]\; dS\,, \qquad (3.19)
\end{aligned}
$$

where for any $\boldsymbol{v} \in [L^2(\mathcal{E}_h)]^2$, we have that $\operatorname{tr}\big([\![\boldsymbol{v}]\!]\big) = \boldsymbol{v}_1 \cdot \boldsymbol{N}_1 + \boldsymbol{v}_2 \cdot \boldsymbol{N}_2$ is the trace of the matrix $[\![\boldsymbol{v}]\!]$ defined in (3.1).

From (3.17) and (3.19) and the definition of a_h we easily obtain $(3.15)_2$ provided that the jump terms involving $\boldsymbol{\sigma}$ and $\nabla\xi$ vanish. From (2.40) both of these quantities are in $H^1(\Omega)$, and hence in $H^1_{loc}(\Omega)$. We use a result due to Evans and Gariepy [77], Section 4.9.2, Theorem 2, according to which functions in $H^1_{loc}(\Omega)$ are continuous across interior edges in Ω. Thus the jump terms involving $\boldsymbol{\sigma}$ and $\nabla\xi$ vanish. This completes the proof. □

Lemma 3.2 (Well-posedness). *The problems (3.13) and (3.14) each have exactly one solution.*

Proof. It suffices to show that ℓ is continuous, j is convex, and lower semicontinuous and the bilinear forms $\overline{a}_h(\cdot,\cdot)$ and $a_h(\cdot,\cdot)$ are continuous and coercive with respect to the norms in (3.8) and (3.9). □

As in the previous lemma, we present the proof for the case of gradient plasticity. We first observe [11] that there exists a positive constant α, independent of the mesh size h, such that

$$\|\boldsymbol{v}_h\|_{L^2(\Omega)} \leq \alpha \left(\sum_K \|\boldsymbol{\varepsilon}(\boldsymbol{v}_h)\|_K^2 + \sum_e \frac{1}{h_e} \|[\![\boldsymbol{v}_h]\!]\|_e^2 \right)^{1/2} . \tag{3.20}$$

Hence

$$\begin{aligned} |\langle \ell, \boldsymbol{z}_h \rangle| &\leq \left(\sum_K \|\boldsymbol{B}\|_K^2 \right)^{1/2} \left(\sum_K \|\boldsymbol{v}_h\|_K^2 \right)^{1/2} \\ &\leq c \left(\sum_K \|\boldsymbol{B}\|_K^2 \right)^{1/2} \|\boldsymbol{z}_h\|_h \, . \end{aligned}$$

Next, we note that j is proper and convex, and is easily shown to be lower semi-continuous on Z_h, with respect to the norm $\|\cdot\|_h$. Now, we show that a_h is continuous with respect to the norm $\|\cdot\|_h$.
Take $\boldsymbol{w}_h = (\boldsymbol{u}_h, \boldsymbol{\varepsilon}_h^p, \xi_h) \in Z_h$ and $\boldsymbol{z}_h = (\boldsymbol{v}_h, \boldsymbol{q}_h, \eta_h) \in Z_h$. We first rewrite a_h as

$$\begin{aligned} &a_h(\boldsymbol{w}_h, \boldsymbol{z}_h) = \\ &\left. \begin{aligned} &\sum_K \int_K \Big(\mathcal{C}(\boldsymbol{\varepsilon}(\boldsymbol{u}_h) - \boldsymbol{\varepsilon}_h^p) : (\boldsymbol{\varepsilon}(\boldsymbol{v}_h) - \boldsymbol{q}_h) + k_1 \boldsymbol{\varepsilon}_h^p : \boldsymbol{q}_h \Big) \, dX \\ &+ \sum_K \int_K \Big(k_2 \xi_h \eta_h + k_3 \nabla \xi_h \cdot \nabla \eta_h \Big) \, dX \end{aligned} \right\} && (Q_1) \\ &- \sum_e \int_e \Big(\{\!\{ \mathcal{C}(\boldsymbol{\varepsilon}(\boldsymbol{u}_h) - \boldsymbol{\varepsilon}_h^p) \}\!\} : [\![\boldsymbol{v}_h]\!] + \{\!\{ \mathcal{C}(\boldsymbol{\varepsilon}(\boldsymbol{v}_h) - \boldsymbol{q}_h) \}\!\} : [\![\boldsymbol{u}_h]\!] \Big) \, dS && (Q_2) \\ &- \sum_e \int_e k_3 \big(\{\!\{ \nabla \xi_h \}\!\} \cdot [\![\eta_h]\!] + \{\!\{ \nabla \eta_h \}\!\} \cdot [\![\xi_h]\!] \big) \, dS && (Q_3) \\ &+ \sum_e \frac{\beta_2}{h_e} \int_e [\![\xi_h]\!] \cdot [\![\eta_h]\!] \, dS + \frac{\beta_1}{h_e} \int_e [\![\boldsymbol{u}_h]\!] : [\![\boldsymbol{v}_h]\!] \, dS \, . && (Q_4) \end{aligned} \tag{3.21}$$

We now need to estimate Q_1, Q_2, Q_3 and Q_4. In doing so, we will use the triangle and Minkowski inequalities.

First, using the norm of $\mathcal{C}$ and the triangle and Minkowski inequalities, we have

$$
\begin{aligned}
&|Q_1| \\
&= \Big|\sum_K \int_K \Big(\mathcal{C}(\boldsymbol{\varepsilon}(\boldsymbol{u}_h) - \boldsymbol{\varepsilon}_h^p) : (\boldsymbol{\varepsilon}(\boldsymbol{v}_h) - \boldsymbol{q}_h) + k_1 \boldsymbol{\varepsilon}_h^p : \boldsymbol{q}_h\Big)\, dX \\
&\quad + \sum_K \int_K \Big(k_2 \xi_h \eta_h + k_3 \nabla \xi_h \cdot \nabla \eta_h\Big)\, dX\Big| \\
&\leq \sum_K \int_K \left(|\mathcal{C}|_\infty |\,(\boldsymbol{\varepsilon}(\boldsymbol{u}_h) - \boldsymbol{\varepsilon}_h^p) : (\boldsymbol{\varepsilon}(\boldsymbol{v}_h) - \boldsymbol{q}_h)\,| + |k_1 \boldsymbol{\varepsilon}_h^p : \boldsymbol{q}_h|\right)\, dX \\
&\quad + \sum_K \int_K \left(|k_2 \xi_h \eta_h| + |k_3 \nabla \xi_h \cdot \nabla \eta_h|\right)\, dX \\
&\leq \sum_K \Big(|\mathcal{C}|_\infty \|\boldsymbol{\varepsilon}(\boldsymbol{u}_h) - \boldsymbol{\varepsilon}_h^p\|_K \|\boldsymbol{\varepsilon}(\boldsymbol{v}_h) - \boldsymbol{q}_h\| + (k_1 \|\boldsymbol{\varepsilon}_h^p\| \|\boldsymbol{q}_h\|_K) \\
&\quad + \max(k_2, k_3) \|\xi_h\|_{1,K} \|\eta_h\|_{1,K}\Big) \\
&\leq \sum_K \Big(|\mathcal{C}|_\infty \left(\|\boldsymbol{\varepsilon}(\boldsymbol{u}_h)\|_K + \|\boldsymbol{\varepsilon}_h^p\|_K\right) \left(\|\boldsymbol{\varepsilon}(\boldsymbol{v}_h)\|_K + \|\boldsymbol{q}_h\|_K\right) + (k_1 \|\boldsymbol{\varepsilon}_h^p\| \|\boldsymbol{q}_h\|_K) \\
&\quad + \max(k_2, k_3) \|\xi_h\|_{1,K} \|\eta_h\|_{1,K}\Big) \\
&\leq \max(|\mathcal{C}|_\infty, k_1, k_2, k_3) \sum_K \Big((\|\boldsymbol{\varepsilon}(\boldsymbol{u}_h)\|_K + \|\boldsymbol{\varepsilon}_h^p\|_K)(\|\boldsymbol{\varepsilon}(\boldsymbol{v}_h)\|_K + \|\boldsymbol{q}_h\|_K) \\
&\qquad + \|\boldsymbol{\varepsilon}_h^p\|_K \|\boldsymbol{q}_h\|_K + \|\xi_h\|_{1,K} \|\eta_h\|_{1,K}\Big) \\
&\leq \max(\Lambda + 2\mu, k_1, k_2, k_3) \|\boldsymbol{w}_h\|_h \; \|\boldsymbol{z}_h\|_h \,. \qquad (3.22)
\end{aligned}
$$

Next,

$$
\begin{aligned}
|Q_2| &= -\sum_e \int_e \left(\{\!\{\mathcal{C}(\boldsymbol{\varepsilon}(\boldsymbol{u}_h) - \boldsymbol{\varepsilon}_h^p)\}\!\} : [\![\boldsymbol{v}_h]\!] + \{\!\{\mathcal{C}(\boldsymbol{\varepsilon}(\boldsymbol{v}_h) - \boldsymbol{q}_h)\}\!\} : [\![\boldsymbol{u}_h]\!]\right)\, dS \\
&\leq \left(\sum_e h_e \|\{\!\{\mathcal{C}(\boldsymbol{\varepsilon}(\boldsymbol{u}_h) - \boldsymbol{\varepsilon}_h^p)\}\!\}\|_e^2\right)^{1/2} \left(\sum_e h_e^{-1} \|[\![\boldsymbol{v}_h]\!]\|_e^2\right)^{1/2} \\
&\quad + \left(\sum_e h_e \|\{\!\{\mathcal{C}(\boldsymbol{\varepsilon}(\boldsymbol{v}_h) - \boldsymbol{q}_h)\}\!\}\|_e^2\right)^{1/2} \left(\sum_e h_e^{-1} \|[\![\boldsymbol{u}_h]\!]\|_e^2\right)^{1/2} . \qquad (3.23)
\end{aligned}
$$

To bound the first term in (3.23), we use the triangle inequality on the averaging operator $\{\!\{\ \}\!\}$, and $(3.4)_1$. For $e \in \mathcal{E}_h^0$, take $e = \partial K_1 \cap \partial K_2$, and set $K_{12} = K_1 \cup K_2$. We have

$$h_e \|\{\!\{\mathcal{C}(\boldsymbol{\varepsilon}(\boldsymbol{u}_h) - \boldsymbol{\varepsilon}_h^p)\}\!\}\|_e^2 = h_e \left\| \mathcal{C}\left(\boldsymbol{\varepsilon}\left(\frac{\boldsymbol{u}_{1h} + \boldsymbol{u}_{2h}}{2}\right) - \left(\frac{\boldsymbol{\varepsilon}_{1h}^p + \boldsymbol{\varepsilon}_{2h}^p}{2}\right)\right)\right\|_e^2$$

$$\leq c_1 |\mathcal{C}|_\infty^2 (\|\boldsymbol{\varepsilon}(\boldsymbol{u}_h)\|_{K_{12}}^2 + \|\boldsymbol{\varepsilon}_h^p\|_{K_{12}}^2)\,.$$

Summing over all edges $e \in \mathcal{E}_h$, we have

$$\sum_e h_e \|\{\!\{\mathcal{C}(\boldsymbol{\varepsilon}(\boldsymbol{u}_h) - \boldsymbol{\varepsilon}_h^p)\}\!\}\|_e^2 \leq c_1 |\mathcal{C}|_\infty^2 \|\boldsymbol{w}_h\|_h^2\,.$$

Therefore,

$$|Q_2| \leq c_1^{1/2}(\Lambda + 2\mu)\|\boldsymbol{w}_h\|_h\, \|\boldsymbol{z}_h\|_h\,. \tag{3.24}$$

Similarly,

$$|Q_3| \leq c_1^{1/2}(\Lambda + 2\mu)\|\boldsymbol{w}_h\|_h\, \|\boldsymbol{z}_h\|_h\,. \tag{3.25}$$

We also have

$$\begin{aligned}
|Q_4| &= \left| \sum_e \frac{\beta_2}{h_e} \int_e [\![\xi_h]\!] \cdot [\![\eta_h]\!]\, dS + \frac{\beta_1}{h_e} \int_e [\![\boldsymbol{u}_h]\!] : [\![\boldsymbol{v}_h]\!]\, dS \right| \\
&\leq \beta_1 \left(\sum_e h_e^{-1} \|[\![\boldsymbol{u}_h]\!]\|_e^2 \right)^{1/2} \left(\sum_e h_e^{-1} \|[\![\boldsymbol{v}_h]\!]\|_e^2 \right)^{1/2} \\
&\quad + \beta_2 \left(\sum_e h_e^{-1} \|\xi_h\|_e^2 \right)^{1/2} \left(\sum_e h_e^{-1} \|\eta_h\|_e^2 \right)^{1/2} \\
&\leq (\beta_1 + \beta_2)\|\boldsymbol{w}_h\|_h\, \|\boldsymbol{z}_h\|_h.
\end{aligned} \tag{3.26}$$

Adding (3.22)–(3.26), we find a constant $c = c(k_1, k_2, k_3, \Lambda, \mu, \beta_1, \Omega) > 0$ such that

$$|a_h(\boldsymbol{w}_h, \boldsymbol{z}_h)| \leq c(k_1, k_2, k_3, \Lambda, \mu, \beta_1, \Omega)\|\boldsymbol{w}_h\|_h \, \|\boldsymbol{z}_h\|_h \qquad \forall \boldsymbol{w}_h,\ \boldsymbol{z}_h \in Z_h \, .$$

Thus a_h is continuous.

Concerning the coercivity of a_h we write, for every $\boldsymbol{w}_h = (\boldsymbol{u}_h, \boldsymbol{\varepsilon}_h^p, \xi_h)$ and $\boldsymbol{z}_h = (\boldsymbol{v}_h, \boldsymbol{q}_h, \eta_h) \in Z_h$,

$$a_h(\boldsymbol{w}_h, \boldsymbol{z}_h) = b(\boldsymbol{u}_h, \boldsymbol{v}_h) - c(\boldsymbol{\varepsilon}_h^p, \boldsymbol{v}_h) - c(\boldsymbol{q}_h, \boldsymbol{u}_h) + d((\boldsymbol{\varepsilon}_h^p, \xi_h), (\boldsymbol{q}_h, \eta_h)) \tag{3.27}$$

where

$$\begin{aligned} b(\boldsymbol{u}_h, \boldsymbol{v}_h) = & \sum_K \int_K \mathcal{C}\boldsymbol{\varepsilon}(\boldsymbol{u}_h) : \boldsymbol{\varepsilon}(\boldsymbol{v}_h) \, dX - \sum_e \int_e \{\!\{\mathcal{C}\boldsymbol{\varepsilon}(\boldsymbol{u}_h)\}\!\} : [\![\boldsymbol{v}_h]\!] \, dS \\ & - \sum_e \int_e \{\!\{\mathcal{C}\boldsymbol{\varepsilon}(\boldsymbol{v}_h)\}\!\} : [\![\boldsymbol{u}_h]\!] \, dS + \sum_e \frac{\beta_1}{h_e} \int_e [\![\boldsymbol{v}_h]\!] : [\![\boldsymbol{v}_h]\!] \, dS, \end{aligned} \tag{3.28}$$

$$c(\boldsymbol{\varepsilon}_h^p, \boldsymbol{v}_h) = \sum_K \int_K \mathcal{C}\boldsymbol{\varepsilon}_h^p : \boldsymbol{\varepsilon}(\boldsymbol{v}_h) \, dX - \sum_e \int_e \{\!\{\mathcal{C}\boldsymbol{\varepsilon}_h^p\}\!\} : [\![\boldsymbol{v}_h]\!] \, dS \, , \tag{3.29}$$

$$\begin{aligned} d((\boldsymbol{\varepsilon}_h^p, \xi_h), (\boldsymbol{q}_h, \eta_h)) = & \sum_K \int_K \left(\mathcal{C}\boldsymbol{\varepsilon}_h^p : \boldsymbol{q}_h + k_1 \boldsymbol{\varepsilon}_h^p : \boldsymbol{q}_h\right) dX \\ & - \sum_e \int_e k_3 \Big(\{\!\{\nabla \xi_h\}\!\} \cdot [\![\eta_h]\!] \, dS + \{\!\{\nabla \eta_h\}\!\} \cdot [\![\xi_h]\!] \Big) \, dS \\ & + \sum_e \frac{\beta_2}{h_e} \int_e [\![\xi_h]\!] \cdot [\![\eta_h]\!] \, dS \\ & + \sum_K \int_K \Big(k_2 \xi_h \eta_h + k_3 \nabla \xi_h \cdot \nabla \eta_h \Big) \, dX \, . \end{aligned} \tag{3.30}$$

The coercivity of a_h is obtained from the following lemma.

Lemma 3.3. *Let $c_1 > 0$ be the constant in (3.4)$_1$. For some positive constants η_1 and η_2 suitably chosen so that*

$$r_1 := \min \left(2\mu - \eta_1 |\mathcal{C}|_\infty^2, \beta_1 - \frac{1}{\eta_1} \right) > 0 \, , \tag{3.31}$$

$$r_2 := \min \left(2\mu + k_1, \beta_2 - \frac{k_3}{\eta_2}, \min \left(k_2 + \frac{k_3}{2c_3}, \frac{k_3}{2} - c_1 k_3 \eta_2 \right) \right) > 0 \, , \tag{3.32}$$

we have

$$\begin{aligned} &b(\boldsymbol{v}_h, \boldsymbol{v}_h) \geq r_1 \|\boldsymbol{v}_h\|_h^2 \ , \\ &d((\boldsymbol{q}_h, \eta_h), (\boldsymbol{q}_h, \eta_h)) \geq r_2 \|(\boldsymbol{q}_h, \eta_h)\|_h^2 \ , \\ &c(\boldsymbol{q}_h, \boldsymbol{v}_h) \leq (\Lambda + 2\mu)(1 + c_1^{1/2}) \|\boldsymbol{q}_h\|_0 \ \|\boldsymbol{v}_h\|_h \, , \end{aligned} \tag{3.33}$$

where

$$\|\boldsymbol{v}_h\|_h^2 = \sum_K \|\boldsymbol{\varepsilon}(\boldsymbol{v}_h)\|_K^2 + \sum_e h_e^{-1} \|[\![\boldsymbol{v}_h]\!]\|_e^2 \ , \tag{3.34}$$

$$\|(\boldsymbol{q}_h, \eta_h)\|_h^2 = \sum_K \|\boldsymbol{q}_h\|_K^2 + \|\eta_h\|_{1,K}^2 + \sum_e h_e^{-1} \|[\![\eta_h]\!]\|_e^2 \ . \tag{3.35}$$

Furthermore, we have the following inequality

$$\|\eta_h\|_K^2 \leq c_3 \|\nabla \eta_h\|_K^2 \, ,$$

where c_3 is a constant.

Proof. The coercivity of a_h is proven by considering the terms (3.28)–(3.30) individually.

We have

$$
\begin{aligned}
b(\boldsymbol{v}_h,\boldsymbol{v}_h) &= \sum_K \int_K \mathcal{C}\boldsymbol{\varepsilon}(\boldsymbol{v}_h) : \boldsymbol{\varepsilon}(\boldsymbol{v}_h)\; dX - 2\sum_e \int_e \{\!\{\mathcal{C}\boldsymbol{\varepsilon}(\boldsymbol{v}_h)\}\!\} : [\![\boldsymbol{v}_h]\!]\; dS \\
&\quad + \sum_e \frac{\beta_1}{h_e} \int_e [\![\boldsymbol{v}_h]\!] : [\![\boldsymbol{v}_h]\!]\; dS \\
&\geq 2\mu \sum_K \|\boldsymbol{\varepsilon}(\boldsymbol{v}_h)\|_K^2 + \beta_1 \sum_e h_e^{-1} \|[\![\boldsymbol{v}_h]\!]\|_e^2 - 2\sum_e \int_e \{\!\{\mathcal{C}\boldsymbol{\varepsilon}(\boldsymbol{v}_h)\}\!\} : [\![\boldsymbol{v}_h]\!]\; dS \\
&\geq 2\mu \sum_K \|\boldsymbol{\varepsilon}(\boldsymbol{v}_h)\|_K^2 + \beta_1 \sum_e h_e^{-1} \|[\![\boldsymbol{v}_h]\!]\|_e^2 \\
&\quad - 2\left[\sum_e \|\{\!\{\mathcal{C}\boldsymbol{\varepsilon}(\boldsymbol{v}_h)\}\!\}\|_e^2\right]^{1/2} \left[\sum_e \|[\![\boldsymbol{v}_h]\!]\|_e^2\right]^{1/2} \qquad \text{(using Hölder's inequality)} \\
&= 2\mu \sum_K \|\boldsymbol{\varepsilon}(\boldsymbol{v}_h)\|_K^2 + \beta_1 \sum_e h_e^{-1} \|[\![\boldsymbol{v}_h]\!]\|_e^2 \\
&\quad - 2\left[\sum_e h_e \|\{\!\{\mathcal{C}\boldsymbol{\varepsilon}(\boldsymbol{v}_h)\}\!\}\|_e^2\right]^{1/2} \left[\sum_e h_e^{-1} \|[\![\boldsymbol{v}_h]\!]\|_e^2\right]^{1/2} \\
&\geq 2\mu \sum_K \|\boldsymbol{\varepsilon}(\boldsymbol{v}_h)\|_K^2 + \beta_1 \sum_e h_e^{-1} \|[\![\boldsymbol{v}_h]\!]\|_e^2 \\
&\quad - \eta_1 \sum_e h_e \|\{\!\{\mathcal{C}\boldsymbol{\varepsilon}(\boldsymbol{v}_h)\}\!\}\|_e^2 - \frac{1}{\eta_1} \sum_e h_e^{-1} \|[\![\boldsymbol{v}_h]\!]\|_e^2 \quad \text{(using Young's inequality)} \\
&\geq 2\mu \sum_K \|\boldsymbol{\varepsilon}(\boldsymbol{v}_h)\|_K^2 - \eta_1 |\mathcal{C}|_\infty^2 \sum_K \|\boldsymbol{\varepsilon}(\boldsymbol{v}_h)\|_K^2 + \beta_1 \sum_e h_e^{-1} \|[\![\boldsymbol{v}_h]\!]\|_e^2 \\
&\quad - \frac{1}{\eta_1} \sum_e h_e^{-1} \|[\![\boldsymbol{v}_h]\!]\|_e^2 \qquad \text{(using (3.5))} \\
&\geq \left(2\mu - \eta_1 |\mathcal{C}|_\infty^2\right) \|\boldsymbol{\varepsilon}(\boldsymbol{v}_h)\|_K^2 + \left(\beta_1 - \frac{1}{\eta_1}\right) \sum_e h_e^{-1} \|[\![\boldsymbol{v}_h]\!]\|_e^2 \\
&\geq \min\left(2\mu - \eta_1 |\mathcal{C}|_\infty^2, \beta_1 - \frac{1}{\eta_1}\right) \|\boldsymbol{v}_h\|_h^2 \\
&= r_1 \|\boldsymbol{v}_h\|_h^2 \,.
\end{aligned}
$$

Thus $b(\boldsymbol{v}_h,\boldsymbol{v}_h)$ is coercive if η_1 and β_1 are chosen such that

$$
\eta_1\beta_1 > 1 \qquad \text{and} \qquad \frac{1}{\beta_1} < \eta_1 < \frac{2\mu}{c_1\left(\Lambda + 2\mu\right)^2} \,. \tag{3.36}
$$

Next, we consider the term

$$c(\boldsymbol{q}_h, \boldsymbol{v}_h) = \sum_K \int_K \mathcal{C}\boldsymbol{q}_h : \boldsymbol{\varepsilon}(\boldsymbol{v}_h)\ dX - \sum_e \int_e \{\!\{\mathcal{C}\boldsymbol{q}_h\}\!\} : [\![\boldsymbol{v}_h]\!]\ dS\,.$$

It follows that

$$\begin{aligned}
|c(\boldsymbol{q}_h, \boldsymbol{v}_h)| &= \left| \sum_K \int_K \mathcal{C}\boldsymbol{q}_h : \boldsymbol{\varepsilon}(\boldsymbol{v}_h)\ dX - \sum_e \int_e \{\!\{\mathcal{C}\boldsymbol{q}_h\}\!\} : [\![\boldsymbol{v}_h]\!]\ dS \right| \\
&\leq |\mathcal{C}|_\infty \sum_K \|\boldsymbol{q}_h\|_K^2 \|\boldsymbol{\varepsilon}(\boldsymbol{v}_h)\|_K^2 + \sum_e \|\{\!\{\mathcal{C}\boldsymbol{q}_h\}\!\}\|_e^2 \|[\![\boldsymbol{v}_h]\!]\|_e^2 \\
&\qquad \text{(using Cauchy–Schwarz inequality)} \\
&\leq |\mathcal{C}|_\infty \left(\sum_K \|\boldsymbol{q}_h\|_K^2 \right)^{1/2} \left(\sum_K \|\boldsymbol{\varepsilon}(\boldsymbol{v}_h)\|_K^2 \right)^{1/2} \\
&\quad + \left(\sum_e h_e \|\{\!\{\mathcal{C}\boldsymbol{q}_h\}\!\}\|_e^2 \right)^{1/2} \left(\sum_e h_e^{-1} \|[\![\boldsymbol{v}_h]\!]\|_e^2 \right)^{1/2} \qquad \text{(using Hölder's inequality)} \\
&\leq |\mathcal{C}|_\infty \left(\sum_K \|\boldsymbol{q}_h\|_K^2 \right)^{1/2} \left(\sum_K \|\boldsymbol{\varepsilon}(\boldsymbol{v}_h)\|_K^2 \right)^{1/2} \\
&\quad + c_1^{1/2} |\mathcal{C}|_\infty \left(\sum_K \|\boldsymbol{q}_h\|_K^2 \right)^{1/2} \left(\sum_e h_e^{-1} \|[\![\boldsymbol{v}_h]\!]\|_e^2 \right)^{1/2} \qquad \text{(using (3.5))} \\
&\leq (\Lambda + 2\mu) \left(1 + c_1^{1/2} \right) \|\boldsymbol{q}_h\|_0 \|\boldsymbol{v}_h\|_h\,.
\end{aligned}$$

Finally, we have

$$
\begin{aligned}
&d((\boldsymbol{q}_h,\eta_h),(\boldsymbol{q}_h,\eta_h))\\
&=\sum_K\int_K(\mathcal{C}\boldsymbol{q}_h:\boldsymbol{q}_h+k_1\boldsymbol{q}_h:\boldsymbol{q}_h)\,dX-2\sum_e\int_e k_3\{\!\{\nabla\eta_h\}\!\}\cdot[\![\eta_h]\!]\,dS\\
&\quad+\sum_e\frac{\beta_2}{h_e}\int_e[\![\eta_h]\!]\cdot[\![\eta_h]\!]\,dS+\sum_K\int_K(k_2\eta_h\eta_h+k_3\nabla\eta_h\cdot\nabla\eta_h)\,dX\\
&\geq(2\mu+k_1)\sum_K\|\boldsymbol{q}_h\|_K^2-2k_3\left(\sum_e h_e\|\{\!\{\nabla\eta_h\}\!\}\|_e^2\right)^{1/2}\left(\sum_e h_e^{-1}\|[\![\eta_h]\!]\|_e^2\right)^{1/2}\\
&\quad+\sum_e\frac{\beta_2}{h_e}\|[\![\eta_h]\!]\|_e^2+\sum_K\left(k_2\|\eta_h\|_K^2+k_3\|\nabla\eta_h\|_K^2\right)\qquad\text{(using Hölder's inequality)}\\
&\geq(2\mu+k_1)\sum_K\|\boldsymbol{q}_h\|_K^2-k_3\eta_2\sum_e h_e\|\{\!\{\nabla\eta_h\}\!\}\|_e^2-\frac{k_3}{\eta_2}\sum_e h_e^{-1}\|[\![\eta_h]\!]\|_e^2\\
&\quad+\sum_e\frac{\beta_2}{h_e}\|[\![\eta_h]\!]\|_e^2+\sum_K\left(k_2\|\eta_h\|_K^2+k_3\|\nabla\eta_h\|_K^2\right)\qquad\text{(using Young's inequality)}\\
&\geq(2\mu+k_1)\sum_K\|\boldsymbol{q}_h\|_K^2+\left(\beta_2-\frac{k_3}{\eta_2}\right)\sum_e h_e^{-1}\|\eta_h\|_e^2\\
&\quad+\left(k_2\sum_K\|\eta_h\|_K^2+(k_3-c_1k_3\eta_2)\sum_K\|\nabla\eta_h\|_K^2\right)\qquad\text{using (3.6)}\,.
\end{aligned}
\tag{3.37}
$$

In order to proceed, we need to bound the last term in (3.37) above. Unlike the continuous problem, we do not have a Poincaré–Friedrichs inequality between η_h and $\nabla\eta_h$. We therefore use an argument based on direct calculus to provide a bound of the form

$$\|\eta_h\|_K^2\leq c_3\|\nabla\eta_h\|_K^2\,.$$

Consider the homogeneous eigenvalue problem

$$-\nabla^2\eta=\lambda\eta\,,$$

where $\lambda\in\mathbb{R}$ is an eigenvalue. The discrete form of the preceeding problem can be expressed in weak form by

$$\int_K \nabla\eta_h \cdot \nabla\psi_h \; dX = \lambda^h \int_K \eta_h \psi_h \; dX \,, \tag{3.38}$$

where ψ_h is an admissible arbitrary test function. The matrix form of the weak problem is obtained from the above relation by interpolating the variables η_h and ψ_h from the nodal values using interpolation functions N_γ according to

$$\eta_h = \sum_{\mathrm{A}=1}^{n^{\mathrm{e}}_{\mathrm{node}}} N^{\mathrm{A}}_\gamma \eta_{\mathrm{A}} \qquad \text{and} \qquad \psi_h = \sum_{\mathrm{A}=1}^{n^{\mathrm{e}}_{\mathrm{node}}} N^{\mathrm{A}}_\gamma \psi_{\mathrm{A}} \,,$$

where $n^{\mathrm{e}}_{\mathrm{node}}$ is the number of nodes per element, and η_{A} and ψ_{A} are the values of η and ψ at node A respectively. Further details of this mapping will be provided in the overview of the finite element method presented in Section 4.3.1.

The gradient of η_h and ψ_h across K are constant and can be interpolated from the nodal values using the matrix $\boldsymbol{B}_\gamma$ which contains constant gradients of N_γ according to

$$\nabla\eta_h = \sum_{\mathrm{A}=1}^{n^{\mathrm{e}}_{\mathrm{node}}} \boldsymbol{B}^A_\gamma \eta_{\mathrm{A}} \qquad \text{and} \qquad \nabla\psi_h = \sum_{\mathrm{A}=1}^{n^{\mathrm{e}}_{\mathrm{node}}} \boldsymbol{B}^A_\gamma \psi_{\mathrm{A}} \,.$$

Substituting the preceding approximations into the weak form of the eigenvalue problem (3.38) we obtain the matrix problem given by

$$\int_K \sum_{\mathrm{A}=1}^{n^{\mathrm{e}}_{\mathrm{node}}} \sum_{\mathrm{B}=1}^{n^{\mathrm{e}}_{\mathrm{node}}} \left(\boldsymbol{B}^{\mathrm{A}}_\gamma \psi_{\mathrm{A}}\right)^T \left(\boldsymbol{B}^{\mathrm{B}}_\gamma \eta_{\mathrm{B}}\right) \; dX = \lambda^h \int_K \sum_{\mathrm{A}=1}^{n^{\mathrm{e}}_{\mathrm{node}}} \sum_{\mathrm{B}=1}^{n^{\mathrm{e}}_{\mathrm{node}}} N^{\mathrm{A}}_\gamma \psi_{\mathrm{A}} N^{\mathrm{B}}_\gamma \eta_{\mathrm{B}} \; dX$$

$$\underbrace{\int_K \boldsymbol{B}^T_\gamma \boldsymbol{B}_\gamma \; dX}_{\boldsymbol{\kappa}} \boldsymbol{\eta} = \lambda_h \underbrace{\int_K \boldsymbol{N}^T_\gamma \boldsymbol{N}_\gamma \; dX}_{\boldsymbol{m}} \boldsymbol{\eta} \,,$$

where $\boldsymbol{B}_\gamma$ and $\boldsymbol{N}_\gamma$ are matrices with entries containing the gradients of the interpolation functions and the interpolation functions respectively. The vector $\boldsymbol{\eta}$ contains the nodal values of η. The eigenvalues λ_h possess the property

$$\lambda^h_1 \leq \lambda^h_2 \leq \ldots \leq \lambda^h_{n^{\mathrm{e}}_{\mathrm{node}}} \,.$$

The L^2-norm of η_h and $\nabla\eta_h$ on element K can be expressed, using the notation introduced above, in matrix form as

$$\|\eta_h\|_K^2 = \boldsymbol{\eta}^T \boldsymbol{m}\boldsymbol{\eta} \qquad \text{and} \qquad \|\nabla\eta_h\|_K^2 = \boldsymbol{\eta}^T \boldsymbol{\kappa}\boldsymbol{\eta}\,.$$

The interpolation functions N_γ are most conveniently constructed on the reference element $\hat{K}$, where they are denoted $\widehat{N}_\gamma$, and then transformed to the actual element K, as depicted in Fig. 3.6. The L^2-norm of η_h and $\nabla\eta_h$ on element K can thus be expressed as

$$\|\eta_h\|_K^2 = \boldsymbol{\eta}^T \underbrace{\int_{\hat{K}} \widehat{\boldsymbol{N}}_\gamma^T \widehat{\boldsymbol{N}}_\gamma \, d\hat{X}}_{\widehat{\boldsymbol{m}}} \boldsymbol{\eta} \; \underbrace{\frac{\text{area}[K]}{\text{area}[\hat{K}]}}_{\alpha},$$

$$\|\nabla\eta_h\|_K^2 = \boldsymbol{\eta}^T \underbrace{\boldsymbol{B}_\gamma^T \boldsymbol{B}_\gamma}_{\hat{\boldsymbol{\kappa}}} \boldsymbol{\eta} \; \text{area}[K]\,.$$

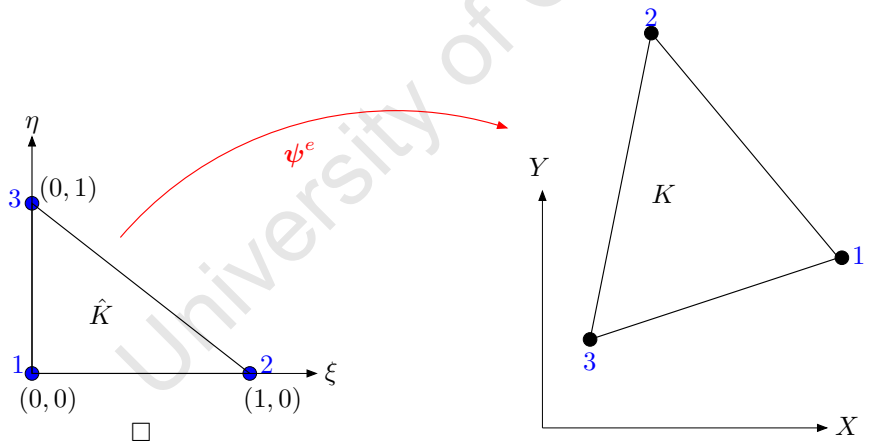

Fig. 3.6. Map between the reference element $\hat{K}$ and the element in the reference configuration K

From the positive definiteness of $\widehat{\boldsymbol{m}}$ we obtain

$$\begin{aligned} \boldsymbol{\eta}^T \boldsymbol{m}\boldsymbol{\eta} &= \boldsymbol{\eta}^T \hat{\boldsymbol{m}}\boldsymbol{\eta}\;\alpha \\ &\leq \lambda_{\max}^{\hat{m}} |\boldsymbol{\eta}|^2\;\alpha\,, \end{aligned} \tag{3.39}$$

where $\lambda_{\max}^{\hat{m}}$ is the maximum eigenvalue of $\hat{\boldsymbol{m}}$. In the same manner, using the positive definiteness of $\widehat{\boldsymbol{\kappa}}$ we get

$$\begin{aligned}\boldsymbol{\eta}^T\boldsymbol{\kappa}\boldsymbol{\eta} &= \boldsymbol{\eta}^T\widehat{\boldsymbol{\kappa}}\boldsymbol{\eta}\ \text{area}[K] \\ &\geq \lambda_{\min}^{\kappa}|\boldsymbol{\eta}|^2\ \text{area}[K]\,,\end{aligned} \tag{3.40}$$

where $\lambda_{\min}^{\hat{\kappa}}$ is the minimum eigenvalue of $\widehat{\boldsymbol{\kappa}}$.

Finally, using (3.39) and (3.40) we obtain the required bound for the L^2-norm of $\nabla\eta_h$ as follows:

$$\begin{aligned}\|\nabla\eta_h\|_K^2 &= \boldsymbol{\eta}^T\boldsymbol{\kappa}\boldsymbol{\eta}\ \text{area}[K] \\ &\geq \lambda_{\min}^{\hat{\kappa}}|\boldsymbol{\eta}|^2\ \text{area}[K] \\ &\geq \frac{\lambda_{\min}^{\hat{\kappa}}\|\eta_h\|_K^2\ \text{area}[K]}{\lambda_{\max}^{\hat{m}}\alpha} \\ &= \frac{\text{area}[\hat{K}]\ \lambda_{\min}^{\hat{\kappa}}}{\lambda_{\max}^{\hat{m}}}\|\eta_h\|_K^2 \\ &= \tfrac{1}{c_3}\|\eta_h\|_K^2\,.\end{aligned} \tag{3.41}$$

Returning to (3.37) and using (3.41) we obtain

$$
\begin{aligned}
&d((\boldsymbol{q}_h,\eta_h),(\boldsymbol{q}_h,\eta_h))\\
&\quad\geq (2\mu+k_1)\sum_K \|\boldsymbol{q}_h\|_K^2+\left(\beta_2-\frac{k_3}{\eta_2}\right)\sum_e h_e^{-1}\|\eta_h\|_e^2\\
&\qquad+\left(k_2\sum_K\|\eta_h\|_K^2+(k_3-c_1k_3\eta_2)\sum_K\|\nabla\eta_h\|_K^2\right)\\
&\quad=(2\mu+k_1)\sum_K \|\boldsymbol{q}_h\|_K^2+\left(\beta_2-\frac{k_3}{\eta_2}\right)\sum_e h_e^{-1}\|\eta_h\|_e^2\\
&\qquad+\left(k_2\sum_K\|\eta_h\|_K^2+\frac{k_3}{2}\sum_K\|\nabla\eta_h\|_K^2\right)+\left(\frac{k_3}{2}-c_1k_3\eta_2\right)\sum_K\|\nabla\eta_h\|_K^2\\
&\quad\geq (2\mu+k_1)\sum_K \|\boldsymbol{q}_h\|_K^2+\left(\beta_2-\frac{k_3}{\eta_2}\right)\sum_e h_e^{-1}\|\eta_h\|_e^2\\
&\qquad+\left(k_2+\frac{k_3}{2c_3}\right)\sum_K\|\eta_h\|_K^2+\left(\frac{k_3}{2}-c_1k_3\eta_2\right)\sum_K\|\nabla\eta_h\|_K^2\quad\text{(using (3.41))}\\
&\quad\geq (2\mu+k_1)\sum_K \|\boldsymbol{q}_h\|_K^2+\left(\beta_2-\frac{k_3}{\eta_2}\right)\sum_e h_e^{-1}\|\eta_h\|_e^2\\
&\qquad+\min\left(k_2+\frac{k_3}{2c_3},\frac{k_3}{2}-c_1k_3\eta_2\right)\sum_K\|\eta_h\|_{1,K}^2\\
&\quad\geq \min\left(2\mu+k_1,\beta_2-\frac{k_3}{\eta_2},\min\left(k_2+\frac{k_3}{2c_3},\frac{k_3}{2}-c_1k_3\eta_2\right)\right)\|(\boldsymbol{q}_h,\eta_h)\|_h^2\\
&\quad=r_2\|(\boldsymbol{q}_h,\eta_h)\|_h^2\,,
\end{aligned}
$$

provided that we choose η_2 and β_2 such that

$$
\frac{k_3}{\beta_2}>\eta_2>\frac{1}{2c_1}\,. \tag{3.42}
$$

Furthermore, we need to choose the gradient hardening constant k_3 such that

$$
k_3>-2k_2c_3\,. \tag{3.43}
$$

Now with η_1, η_2, β_1 and β_2 as in (3.36) and (3.42) we obtain for every $\boldsymbol{z}_h=(\boldsymbol{v}_h,\boldsymbol{q}_h,\eta_h)\in Z_h$

$$
\begin{aligned}
&a_h(\boldsymbol{z}_h,\boldsymbol{z}_h) \\
&\quad = b(\boldsymbol{v}_h,\boldsymbol{v}_h) - 2c(\boldsymbol{q}_h,\boldsymbol{v}_h) + d((\boldsymbol{q}_h,\eta_h),(\boldsymbol{q}_h,\eta_h)) \\
&\quad = r_1\|\boldsymbol{v}_h\|_h^2 - 2(\Lambda+2\mu)(1+c_1^{1/2})\|\boldsymbol{q}_h\|_0^2\|\boldsymbol{v}_h\|_h^2 + r_2(\|\boldsymbol{q}_h\|_0^2 + \|\eta_h\|_h^2) \\
&\quad \geq r_1\|\boldsymbol{v}_h\|_h^2 - (\Lambda+2\mu)(1+c_1^{1/2})\eta_3\|\boldsymbol{q}_h\|_0^2 - \frac{(\Lambda+2\mu)(1+c_1^{1/2})}{\eta_3}\|\boldsymbol{v}_h\|_h^2 \\
&\qquad + r_2(\|\boldsymbol{q}_h\|_0^2 + \|\eta_h\|_h^2) \qquad \text{(using Young's inequality)} \\
&\quad = \Big[r_1 - \frac{(\Lambda+2\mu)(1+c_1^{1/2})}{\eta_3}\Big]\|\boldsymbol{v}_h\|_h^2 + r_2\|\eta_h\|_h^2 \\
&\qquad + \Big[r_2 - (\Lambda+2\mu)(1+c_1^{1/2})\eta_3\Big]\|\boldsymbol{q}_h\|_0^2 \,.
\end{aligned}
$$

Thus by taking η_3 such that

$$
\frac{(\Lambda+2\mu)(1+c_1^{1/2})}{r_1} < \eta_3 < \frac{r_2}{(\Lambda+2\mu)(1+c_1^{1/2})}, \tag{3.44}
$$

we find for some constant $c = c(k_1,k_2,k_3,\mu,\Lambda,\beta_1,\beta_2,\Omega) > 0$ that

$$
a_h(\boldsymbol{z}_h,\boldsymbol{z}_h) \;\geq\; c\|\boldsymbol{z}_h\|_h^2 \;.
$$

□

Remark 3.4. The choice of the positive constants η_1, η_2 and η_3 is subject to the constraint that both the kinematic and isotropic hardening constants are sufficiently large. From (3.32) it follows that k_1 satisfy

$$
k_1 > -2\mu \,.
$$

The formulation is thus able to accommodate a certain amount of kinematic softening, that is, $k_1 < 0$. Furthermore, due to the regularising effect of the gradient plasticity model, the formulation is able to accommodate a certain amount of isotropic softening ($k_2 < 0$) subject to the constraint that (see (3.32))

$$
k_3 > -2k_2c_3 \,.
$$

Therefore, the coercivity of the bilinear form a_h is obtained under the same conditions as the constraints on the constants η_1, η_2 and η_3.

The inability of classical models of plasticity with isotropic hardening only to accommodate softening is clearly seen if we omit all terms related to gradient hardening in (3.37). Coercivity of the bilinear form a_h is thus only achieved in this case for $k_2 > 0$.

Remark 3.5. The proof concerning the coercivity of the bilinear form a_h presented in Djoko et al. [67] is not able to account for softening.

3.2 Continuous-in-time a priori error estimate

In this section an a priori error estimate for the continuous-in-time problem is derived. We first collect some useful results.

For a scalar-valued function $\eta \in H^2(\Omega)$ let $\Pi_K : H^2(\Omega) \to P_1(K)$ denote the usual interpolation operator [51], which satisfies the error estimate

$$\|\eta - \Pi_K \eta\|_{H^1(K)} \leq c h_K |\eta|_{H^2(K)} \,. \tag{3.45}$$

The estimate is extended in a straightforward way to be valid for vector- and matrix-valued functions.

For $\boldsymbol{q} \in [H^1(\Omega)]^{2\times 2}$ let Π_K be the local L^2-orthogonal projection operator onto $P_0(K)$ (in fact on each element $K \in \mathcal{T}_h$, and $\boldsymbol{q} \in Q$, $\Pi_K \boldsymbol{q}$ is the average value of $\boldsymbol{q}$ on K). We then have

$$\|\Pi_K \boldsymbol{q} - \boldsymbol{q}\|_{L^2(K)} \leq c h_K |\boldsymbol{q}|_{H^1(K)} \,. \tag{3.46}$$

Next, we have the following interpolation result.

Lemma 3.6. *Let $\boldsymbol{w}(t) \in Z$. Then there exists $\boldsymbol{w}_I(t) \in Z_h$ with $\dot{\boldsymbol{w}}_I(t) \in Z_h$ and*

$$\begin{aligned} &\|\boldsymbol{w}_I(t) - \boldsymbol{w}(t)\|_h \leq ch \,, \\ &\|\dot{\boldsymbol{w}}_I(t) - \dot{\boldsymbol{w}}(t)\|_h \leq ch \,. \end{aligned} \tag{3.47}$$

Remark 3.7. We note that, for $\boldsymbol{w}_I(t) \in Z_h$, $\dot{\boldsymbol{w}}_I(t) \in Z_h$ from the definition of the time derivative and the fact that Z_h is a closed subspace.

Proof. The proof is constructed in two steps: first, we construct $\boldsymbol{w}_I(t)$, and secondly we derive the error estimates (3.47).

For $\boldsymbol{w}(t) = (\boldsymbol{u}(t), \boldsymbol{\varepsilon}^p(t), \xi(t)) \in Z$ we define $\boldsymbol{w}_I(t) \in Z_h$ by

$$a_h(\boldsymbol{w}_I(t) - \boldsymbol{w}(t), \boldsymbol{z}_h) = 0 \ , \quad \boldsymbol{z}_h \in Z_h \, . \tag{3.48}$$

Since the bilinear form $a_h(\cdot, \cdot)$ is continuous and coercive on Z_h, $\boldsymbol{w}_I(t)$ is well defined.

Let $\Pi \boldsymbol{w}(t) \in Z_h$ be defined by

$$\Pi \boldsymbol{w}(t)|_K = (\Pi_K \boldsymbol{u}(t), \Pi_K \boldsymbol{\varepsilon}^p(t), \Pi_K \xi(t)) \, ;$$

setting $\boldsymbol{z}_h = \boldsymbol{w}_I(t) - \Pi \boldsymbol{w}(t)$ in (3.48) we obtain

$$c \| \boldsymbol{w}_I(t) - \rho_h \boldsymbol{w}(t) \|_{h1}^2 \leq a_h(\boldsymbol{w}_I(t) - \rho_h \boldsymbol{w}(t), \boldsymbol{w}_I(t) - \rho_h \boldsymbol{w}(t)) = R \tag{3.49}$$

with

$$R := a_h(\boldsymbol{w}(t) - \rho_h \boldsymbol{w}(t), \boldsymbol{w}_I(t) - \rho_h \boldsymbol{w}(t)) = Q_5 + Q_6 + Q_7 + Q_8 \, ,$$

where

$$
\begin{aligned}
Q_5 = \sum_K \int_K \Big\{ & \mathcal{C}[\boldsymbol{\varepsilon}(\boldsymbol{u}(t) - \boldsymbol{\Pi}_K \boldsymbol{u}(t)) - (\boldsymbol{\varepsilon}^p(t) - \boldsymbol{\Pi}_K \boldsymbol{\varepsilon}^p(t))] \\
& : [\boldsymbol{\varepsilon}(\boldsymbol{u}_I(t) - \boldsymbol{\Pi}_K \boldsymbol{u}(t)) - (\boldsymbol{\varepsilon}_I^p(t) - \boldsymbol{\Pi}_K \boldsymbol{\varepsilon}^p(t))] \\
& + k_1(\boldsymbol{\varepsilon}^p(t) - \boldsymbol{\Pi}_K \boldsymbol{\varepsilon}^p(t)) : (\boldsymbol{\varepsilon}_I^p(t) - \boldsymbol{\Pi}_K \boldsymbol{\varepsilon}^p(t)) \\
& + k_3 \nabla(\xi(t) - \Pi_K \xi(t)) \cdot \nabla(\xi_I(t) - \Pi_K \xi(t)) \Big\} \, dX \ , \\
Q_6 = & - \sum_e \int_e \mathcal{C}[\boldsymbol{\varepsilon}(\boldsymbol{u}(t) - \boldsymbol{\Pi}_K \boldsymbol{u}(t)) - (\boldsymbol{\varepsilon}^p(t) - \boldsymbol{\Pi}_K \boldsymbol{\varepsilon}^p(t))] : [\![\boldsymbol{u}_I(t) - \boldsymbol{\Pi}_K \boldsymbol{u}(t)]\!] \, dS \\
& - \sum_e \int_e k_3 \{\nabla(\xi(t) - \Pi_K \xi(t))\} \cdot [\![\xi_I(t) - \Pi_K \xi(t)]\!] \, dS \ , \\
Q_7 = & - \sum_e \int_e \mathcal{C}[\boldsymbol{\varepsilon}(\boldsymbol{u}_I(t) - \boldsymbol{\Pi}_K \boldsymbol{u}(t)) - (\boldsymbol{\varepsilon}_I^p(t) - \boldsymbol{\Pi}_K \boldsymbol{\varepsilon}^p(t)))] : [\![\boldsymbol{u}(t) - \boldsymbol{\Pi}_K \boldsymbol{u}(t)]\!] \, dS \\
& - \sum_e \int_e k_3 \left\{\nabla(\xi_I(t) - \Pi_K \xi(t))\right\} \cdot [\![\xi(t) - \Pi_K \xi(t)]\!] \, dS \ , \\
Q_8 = & \sum_e \int_e \frac{\beta_1}{h_e} [\![\boldsymbol{u}(t) - \boldsymbol{\Pi}_K \boldsymbol{u}(t)]\!] : [\![\boldsymbol{u}_I(t) - \boldsymbol{\Pi}_K \boldsymbol{u}(t)]\!] \, dS \\
& + \sum_e \int_e \frac{\beta_2}{h_e} [\![\xi(t) - \Pi_K \xi(t)]\!] \cdot [\![\xi_I(t) - \Pi_K \xi(t)]\!] \, dS \ .
\end{aligned}
$$

We now estimate Q_5–Q_8 using the Cauchy–Schwarz, Minkowski, and Young inequalities, (3.45) and (3.46).

First, Q_6 is treated thanks to $(3.4)_2$, to obtain

$$
\begin{aligned}
&|Q_6| \\
&\le \left(\sum_e h_e \|\{\mathcal{C}(\boldsymbol{\varepsilon}(\boldsymbol{u}(t)-\boldsymbol{\Pi}_K\boldsymbol{u}(t))-(\boldsymbol{\varepsilon}^p(t)-\boldsymbol{\Pi}_K\boldsymbol{\varepsilon}^p(t))\}\|_e^2\right)^{1/2} \\
&\quad\times\left(\sum_e h_e^{-1}\|[\![\boldsymbol{u}_I(t)-\boldsymbol{\Pi}_K\boldsymbol{u}(t)]\!]\|_e^2\right)^{1/2} \\
&\quad+k_3\left(\sum_e h_e\|\{\nabla(\xi(t)-\Pi_K\xi(t))\}\|_e^2\right)^{1/2}\left(\sum_e h_e^{-1}\|[\![\xi_I(t)-\Pi_K\xi(t)]\!]\|_e^2\right)^{1/2} \\
&\le \frac{1}{2\varepsilon}\sum_e h_e\|\{\mathcal{C}(\boldsymbol{\varepsilon}(\boldsymbol{u}(t)-\boldsymbol{\Pi}_K\boldsymbol{u}(t))-(\boldsymbol{\varepsilon}^p(t)-\boldsymbol{\Pi}_K\boldsymbol{\varepsilon}^p(t)))\}\|_e^2 \\
&\quad+k_3h_K^2\|\nabla^2(\xi(t)-\Pi_K\xi(t))\|_K^2+\varepsilon\|\boldsymbol{w}_I(t)-\boldsymbol{\Pi}\boldsymbol{w}(t)\|_h^2 \\
&\le c\sum_K\left(h_K^2+h_K^2\|\operatorname{div}(\boldsymbol{\sigma}(t)-\mathcal{C}(\boldsymbol{\varepsilon}(\boldsymbol{\Pi}_K\boldsymbol{u}(t))-\boldsymbol{\Pi}_K\boldsymbol{\varepsilon}^p(t)))\|_K^2\right) \\
&\quad+k_3\sum_K h_K^2\|\nabla^2(\xi(t)-\Pi_K\xi(t))\|_K^2+\varepsilon\|\boldsymbol{w}_I(t)-\boldsymbol{\Pi}\boldsymbol{w}(t)\|_h^2 \\
&\le ch^2+\varepsilon\|\boldsymbol{w}_I(t)-\boldsymbol{\Pi}\boldsymbol{w}(t)\|_h^2\,.
\end{aligned}
\tag{3.50}
$$

Next,

$$
\begin{aligned}
|Q_5| &\le c\Big(\sum_K|\boldsymbol{u}(t)-\boldsymbol{\Pi}_K\boldsymbol{u}(t)|_{1,K}^2+\|\boldsymbol{\varepsilon}^p(t)-\boldsymbol{\Pi}_K\boldsymbol{\varepsilon}^p(t)\|_K^2+\|\xi(t)-\Pi_K\xi(t)\|_{1,K}^2\Big)^{1/2} \\
&\quad\times\Big(\sum_K\|\boldsymbol{\varepsilon}(\boldsymbol{u}_I(t)-\boldsymbol{\Pi}_K\boldsymbol{u}(t))\|_K^2+\|\boldsymbol{\varepsilon}_I^p(t)-\boldsymbol{\Pi}_K\boldsymbol{\varepsilon}^p(t)\|_K^2 \\
&\qquad+\|\xi_I(t)-\Pi_K\xi(t)\|_{1,K}^2\Big)^{1/2} \\
&\le ch^2+\frac{\varepsilon}{2}\|\boldsymbol{w}_I(t)-\boldsymbol{\Pi}\boldsymbol{w}(t)\|_h^2\,.
\end{aligned}
\tag{3.51}
$$

The term Q_7 is treated by using $(3.4)_1$, to get

$$
\begin{aligned}
&|Q_7| \\
&\quad \leq c \left(\sum_K \|\mathcal{C}(\boldsymbol{\varepsilon}(\boldsymbol{u}_I(t) - \boldsymbol{\Pi}_K \boldsymbol{u}(t)) - (\boldsymbol{\varepsilon}^p_I(t) - \boldsymbol{\Pi}_K \boldsymbol{\varepsilon}^p(t)))\|^2_K \right)^{1/2} \\
&\qquad \times \left(\sum_K \|\nabla(\boldsymbol{u}(t) - \boldsymbol{\Pi}_K \boldsymbol{u}(t))\|^2_K \right)^{1/2} \\
&\qquad + c k_3 \left(\sum_e \|\nabla(\xi_I(t) - \Pi_K \xi(t))\|^2_e \right)^{1/2} \left(\sum_K \|\nabla(\xi(t) - \Pi_K \xi(t))\|^2_K \right)^{1/2} \\
&\quad \leq c h^2 + \varepsilon \|\boldsymbol{w}_I(t) - \boldsymbol{\Pi} \boldsymbol{w}(t)\|^2_h \,. \qquad (3.52)
\end{aligned}
$$

Finally,

$$
\begin{aligned}
|Q_8| &\leq \frac{\beta_1^2 + \beta_2^2}{2\varepsilon} \sum_e h_e^{-1} \|[\![\boldsymbol{u}(t) - \boldsymbol{\Pi}_K \boldsymbol{u}(t)]\!]\|^2_e + h_e^{-1} \|[\![\xi(t) - \Pi_K \xi(t)]\!]\|^2_e \\
&\quad + \varepsilon \|\boldsymbol{w}_I(t) - \boldsymbol{\Pi} \boldsymbol{w}(t)\|^2_h \\
&\leq c(\beta_1^2 + \beta_2^2) \|\nabla(\boldsymbol{u}(t) - \boldsymbol{\Pi}_K \boldsymbol{u}(t))\|^2_0 + \|\nabla(\xi(t) - \Pi_K \xi(t))\|^2_0 \\
&\quad + \varepsilon \|\boldsymbol{w}_I(t) - \boldsymbol{\Pi} \boldsymbol{w}(t)\|^2_h \\
&\leq c h^2 + \varepsilon \|\boldsymbol{w}_I(t) - \boldsymbol{\Pi} \boldsymbol{w}(t)\|^2_h \,. \qquad (3.53)
\end{aligned}
$$

Replacing (3.52)–(3.53) in (3.49) and taking ε sufficiently small, we obtain

$$
\|\boldsymbol{w}_I(t) - \boldsymbol{\Pi} \boldsymbol{w}(t)\|_h \leq c h. \qquad (3.54)
$$

The first of (3.47) is obtained using the triangle inequality, (3.54), and the interpolation estimate

$$
\|\boldsymbol{\Pi} \boldsymbol{w}(t) - \boldsymbol{w}(t)\|_h \leq c h \,.
$$

The second estimate is obtained by first differentiating (3.48) with respect to time to get

$$
a_h(\dot{\boldsymbol{w}}_I(t) - \dot{\boldsymbol{w}}(t), \boldsymbol{z}_h) = 0 \,, \qquad (3.55)
$$

and by repeating the analysis. □

With these preliminary results in place, we then have the following.

Theorem 3.8. *Let $\boldsymbol{w}_I(t) \in Z_h$ defined by (3.48), and let $\boldsymbol{w}_h(t)$ be the solution of (3.14). Assume that $\boldsymbol{B}(t) \in H^1(\Omega)^2$, and that $\boldsymbol{w} = (\boldsymbol{u}, \boldsymbol{\varepsilon}^p, \xi)$ is the solution of (2.34). Then there exists a positive constant c, independent of h, such that*

$$\begin{aligned}\|\boldsymbol{w} - \boldsymbol{w}_h\|_{L^\infty(0,T;Z_h+Z)} &\le \|\boldsymbol{w} - \boldsymbol{w}_I\|_{L^\infty(0,T;Z_h+Z)} \\ &+ c\|\dot{\boldsymbol{w}}_I - \dot{\boldsymbol{w}}\|_{L^2(0,T;Z_h+Z)} + c\left(\inf_{\boldsymbol{z}_h \in L^2(0,T;Z_h)} \|\boldsymbol{z}_h - \dot{\boldsymbol{w}}\|^{1/2}_{L^2(0,T;Z_h+Z)}\right. \\ &\left. + \inf_{\boldsymbol{v}_h \in L^2(0,T;V_h)} \|\boldsymbol{v}_h - \dot{\boldsymbol{u}}\|^{1/2}_{L^2(0,T;V_h+V)} + \inf_{\boldsymbol{q}_h \in L^2(0,T;Q_h)} \|\boldsymbol{q}_h - \dot{\boldsymbol{\varepsilon}}^p\|^{1/2}_{L^2(0,T;Q)}\right) . \end{aligned} \tag{3.56}$$

Proof. Taking $\boldsymbol{z}_h = \dot{\boldsymbol{w}}_h(t)$ in (3.15_2), and adding (3.14), we get for all $\boldsymbol{z}_h \in Z_h$,

$$\begin{aligned}-a_h(\boldsymbol{w}_h(t), \boldsymbol{z}_h - \dot{\boldsymbol{w}}_h(t)) \le& a_h(\boldsymbol{w}(t), \dot{\boldsymbol{w}}_h(t) - \dot{\boldsymbol{w}}(t)) + j(\boldsymbol{z}_h) - j(\dot{\boldsymbol{w}}(t)) \\ &- \langle \ell(t), \boldsymbol{z}_h - \dot{\boldsymbol{w}}(t)\rangle . \end{aligned} \tag{3.57}$$

Now a_h is continuous and coercive on Z_h, so that $\|\boldsymbol{z}_h\|^2_{a_h} = a_h(\boldsymbol{z}_h, \boldsymbol{z}_h)$ is a norm on Z_h, equivalent to $\|\boldsymbol{z}_h\|_h$. Using (3.57) and (3.48) we obtain, for $\boldsymbol{z}_h \in Z_h$,

$$\begin{aligned}&\frac{1}{2}\frac{d}{dt}\|\boldsymbol{w}_I(t) - \boldsymbol{w}_h(t)\|^2_{a_h} \\ &\quad = a_h(\boldsymbol{w}_I(t) - \boldsymbol{w}_h(t), \dot{\boldsymbol{w}}_I(t) - \boldsymbol{z}_h) + a_h(\boldsymbol{w}_I(t), \boldsymbol{z}_h - \dot{\boldsymbol{w}}_h(t)) \\ &\qquad - a_h(\boldsymbol{w}_h(t), \boldsymbol{z}_h - \dot{\boldsymbol{w}}_h(t)) \\ &\quad \le a_h(\boldsymbol{w}_I(t) - \boldsymbol{w}_h(t), \dot{\boldsymbol{w}}_I(t) - \dot{\boldsymbol{w}}(t)) + a_h(\boldsymbol{w}_I(t) - \boldsymbol{w}_h(t), \dot{\boldsymbol{w}}(t) - \boldsymbol{z}_h) \\ &\qquad + a_h(\boldsymbol{w}(t), \boldsymbol{z}_h - \dot{\boldsymbol{w}}(t)) + j(\boldsymbol{z}_h) - j(\dot{\boldsymbol{w}}(t)) - \langle \ell(t), \boldsymbol{z}_h - \dot{\boldsymbol{w}}(t)\rangle . \end{aligned} \tag{3.58}$$

We now have to estimate each term on the right-hand side of (3.58).

Using Lemma 3.6 we have

$$\begin{aligned}a_h(\boldsymbol{w}_I(t) - \boldsymbol{w}_h(t), \dot{\boldsymbol{w}}_I(t) - \dot{\boldsymbol{w}}(t)) &\le c\left(\|\boldsymbol{w}_I(t) - \boldsymbol{w}_h(t)\|^2_{a_h} + \|\dot{\boldsymbol{w}}_I(t) - \dot{\boldsymbol{w}}(t)\|^2_h\right) , \\ a_h(\boldsymbol{w}_I(t) - \boldsymbol{w}_h(t), \dot{\boldsymbol{w}}(t) - \boldsymbol{z}_h) &\le c\left(\|\boldsymbol{w}_I(t) - \boldsymbol{w}_h(t)\|^2_{a_h} + c\|\dot{\boldsymbol{w}}(t) - \boldsymbol{z}_h\|^2_h\right) . \end{aligned}$$

(3.59)

This leaves the terms in (3.58) involving j and ℓ. Bearing in mind the definition (2.24) of j in Section 2.2.1 we have, for any $\hat{\boldsymbol{z}}_h = (\boldsymbol{v}_h, \boldsymbol{q}_h, |\boldsymbol{q}_h|) \in W_h$,

$$\begin{aligned} j(\hat{\boldsymbol{z}}_h) - j(\dot{\boldsymbol{w}}(t)) - \langle \ell(t), \hat{\boldsymbol{z}}_h - \dot{\boldsymbol{w}}(t) \rangle \\ \leq \sum_K \int_K |\boldsymbol{q}_h(t) - \dot{\boldsymbol{\varepsilon}}^p(t)| + \boldsymbol{B}(t) \cdot (\boldsymbol{v}_h(t) - \dot{\boldsymbol{u}}(t)) \, dX \\ \leq c\|\boldsymbol{q}_h(t) - \dot{\boldsymbol{\varepsilon}}^p(t)\|_0 + c\|\boldsymbol{v}_h(t) - \dot{\boldsymbol{u}}(t)\|_0 \,. \end{aligned} \tag{3.60}$$

Combining (3.58)–(3.60), we obtain, for $\boldsymbol{z}_h = (\boldsymbol{v}_h, \boldsymbol{q}_h, \eta_h) \in Z_h$,

$$\begin{aligned} \frac{d}{dt}\|\boldsymbol{w}_I(t) - \boldsymbol{w}_h(t)\|_{a_h}^2 \leq c \left(\|\boldsymbol{w}_I(t) - \boldsymbol{w}_h(t)\|_{a_h}^2 + c\|\dot{\boldsymbol{w}}_I(t) - \dot{\boldsymbol{w}}(t)\|_h^2 \right. \\ \left. + \|\boldsymbol{z}_h - \dot{\boldsymbol{w}}(t)\|_h + \|\boldsymbol{q}_h - \dot{\boldsymbol{\varepsilon}}^p(t)\|_0 + \|\boldsymbol{v}_h - \dot{\boldsymbol{u}}(t)\|_0 \right) \,. \end{aligned} \tag{3.61}$$

In order to proceed we use Gronwall's Lemma and the Sobolev Embedding Theorem. Applying Gronwall's Lemma with $\boldsymbol{w}_h(\boldsymbol{0}) = \boldsymbol{0}$, the Sobolev embedding result, and the equivalence between $\|\cdot\|_{a_h}$ and $\|\cdot\|_h$, we obtain

$$\begin{aligned} \|\boldsymbol{w}_I(t) - \boldsymbol{w}_h(t)\|_h \leq c \left(\|\dot{\boldsymbol{w}}_I - \dot{\boldsymbol{w}}\|_{L^2(0,T;Z_h+Z)} + \|\boldsymbol{z}_h - \dot{\boldsymbol{w}}\|_{L^2(0,T;Z_h+Z)}^{1/2} \right. \\ \left. + \|\boldsymbol{q}_h - \dot{\boldsymbol{\varepsilon}}^p(t)\|_{L^2(0,T;Q)} + \|\boldsymbol{v}_h - \dot{\boldsymbol{u}}(t)\|_{L^2(0,T;V_h+V)} \right) \,. \end{aligned} \tag{3.62}$$

The theorem follows after application of the triangle inequality. □

Remark 3.9. Choosing $\boldsymbol{z}_h$ such that $\boldsymbol{z}_h|_K = \Pi_K \dot{\boldsymbol{w}}_I(t)$, we obtain

$$\|\boldsymbol{w} - \boldsymbol{w}_h\|_{L^\infty(0,T;Z_h+Z)} \leq ch^{1/2} \,.$$

This is the same rate of convergence as that obtained for classical plasticity using the conventional Galerkin method in Han and Reddy [94]. It should be mentioned that Carstensen [34] has demonstrated linear convergence under the assumptions that $u \in H^2(\Omega)$ and that the data is piecewise constant on an element.

3.3 Fully-discrete discontinuous Galerkin approximations

In this section we discretise the variational inequality governing the discontinuous Galerkin gradient plasticity problem (2.34) in time using the backward Euler scheme. We denote the function ψ evaluated at time $t_{\rm n}$ by $\psi^{\rm n}$. We first discretise the time interval $[0,T]$ into N subintervals with node points $t_{\rm n} = nk$, $0 \leq n \leq N$, where $k = t_{\rm n} - t_{\rm n-1} = T/N$ is the step-size. We set $\delta \boldsymbol{w}^{\rm n} = \Delta \boldsymbol{w}^{\rm n}/k$ where $\Delta \boldsymbol{w}^{\rm n} = \boldsymbol{w}^{\rm n} - \boldsymbol{w}^{\rm n-1}$.

Further details concerning the technique used in the proof of the main result of this section can be found in Han and Reddy [94].

Consider the following fully-discrete discontinuous Galerkin approximation of Problem (2.34):

given $\ell \in H^1(0,T;Z')$, and $\boldsymbol{w}_h^0 = \boldsymbol{0}$, find a sequence $(\boldsymbol{w}_h^{\rm n})_{\rm n=1}^N$ in W_h, with $\delta w_h^n \in W_h$ satisfying

$$a_h(\boldsymbol{w}_h^{\rm n}, \boldsymbol{z}_h - \delta \boldsymbol{w}_h^{\rm n}) + j(\boldsymbol{z}_h) - j(\delta \boldsymbol{w}_h^{\rm n}) \geq \langle \ell^n, \boldsymbol{z}_h - \delta \boldsymbol{w}_h^{\rm n} \rangle \ , \qquad \forall \boldsymbol{z}_h \in Z_h \, . \tag{3.63}$$

The existence of a unique solution to Problem (3.63) follows from the arguments presented in Lemma 3.2.

We have the following stability result, which follows directly from [94, Lemma 7.2].

Lemma 3.10. *The solution $(\boldsymbol{w}_h^{\rm n})_{\rm n=1}^N$ is stable in the sense there exist positive constants c_1, c_2 independent of k, such that*

$$\sum_{\rm n=1}^{N} \|\delta \boldsymbol{w}_h^{\rm n}\|_h^2 k \leq c_1 \|\dot{\ell}\|^2_{L^2(0,T;Z')} \quad \textit{and} \quad \max_{1 \leq {\rm n} \leq N} \|\boldsymbol{w}_h^n\|_h \leq c_2 \|\dot{\ell}\|_{L^1(0,T;Z')} \, . \tag{3.64}$$

The following result concerning the time derivative of the interpolant $\boldsymbol{w}_I(t)$ of $\boldsymbol{w}(t)$ will be used in the upcoming proof of Theorem 3.12.

Lemma 3.11. *If $\ddot{\boldsymbol{w}} \in L^1(0,T;Z)$, and $\dot{\boldsymbol{w}}_I(t)$ is the interpolant of $\dot{\boldsymbol{w}}(t)$, then there exists a positive constant c, independent of h and k, such that*

$$\left|\left| \frac{\boldsymbol{w}_I(t_{m+1}) - \boldsymbol{w}_I(t_m)}{k} - \dot{\boldsymbol{w}}_I(t_m) \right|\right|_h \leq c \|\ddot{\boldsymbol{w}}\|_{L^1(t_m, t_{m+1}; Z + Z_h)} \, . \tag{3.65}$$

The proof is obtained by using (3.48) to show that $\ddot{\boldsymbol{w}}_I \in L^1(0,T;Z_h)$, followed by a Taylor expansion of $\boldsymbol{w}_I$ about t_m with integral remainder [see 94, Lemma 11.4].

Next we state the main result regarding the accuracy of the solution $\boldsymbol{w}_h^{\mathrm{n}}$ of problem (3.63).

Theorem 3.12. *Let $(\boldsymbol{w}_h^{\mathrm{n}})_{\mathrm{n}=1}^N$ be a sequence of solutions of (3.63). If $\boldsymbol{B}(t) \in L^2(\Omega)^2$ and the solution $\boldsymbol{w} = (\boldsymbol{u}, \boldsymbol{\varepsilon}^p, \xi)$ of (2.34) satisfies $\ddot{\boldsymbol{w}} \in L^1(0,T;Z)$, then there exists a positive constant c, independent of the mesh size h and k, such that*

$$\max_{1\le \mathrm{n}\le N} \|\boldsymbol{w}^{\mathrm{n}} - \boldsymbol{w}_h^n\|_h \le ck + c\left[k\sum_{i=1}^{N} \inf_{\boldsymbol{z}_h\in Z_h} \|\dot{\boldsymbol{w}}^i - \boldsymbol{z}_h\|_h\right]^{1/2}. \tag{3.66}$$

Proof. We follow closely the proof of Theorem 11.7 in [94]. Let $\boldsymbol{e}^{\mathrm{n}} = \boldsymbol{w}^{\mathrm{n}} - \boldsymbol{w}_h^{\mathrm{n}} = \boldsymbol{\eta}^{\mathrm{n}} + \boldsymbol{e}_h^{\mathrm{n}}$, for $1 \le \mathrm{n} \le N$ where $\boldsymbol{\eta}^{\mathrm{n}} = \boldsymbol{w}^{\mathrm{n}} - \boldsymbol{w}_I^{\mathrm{n}}$, $\boldsymbol{e}_h^{\mathrm{n}} = \boldsymbol{w}_I^{\mathrm{n}} - \boldsymbol{w}_h^{\mathrm{n}}$, and $\boldsymbol{w}_I^{\mathrm{n}} = \boldsymbol{w}_I(t_{\mathrm{n}})$. Set

$$A_{\mathrm{n}} = a_h(\boldsymbol{e}_h^{\mathrm{n}}, \delta\boldsymbol{e}_h^{\mathrm{n}}) = \frac{1}{k}a_h(\boldsymbol{e}_h^{\mathrm{n}}, \boldsymbol{e}_h^{\mathrm{n}}) - \frac{1}{k}a_h(\boldsymbol{e}_h^{\mathrm{n}}, \boldsymbol{e}_h^{\mathrm{n}-1}).$$

Using the Cauchy–Schwarz and Young's inequalities we obtain

$$A_{\mathrm{n}} \ge \frac{1}{2k}(\|\boldsymbol{e}_h^{\mathrm{n}}\|_{a_h}^2 - \|\boldsymbol{e}_h^{\mathrm{n}-1}\|_{a_h}^2). \tag{3.67}$$

Next, we have to find an upper bound for A_{n}. From the linearity of $a_h(\cdot,\cdot)$,

$$A_{\mathrm{n}} = a_h(\boldsymbol{w}_I^{\mathrm{n}}, \delta\boldsymbol{w}_I^{\mathrm{n}} - \delta\boldsymbol{w}_h^{\mathrm{n}}) - a_h(\boldsymbol{w}_h^{\mathrm{n}}, \delta\boldsymbol{w}_I^{\mathrm{n}} - \boldsymbol{z}_h) - a_h(\boldsymbol{w}_h^{\mathrm{n}}, \boldsymbol{z}_h - \delta\boldsymbol{w}_h^{\mathrm{n}}). \tag{3.68}$$

Now combining (3.63), and $(3.15)_2$ with $t = t_{\mathrm{n}}$ and $\boldsymbol{z}_h = \delta\boldsymbol{w}_h^{\mathrm{n}}$, we obtain

$$-a_h(\boldsymbol{w}_h^{\mathrm{n}}, \boldsymbol{z}_h - \delta\boldsymbol{w}_h^{\mathrm{n}}) \le j(\boldsymbol{z}_h) - j(\dot{\boldsymbol{w}}^n) - \langle \ell^n, \boldsymbol{z}_h - \dot{\boldsymbol{w}}^n\rangle + a_h(\boldsymbol{w}^{\mathrm{n}}, \delta\boldsymbol{w}_h^{\mathrm{n}} - \dot{\boldsymbol{w}}^{\mathrm{n}}). \tag{3.69}$$

Combining (3.69), (3.68), (3.48), and using $\delta\boldsymbol{e}_h^{\mathrm{n}} = \delta\boldsymbol{w}_I^{\mathrm{n}} - \delta\boldsymbol{w}_h^{\mathrm{n}} = (\boldsymbol{e}_h^{\mathrm{n}} - \boldsymbol{e}_h^{\mathrm{n}-1})/k$, we get

$$
\begin{aligned}
A_{\mathrm{n}} &\le a_h(\boldsymbol{w}_I^n - \boldsymbol{w}^{\mathrm{n}}, \delta\boldsymbol{w}_I^{\mathrm{n}} - \delta\boldsymbol{w}_h^{\mathrm{n}}) + a_h(\boldsymbol{w}^{\mathrm{n}}, \delta\boldsymbol{w}_I^{\mathrm{n}} - \delta\boldsymbol{w}_h^{\mathrm{n}}) \\
&\quad - a_h(\boldsymbol{w}_h^{\mathrm{n}}, \delta\boldsymbol{w}_I^{\mathrm{n}} - \boldsymbol{z}_h) + a_h(\boldsymbol{w}^{\mathrm{n}}, \delta\boldsymbol{w}_h^{\mathrm{n}} - \dot{\boldsymbol{w}}^{\mathrm{n}}) + j(\boldsymbol{z}_h) - j(\dot{\boldsymbol{w}}^{\mathrm{n}}) - \langle \ell^{\mathrm{n}}, \boldsymbol{z}_h - \dot{\boldsymbol{w}}^{\mathrm{n}} \rangle \\
&\le a_h(\boldsymbol{w}^{\mathrm{n}}, \delta\boldsymbol{w}_I^{\mathrm{n}} - \delta\boldsymbol{w}_h^{\mathrm{n}}) - a_h(\boldsymbol{w}_h^{\mathrm{n}}, \delta\boldsymbol{w}_I^{\mathrm{n}} - \boldsymbol{z}_h) \\
&\quad + a_h(\boldsymbol{w}^{\mathrm{n}}, \delta\boldsymbol{w}_h^{\mathrm{n}} - \dot{\boldsymbol{w}}^{\mathrm{n}}) + j(\boldsymbol{z}_h) - j(\dot{\boldsymbol{w}}^{\mathrm{n}}) - \langle \ell^{\mathrm{n}}, \boldsymbol{z}_h - \dot{\boldsymbol{w}}^{\mathrm{n}} \rangle \\
&\le \underbrace{a_h(\boldsymbol{e}_h^{\mathrm{n}}, \delta\boldsymbol{w}_I^{\mathrm{n}} - \boldsymbol{z}_h) + a_h(\boldsymbol{w}^{\mathrm{n}}, \boldsymbol{z}_h - \dot{\boldsymbol{w}}^{\mathrm{n}})}_{Q_9} + \underbrace{j(\boldsymbol{z}_h) - j(\dot{\boldsymbol{w}}^{\mathrm{n}}) - \langle \ell^{\mathrm{n}}, \boldsymbol{z}_h - \dot{\boldsymbol{w}}^{\mathrm{n}} \rangle}_{Q_{10}} \,.
\end{aligned}
\tag{3.70}
$$

From (3.67) and (3.70) we obtain, choosing $\boldsymbol{z}_h = (\boldsymbol{v}_h, \boldsymbol{q}_h, \eta_h) \in Z_h$ in the term Q_9 and $\boldsymbol{z}_h = \hat{\boldsymbol{z}}_h := (\boldsymbol{v}_h, \boldsymbol{q}_h, |\boldsymbol{q}_h|)$ in Q_{10},

$$
\begin{aligned}
&\frac{1}{2k}\left(\|\boldsymbol{e}_h^{\mathrm{n}}\|_{a_h}^2 - \|\boldsymbol{e}_h^{\mathrm{n}-1}\|_{a_h}^2\right) \\
&\quad \le Q_9 + Q_{10} \\
&\quad \le c\big(\|\boldsymbol{e}_h^{\mathrm{n}}\|_{a_h}\ \|\delta\boldsymbol{w}_I^{\mathrm{n}} - \boldsymbol{z}_h\|_{a_h} + \|\boldsymbol{w}^{\mathrm{n}}\|_{a_h}\|\boldsymbol{z}_h^{\mathrm{n}} - \dot{\boldsymbol{w}}^{\mathrm{n}}\|_{a_h} \\
&\qquad + \|\boldsymbol{q}_h - \dot{\boldsymbol{\varepsilon}^p}^{\mathrm{n}}\|_0 + \|\boldsymbol{v}_h - \dot{\boldsymbol{u}}^{\mathrm{n}}\|_0\big)\,.
\end{aligned}
\tag{3.71}
$$

Now replacing n with i, summing over i with $1 \le i \le n$ and with $\boldsymbol{e}_h^0 = \boldsymbol{0}$, we obtain

$$
\begin{aligned}
\|\boldsymbol{e}_h^{\mathrm{n}}\|_{a_h}^2 &\le ckM \sum_{i=1}^{\mathrm{n}} \|\delta\boldsymbol{w}_I^i - \boldsymbol{z}_h\|_{a_h} \\
&\quad + ck \sum_{i=1}^{\mathrm{n}} \Big(\|\boldsymbol{z}_h - \dot{\boldsymbol{w}}^i\|_{a_h} + \|\boldsymbol{q}_h^i - \dot{\boldsymbol{\varepsilon}^p}^i\|_0 + \|\boldsymbol{v}_h^i - \dot{\boldsymbol{u}}^i\|_0 \Big)\,,
\end{aligned}
$$

where $M = \max_i \|\boldsymbol{e}_h^i\|_{a_h}$ and we have also used the property $\max_{\mathrm{n}} \|\boldsymbol{w}^{\mathrm{n}}\|_Z \le c\|\dot{\ell}\|_{Z'}$, which follows from [94, Lemma 7.2]. Finally,

$$
M^2 \le ckM \sum_{i=1}^{N} \|\delta\boldsymbol{w}_I^i - \boldsymbol{z}_h\|_{a_h} + ck \sum_{i=1}^{N} \|\boldsymbol{z}_h - \dot{\boldsymbol{w}}^i\|_{a_h}\,. \tag{3.72}
$$

Noting that a, b, $x \ge 0$ and $x^2 \le ax + b$ imply that $x \le a + \sqrt{2b}$, we obtain

$$M \leq ck \sum_{i=1}^{N} \|\delta \boldsymbol{w}_I^i - \boldsymbol{z}_h\|_{a_h} + ck^{1/2} \left(\sum_{i=1}^{N} \|\boldsymbol{z}_h - \dot{\boldsymbol{w}}^i\|_{a_h} \right)^{1/2} . \tag{3.73}$$

The result follows by choosing $\boldsymbol{z}_h = \dot{\boldsymbol{w}}_I(t)$ in (3.73) and using Lemma 3.11. □

Remark 3.13. Again, as with the case of the semi-discrete approximations, by using the interpolation error estimates (3.45) and (3.46) and the regularity of the solution, it is seen that the order of spatial convergence is the same as that obtained for the classical problem with the conventional Galerkin method.

Remark 3.14. It is possible, using the approach in [94, Theorem 11.6], to obtain $O(k^2)$ convergence with the use of a Crank–Nicolson, as opposed to a backward Euler, approximation in time.

4

Algorithms for a discontinuous Galerkin formulation of classical and gradient plasticity at infinitesimal strains

Solution algorithms for problems in elastoplasticity are frequently of the two-step, predictor–corrector (Newton–Raphson) type. The properties of these algorithms based on the primal formulation of plasticity were first investigated by Martin and coworkers [26, 122]. They demonstrated that the solution algorithms used for the classical dual problem (see Simo and Hughes [166] for an overview) could be recovered by adopting particular quadratic approximations for the dissipation function D. A general presentation of this approach, together with convergence analyses, is presented in Han and Reddy [94].

The bilinear forms that arise in standard finite element approximations of elastoplastic problems are symmetric with the consequence that the variational inequalities corresponding to the incremental problem in time are equivalent to certain minimisation problems. The approach taken in the aforementioned works [26, 122, 94] is to analyse the convergence and accuracy of the approximate solution by producing a minimising sequence. The objective here, however, is to establish convergence of the algorithms without exploiting the symmetry of the bilinear form so as to allow for discontinuous Galerkin formulations which are not symmetric.

The present chapter begins with an overview of the predictor–corrector solution procedure using two simple example problems. The examples introduce many of the key features of the solution algorithm that are present in the considerably more complex problem of elastoplasticity. The concepts of stability and accuracy (that is, the rate of convergence) of the solution algorithm for various choices of predictors are also presented.

The equivalence of the primal and dual formulations of the flow law is demonstrated in the second example problem. It is important to emphasise this equivalence as we have chosen to use the primal form for the analysis of the discontinuous Galerkin problem, but will make use of both the dual and primal approaches when developing the solution algorithm.

We then proceed to the convergence analysis of an abstract problem whose general structure allows results for particular predictors to be deduced as special cases. Furthermore, an error estimate for the convergence rate of the discrete problem is obtained without assuming that the bilinear form is symmetric.

The convergence analysis and subsequent algorithm applies to the problem of gradient plasticity with linear isotropic hardening and a discontinuous Galerkin approximation of the hardening parameter field only. Kinematic hardening and a discontinuous Galerkin approximation of the displacement field were considered in the analysis of the gradient plasticity model presented in Chapter 3. The kinematic hardening effects are as for classical plasticity and their treatment is standard; they are thus excluded. A discontinuous Galerkin approximation of the displacement field provides an elegant method to circumvent locking related problems due to the assumption of incompressible plastic deformation as demonstrated by, for example, Wihler [190] in the context of linear elasticity and ten Eyck and Lew [180] for the nonlinear theory. The emphasis of the work presented here is on the model of gradient plasticity and thus, while a discontinuous Galerkin approximation of the displacement field is clearly attractive, it does not directly influence the plasticity model and is thus not considered henceforth.

The chapter concludes with a detailed account of the predictor–corrector solution algorithm for the model of gradient plasticity considered here within the framework of the finite element method. Relevant aspects of the finite element method are briefly introduced. Thereafter, features of the algorithm unique to the gradient problem, such as the treatment of the moving elastoplastic boundary and the identification of the plastic subdomain, are given. Finally, the form of the consistent tangent modulus for the gradient plasticity formulation is derived. The algorithm is used in Chapter 5 to solve a variety of example problems.

4.1 Overview of predictor–corrector solution schemes

The nonlinear system of equations governing the elastoplasticity problem, be it for the classical or the gradient case, is solved using a predictor–corrector (Newton–Raphson) strategy. The objective of this section is to introduce the predictor–corrector approach and associated terminology using two simple example problems. The first example is that of a nonlinear spring, while the second example concerns classical perfect plasticity.

The focus of the nonlinear spring example is on the predictor step, with a particular emphasis placed on the effect that the choice of the predictor has on both the stability and efficiency of the algorithm. The equivalence of the primal and dual formulations of the plastic flow law is demonstrated in the second example problem. This equivalence will be exploited later in the chapter when discussing the algorithm for the model of gradient plasticity.

In both examples we consider a partition of the time domain $[0, T]$ into N intervals of duration $\Delta t = T/N$. The complete state of the system is assumed known at the beginning of the current time step t_{n} from the equilibrium state at the end of the previous time step at time $t_{\mathrm{n}-1}$.

The predictor–corrector scheme is an iterative process for all but the most simple constitutive relations. The current iterate is denoted i and the following notation adopted to distinguish between quantities updated in a total manner from the converged initial conditions at the beginning of the time step, and those updated from the previous iteration:

$$\Delta(\cdot) := (\cdot)^{\mathrm{i}}_{\mathrm{n}} - (\cdot)^{0}_{\mathrm{n}} = (\cdot)^{\mathrm{i}}_{\mathrm{n}} - (\cdot)_{\mathrm{n}-1} \quad \text{and} \quad \delta(\cdot) := (\cdot)^{\mathrm{i}}_{\mathrm{n}} - (\cdot)^{\mathrm{i}-1}_{\mathrm{n}} \ .$$

We distinguish indices unrelated to the number of space dimensions from those related to the number of space dimensions by using upright font for the former. The objective of the predictor–corrector scheme is to determine the equilibrium state at the end of the current time step taking into account the increment in loading.

4.1.1 A nonlinear spring

Consider a nonlinear spring where the stiffness of the spring, denoted E, is constant up to a displacement d of d_y, after which E is a function of the current displacement as depicted in Fig. 4.1. The stiffness of the spring in the linear and nonlinear regimes in denoted E^e and E^{ep} respectively. An external force of magnitude F acts upon the spring. A simple balance of internal and external forces yields the equation

$$Ed = F$$

for the displacement of the spring.

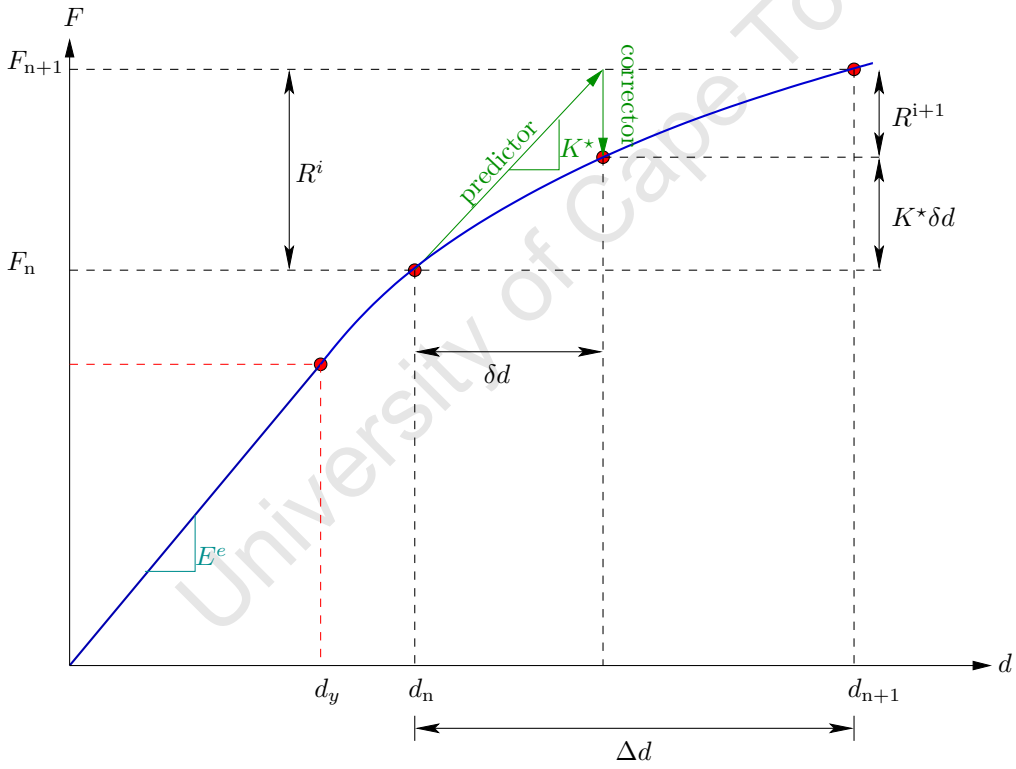

Fig. 4.1. Schematic of the predictor–corrector solution strategy for the example of a nonlinear spring

The residual expression to be satisfied is given by

$$R := F - Ed = 0\,,$$

where R is the residual. Applying a Taylor series expansion of the residual function in the neighbourhood of the iterate $i-1$ we obtain

$$R^{\mathrm{i}} \approx R^{\mathrm{i}-1} + \frac{\mathrm{d}R^{i-1}}{\mathrm{d}d}\delta d + \frac{1}{2}\frac{\mathrm{d}^2 R^{i-1}}{\mathrm{d}d^2}\delta d^2 + \ \cdots .$$

Ignoring higher-order terms and noticing that F is not, here, a function of the displacement, the expansion above implies that

$$\begin{aligned}\delta d &= -\left[\underbrace{\frac{-\mathrm{d}E^{\mathrm{i}-1}}{\mathrm{d}d}}_{K}\right]^{-1} R^{\mathrm{i}-1} \\ &= K^{-1}R^{\mathrm{i}-1}\,,\end{aligned} \tag{4.1}$$

where K is the tangent.

Under certain circumstances an exact expression for the tangent K is either not known or its calculation is prohibitively computationally expensive. An approximation, or a numerical evaluation, of the tangent, denoted $K^\star$, could, in this case, be used instead.

The *predictor* step entails solving the system (4.1) for δd. The choice of the predictor, that is the choice of the approximation $K^\star$, determines the stability and efficiency of the solution scheme. Two common choices of predictors, namely the elastic and consistent tangent, are depicted in Figs 4.2 and 4.3.

For the choice of the elastic predictor, the tangent is set to the elastic stiffness for each iteration. Convergence of the algorithm using an elastic predictor is guaranteed but the rate of convergence can be prohibitively slow for more complex problems. The consistent tangent formulation uses an elastic predictor for the first increment of the iterative process. The terminology "consistent tangent" is not truly appropriate in this example as the corrector step is trivial and consistency of the predictor is not an issue. This slight abuse of terminology is intended to emphasise various features of the solution algorithms in elastoplasticity. For the second and subsequent iterations, the tangent direction to the force versus displacement relationship is used as the tangent.

The rate of convergence of the scheme using the consistent tangent predictor is far higher than that obtained when using the elastic predictor as shown in Fig. 4.3(a). Convergence is not, however, guaranteed as depicted in Fig. 4.3(b). Guaranteed convergence can be recovered by incorporating a line-search algorithm [32], for example, into the predictor step. This is a standard technique in root finding and the numerical solution of nonlinear sets of equations (see, for example, [149]).

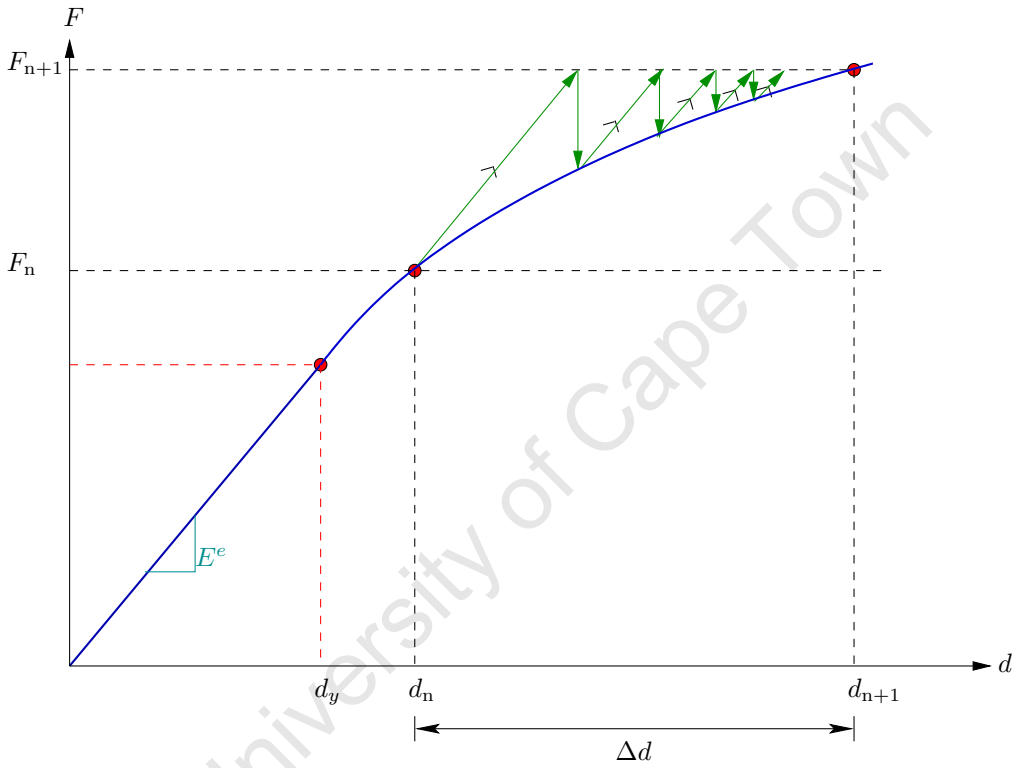

Fig. 4.2. Schematic of the elastic predictor for the example of a nonlinear spring

The *corrector step* involves constructing the updated residual, a trivial matter for the current example.

4.1.2 Classical perfect plasticity

In order to gain further insight into the primal formulation of plasticity, the relation of this to the more widely adopted dual formulation, and the predictor–corrector

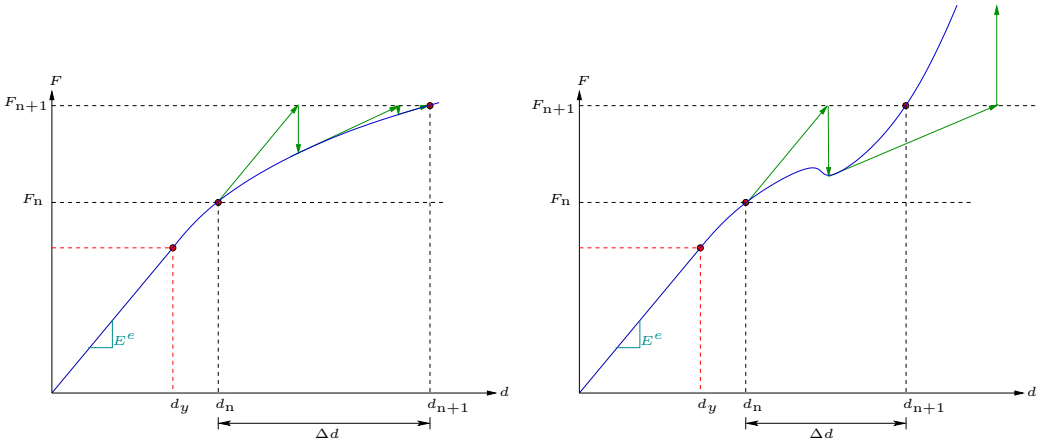

(a) Convergent (b) Possibly divergent

Fig. 4.3. Schematic of the consistent tangent predictor for the example of a nonlinear spring

solution algorithm, we consider here a classical perfectly-plastic material. The von Mises yield criterion in the absence of kinematic or isotropic hardening is given by

$$f(\boldsymbol{\sigma}) = |\operatorname{dev}[\boldsymbol{\sigma}]| - \sqrt{\tfrac{2}{3}}\sigma_0 \leq 0\,, \tag{4.2}$$

where $\sigma_0 > 0$ is related to the yield stress of the material in uniaxial tension. The plastic strain is assumed incompressible, so that $\operatorname{tr}[\boldsymbol{\varepsilon}^p] = \boldsymbol{\varepsilon}^p_{ii} = 0$. It follows that the plastic strain is a deviatoric quantity.

We shall restrict attention to a single quadrature point. This restriction in no way limits the scope of the example as the corrector part of the solution algorithm for classical problems in elastoplasticity is performed at the level of the quadrature point. This, however, is no longer the case for the model of gradient plasticity considered here.

The complete state of the system, that is, the strain $\boldsymbol{\varepsilon}$, the plastic strain $\boldsymbol{\varepsilon}^p$, and the stress $\boldsymbol{\sigma}$, is assumed known from the converged solution at time t_{n-1}. The product of the predictor step is the total strain $\boldsymbol{\varepsilon}$ at time t_n. The total strain obtained in the predictor is used to assess if plastic flow occurred at the quadrature point. The objective of the corrector step is then to determine the current stress state taking into account the possible evolution of plastic deformation.

The state of activity of the quadrature point, that is, if the point is elastic (inactive) or undergoing plastic deformation (active), is assessed by making an assumption as to the evolution of plastic flow during the strain increment. Typically it is assumed that the step is fully elastic; that is, plastic flow is "frozen" at the beginning of the time step. The trial stress deviator $\mathrm{dev}[\boldsymbol{\sigma}^\star]$ is thus defined, using the elastic constitutive relations, by

$$\mathrm{dev}[\boldsymbol{\sigma}^\star] = 2\mu \underbrace{(\mathrm{dev}[\boldsymbol{\varepsilon}_\mathrm{n}] - \boldsymbol{\varepsilon}_0^p)}_{\boldsymbol{\varepsilon}^{e\star}},$$

where $\boldsymbol{\varepsilon}^{e\star}$ is the associated trial elastic strain. The yield function is then evaluated using the trial stress state as

$$f^\star := f(\boldsymbol{\sigma}^\star) = |\,\mathrm{dev}[\boldsymbol{\sigma}^\star]| - \sqrt{\tfrac{2}{3}}\sigma_0\,,$$

where $f^\star$ is termed the trial yield function. The quadrature point is active if $f^\star > 0$, otherwise the point is inactive and the trial stress state is the actual stress state.

We now consider the form of the corrector step for the primal and dual formulations of the perfect plasticity problem under the assumption that the quadrature point is active. Recall that the objective of the corrector step is to determine the stress state while ensuring that the yield condition is satisfied at the end of the time step.

Primal formulation

The dissipation function $D(\Delta\boldsymbol{\varepsilon}^p)$ for the incremental problem of perfect plasticity is determined as follows:

$$\begin{aligned} D(\Delta\boldsymbol{\varepsilon}^p) &= \sup\,[\boldsymbol{\sigma} : \Delta\boldsymbol{\varepsilon}^p] \\ &= \sup\,[\mathrm{dev}[\boldsymbol{\sigma}] : \Delta\boldsymbol{\varepsilon}^p] \\ &= \sup\,[|\,\mathrm{dev}[\boldsymbol{\sigma}]|\;|\Delta\boldsymbol{\varepsilon}^p|] \\ &= \sqrt{\tfrac{2}{3}}\sigma_0|\Delta\boldsymbol{\varepsilon}^p| \qquad \text{using (4.2).} \end{aligned} \tag{4.3}$$

The quadrature point is assumed active and the yield surface is smooth; the primal expression of the flow rule, therefore, becomes the equality

$$\begin{aligned}\operatorname{dev}[\boldsymbol{\sigma}] &= \frac{\partial D(\Delta\boldsymbol{\varepsilon}^p)}{\partial \Delta\boldsymbol{\varepsilon}^p} \\ &= \sqrt{\tfrac{2}{3}}\sigma_0 \frac{\Delta\boldsymbol{\varepsilon}^p}{|\Delta\boldsymbol{\varepsilon}^p|}\,.\end{aligned}$$

The primal flow rule above states that the stress deviator has a maximum value equal to the effective yield stress $\sqrt{2/3}\sigma_0$ and is in the direction $\Delta\boldsymbol{\varepsilon}^p/|\Delta\boldsymbol{\varepsilon}^p|$.

Consider now the incremental problem. The product of the predictor step is the strain at time t_{n}, and hence the increment in strain $\Delta\boldsymbol{\varepsilon} = \boldsymbol{\varepsilon}_{\mathrm{n}} - \boldsymbol{\varepsilon}_0$.

The yield surface in deviatoric strain space at time $t_{\mathrm{n-1}}$ is depicted schematically in Fig. 4.4. In strain space the yield surface is a hypersphere centred on $\boldsymbol{\varepsilon}_0^p$ with radius $\sigma_0/(\sqrt{6}\mu)$. This can be seen be rewriting the yield condition (4.2) as

$$\begin{aligned}f(\boldsymbol{\sigma}) &= |\operatorname{dev}[\boldsymbol{\sigma}]| - \sqrt{\tfrac{2}{3}}\sigma_0 \\ &= |2\mu \operatorname{dev}[\boldsymbol{\varepsilon}^e]| - \sqrt{\tfrac{2}{3}}\sigma_0 \\ &= 2\mu|\operatorname{dev}[\boldsymbol{\varepsilon}] - \boldsymbol{\varepsilon}^p| - \sqrt{\tfrac{2}{3}}\sigma_0\,.\end{aligned}$$

The equation for the yield surface ($f = 0$) is obtained by taking the square of the yield function:

$$[\operatorname{dev}[\boldsymbol{\varepsilon}] - \boldsymbol{\varepsilon}^p] : [\operatorname{dev}[\boldsymbol{\varepsilon}] - \boldsymbol{\varepsilon}^p] = \frac{1}{6\mu^2}{\sigma_0}^2\,;$$

that is, the equation of a hypersphere centred on $\boldsymbol{\varepsilon}_0^p$ with radius $\sigma_0/(\sqrt{6}\mu)$. The total strain $\boldsymbol{\varepsilon}_0$ is also indicated in Fig. 4.4.

The stress deviator at time $t_{\mathrm{n-1}}$ is obtained from the elastic constitutive law as

$$\operatorname{dev}[\boldsymbol{\sigma}_{\mathrm{n-1}}] = 2\mu \underbrace{\left(\operatorname{dev}[\boldsymbol{\varepsilon}_{\mathrm{n-1}}] - \boldsymbol{\varepsilon}^p_{\mathrm{n-1}}\right)}_{\operatorname{dev}[\boldsymbol{\varepsilon}^e_{\mathrm{n-1}}]}\,,$$

where $\operatorname{dev}[\boldsymbol{\varepsilon}^e_{\mathrm{n-1}}]$ is the elastic strain deviator at time $t_{\mathrm{n-1}}$.

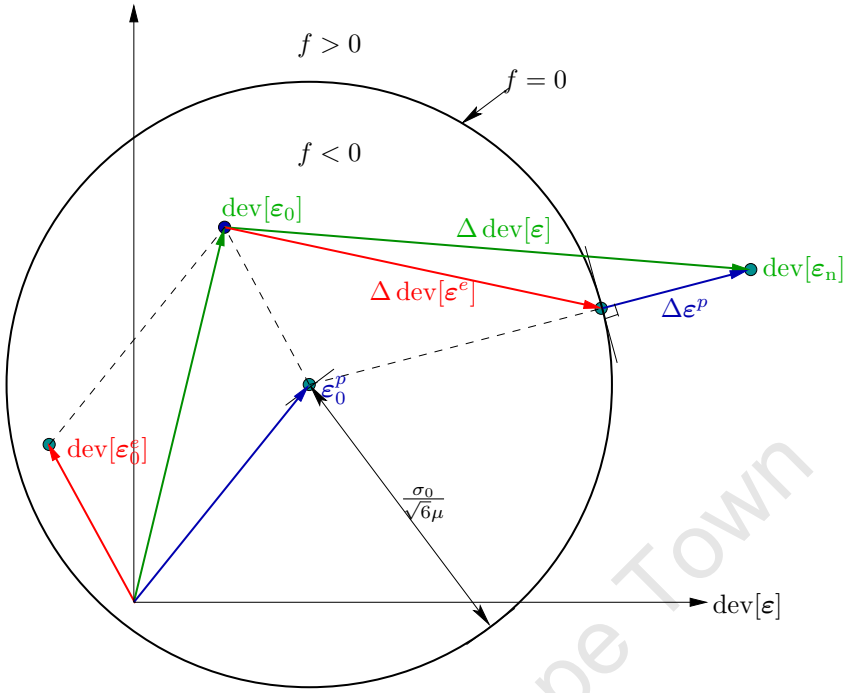

Fig. 4.4. The von Mises yield function in strain deviator space at time $t_{\mathrm{n}-1}$ for a perfectly plastic material

The increment in the strain deviator is

$$\Delta\,\mathrm{dev}[\boldsymbol{\varepsilon}] = \mathrm{dev}[\boldsymbol{\varepsilon}_\mathrm{n}] - \mathrm{dev}[\boldsymbol{\varepsilon}_0]\,,$$

resulting in a violation of the yield condition as depicted in Fig. 4.4. The magnitude of the plastic strain increment is determined from

$$\begin{aligned}
\Delta\boldsymbol{\varepsilon}^p &= \Delta\left(\mathrm{dev}[\boldsymbol{\varepsilon}_\mathrm{n}] - \mathrm{dev}[\boldsymbol{\varepsilon}^e_\mathrm{n}]\right) \\
&= \left(\mathrm{dev}[\boldsymbol{\varepsilon}_\mathrm{n}] - \mathrm{dev}[\boldsymbol{\varepsilon}_0]\right) - \left(\mathrm{dev}[\boldsymbol{\varepsilon}^e_\mathrm{n}] - \mathrm{dev}[\boldsymbol{\varepsilon}^e_0]\right) \\
&= \mathrm{dev}[\boldsymbol{\varepsilon}_\mathrm{n}] - \mathrm{dev}[\boldsymbol{\varepsilon}^e_\mathrm{n}] - \boldsymbol{\varepsilon}^p_0 \\
&= \mathrm{dev}[\boldsymbol{\varepsilon}_\mathrm{n}] - \frac{1}{2\mu}\,\mathrm{dev}[\boldsymbol{\sigma}_\mathrm{n}] - \boldsymbol{\varepsilon}^p_0 \\
&= \mathrm{dev}[\boldsymbol{\varepsilon}_\mathrm{n}] - \frac{\sigma_0}{\sqrt{6}\mu}\frac{\Delta\boldsymbol{\varepsilon}^p}{|\Delta\boldsymbol{\varepsilon}^p|} - \boldsymbol{\varepsilon}^p_0\,.
\end{aligned}$$

Rearranging the equation above we obtain

$$
\begin{aligned}
&\Delta\boldsymbol{\varepsilon}^p + \frac{\sigma_0}{\sqrt{6}\mu}\frac{\Delta\boldsymbol{\varepsilon}^p}{|\Delta\boldsymbol{\varepsilon}^p|} = \operatorname{dev}[\boldsymbol{\varepsilon}_{\mathrm{n}}] - \boldsymbol{\varepsilon}_0^p\,,\\
&\Delta\boldsymbol{\varepsilon}^p\left(1 + \frac{\sigma_0}{\sqrt{6}\mu|\Delta\boldsymbol{\varepsilon}^p|}\right) = \operatorname{dev}[\boldsymbol{\varepsilon}_{\mathrm{n}}] - \boldsymbol{\varepsilon}_0^p\,,\\
&|\Delta\boldsymbol{\varepsilon}^p|\left(1 + \frac{\sigma_0}{\sqrt{6}\mu|\Delta\boldsymbol{\varepsilon}^p|}\right) = |\operatorname{dev}[\boldsymbol{\varepsilon}_{\mathrm{n}}] - \boldsymbol{\varepsilon}_{\mathrm{n}}^p|\,,\\
&|\Delta\boldsymbol{\varepsilon}^p| = |\operatorname{dev}[\boldsymbol{\varepsilon}_{\mathrm{n}}] - \boldsymbol{\varepsilon}_{\mathrm{n}}^p| - \frac{\sigma_0}{\sqrt{6}\mu}\,.
\end{aligned}
\tag{4.4}
$$

The plastic strain increment follows a straight line normal to the yield surface in deviatoric strain space, as indicated in Fig. 4.4. For a perfectly plastic material, the increment in the strain deviator can be additively decomposed into two sequential parts: an elastic part $\Delta\operatorname{dev}[\boldsymbol{\varepsilon}^e]$ and a plastic part $\Delta\boldsymbol{\varepsilon}^p$ which takes place at a constant deviator stress.

The predictor–corrector approach as described above is effectively the well known radial return algorithm and the strain path is the minimum work path; that is, the incremental work density $\mathrm{d}W$, given by

$$
\mathrm{d}W = \int_{\operatorname{dev}[\boldsymbol{\varepsilon}_0]}^{\operatorname{dev}[\boldsymbol{\varepsilon}_{\mathrm{n}}]} \operatorname{dev}[\boldsymbol{\sigma}]\; d\operatorname{dev}[\boldsymbol{\varepsilon}]\,,
$$

takes its least value [121].

Dual formulation

The active state of the quadrature point and the smoothness of the yield surface allow the dual form of the flow rule to be written as

$$
\begin{aligned}
\Delta\boldsymbol{\varepsilon}^p &= \Delta\gamma\frac{\partial f(\boldsymbol{\sigma})}{\partial\operatorname{dev}[\boldsymbol{\sigma}]}\\
&= \Delta\gamma\,\underbrace{\frac{\operatorname{dev}[\boldsymbol{\sigma}]}{|\operatorname{dev}[\boldsymbol{\sigma}]|}}_{\boldsymbol{\nu}}\,,
\end{aligned}
$$

where $\boldsymbol{\nu}$ is the normal to the yield surface at $\operatorname{dev}[\boldsymbol{\sigma}]$. The classical return mapping algorithms (see, for example, Simo [164]) allow the stress deviator at t_{n} to be deter-

mined using the trial stress state from

$$\operatorname{dev}[\boldsymbol{\sigma}_{\mathrm{n}}] = \operatorname{dev}[\boldsymbol{\sigma}^{\star}] - 2\mu\Delta\gamma\boldsymbol{\nu}^{\star}\,, \tag{4.5}$$

where the consistency parameter is equal to the increment in plastic strain, that is,

$$\Delta\gamma = |\Delta\boldsymbol{\varepsilon}^{p}|\,,$$

and

$$\boldsymbol{\nu}^{\star} = \frac{\operatorname{dev}[\boldsymbol{\sigma}^{\star}]}{|\operatorname{dev}[\boldsymbol{\sigma}^{\star}]|} = \frac{\operatorname{dev}[\boldsymbol{\sigma}_{\mathrm{n}}]}{|\operatorname{dev}[\boldsymbol{\sigma}_{\mathrm{n}}]|}\,.$$

Following Simo [164], we take the inner product of (4.5) with $\boldsymbol{\nu}_{\mathrm{n}}$ to obtain the equation

$$|\operatorname{dev}[\boldsymbol{\sigma}]| - 2\mu\Delta\gamma = \sqrt{\tfrac{2}{3}}\sigma_0$$

that determines the consistency parameter. Manipulation of the above yields an algebraic equation for $\Delta\gamma$ as follows:

$$
\begin{aligned}
&|\operatorname{dev}[\boldsymbol{\sigma}]| = \sqrt{\tfrac{2}{3}}\sigma_0 + 2\mu\Delta\gamma\,,\\
&2\mu|\operatorname{dev}[\boldsymbol{\varepsilon}_{\mathrm{n}}] - \boldsymbol{\varepsilon}_0^p - \Delta\boldsymbol{\varepsilon}^p| = \sqrt{\tfrac{2}{3}}\sigma_0 + 2\mu\Delta\gamma\,,\\
&|\operatorname{dev}[\boldsymbol{\varepsilon}^{e\star}] - \Delta\boldsymbol{\varepsilon}^p| = \frac{\sigma_0}{3\sqrt{2}\mu} + \Delta\gamma\,,\\
&|\operatorname{dev}[\boldsymbol{\varepsilon}^{e\star}] - \Delta\gamma\boldsymbol{\nu}| = \frac{\sigma_0}{3\sqrt{2}\mu} + \Delta\gamma\,,\\
&\left[|\operatorname{dev}[\boldsymbol{\varepsilon}^{e\star}]| - 2\operatorname{dev}[\boldsymbol{\varepsilon}^{e\star}]\Delta\gamma\boldsymbol{\nu} + \Delta\gamma^2|\boldsymbol{\nu}|^2\right]^{1/2} = \frac{\sigma_0}{3\sqrt{2}\mu} + \Delta\gamma\,,\\
&\left[|\operatorname{dev}[\boldsymbol{\varepsilon}^{e\star}]| - 2|\operatorname{dev}[\boldsymbol{\varepsilon}^{e\star}]|\Delta\gamma + \Delta\gamma^2\right]^{1/2} = \frac{\sigma_0}{3\sqrt{2}\mu} + \Delta\gamma\\
&\qquad (\text{using } \operatorname{dev}[\boldsymbol{\varepsilon}^{e\star}] : \boldsymbol{\nu} = |\operatorname{dev}[\boldsymbol{\varepsilon}^{e\star}]| \text{ and } |\boldsymbol{\nu}| = 1)\\
&|\operatorname{dev}[\boldsymbol{\varepsilon}^{e\star}]| - \Delta\gamma = \frac{\sigma_0}{3\sqrt{2}\mu} + \Delta\gamma\,,\\
&2\Delta\gamma = |\operatorname{dev}[\boldsymbol{\varepsilon}^{e\star}]| - \frac{\sigma_0}{3\sqrt{2}\mu}\,,\\
&\Delta\gamma = \frac{f^\star}{2\mu}\,.
\end{aligned}
$$

It is easily shown that the above statement is identical to the expression for the increment in plastic strain (4.4) obtained using the primal approach. Thus, the two approaches are equivalent.

4.2 Convergence analysis for the solution algorithm

The convergence analysis is initially performed for an abstract problem with the same general structure as the discontinuous Galerkin formulation of the model of gradient plasticity developed in Section 3.3 of the previous chapter. We focus here on a model gradient plasticity restricted to isotropic hardening. Furthermore, we consider a discontinuous Galerkin approximation of the hardening parameter field only.

We recall the fully-discrete problem here to emphasise the connection between the abstract and the actual problem. The fully-discrete problem reads:

given $\ell(t) \in Z'$ and $\boldsymbol{w}_h^0 = (\boldsymbol{u}_h^0, \boldsymbol{\varepsilon}^{p0}_h, \xi_h^0) = \mathbf{0}$, find a sequence $\{\boldsymbol{w}_h^n\}_{n=1}^N$ in W_h such that

$$a_h(\boldsymbol{w}_h^n, \boldsymbol{z}_h - \Delta\boldsymbol{w}_h) + j(\boldsymbol{z}_h) - j(\Delta\boldsymbol{w}_h) \geq \langle \ell^n, \boldsymbol{z}_h - \Delta\boldsymbol{w}_h \rangle \ , \quad \forall \boldsymbol{z}_h \in Z_h \ , \tag{4.6}$$

where

$$\begin{aligned}
&a_h((\boldsymbol{u}_h,\boldsymbol{\varepsilon}_h^p,\xi_h),(\boldsymbol{v}_h,\boldsymbol{q}_h,\eta_h)) \\
&\quad = \sum_K \int_K \Big(\mathcal{C}(\boldsymbol{\varepsilon}(\boldsymbol{u}_h) - \boldsymbol{\varepsilon}_h^p) : (\boldsymbol{\varepsilon}(\boldsymbol{v}_h) - \boldsymbol{q}_h) + k_2 \xi_h \eta_h \Big) \, dX \\
&\qquad + \sum_K \int_K k_3 \nabla\xi_h \cdot \nabla\eta_h \, dX \\
&\qquad - \sum_e \int_e k_3 \Big(\{\!\{ \nabla\xi_h \}\!\} \cdot [\![\eta_h]\!] + \{\!\{ \nabla\eta_h \}\!\} \cdot [\![\xi_h]\!] \Big) \, dS \\
&\qquad + \sum_e \frac{\beta_2}{h_e} \int_e [\![\xi_h]\!] \cdot [\![\eta_h]\!] \, dS \ .
\end{aligned}$$

Furthermore, we define the bilinear forms $b,\ c$ and d by

$$\begin{aligned}
b(\boldsymbol{u}_h, \boldsymbol{v}_h) &= \sum_K \int_K \mathcal{C}\boldsymbol{\varepsilon}(\boldsymbol{u}_h) : \boldsymbol{\varepsilon}(\boldsymbol{v}_h) \ dX \ , \\
c(\boldsymbol{\varepsilon}_h^p, \boldsymbol{v}_h) &= \sum_K \int_K \mathcal{C}\boldsymbol{\varepsilon}_h^p : \boldsymbol{\varepsilon}(\boldsymbol{v}_h) \ dX \ , \\
d((\boldsymbol{\varepsilon}_h^p, \xi_h), (\boldsymbol{q}_h, \eta_h)) &= \sum_K \int_K \mathcal{C}\boldsymbol{\varepsilon}_h^p : \boldsymbol{q}_h \ dX \\
&\qquad - \sum_e \int_e k_3 \Big(\{\!\{ \nabla\xi_h \}\!\} \cdot [\![\eta_h]\!] \ dS + \{\!\{ \nabla\eta_h \}\!\} \cdot [\![\xi_h]\!] \Big) \ dS \\
&\qquad + \sum_e \frac{\beta k_3}{h_e} \int_e [\![\xi_h]\!] \cdot [\![\eta_h]\!] \ dS \\
&\qquad + \sum_K \int_K \Big(k_2 \xi_h \eta_h + k_3 \nabla\xi_h \cdot \nabla\eta_h \Big) \ dX \ .
\end{aligned}$$

The fully-discrete problem (4.6) is obtained from combining the weak form of the statement of equilibrium and the primal expression of the flow law, respectively given for the semi-discrete problem by

$$\sum_K \int_K \mathcal{C}(\boldsymbol{\varepsilon}(\boldsymbol{u}_h) - \boldsymbol{\varepsilon}_h^p) : (\boldsymbol{\varepsilon}(\boldsymbol{v}_h) - \boldsymbol{q}_h)\ dX = \sum_K \int_K \boldsymbol{B} \cdot (\boldsymbol{v}_h - \boldsymbol{q}_h)\ dX\,,$$

$$\begin{aligned} j(\boldsymbol{z}_h) \geq j(\dot{\boldsymbol{w}}_h) &+ \sum_K \int_K \mathcal{C}(\boldsymbol{\varepsilon}(\boldsymbol{u}_h) - \boldsymbol{\varepsilon}_h^p) : (\boldsymbol{q}_h - \dot{\boldsymbol{\varepsilon}}_h^p)\ dX \\ &- \sum_K \int_K k_2 \xi_h (\eta_h - \dot{\xi}_h)\ dX - \sum_K \int_K k_3 \nabla \xi_h \cdot (\nabla[\eta_h - \dot{\xi}_h])\, dX \\ &+ \sum_e \int_e k_3 \Big(\{\!\{\nabla \xi_h\}\!\} \cdot [\![\eta_h - \dot{\xi}_h]\!] + \{\!\{\nabla[\eta_h - \dot{\xi}_h]\}\!\} \cdot [\![\xi_h]\!] \Big)\, dS \\ &- \sum_e \frac{\beta_2}{h_e} \int_e [\![\xi_h]\!] \cdot [\![\eta_h - \dot{\xi}_h]\!]\, dS\,. \end{aligned}$$

For further details see Section 2.2.1 where the key steps in the construction of the variational inequality corresponding to the primal formulation of classical plasticity are given.

4.2.1 Abstract formulation

We begin by introducing the various spaces, functionals, and assumptions required for the abstract problem.

- Let V and Λ be two Hilbert spaces.
- Let $b : V \times V \to \mathbb{R}$, $c : V \times \Lambda \to \mathbb{R}$ and $d : \Lambda \times \Lambda \to \mathbb{R}$ be continuous, with b and d not necessarily symmetric, bilinear forms, that is,

$$\begin{aligned} &|b(\boldsymbol{u}, \boldsymbol{v})| \leq \bar{c} \|\boldsymbol{u}\|_V \|\boldsymbol{v}\|_V\,, \quad |c(\boldsymbol{u}, \lambda)| \leq \bar{c} \|\boldsymbol{u}\|_V \|\lambda\|_\Lambda\,, \quad |d(\lambda, \mu)| \leq \bar{c} \|\lambda\|_\Lambda \|\mu\|_\Lambda\,, \\ &b(\boldsymbol{v}, \boldsymbol{v}) \geq c_0 \|\boldsymbol{v}\|_V^2 \quad \forall \boldsymbol{v} \in V\,, \quad d(\lambda, \lambda) \geq (c_0 + k_0) \|\lambda\|_\Lambda^2 \quad \forall \lambda \in \Lambda\,, \end{aligned}$$

  for positive constants c_0, $\bar{c}$ and k_0.
- Let $l_1 : V \to \mathbb{R}$ and $l_2 : \Lambda \to \mathbb{R}$ be two continuous linear forms.
- Let $j : \Lambda \to \mathbb{R}$ be a nonnegative convex and Lipschitz continuous functional. It should be noted that these smoothness assumptions restrict the subsequent algorithm to problems having smooth yield surfaces. The treatment of nonsmooth yield surfaces, for example, the one corresponding to the assumption of a Tresca yield condition, is considered in [155, 170].

- For $\boldsymbol{w} = (\boldsymbol{u}, \lambda),\ z = (\boldsymbol{v}, \mu) \in V \times \Lambda$ we define

$$a(\boldsymbol{w}, \boldsymbol{z}) = b(\boldsymbol{u}, \boldsymbol{v}) - c(\lambda, \boldsymbol{v}) - c(\mu, \boldsymbol{u}) + d(\lambda, \mu)\,.$$

Crucial to the algorithm is the consideration of the variational inequality as a combination of an equation and an inequality as detailed above for the fully-discrete problem. This allows us to state the abstract problem as follows:

find $\boldsymbol{u} \in V$ and $\lambda \in \Lambda$ such that

$$b(\boldsymbol{u}, \boldsymbol{v}) - c(\lambda, \boldsymbol{v}) = \langle l_1, \boldsymbol{v} \rangle \qquad \forall \boldsymbol{v} \in V, \tag{4.7}$$

$$j(\mu) - j(\lambda) - c(\mu - \lambda, \boldsymbol{u}) + d(\lambda, \mu - \lambda) \geq \langle l_2, \mu - \lambda \rangle \qquad \forall \mu \in \Lambda. \tag{4.8}$$

The abstract problem (4.7)–(4.8) has a unique solution $\boldsymbol{w} = (\boldsymbol{u}, \lambda) \in V \times \Lambda$.

The predictor–corrector algorithm for the solution of the abstract problem is given in Alg. 4.1. In a typical iteration we have estimates $u^{\mathrm{i}-1}$ and $\lambda^{\mathrm{i}-1}$. The objective of the iteration is to provide an updated and improved estimate of u^{i} and λ^{i}. We denote by u^0 and λ^0 some initial estimate. The outcome of the predictor step is an updated value for u, denoted u^{i}, and an intermediate value for λ, denoted $\lambda^{*\mathrm{i}}$. The rate of convergence of the algorithm is governed by the approximation of the dissipation function used in the predictor step. In the corrector step, an updated value for λ, denoted λ^{i}, is computed.

Theorem 4.1. *Under the assumptions on the functionals and the structural inequality*

$$r_3 := \frac{\bar{c}^2}{c_0(c_0 + k_0)} < \frac{1}{3}\,, \tag{4.16}$$

the predictor–corrector algorithm given above converges. That is,

$$\boldsymbol{u}^{\mathrm{i}} \to \boldsymbol{u} \text{ in } V \quad \text{and} \quad \lambda^{\mathrm{i}} \to \lambda \text{ in } \Lambda \quad \text{as } \mathrm{i} \to \infty\,,$$

where $\boldsymbol{w} = (\boldsymbol{u}, \lambda)$ is the solution of the abstract problem (4.7)–(4.8). Furthermore, the following error estimate holds:

Algorithm 4.1 Algorithm for the solution of the abstract problem

Initial conditions

Given initial data $\boldsymbol{w}^0 = (\boldsymbol{u}^0, \lambda^0) \in V \times \Lambda$.

Predictor

Compute $(\boldsymbol{u}^{\mathrm{i}}, \lambda^{*\mathrm{i}}) \in V \times \Lambda$ such that

$$b(\boldsymbol{u}^{\mathrm{i}}, \boldsymbol{v} - \boldsymbol{u}^{\mathrm{i}}) - c(\lambda^{*\mathrm{i}}, \boldsymbol{v} - \boldsymbol{u}^{\mathrm{i}}) = \langle l_1, \boldsymbol{v} - \boldsymbol{u}^{\mathrm{i}} \rangle \qquad \forall \boldsymbol{v} \in V\,, \tag{4.9}$$

$$j^{(\mathrm{i})}(\mu) - j^{(\mathrm{i})}(\lambda^{*\mathrm{i}}) + d(\lambda^{*\mathrm{i}}, \mu - \lambda^{*\mathrm{i}}) \geq \langle l_2, \mu - \lambda^{*\mathrm{i}} \rangle + c(\mu - \lambda^{*\mathrm{i}}, \boldsymbol{u}^{\mathrm{i}}) \quad \forall \mu \in \Lambda\,, \tag{4.10}$$

where

$$j^{(\mathrm{i})}(\mu) = \int_\Omega D^{(\mathrm{i})}(\mu)\, dX\,, \tag{4.11}$$

and $D^{(\mathrm{i})}$ is a smooth convex function which satisfies (see Fig. 4.5 for an example):

$$D^{(\mathrm{i})}(\lambda^{\mathrm{i}-1}) = D(\lambda^{\mathrm{i}-1})\,, \tag{4.12}$$

$$\nabla D^{(\mathrm{i})}(\lambda^{\mathrm{i}-1}) = \nabla D(\lambda^{\mathrm{i}-1})\,, \tag{4.13}$$

$$D(\mu) \leq D^{(\mathrm{i})}(\mu) \quad \forall \mu \in \Lambda\,. \tag{4.14}$$

Corrector

Compute $\lambda^i \in \Lambda$ such that

$$j(\mu) - j(\lambda^{\mathrm{i}}) + d(\lambda^{\mathrm{i}}, \mu - \lambda^{\mathrm{i}}) \geq \langle l_2, \mu - \lambda^{\mathrm{i}} \rangle + c(\mu - \lambda^{\mathrm{i}}, \boldsymbol{u}^{\mathrm{i}}) \qquad \forall \mu \in \Lambda\,. \tag{4.15}$$

$$\|\boldsymbol{w}^{\mathrm{i}} - \boldsymbol{w}\|_{V\times\Lambda} \leq \frac{2r_3}{1 - r_3} \|\boldsymbol{w}^{\mathrm{i}} - \boldsymbol{w}^{\mathrm{i}-1}\|_{V\times\Lambda}\,, \tag{4.17}$$

where $\boldsymbol{w}^{\mathrm{i}} = (\boldsymbol{u}^{\mathrm{i}}, \lambda^{\mathrm{i}})$.

Proof. Equation (4.9) in the predictor step is rewritten as

$$b(\boldsymbol{u}^{\mathrm{i}}, \boldsymbol{v} - \boldsymbol{u}^{\mathrm{i}}) - c(\lambda^{\mathrm{i}-1}, \boldsymbol{v} - \boldsymbol{u}^{\mathrm{i}}) = c(\lambda^{*\mathrm{i}} - \lambda^{\mathrm{i}-1}, \boldsymbol{v} - \boldsymbol{u}^{\mathrm{i}}) + \langle l_1, \boldsymbol{v} - \boldsymbol{u}^{\mathrm{i}} \rangle \qquad \forall \boldsymbol{v} \in V\,. \tag{4.18}$$

Setting arbitrary $\boldsymbol{v}$ to equal $\boldsymbol{u}^{\mathrm{i}-1}$ in (4.18) above we obtain

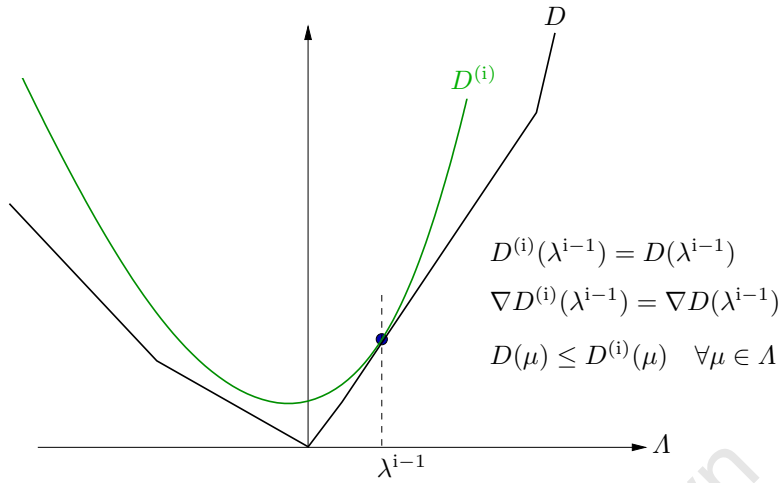

Fig. 4.5. The approximation $D^{(\mathrm{i})}$ of the dissipation function D

$$b(\boldsymbol{u}^{\mathrm{i}}, \boldsymbol{u}^{\mathrm{i}-1} - \boldsymbol{u}^{\mathrm{i}}) - c(\lambda^{\mathrm{i}-1}, \boldsymbol{u}^{\mathrm{i}-1} - \boldsymbol{u}^{\mathrm{i}}) = c(\lambda^{*\mathrm{i}} - \lambda^{\mathrm{i}-1}, \boldsymbol{u}^{\mathrm{i}-1} - \boldsymbol{u}^{\mathrm{i}}) + \langle l_1, \boldsymbol{u}^{\mathrm{i}-1} - \boldsymbol{u}^{\mathrm{i}} \rangle \,. \tag{4.19}$$

Rewriting (4.18) at iteration $i-1$ and take $\boldsymbol{v} = \boldsymbol{u}^{\mathrm{i}}$ to obtain

$$b(\boldsymbol{u}^{\mathrm{i}-1}, \boldsymbol{u}^{\mathrm{i}} - \boldsymbol{u}^{\mathrm{i}-1}) - c(\lambda^{\mathrm{i}-2}, \boldsymbol{u}^{\mathrm{i}} - \boldsymbol{u}^{\mathrm{i}-1}) = c(\lambda^{*(\mathrm{i}-1)} - \lambda^{\mathrm{i}-2}, \boldsymbol{u}^{\mathrm{i}} - \boldsymbol{u}^{\mathrm{i}-1}) + \langle l_1, \boldsymbol{u}^{\mathrm{i}} - \boldsymbol{u}^{\mathrm{i}-1} \rangle \,. \tag{4.20}$$

Adding (4.19) and (4.20) we obtain

$$\underbrace{b(\boldsymbol{u}^{\mathrm{i}}, \boldsymbol{u}^{\mathrm{i}-1} - \boldsymbol{u}^{\mathrm{i}}) + b(\boldsymbol{u}^{\mathrm{i}-1}, \boldsymbol{u}^{\mathrm{i}} - \boldsymbol{u}^{\mathrm{i}-1})}_{A} + \underbrace{\big(-c(\lambda^{\mathrm{i}-1}, \boldsymbol{u}^{\mathrm{i}-1} - \boldsymbol{u}^{\mathrm{i}}) - c(\lambda^{\mathrm{i}-2}, \boldsymbol{u}^{\mathrm{i}} - \boldsymbol{u}^{\mathrm{i}-1})\big)}_{B}$$
$$= \underbrace{c(\lambda^{*\mathrm{i}} - \lambda^{\mathrm{i}-1}, \boldsymbol{u}^{\mathrm{i}-1} - \boldsymbol{u}^{\mathrm{i}})}_{C} + \underbrace{c(\lambda^{*(\mathrm{i}-1)} - \lambda^{\mathrm{i}-2}, \boldsymbol{u}^{\mathrm{i}} - \boldsymbol{u}^{\mathrm{i}-1})}_{D} ,$$

or

$$A = C + D - B \,.$$

Manipulating the individual contributions A, B, C and D, we obtain

$$
\begin{aligned}
A &= -b\left(\boldsymbol{u}^{\mathrm{i}} - \boldsymbol{u}^{\mathrm{i}-1}, \boldsymbol{u}^{\mathrm{i}} - \boldsymbol{u}^{\mathrm{i}-1}\right) , \\
-B &= -c\left(\lambda^{\mathrm{i}-1} - \lambda^{\mathrm{i}-2}, \boldsymbol{u}^{\mathrm{i}} - \boldsymbol{u}^{\mathrm{i}-1}\right) , \\
C &= -c\left(\lambda^{*\mathrm{i}} - \lambda^{\mathrm{i}-1}, \boldsymbol{u}^{\mathrm{i}} - \boldsymbol{u}^{\mathrm{i}-1}\right) , \\
D &= -c\left(\lambda^{*(\mathrm{i}-1)} - \lambda^{\mathrm{i}-2}, \boldsymbol{u}^{\mathrm{i}} - \boldsymbol{u}^{\mathrm{i}-1}\right) .
\end{aligned}
$$

Combining the individual contributions and exploiting the coercivity of b and the continuity of c we get

$$
\begin{aligned}
b\left(\boldsymbol{u}^{\mathrm{i}} - \boldsymbol{u}^{\mathrm{i}-1}, \boldsymbol{u}^{\mathrm{i}} - \boldsymbol{u}^{\mathrm{i}-1}\right) &= c\left(\lambda^{\mathrm{i}-1} - \lambda^{\mathrm{i}-2}, \boldsymbol{u}^{\mathrm{i}} - \boldsymbol{u}^{\mathrm{i}-1}\right) \\
&\quad + c\left(\lambda^{*\mathrm{i}} - \lambda^{\mathrm{i}-1}, \boldsymbol{u}^{\mathrm{i}} - \boldsymbol{u}^{\mathrm{i}-1}\right) + c\left(\lambda^{*(\mathrm{i}-1)} - \lambda^{\mathrm{i}-2}, \boldsymbol{u}^{\mathrm{i}} - \boldsymbol{u}^{\mathrm{i}-1}\right), \\
c_0\|\boldsymbol{u}^{\mathrm{i}} - \boldsymbol{u}^{\mathrm{i}-1}\|_V^2 &\le |c\left(\lambda^{\mathrm{i}-1} - \lambda^{\mathrm{i}-2}, \boldsymbol{u}^{\mathrm{i}} - \boldsymbol{u}^{\mathrm{i}-1}\right)| + |c\left(\lambda^{*\mathrm{i}} - \lambda^{\mathrm{i}-1}, \boldsymbol{u}^{\mathrm{i}} - \boldsymbol{u}^{\mathrm{i}-1}\right)| \\
&\quad + |c\left(\lambda^{*(\mathrm{i}-1)} - \lambda^{\mathrm{i}-2}, \boldsymbol{u}^{\mathrm{i}} - \boldsymbol{u}^{\mathrm{i}-1}\right)| \qquad \text{(using the coercivity of } b), \\
c_0\|\boldsymbol{u}^{\mathrm{i}} - \boldsymbol{u}^{\mathrm{i}-1}\|_V^2 &\le \bar{c}\|\lambda^{\mathrm{i}-1} - \lambda^{\mathrm{i}-2}\|_\Lambda\|\boldsymbol{u}^{\mathrm{i}} - \boldsymbol{u}^{\mathrm{i}-1}\|_V \\
&\quad + \bar{c}\|\lambda^{*\mathrm{i}} - \lambda^{\mathrm{i}-1}\|_\Lambda\|\boldsymbol{u}^{\mathrm{i}} - \boldsymbol{u}^{\mathrm{i}-1}\|_V + \bar{c}\|\lambda^{\mathrm{i}-2} - \lambda^{*(\mathrm{i}-1)}\|_\Lambda\|\boldsymbol{u}^{\mathrm{i}} - \boldsymbol{u}^{\mathrm{i}-1}\|_V \\
&\quad \text{(using the continuity of } c), \\
c_0\|\boldsymbol{u}^{\mathrm{i}} - \boldsymbol{u}^{\mathrm{i}-1}\|_V &\le \bar{c}\Big[\|\lambda^{\mathrm{i}-1} - \lambda^{\mathrm{i}-2}\|_\Lambda + \|\lambda^{*\mathrm{i}} - \lambda^{\mathrm{i}-1}\|_\Lambda + \|\lambda^{*(\mathrm{i}-1)} - \lambda^{\mathrm{i}-2}\|_\Lambda\Big] . \qquad (4.21)
\end{aligned}
$$

Next, taking $\mu = \lambda^{\mathrm{i}-1}$ in (4.10) we obtain

$$
j^{(\mathrm{i})}(\lambda^{\mathrm{i}-1}) - j^{(\mathrm{i})}(\lambda^{*\mathrm{i}}) + d(\lambda^{*\mathrm{i}}, \lambda^{\mathrm{i}-1} - \lambda^{*\mathrm{i}}) \ge \langle l_2, \lambda^{\mathrm{i}-1} - \lambda^{*\mathrm{i}}\rangle + c(\lambda^{\mathrm{i}-1} - \lambda^{*\mathrm{i}}, \boldsymbol{u}^{\mathrm{i}}) . \quad (4.22)
$$

We write (4.15) at step $i-1$ and take $\mu = \lambda^{*\mathrm{i}}$ to get

$$
j(\lambda^{*\mathrm{i}}) - j(\lambda^{\mathrm{i}-1}) + d(\lambda^{\mathrm{i}-1}, \lambda^{*\mathrm{i}} - \lambda^{\mathrm{i}-1}) \ge \langle l_2, \lambda^{*\mathrm{i}} - \lambda^{\mathrm{i}-1}\rangle + c(\lambda^{*\mathrm{i}} - \lambda^{\mathrm{i}-1}, \boldsymbol{u}^{\mathrm{i}-1}) . \quad (4.23)
$$

Adding the inequalities (4.22) and (4.23) and rearranging we obtain

$$
\begin{aligned}
&\left(j^{(\mathrm{i})}(\lambda^{\mathrm{i}-1}) - j(\lambda^{\mathrm{i}-1})\right) + \left(j(\lambda^{*\mathrm{i}}) - j^{(\mathrm{i})}(\lambda^{*\mathrm{i}})\right) - d\left(\lambda^{*\mathrm{i}} - \lambda^{\mathrm{i}-1}, \lambda^{*\mathrm{i}} - \lambda^{\mathrm{i}-1}\right) \\
&\quad \le -c\left(\lambda^{*\mathrm{i}} - \lambda^{\mathrm{i}-1}, \boldsymbol{u}^{\mathrm{i}} - \boldsymbol{u}^{\mathrm{i}-1}\right)
\end{aligned}
$$

Using the properties of the approximation of the dissipation D listed in (4.12) – (4.14) and the definition of the functional j, the inequality above reduces to

$$d\left(\lambda^{*\mathrm{i}} - \lambda^{\mathrm{i}-1}, \lambda^{*\mathrm{i}} - \lambda^{\mathrm{i}-1}\right) \geq c\left(\lambda^{*\mathrm{i}} - \lambda^{\mathrm{i}-1}, \boldsymbol{u}^{\mathrm{i}} - \boldsymbol{u}^{\mathrm{i}-1}\right) .$$

Finally, using the coercivity of d and the continuity of c, we obtain

$$(c_0 + k_0)\|\lambda^{*\mathrm{i}} - \lambda^{\mathrm{i}-1}\|_{\Lambda} \leq \bar{c}\|\boldsymbol{u}^{\mathrm{i}} - \boldsymbol{u}^{\mathrm{i}-1}\|_V . \tag{4.24}$$

Combining (4.21) and (4.24) we get

$$\left(c_0 - \frac{\bar{c}^2}{c_0 + k_0}\right)\|\boldsymbol{u}^{\mathrm{i}} - \boldsymbol{u}^{\mathrm{i}-1}\|_V \leq \bar{c}\|\lambda^{\mathrm{i}-1} - \lambda^{\mathrm{i}-2}\|_{\Lambda} + \frac{\bar{c}^2}{c_0 + k_0}\|\boldsymbol{u}^{\mathrm{i}-1} - \boldsymbol{u}^{\mathrm{i}-2}\|_V . \tag{4.25}$$

Now we take $\mu = \lambda^{\mathrm{i}-1}$ in (4.15), then we consider (4.15) in the corrector step with $\mu = \lambda^{\mathrm{i}-1}$. This yields

$$j(\lambda^{\mathrm{i}-1}) - j(\lambda^{\mathrm{i}}) + d(\lambda^{\mathrm{i}}, \lambda^{\mathrm{i}-1} - \lambda^{\mathrm{i}}) \geq \langle l_2, \lambda^{\mathrm{i}-1} - \lambda^{\mathrm{i}}\rangle + c(\lambda^{\mathrm{i}-1} - \lambda^{\mathrm{i}}, \boldsymbol{u}^{\mathrm{i}}) , \tag{4.26}$$

$$j(\lambda^{\mathrm{i}}) - j(\lambda^{\mathrm{i}-1}) + d(\lambda^{\mathrm{i}-1}, \lambda^{\mathrm{i}} - \lambda^{\mathrm{i}-1}) \geq \langle l_2, \lambda^{\mathrm{i}} - \lambda^{\mathrm{i}-1}\rangle + c(\lambda^{\mathrm{i}} - \lambda^{\mathrm{i}-1}, \boldsymbol{u}^{\mathrm{i}-1}) . \tag{4.27}$$

Adding the above two inequalities and rearranging we get

$$d\left(\lambda^{\mathrm{i}} - \lambda^{\mathrm{i}-1}, \lambda^{\mathrm{i}} - \lambda^{\mathrm{i}-1}\right) \leq c\left(\lambda^{\mathrm{i}} - \lambda^{\mathrm{i}-1}, \boldsymbol{u}^{\mathrm{i}} - \boldsymbol{u}^{\mathrm{i}-1}\right) , \tag{4.28}$$

from which we obtain, using the coercivity of d and the continuity of c, the inequality

$$(c_0 + k_0)\|\lambda^{\mathrm{i}} - \lambda^{\mathrm{i}-1}\|_{\Lambda} \leq \bar{c}\|\boldsymbol{u}^{\mathrm{i}} - \boldsymbol{u}^{\mathrm{i}-1}\|_V . \tag{4.29}$$

From (4.25) and (4.29) we then obtain

$$\left(c_0 - \frac{\bar{c}^2}{c_0 + k_0}\right)\|\boldsymbol{u}^{\mathrm{i}} - \boldsymbol{u}^{\mathrm{i}-1}\|_V \leq \frac{2\bar{c}^2}{c_0 + k_0}\|\boldsymbol{u}^{\mathrm{i}-1} - \boldsymbol{u}^{\mathrm{i}-2}\|_V ,$$

which gives

$$\|\boldsymbol{u}^{\mathrm{i}} - \boldsymbol{u}^{\mathrm{i}-1}\|_V \leq \frac{2r_3}{1-r_3}\|\boldsymbol{u}^{\mathrm{i}-1} - \boldsymbol{u}^{\mathrm{i}-2}\|_V\,, \tag{4.30}$$

with r_3 given in (4.16).

Rewriting (4.29) as

$$\|\lambda^{\mathrm{i}} - \lambda^{\mathrm{i}-1}\|_{\Lambda} \leq \frac{\bar{c}}{c_0 + k_0}\|\boldsymbol{u}^{\mathrm{i}} - \boldsymbol{u}^{\mathrm{i}-1}\|_V\,,$$

and adding it to (4.30), we obtain

$$\begin{aligned}
&\|\lambda^{\mathrm{i}} - \lambda^{\mathrm{i}-1}\|_{\Lambda} + \|\boldsymbol{u}^{\mathrm{i}} - \boldsymbol{u}^{\mathrm{i}-1}\|_V \leq \frac{\bar{c}}{c_0 + k_0}\|\boldsymbol{u}^{\mathrm{i}} - \boldsymbol{u}^{\mathrm{i}-1}\|_V + \frac{2r_3}{1-r_3}\|\boldsymbol{u}^{\mathrm{i}-1} - \boldsymbol{u}^{\mathrm{i}-2}\|_V\,,\\
&\|\boldsymbol{w}^{\mathrm{i}} - \boldsymbol{w}^{\mathrm{i}-1}\|_{V\times\Lambda} \leq \frac{\bar{c}}{c_0 + k_0}\|\boldsymbol{u}^{i} - \boldsymbol{u}^{\mathrm{i}-1}\|_V + \frac{2r_3}{1-r_3}\|\boldsymbol{u}^{\mathrm{i}-1} - \boldsymbol{u}^{\mathrm{i}-2}\|_V\,,\\
&\|\boldsymbol{w}^{\mathrm{i}} - \boldsymbol{w}^{\mathrm{i}-1}\|_{V\times\Lambda} \leq \frac{\bar{c}}{c_0 + k_0}\|\boldsymbol{w}^{i} - \boldsymbol{w}^{\mathrm{i}-1}\|_{V\times\Lambda} + \frac{2r_3}{1-r_3}\|\boldsymbol{w}^{\mathrm{i}-1} - \boldsymbol{w}^{\mathrm{i}-2}\|_{V\times\Lambda}\\
&\qquad \text{(using the obvious inequality } \|\boldsymbol{u}^{\mathrm{i}} - \boldsymbol{u}^{\mathrm{i}-1}\|_V \leq \|\boldsymbol{w}^{\mathrm{i}} - \boldsymbol{w}^{\mathrm{i}-1}\|_{V\times\Lambda})\,,\\
&\|\boldsymbol{w}^{\mathrm{i}} - \boldsymbol{w}^{\mathrm{i}-1}\|_{V\times\Lambda} \leq \|\boldsymbol{w}^{\mathrm{i}} - \boldsymbol{w}^{\mathrm{i}-1}\|_{V\times\Lambda} + \frac{2r_3}{1-r_3}\|\boldsymbol{w}^{\mathrm{i}-1} - \boldsymbol{w}^{\mathrm{i}-2}\|_{V\times\Lambda}\\
&\qquad \text{(using } \frac{\bar{c}}{c_0 + k_0} < 1)\,.
\end{aligned}$$

The difference in $\|\boldsymbol{w}^{\mathrm{i}} - \boldsymbol{w}^{\mathrm{i}-1}\|_{V\times\Lambda}$ between successive iterations is thus $\dfrac{2r_3}{1-r_3}$. The difference between successive iterates can thus be expressed in terms of the difference between the first iterate and the initial condition as

$$\|\boldsymbol{w}^{i} - \boldsymbol{w}^{\mathrm{i}-1}\|_{V\times\Lambda} \leq \underbrace{\left(\frac{2r_3}{1-r_3}\right)}_{\bar{r}}^{(\mathrm{i}-1)}\|\boldsymbol{w}^1 - \boldsymbol{w}^0\|_{V\times\Lambda}\,.$$

Note, in the above $\bar{r}$ is raised to the power of $(i-1)$. Using $r_3 < 1/3$, we find that $\bar{r} < 1$ and $\{\boldsymbol{w}^{\mathrm{i}}\}_{\mathrm{i}\geq 1}$ is thus a Cauchy sequence in the Hilbert space $V \times \Lambda$, which converges to $\boldsymbol{w}^\star = (\boldsymbol{u}^\star, \lambda^\star) \in V \times \Lambda$.

Using the continuity of the bilinear and linear forms we can pass to the limit in (4.9) and (4.15) and find that $\boldsymbol{w}^\star = (\boldsymbol{u}^\star, \lambda^\star)$ solves the abstract problem (4.7)–(4.8).

By the uniqueness of the solution it follows that $\boldsymbol{w}^\star = \boldsymbol{w}$. Therefore, the sequence $\{\boldsymbol{w}^{\mathrm{i}}\}_{\mathrm{i}\geq 1}$ converges to $\boldsymbol{w}$.

It remains to obtain the error estimate (4.17). To this end, we first take $\boldsymbol{v} = \boldsymbol{u}^{\mathrm{i}} - \boldsymbol{u}$ in (4.7) and $\mu = \lambda^{\mathrm{i}}$ in (4.8) to get, respectively,

$$b(\boldsymbol{u}, \boldsymbol{u}^{\mathrm{i}} - \boldsymbol{u}) - c(\lambda, \boldsymbol{u}^{\mathrm{i}} - \boldsymbol{u}) = \langle l_1, \boldsymbol{u}^{\mathrm{i}} - \boldsymbol{u}\rangle \ , \tag{4.31}$$

$$j(\lambda^{\mathrm{i}}) - j(\lambda) + d(\lambda, \lambda^{\mathrm{i}} - \lambda) \ \geq \ \langle l_2, \lambda^{\mathrm{i}} - \lambda\rangle + c(\lambda^{\mathrm{i}} - \lambda, \boldsymbol{u})\,. \tag{4.32}$$

Now we take $\boldsymbol{v} = \boldsymbol{u} - \boldsymbol{u}^{\mathrm{i}}$ in (4.9) and $\mu = \lambda$ in (4.15) and get respectively

$$b(\boldsymbol{u}^{\mathrm{i}}, \boldsymbol{u} - u^{\mathrm{i}}) = \langle l_1, \boldsymbol{u} - \boldsymbol{u}^{\mathrm{i}}\rangle + c(\lambda^{*\mathrm{i}}, \boldsymbol{u} - \boldsymbol{u}^{\mathrm{i}}) \tag{4.33}$$

and

$$j(\lambda) - j(\lambda^{\mathrm{i}}) + d(\lambda^{\mathrm{i}}, \lambda - \lambda^{\mathrm{i}}) \geq \langle l_2, \lambda - \lambda^{\mathrm{i}}\rangle + c(\lambda - \lambda^{\mathrm{i}}, \boldsymbol{u}^{\mathrm{i}})\,. \tag{4.34}$$

Similarly to the inequality we find from (4.31) and (4.33) that

$$c_0\|\boldsymbol{u}^{\mathrm{i}} - \boldsymbol{u}\|_V \leq \bar{c}\|\lambda^{*\mathrm{i}} - \lambda\|_\Lambda \leq \bar{c}\Big[\|\lambda^{*\mathrm{i}} - \lambda^{\mathrm{i}-1}\|_\Lambda + \|\lambda - \lambda^{\mathrm{i}-1}\|_\Lambda\Big]\,. \tag{4.35}$$

Furthermore, from (4.26) and (4.27) we obtain

$$(c_0 + k_0)\|\lambda^{\mathrm{i}} - \lambda\|_\Lambda \leq \bar{c}\|\boldsymbol{u}^{\mathrm{i}} - \boldsymbol{u}\|_V\,, \tag{4.36}$$

which together with (4.35) imply that

$$\|\boldsymbol{u}^{\mathrm{i}} - \boldsymbol{u}\|_V \leq \frac{r_3}{1 - r_3}\|\boldsymbol{u}^{\mathrm{i}} - \boldsymbol{u}^{\mathrm{i}-1}\|_V\,. \tag{4.37}$$

Similarly using (4.36), (4.30) and (4.37) we obtain

$$\|\lambda^{\mathrm{i}} - \lambda\|_\Lambda \leq \frac{2r_3}{1 - r_3}\|\lambda^{\mathrm{i}-1} - \lambda^{\mathrm{i}-2}\|_\Lambda\,. \tag{4.38}$$

Finally, adding (4.37) and (4.38) we obtain

$$\begin{aligned}\|\boldsymbol{u}^{\mathrm{i}} - \boldsymbol{u}\|_V + \|\lambda^{\mathrm{i}} - \lambda\|_\Lambda &\leq \frac{r_3}{1-r_3}\|\boldsymbol{u}^{\mathrm{i}} - \boldsymbol{u}^{\mathrm{i}-1}\|_V + \frac{2r_3}{1-r_3}\|\lambda^{\mathrm{i}} - \lambda^{\mathrm{i}-1}\|_\Lambda \\ &\leq \frac{2r_3}{1-r_3}\left(\|\boldsymbol{u}^{\mathrm{i}} - \boldsymbol{u}^{\mathrm{i}-1}\|_V + \|\lambda^{\mathrm{i}} - \lambda^{\mathrm{i}-1}\|_\Lambda\right) .\end{aligned}$$

Rewriting the above gives

$$\|\boldsymbol{w}^{\mathrm{i}} - \boldsymbol{w}\|_{V\times\Lambda} \leq \frac{2r_3}{1-r_3}\|\boldsymbol{w}^{\mathrm{i}} - \boldsymbol{w}^{\mathrm{i}-1}\|_{V\times\Lambda} ,$$

which is the error estimate given in (4.17). This ends the proof. □

The elastic predictor

In the algorithm for the elastic predictor we take $\lambda^{*\mathrm{i}} = \lambda^{\mathrm{i}-1}$ and there is thus no need to define the functional $j^{(\mathrm{i})}$; that is, we assume zero plastic deformation. This is analogous to the nonlinear spring example presented in Section 4.1.1 where, for the elastic predictor, we assumed the spring stiffness was the initial constant spring stiffness. Convergence of the algorithm is guaranteed but the rate of convergence can be prohibitively slow for large computations.

The secant predictor

The algorithm corresponding to the secant predictor is obtained by choosing $D^{(\mathrm{i})}$ to be the quadratic function whose graph lies (at least locally around $\lambda^{\mathrm{i}-1}$) inside the cone with boundary the graph of D, and satisfying (4.12)–(4.13) as depicted in Fig. 4.6.

More precisely, for vectorial (λ, μ) we seek a vector $\boldsymbol{a}$ and a symmetric positive definite matrix $\boldsymbol{B}$ such that the function

$$D^i(\lambda) = D(\lambda^{\mathrm{i}-1}) + \boldsymbol{a}\cdot(\mu - \lambda^{\mathrm{i}-1}) + \tfrac{1}{2}(\mu - \lambda^{\mathrm{i}}) : \boldsymbol{B}(\mu - \lambda^{\mathrm{i}-1})$$

satisfies (4.12)–(4.14). We find that $\boldsymbol{a} = \nabla D(\lambda^{\mathrm{i}-1})$ and $\boldsymbol{B}$ is to be chosen such that

$$D(\mu) \leq D(\lambda^{\mathrm{i}-1}) + \nabla D(\lambda^{\mathrm{i}-1})\cdot(\mu - \lambda^{\mathrm{i}-1}) + \tfrac{1}{2}(\mu - \lambda^{\mathrm{i}}) : \boldsymbol{B}(\mu - \lambda^{\mathrm{i}-1})$$

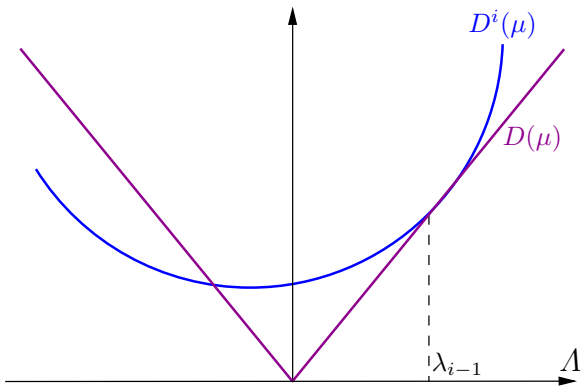

Fig. 4.6. Approximation D^{i} of D for the secant predictor

at least in a small neighbourhood of $\lambda^{\mathrm{i}-1}$. Then all of the conditions (4.12)–(4.14) are satisfied.

The consistent tangent predictor

Formulations in which the predictor step is consistent with the corrector step are termed consistent tangent formulations and the tangent matrix is the consistent tangent. Consistent predictors ensure that the algorithm converges quadratically as normally expected of a Newton–Raphson scheme when the tangent can be calculated directly. This seminal contribution to computational plasticity was made by Simo and Taylor [169] for the conventional dual problem. Bird and Martin [27] developed the equivalent consistent formulation within the context of the primal approach by defining the approximation $D^{(\mathrm{i})}$ as the second-order Taylor expansion of D about $\lambda^{\mathrm{i}-1}$; that is,

$$D^{\mathrm{i}}(\mu) = D(\lambda^{\mathrm{i}-1}) + \nabla D(\lambda^{\mathrm{i}-1}) \cdot (\mu - \lambda^{\mathrm{i}-1}) + \tfrac{1}{2}(\mu - \lambda^{\mathrm{i}-1}) : \left[\boldsymbol{H}(\lambda^{\mathrm{i}-1})](\mu - \lambda^{\mathrm{i}-1})\right] , \tag{4.39}$$

where $\boldsymbol{H}(\lambda^{\mathrm{i}-1})$ is the Hessian matrix of D at $\lambda^{\mathrm{i}-1}$; that is,

$$\boldsymbol{H} = \nabla^2 D(\lambda^{\mathrm{i}-1}) . \tag{4.40}$$

Use of the consistent tangent predictor as given in (4.39) is not guaranteed to produce monotonically convergent results as demonstrated by Martin and Caddemi [122] using the approach based on constructing minimising sequences. A line-search can be used in conjunction with the consistent–tangent predictor in order to recover monotonic convergence of the algorithm (see, for example, [32, 94] for further details).

An alternative approach to guarantee convergence of the algorithm corresponding to the consistent tangent predictor is to use the following modified second-order Taylor expansion of the function D about $\lambda^{\mathrm{i}-1}$:

$$\begin{aligned} D^{\mathrm{i}}(\mu) =& D(\lambda^{\mathrm{i}-1}) + \nabla D(\lambda^{\mathrm{i}-1}) \cdot (\mu - \lambda^{\mathrm{i}-1}) \\ &+ \tfrac{1}{2}(\mu - \lambda^{\mathrm{i}-1}) : [\boldsymbol{H}(\lambda^{\mathrm{i}-1}) + \epsilon \boldsymbol{I}](\mu - \lambda^{\mathrm{i}-1}) \,. \end{aligned}$$

Here $\boldsymbol{I}$ is the identity matrix of the same size as $\boldsymbol{H}(\lambda^{\mathrm{i}-1})$. In order that (4.14) is satisfied it is essential that $\epsilon > 0$, the magnitude of ϵ being chosen so that D^{i} satisfies (4.14) at least in a small neighbourhood of $\lambda^{\mathrm{i}-1}$.

4.2.2 Application of the solution algorithm to the discrete problem

To apply the abstract problem above to the discrete discontinuous Galerkin problem (4.6) we decompose the discrete bilinear form a_h as in (3.27)–(3.30) (the decomposition is performed in a manner similar to the proof of its coercivity in Lemma 3.2 in Chapter 3). The bilinear form and the decomposition was repeated at the beginning of this section.

The coercivity of the bilinear form $a_h(\cdot, \cdot)$, which is crucial in establishing the well-posedness of the discrete problem (4.6), was proven in Lemma 3.3 in the previous chapter. As remarked there, the choice of the positive constants η_1, η_2, η_3 is obtained provided that, in the case of softening behaviour, the parameter k_3 is sufficiently large. The parameter k_3 effectively introduces a physical length scale into the formulation. The influence of the length scale for problems with softening and hardening materials will be demonstrated using various example problems in Chapter 5.

Using the constants in Lemma 3.3 we apply Theorem 4.1 to obtain the following theorem on the convergence of the discrete problem.

Theorem 4.2. *Let β_1, β_2, η_1 and η_2 given by (3.36) and (3.42). For*

$$r_4 = \frac{(1 + c_1^{1/2})^2(\Lambda + 2\mu)^2}{r_1 r_2} < \frac{1}{3} \ , \tag{4.41}$$

$\lim_{i\to\infty} \|\boldsymbol{w}_h^{\mathrm{i}} - \boldsymbol{w}_h\|_h = 0$. *More precisely,*

$$\|\boldsymbol{w}_h^{\mathrm{i}} - \boldsymbol{w}_h\|_h \leq r_5 \|\boldsymbol{w}_h^{\mathrm{i}} - \boldsymbol{w}_h^{\mathrm{i}-1}\|_h \ , \tag{4.42}$$

where $(\boldsymbol{u}_h, \boldsymbol{\varepsilon}_h^p, \xi_h)$ is solution of (4.6) and $r_5 = \dfrac{2r_4}{1 - r_4}$.

4.3 Implementation of the predictor–corrector solution strategy

As mentioned previously, the presence of the Laplacian term in the yield function for the gradient plasticity formulation under consideration renders solution strategies devised for the classical problem inappropriate. In this section we detail a predictor–corrector strategy for the solution of the gradient plasticity problem using the finite element method that closely follows the well-established approach utilised for classical plasticity. In contrast to the classical problem, the estimation of the equivalent plastic strain in the corrector step for the gradient formulation is a nonlocal problem.

The predictor–corrector procedure described here is equivalent to the widely used Newton–Raphson solution strategy [123]. Indeed, we will exploit this relationship when developing the consistent tangent predictor for both classical and gradient plasticity. It will prove convenient to move between the dual and primal approaches when developing the algorithm. This is easily done, as demonstrated in the second example problem in Section 4.1.2, as the variational inequality governing the evolution of plastic flow becomes an equality during plastic flow.

As demonstrated previously in this chapter, it is the form of the predictor that determines the stability and accuracy of the algorithm. A predictor–corrector solution procedure is chosen here as the link to the underlying mechanical principles is strong [27] and can be readily exploited for the gradient problem at hand.

First we present a brief overview of some aspects of finite element method in order to clarify terminology and notation. Earlier chapters have introduced other finite element concepts and notation. Comprehensive expositions on this mature and extensive topic can be found in [175, 51, 102, 196], amongst others.

4.3.1 A brief overview of the finite element method

The coordinates of the local nodes of a generic element K are labelled in a counter-clockwise direction as follows:

$$\{\boldsymbol{X}^e_{\mathrm{a}} \in \mathbb{R}^{n_{\mathrm{dim}}} \ : \ \mathrm{a} = 1, \ldots, n^{\mathrm{e}}_{\mathrm{node}}\} \ .$$

The local node numbering $\boldsymbol{X}^e_{\mathrm{a}}$ is related to the global node numbering $\boldsymbol{X}_{\mathrm{A}}$ using standard conventions (see, for example, [102, 166]) according to

$$\boldsymbol{X}_{\mathrm{A}} = \boldsymbol{X}^e_{\mathrm{a}} \quad \text{with} \quad \mathrm{A} = ID(e, \mathrm{a}), \ e = 1, \ldots, n_{\mathrm{elem}}, \ \mathrm{A} = 1, \ldots, n_{\mathrm{node}} \ , \tag{4.43}$$

where the $n_{\mathrm{elem}} \times n^{\mathrm{e}}_{\mathrm{node}}$ array ID is defined by the global numbering system.

We denote by $N^{\mathrm{a}}(\boldsymbol{\xi})$ the local polynomial basis functions defined on the reference element $\hat{K} \in \square$, where $\boldsymbol{\xi} = (\xi, \eta) \in \square$ are coordinates (see Fig. 4.7). The local element shape functions are constructed so as to satisfy the completeness condition, that is $N^{\mathrm{a}}(\boldsymbol{\xi}_{\mathrm{b}}) = \delta_{\mathrm{ab}}$ where $\boldsymbol{\xi}_{\mathrm{b}}$ is the coordinate of node $\mathrm{b} \in \hat{K}$, as depicted in Fig. 4.8. The local element coordinate system is obtained from the reference element via the isoparametric map $\boldsymbol{\psi}^e$ as follows (see Fig. 4.7):

$$\boldsymbol{X}_h = \boldsymbol{\psi}^e(\boldsymbol{\xi}) = \sum_{\mathrm{a}=1}^{n^{\mathrm{e}}_{\mathrm{node}}} N^{\mathrm{a}}(\xi, \eta) \boldsymbol{X}^e_a \, .$$

The local shape functions are pieced together to yield the global finite element basis functions denoted $N^{\mathrm{A}} \ : \ \Omega \to \mathbb{R}, \ \mathrm{A} = 1, \ldots, n_{\mathrm{node}}$.

In a conforming finite element approximation certain problem-dependent continuity requirements need to be satisfied, while in the discontinuous Galerkin finite element method these requirements are imposed in a weak sense. For example, in

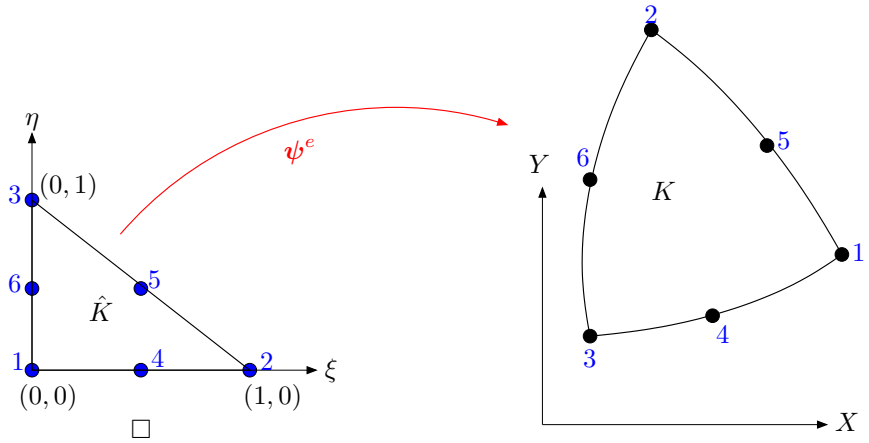

Fig. 4.7. The isoparametric map between the reference element $\hat{K}$ and a typical element K in the reference configuration

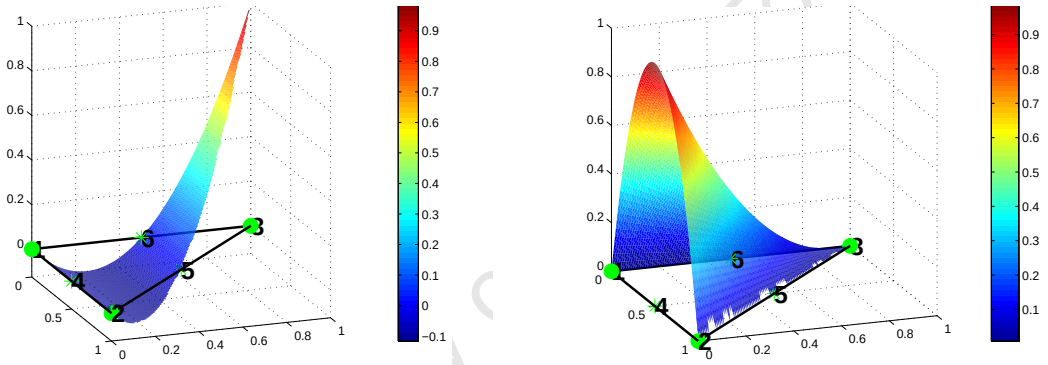

(a) N^3 (b) N^4

Fig. 4.8. The local element shape functions associated with nodes 3 and 4 of a quadratic triangular element

the case of conforming approximations of the elasticity or heat conduction problems we require global C^0 continuity of the approximation field; that is, the solution is in $H^1(\Omega)$. A discontinuous Galerkin approximation requires only that the approximate solution be in $L^2(\Omega)$. Figure 4.9(a) shows a conforming finite element approximation, obtained using the finite element code developed here, of the Poisson equation, while Fig. 4.9(b) shows the discontinuous Galerkin approximation. Figure 4.9(c) shows the effect of imposing interelement continuity poorly in the discontinuous Galerkin problem. Jumps in the approximation are clearly visible at element boundaries.

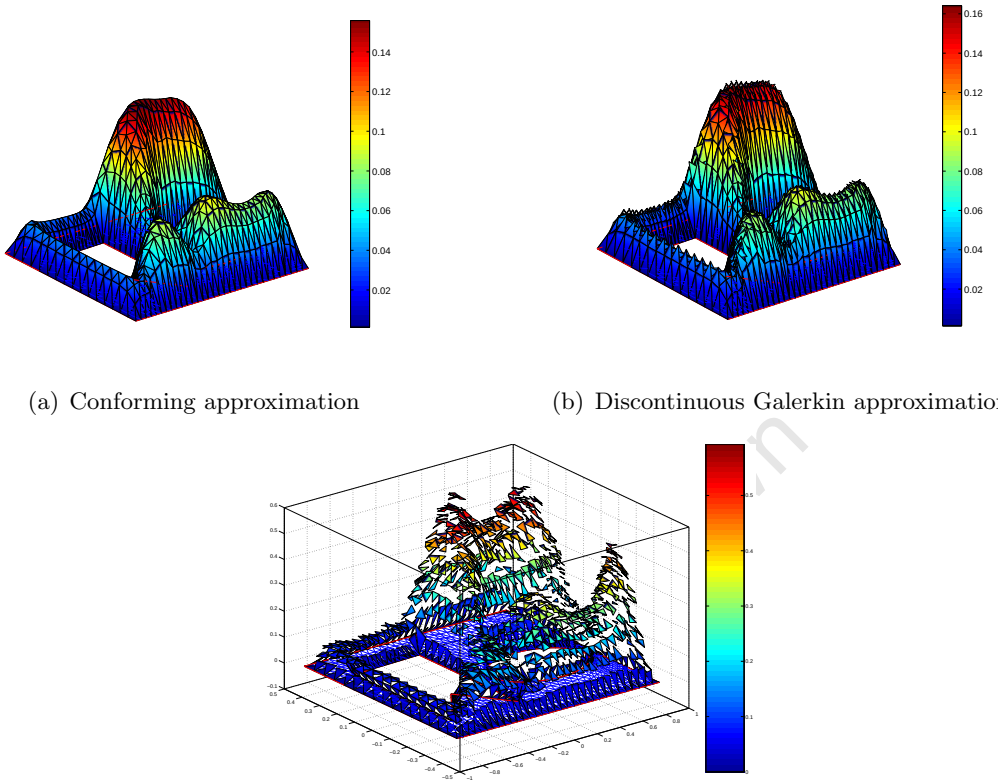

(a) Conforming approximation

(b) Discontinuous Galerkin approximation

(c) Discontinuous Galerkin approximation with a low penalty parameter

Fig. 4.9. Conforming and discontinuous Galerkin finite element approximations of the Poisson problem

We distinguish henceforth the element shape functions used to interpolate the displacement field, denoted N_{φ}^{A}, from those used to interpolate the internal hardening parameter field and denoted N_{γ}^{A}. The displacement field approximation, denoted $\boldsymbol{u}_h$, is written in terms of the nodal displacements $\boldsymbol{d}_{\mathrm{A}} \in \mathbb{R}^{n_{\mathrm{dim}}}$ as

$$\boldsymbol{u}_h(\boldsymbol{X}) = \sum_{\mathrm{A}=1}^{n_{\mathrm{node}}} N_{\varphi}^{\mathrm{A}}(\boldsymbol{X}) \boldsymbol{d}_{\mathrm{A}} \ .$$

Following standard Bubnov–Galerkin finite element procedure, an arbitrary test function $\boldsymbol{v}_h \in V_h$ is approximated from the nodal values, denoted $\boldsymbol{q}_A$, $\mathrm{A} = 1, \ldots, n_{\mathrm{node}}$, in the same manner as the displacement field as

$$\boldsymbol{v}_h(\boldsymbol{X}) = \sum_{\mathrm{A}=1}^{n_{\mathrm{node}}} N_{\varphi}^{\mathrm{A}}(\boldsymbol{X})\boldsymbol{q}_{\mathrm{A}} \ .$$

The approximation of the hardening parameter γ_h and arbitrary member $\eta_h \in M_h$ is done using a discontinuous Galerkin approximation and represented at element level by

$$\gamma_h^e = \sum_{\mathrm{a}=1}^{n^{\mathrm{e}}_{\gamma\mathrm{node}}} N_{\gamma}^{\mathrm{a}}\gamma_{\mathrm{a}}^e \qquad \text{and} \qquad \eta_h^e = \sum_{\mathrm{a}=1}^{n^{\mathrm{e}}_{\gamma\mathrm{node}}} N_{\gamma}^{\mathrm{a}}\eta_{\mathrm{a}}^e \,, \tag{4.44}$$

where $n^{\mathrm{e}}_{\gamma\mathrm{node}}$ denotes the number of nodes per element associated with the hardening parameter. The nodal values of the field are distinguished from the field itself via a subscript for the nodal point in the former. That is, $\gamma_h^e(\boldsymbol{X})$ refers to the value of the field at a point $\boldsymbol{X} \in K$, while γ_{a} refers to the value of the field at node a. This is done in an attempt to prevent the unnecessary proliferation of symbols.

The infinitesimal-strain field $\boldsymbol{\varepsilon}_h$ and the gradient of the hardening variable $\nabla\gamma_h$ are approximated at element level by

$$\boldsymbol{\varepsilon}_h^e = \left[\sum_{\mathrm{a}=1}^{n^{\mathrm{e}}_{\mathrm{node}}} \boldsymbol{u}_{\mathrm{a}}^e \otimes \nabla N_{\varphi}^{\mathrm{a}}\right]^{\mathrm{sym}} \ , \tag{4.45}$$

$$\nabla\gamma_h^e = \sum_{\mathrm{a}=1}^{n^{\mathrm{e}}_{\gamma\mathrm{node}}} \nabla N_{\gamma}^{\mathrm{a}}\gamma_{\mathrm{a}}^e \,. \tag{4.46}$$

The jump and average terms arising in the discontinuous Galerkin formulation are constructed from the finite element approximation fields evaluated on either side of the common edge between two neighbouring elements.

We shall occasionally adopt Voigt notation to represent the components of second- and fourth-order tensors as column vectors and matrices respectively. For a concise overview of Voigt notation the reader is referred to [23], amongst others. Variables expressed in Voigt notation are distinguished from their tensorial expression via the use of upright font. For example, the Voigt representation of the second-order strain tensor $\boldsymbol{\varepsilon}$ in $\mathbb{R}^3$ is

$$\boldsymbol{\varepsilon} = \Big[\varepsilon_{11}\ \varepsilon_{22}\ \varepsilon_{33}\ 2\varepsilon_{23}\ 2\varepsilon_{13}\ 2\varepsilon_{12}\Big]^T \ .$$

The relationship between the infinitesimal-strain field over an element and the vector of element nodal displacements, denoted $\boldsymbol{d}^e$, is expressed in Voigt notation as

$$\boldsymbol{\varepsilon}_h^e = \boldsymbol{B}_\varphi^e \boldsymbol{d}^e \ , \tag{4.47}$$

where the matrix $\boldsymbol{B}_\varphi$ contains the material gradients of the element shape functions obtained using the relationship

$$\frac{\partial N^{\mathrm{A}}(\boldsymbol{\xi})}{\partial \boldsymbol{X}} = \underbrace{\left[\frac{\partial \boldsymbol{X}_h^e(\boldsymbol{\xi})}{\partial \boldsymbol{\xi}}\right]^{-T}}_{\boldsymbol{J}(\boldsymbol{\xi})} \frac{\partial N^{\mathrm{A}}}{\partial \boldsymbol{\xi}} \ .$$

The matrix $\boldsymbol{J}(\boldsymbol{\xi})$ is referred to as the Jacobian matrix. The interpolation of the displacement field can be expressed in matrix format according to

$$\boldsymbol{u}_h^e = \boldsymbol{N}_\varphi \boldsymbol{d}^e \ .$$

The plastic strain field $\boldsymbol{\varepsilon}_h^p$ is able to be treated locally at the level of the quadrature point, as in the classical formulation, so that it requires no explicit representation.

The matrix representations of the fourth-order elasticity tensor $\mathcal{C}$ and the algorithmic consistent tangent constitutive tensor $\mathcal{C}^{\mathrm{con}}$ are given as C and $\mathrm{C}^{\mathrm{con}}$ respectively. The matrix associated with a general algorithmic tangent modulus is denoted $\mathrm{C}^\star$. The standard operation of assembling the local element contributions to the global structural level using the array ID is denoted $\mathop{\mathsf{A}}_{K}$.

4.3.2 Predictor–corrector solution strategy

An overview of the solution procedure is given in Alg. 4.2. The full state of the system is assumed known at the beginning of the current time step n from the equilibrium state at the end of the previous time step $\mathrm{n}-1$. The current iterate is denoted i and

the following notation adopted, as before, to distinguish between quantities updated in a total manner from the converged initial conditions at the beginning of the time step, and those updated from the previous iteration:

$$\Delta(\cdot) := (\cdot)^i_{\rm n} - (\cdot)^0_{\rm n} = (\cdot)^i_{\rm n} - (\cdot)_{\rm n-1} \quad \text{and} \quad \delta(\cdot) := (\cdot)^i_{\rm n} - (\cdot)^{i-1}_{\rm n} \ .$$

Unless explicitly stated otherwise, all quantities referred to at a specific iterate are for the current time step n, that is, $(\cdot)^i := (\cdot)^i_{\rm n}$. The subscript h, used to denote a finite-dimensional approximation, is dropped henceforth to simplify the notation. The assumption of linear isotropic hardening is made to simplify the subsequent presentation without loss of generality. Each of the steps in the algorithm are discussed in more detail in the sections that follow.

The predictor step

Irrespective as to the form of the approximation of the dissipation function, the predictor step can be linearised and expressed in matrix form as

$$\boldsymbol{K}^i \delta\boldsymbol{d} = \boldsymbol{F}_{\rm ext} - \boldsymbol{F}^i_{\rm int} = \boldsymbol{R}^i \,, \tag{4.48}$$

where the global stiffness matrix $\boldsymbol{K}$ is assembled from the element contributions as

$$\boldsymbol{K} = \mathop{\mathsf{A}}_{K\in\mathcal{T}_h} \boldsymbol{k}^e := \mathop{\mathsf{A}}_{K\in\mathcal{T}_h} \int_K \boldsymbol{B}^{e\,T}_{\varphi} \mathrm{C}^\star \boldsymbol{B}^e_{\varphi} \, dX \ .$$

The global vector of incremental nodal displacements is denoted $\delta\boldsymbol{d}$. The global vector field of prescribed nodal forces, denoted $\boldsymbol{F}_{\rm ext}$, contains components

$$\boldsymbol{F}^{\rm A}_{\rm ext} = \int_\Omega N^{\rm A}_\varphi \boldsymbol{B} \, dX + \int_{\Gamma_T} N^{\rm A}_\varphi \boldsymbol{t}^N \, dS \,, \qquad {\rm A} = 1, \ldots, n_{\rm node} \,,$$

and the global internal nodal force vector at the current iteration, denoted $\boldsymbol{F}_{\rm int}$, contains the components

$$\boldsymbol{F}^{\rm A}_{\rm int} = \int_\Omega \boldsymbol{\sigma}^i [\nabla N^{\rm A}] \, dX \,, \qquad {\rm A} = 1, \ldots, n_{\rm node} \,.$$

Algorithm 4.2 Algorithm for solution of the small-strain, gradient-enhanced discontinuous Galerkin plasticity problem at iteration i of time step n

Initial conditions
if $i == 0$ **then**
  Set tangent stiffness matrix to elastic stiffness matrix
  $\boldsymbol{K}_i = \boldsymbol{K}^{\text{elas}} := \mathop{\mathsf{A}}_{K\in\mathcal{T}_h} \int_K \boldsymbol{B}_\varphi^{e\,T} \mathrm{C} \boldsymbol{B}_\varphi^e \, dX$
  Assemble global external force vector $\boldsymbol{F}_{\text{ext}}$
  At each quadrature point $\boldsymbol{\sigma}_0 = \boldsymbol{\sigma}_{\text{n}-1}, \quad g_0 = g_{n-1}, \quad \gamma_0 = \gamma_{\text{n}-1}$
else
  Assemble tangent stiffness matrix $\boldsymbol{K}^i = \boldsymbol{K}_i^{\tan} := \mathop{\mathsf{A}}_{K\in\mathcal{T}_h} \int_K \boldsymbol{B}_\varphi^{e\,T} \mathrm{C}^\star \boldsymbol{B}_\varphi^e \, dX$
  Update all incremental quantities $(\cdot)_i = (\cdot)_{i-1}$
end if
Assemble internal force vector $\boldsymbol{F}_{\text{int}}$
Impose Dirichlet boundary conditions on Γ_φ
Predictor step
Solve $\boldsymbol{K}^i \delta\boldsymbol{d} = \boldsymbol{R}^i$ for incremental nodal displacements $\delta\boldsymbol{d}$
Update current total incremental displacement $\Delta\boldsymbol{d}^i = \Delta\boldsymbol{d}^{i-1} + \delta\boldsymbol{d}$
for each integration point **do**
  Calculate the total increment in strain $\Delta\boldsymbol{\epsilon} = \boldsymbol{B}_\varphi^e(\boldsymbol{X})\Delta\boldsymbol{d}$
  Calculate the trial stress $\boldsymbol{\sigma}^\star = \boldsymbol{\sigma}_0 + \mathcal{C}\Delta\boldsymbol{\varepsilon}$
  if $f(\boldsymbol{\sigma}^\star, g_0) < 0$ **then**
    Elastic state $\boldsymbol{\sigma}^i = \boldsymbol{\sigma}^\star$
  else
    Record the current quadrature point as active
  end if
end for
Corrector step
Assemble the unique set of active elements and neighbours $\mathcal{AE}$
Solve the discontinuous Galerkin problem (4.53) over $\mathcal{AE}$ for $\Delta\boldsymbol{\gamma}$
for each quadrature point in $\mathcal{AE}$ **do**
  Calculate $\nabla^2[\gamma]$ according to (4.54)
  Update g according to (4.55)
  Calculate the increment in plastic strain using (4.56) if quadrature point is active
  Update the stress if the quadrature point is active
end for
Check global convergence. If convergence is not attained, return to predictor step and increment i

The global nodal vector $\boldsymbol{R}^i$ is termed the residual.

The predictor step involves solving (4.48) for $\delta\boldsymbol{d}$. The total strain increment $\Delta\boldsymbol{\varepsilon}$ at each quadrature point in the domain is then obtained from the strain displacement relationship given in (4.47).

The proportion of the deformation that is plastic, if any, is not known at this point in the solution procedure. The identification of the active quadrature points is estimated locally by evaluating the yield condition under the assumption that the strain increment is completely elastic, that is, $\Delta\boldsymbol{\varepsilon}^p = \boldsymbol{0}$. The conjugate stress to this estimate of the elastic strain state is referred to as the trial stress and denoted by $\boldsymbol{\sigma}^\star$. The yield function evaluated using the trial stress state, termed the trial yield function, is denoted

$$f^\star := f\left(\boldsymbol{\sigma}^\star, g_0\right) = |\operatorname{dev}[\boldsymbol{\sigma}^\star]| - (\kappa - g_0) \ ,$$

where $\operatorname{dev}[\boldsymbol{\sigma}^\star] := 2\mu(\operatorname{dev}[\boldsymbol{\varepsilon}_{\mathrm{n}}] - \boldsymbol{\varepsilon}_0^p)$ is the trial stress deviator. If $f\left(\boldsymbol{\sigma}^\star, g_0\right) > 0$ then the quadrature point is deemed active, otherwise the quadrature point is inactive and the trial stress is the actual stress. Active quadrature points are recorded in the set $\mathcal{AP}$.

Updating of the variables is done in a "total incremental" manner as recommended by Pamin [145], amongst others; that is, in every iteration i total increments are determined from the converged state at the end of the previous step, to prevent spurious unloading. The product of the predictor step is thus the total strain increment at each quadrature point and the classification of each quadrature point as active or inactive based on the evaluation of $f^\star$.

Critical to the performance of the predictor–corrector solution algorithm is the formulation of the algorithmic consistent tangent modulus $\mathrm{C}^{\mathrm{con}}$, the derivation of which will be given shortly for both the classical and gradient cases.

The corrector step

In the corrector step we seek to determine the stress state arising from the strain field approximation obtained in the predictor step taking into account the possible evolu-

tion of plastic deformation. The presence of higher-order terms in the yield function for the gradient plasticity formulation under consideration negates the use of conventional return mapping algorithms, as detailed, for example, by Simo and Hughes [166], as the statement of the discrete consistency condition, that is $f(\boldsymbol{\sigma}_{\mathrm{n}}, g_{\mathrm{n}}) = 0$, used to determine the change in γ is no longer an algebraic one at the local level of the quadrature point, but rather a differential equation.

Furthermore, in contrast to the problem of classical plasticity, boundary conditions on the hardening parameter need to specified. The choice of appropriate boundary conditions is governed by the material and problem under consideration. These additional boundary conditions need to specified on the boundary of the elastoplastic domain, denoted $\partial\Omega^p$. The boundary $\partial\Omega^p$ can be in the interior of Ω or on the boundary of Ω as depicted in Fig. 4.10. These additional boundary conditions are specified explicitly when we present the example problems in the next chapter.

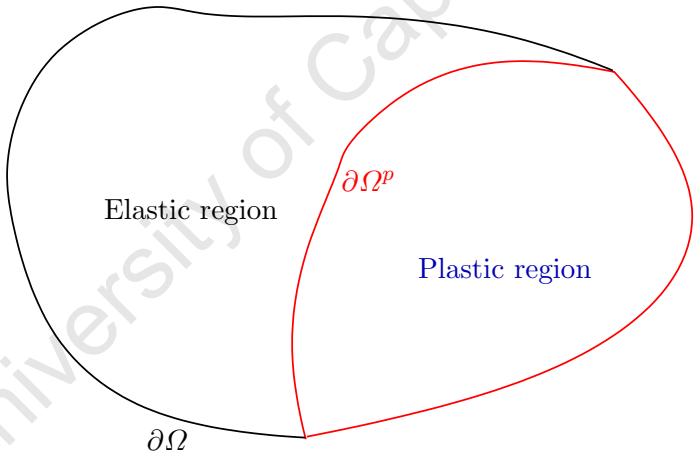

Fig. 4.10. Schematic of the domain Ω divided into elastic and plastic regions and the elastoplastic boundary

In this section we choose to solve the nonlocal statement of the flow law over an active subset of the domain as in de Borst and Pamin [63], Svedberg and Runesson [176] and Liebe and Steinmann [115], amongst others. The active subdomain is denoted by $\Omega^p \subseteq \Omega$. The identification of the active subdomain is achieved as follows. Firstly, the unique set of all elements containing active quadrature points, denoted $\mathcal{AE}$, is determined. The unique set of all elements in $\mathcal{AE}$ and elements that share a

common edge, denoted $\overline{\mathcal{AE}}$, is then determined. The unique set of all element edges in $\overline{\mathcal{AE}}$ is denoted $\mathit{\Gamma}_{\overline{\mathcal{AE}}}$. The union of all elements in $\overline{\mathcal{AE}}$ is the active subset Ω^p. The procedure outlined above is implemented in such a manner that multiple disconnected active regions can arise.

It should be noted that the method described above to determine the plastic subdomain is done at the element level. Thus, an element containing an active quadrature point is deemed active. For coarse meshes this could introduce errors. The discontinuous Galerkin methods appears to be a possible strategy to accurately resolve the moving elastoplastic boundary without resorting to local remeshing in the vicinity of the interface, a computationally expensive option. Dolbow and coworkers [69, 107, 106] have examined various finite element methodologies for evolving interface problems, including Nitsche's method [139], a symmetric interior penalty formulation. Hansbo and Larson [97] used Nitsche's method to impose the solid boundary in arbitrary Lagrange–Euler fluid–structure interaction problems. Other related work includes that of Rivière and Girault [158] on incompressible flows on subdomains with nonmatching interfaces and Duarte et al. [70] who use a discontinuous finite element formulation to model crack propagation in elastic domains. Furthermore, discontinuous Galerkin time integration schemes appear to be ideally suited to evolving interface problems, as demonstrated by Alberty and Carstensen [6].

The solution strategy adopted here solves the corrector step in two stages. In the first stage a nonlocal expression of consistency condition for the increment in the scalar hardening parameter $\Delta\gamma$ is solved using the symmetric interior penalty discontinuous Galerkin finite element formulation. In the second stage the value of $\Delta\gamma$ is used to determine the increment in plastic strain $\Delta\boldsymbol{\varepsilon}^p$ at active quadrature points.

Before proceeding, we state certain results. The discrete dissipation function $D(\Delta\boldsymbol{\varepsilon}^p)$ for the gradient problem with linear isotropic hardening is obtained from

$$\begin{aligned} D(\Delta\boldsymbol{\varepsilon}^p) &= \sup\left[\boldsymbol{\sigma}_{\mathrm{n}} : \Delta\boldsymbol{\varepsilon}^p\right] \\ &= \sup\left[\operatorname{dev}[\boldsymbol{\sigma}_{\mathrm{n}}] : \Delta\boldsymbol{\varepsilon}^p\right] \\ &= \sup\left[|\operatorname{dev}[\boldsymbol{\sigma}_{\mathrm{n}}]|\ |\Delta\boldsymbol{\varepsilon}^p|\right] \\ &= (\kappa - g_n)\,|\Delta\boldsymbol{\varepsilon}^p|\,. \end{aligned}$$

The steps in the derivation above are near-identical to those presented in the second example problem at the beginning of this chapter (see (4.3)).

Assuming plastic flow at the quadrature point under consideration, we have

$$\operatorname{dev}[\boldsymbol{\sigma}_{\mathrm{n}}] = \operatorname{dev}[\boldsymbol{\sigma}^{\star}] - 2\mu\boldsymbol{\nu}\Delta\gamma\,, \tag{4.49}$$

where the normal to the yield surface, denoted $\boldsymbol{\nu}$, is given by

$$\boldsymbol{\nu} = \frac{\operatorname{dev}[\boldsymbol{\sigma}]}{|\operatorname{dev}[\boldsymbol{\sigma}]|} = \frac{\operatorname{dev}[\boldsymbol{\sigma}^{\star}]}{|\operatorname{dev}[\boldsymbol{\sigma}^{\star}]|}\,.$$

Squaring the norm of both sides of (4.49) and recalling that $\Delta\gamma = \lambda = |\Delta\boldsymbol{\varepsilon}^{p}|$, we obtain

$$\begin{aligned}
|\operatorname{dev}[\boldsymbol{\sigma}_{\mathrm{n}}]|^2 &= |\operatorname{dev}[\boldsymbol{\sigma}^{\star}] - 2\mu\Delta\gamma\boldsymbol{\nu}|^2 \\
&= |\operatorname{dev}[\boldsymbol{\sigma}^{\star}]|^2 - 4\mu\Delta\gamma\operatorname{dev}[\boldsymbol{\sigma}^{\star}] : \boldsymbol{\nu} + 4\mu^2(\Delta\gamma)^2|\boldsymbol{\nu}|^2 \\
&= |\operatorname{dev}[\boldsymbol{\sigma}^{\star}]|^2 - 4\mu\Delta\gamma|\operatorname{dev}[\boldsymbol{\sigma}^{\star}]| + 4\mu^2(\Delta\gamma)^2 \\
&\qquad (\text{using } \operatorname{dev}[\boldsymbol{\sigma}^{\star}] : \boldsymbol{\nu} = |\operatorname{dev}[\boldsymbol{\sigma}^{\star}]| \text{ and } |\boldsymbol{\nu}| = 1) \\
&= (|\operatorname{dev}[\boldsymbol{\sigma}^{\star}]| - 2\mu\Delta\gamma)^2\,.
\end{aligned}$$

Thus, we have

$$|\operatorname{dev}[\boldsymbol{\sigma}]| = |\operatorname{dev}[\boldsymbol{\sigma}^{\star}]| - 2\mu\Delta\gamma\,. \tag{4.50}$$

A nonlocal variational expression of the consistency condition, equivalent to the weak form of the flow law in the primal form, is obtained by testing the local consistency condition $f(\boldsymbol{\sigma}_{\mathrm{n}}, g_{\mathrm{n}}) = 0$ with an arbitrary test function $\varrho \in M$ and integrating over the plastic subdomain Ω^{p}. This yields

$$
\begin{aligned}
0 &= \int_{\Omega^p} f\left(\boldsymbol{\sigma}_{\mathrm{n}}, \gamma_{\mathrm{n}}, \nabla^2[\gamma_{\mathrm{n}}]\right) \varrho \, dX \\
&= \int_{\Omega^p} \left(|\operatorname{dev}[\boldsymbol{\sigma}]_{\mathrm{n}}| - \left(\kappa - g(\gamma_{\mathrm{n}}, \nabla^2[\gamma_{\mathrm{n}}])\right)\right) \varrho \, dX \\
&= \int_{\Omega^p} \left(|\operatorname{dev}[\boldsymbol{\sigma}^\star]| - 2\mu\Delta\gamma - \left[\kappa - g\left(\gamma_0, \nabla^2\gamma_0\right) - g\left(\Delta\gamma, \nabla^2[\Delta\gamma]\right)\right]\right) \varrho \, dX \\
&\quad \text{(using (4.50))} \\
&= \int_{\Omega^p} \Big[|\operatorname{dev}[\boldsymbol{\sigma}^\star]| - 2\mu\Delta\gamma - \left(\kappa - g\left(\gamma_0, \nabla^2[\gamma_0]\right) - \left(-k_2\Delta\gamma + k_3\nabla^2[\Delta\gamma]\right)\right)\Big] \varrho \, dX \, .
\end{aligned}
$$

Rearranging, we obtain

$$
\begin{aligned}
&\int_{\Omega} \left((2\mu + k_2)\, \Delta\gamma - k_3\nabla^2[\Delta\gamma]\right) \varrho \, dX \\
&\quad = \int_{\Omega} \left(|\operatorname{dev}[\boldsymbol{\sigma}^\star]| - \left(\kappa - g\left(\gamma_0, \nabla^2[\gamma_0]\right)\right)\right) \varrho \, dX \\
&\quad = \int_{\Omega} f\left(\boldsymbol{\sigma}^\star, g_0\right) \varrho \, dX \, .
\end{aligned} \tag{4.51}
$$

In the absence of the higher-order terms (4.51) is equivalent to a nonlocal expression of the classical consistency condition. Indeed, the key steps in the derivation of (4.51) follow those used to obtain the local algebraic form of the consistency condition for classical plasticity as described by Simo and Hughes [166]. Thus (4.51) is the extension to gradient plasticity of the classical algebraic consistency condition.

Next we consider the symmetric interior penalty discontinuous Galerkin formulation corresponding to (4.51), which takes the form

$$
\begin{aligned}
&\mathop{\mathsf{A}}_{K\in\mathcal{AE}} \int_K \left[(2\mu + k_2)\, (\Delta\gamma^e)\, \varrho + k_3 \nabla[\Delta\gamma^e] \cdot \nabla\varrho \right] \, dX \\
&\qquad - \mathop{\mathsf{A}}_{\Gamma\in\Gamma_{\mathcal{AE}}} \int_\Gamma k_3 \left([\![\varrho]\!] \cdot \{\!\{\nabla[\Delta\gamma^e]\}\!\} + \{\!\{\nabla[\varrho]\}\!\} \cdot [\![\Delta\gamma^e]\!] \right) \, dS \\
&\qquad + \mathop{\mathsf{A}}_{\Gamma\in\Gamma_{\mathcal{AE}}} \int_\Gamma \frac{k_3\beta_2}{h_e} [\![\Delta\gamma^e]\!] \cdot [\![\varrho]\!] \, dS \\
&\qquad = \mathop{\mathsf{A}}_{K\in\mathcal{AE}} \int_K f\left(\boldsymbol{\sigma}^\star, g_0\right) \varrho \, dX \, .
\end{aligned} \tag{4.52}
$$

We have assumed here, without loss of generality, that either homogeneous Dirichlet or Neumann boundary conditions on the boundary of the active plastic subdomain $\partial\Omega^p$ are appropriate. This choice will be specified when presenting the example problems in Chapter 5. The spatially discrete form of the discontinuous Galerkin problem (4.52) can be obtained by approximating the trial and test functions using the approximations given in (4.46) resulting in the following matrix problem for the increment in the global nodal hardening parameter vector field (denoted $\Delta\boldsymbol{\gamma}$):

$$\boldsymbol{K}^{\gamma}\Delta\boldsymbol{\gamma} = \boldsymbol{F}^{\gamma}\,. \tag{4.53}$$

Equation (4.53) is solved for $\Delta\boldsymbol{\gamma}$ and the results extrapolated back to the quadrature points. An estimate for $\nabla^2[\Delta\gamma]$ is then obtained locally at quadrature point level using the yield condition as follows:

$$\nabla^2[\Delta\gamma] = \frac{(2\mu + k_2)\,\Delta\gamma - f\left(\boldsymbol{\sigma}^{\star}, g_0\right)}{k_3}\,. \tag{4.54}$$

The value of g_n is then updated at all quadrature points in $\overline{\mathcal{AE}}$ using the current estimates of $\Delta\gamma$ and $\nabla^2[\Delta\gamma]$, to obtain

$$g_{\mathrm{n}} = g_0 - k_2(\Delta\gamma) + k_3\nabla^2[\Delta\gamma]\,. \tag{4.55}$$

A crucial detail of the gradient formulation is that it allows for the spreading of the plastic zone for softening problems. This detail is essential to overcome the pathological behaviour associated with classical treatments of softening materials as it allows for the spreading of the localisation zone. The contribution of the Laplacian term can either increase or decrease the effective yield strength.

An idealised yield surface for a von Mises yield criterion with linear isotropic gradient dependent hardening is shown in Fig. 4.11 (adapted from [145]). The yield surface for the classical case is denoted $f(\boldsymbol{\sigma}, \bar{g}(\gamma)) = 0$ where the Laplacian contribution is zero. For the gradient plasticity formulation the presence of the Laplacian term will have an additional effect. A negative Laplacian contribution would increase the extent of the yield surface thereby giving the material additional load-carrying capacity.

Conversely, a positive Laplacian contribution would decrease the extent of the yield surface, thereby reducing the load-carrying capacity of the material. Also shown in Fig. 4.11 is an idealised distribution of γ for a problem in $\mathbb{R}$ in which a region of localised plastic flow occurs. The negative curvature of the γ curve in the middle of the localisation zone would increase the effective yield strength, giving this region additional load-carrying capacity. The positive curvature on the edges of the localised zone weaken the material, thereby allowing the plastic zone to spread. The spreading of the plastic zone is essential to overcome the pathological mesh-dependence, characterised by the localisation of the plastic zone to the element level, exhibited by classical analyses of softening problems.

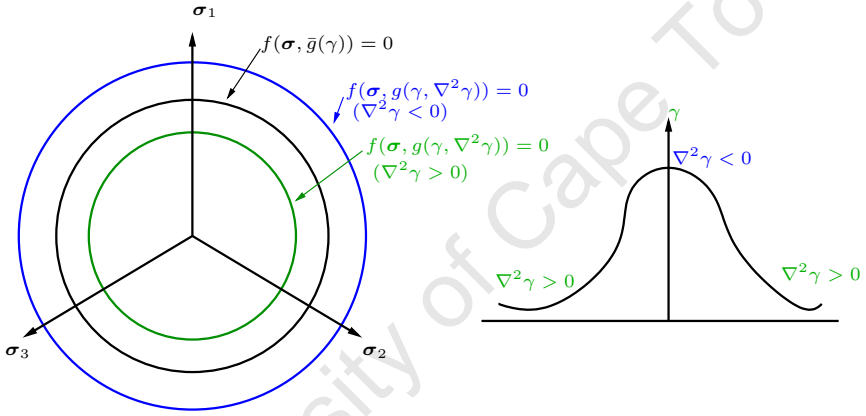

Fig. 4.11. The contribution of the gradient term to the yield strength (from [145])

The flow law may be written in the primal form, that is, $\boldsymbol{\sigma} \in \partial D(\Delta\boldsymbol{\varepsilon}^p) \Leftrightarrow \boldsymbol{\sigma} = \partial D/\partial(\Delta\boldsymbol{\varepsilon}^p)$ for $\Delta\boldsymbol{\varepsilon}^p \neq 0$, most conveniently using (2.6a) together with (2.3) and (2.6b), to give the time-discrete expression

$$2\mu\left(\boldsymbol{\varepsilon}_{\mathrm{n}} - \boldsymbol{\varepsilon}_0^p - \Delta\boldsymbol{\varepsilon}^p\right) = (\kappa - g_{\mathrm{n}})\,\frac{\Delta\boldsymbol{\varepsilon}^p}{|\Delta\boldsymbol{\varepsilon}^p|}\,, \tag{4.56}$$

which is solved locally at each active quadrature point for $\Delta\boldsymbol{\varepsilon}^p$ and the stress state at all active quadrature points calculated using

$$\boldsymbol{\sigma}^i = \boldsymbol{\sigma}_0 + 3\left(\Lambda + \tfrac{2}{3}\mu\right)\Delta\boldsymbol{\varepsilon}^S + 2\mu(\Delta\,\mathrm{dev}[\boldsymbol{\varepsilon}] - \Delta\boldsymbol{\varepsilon}^p)$$

in which $(\cdot)^S$ denotes the spherical part of a tensor.

The implementation of the corrector step resembles the cutting plane algorithm proposed by Simo and Taylor [169] for classical plasticity where successive return map iterations are performed onto an updated yield surface within the corrector step. A check on the satisfaction of the yield condition at the end of each cutting plane increment is performed to determine whether convergence has been obtained or if another iteration should occur. The yield condition is satisfied exactly if linear isotropic hardening is assumed.

4.3.3 Derivation of the algorithmic tangent modulus for classical and gradient plasticity

The convergence rate and stability of the predictor–corrector algorithm are governed by the form of the approximation of the dissipation function and the resulting algorithmic tangent modulus $\mathrm{C}^\star$ utilised in the predictor step. This was demonstrated for the simple example of a nonlinear spring earlier in this chapter. In order to preserve the quadratic rate of convergence associated with a typical Newton–Raphson solution scheme for the fully-discrete finite element problem of plasticity one needs the formulate the algorithmic tangent modulus in a manner that is consistent with the corrector step. This key contribution to the numerical solution of problems in plasticity was recognised by Simo and Taylor [169]. The derivation of an equivalent consistent algorithmic tangent modulus using the primal formulation of plasticity was initially considered by Bird and Martin [27]. The approach adopted here follows that of Simo and Taylor [169] for the dual formulation. The equivalent primal formulation is not given here but the key steps are given in Bird and Martin [27].

A consistent algorithmic tangent modulus for the case of gradient plasticity that correctly accounts for the form of the corrector step presented in the previous section is detailed here. First, however, some results pertaining to the classical problem are derived.

The fully-discrete form of the equilibrium statement reads

$$\mathop{\mathsf{A}}_{K\in\mathcal{T}_h}\Big[\int_K \boldsymbol{B}\cdot\boldsymbol{v}\;dX+\int_{\Gamma_T}\boldsymbol{t}^N\cdot\boldsymbol{v}\;dS\Big]=\mathop{\mathsf{A}}_{K\in\mathcal{T}_h}\int_K\boldsymbol{\sigma}_n\left(\boldsymbol{u}_n,\boldsymbol{\varepsilon}_n^p\right):\boldsymbol{\varepsilon}\left(\boldsymbol{v}\right)\;dX$$
$$=\mathop{\mathsf{A}}_{K\in\mathcal{T}_h}\int_K\mathcal{C}\left(\boldsymbol{\varepsilon}_n-\boldsymbol{\varepsilon}_0^p-\Delta\boldsymbol{\varepsilon}^p\right):\boldsymbol{\varepsilon}\left(\boldsymbol{v}\right)\;dX\;.$$

The above relationship can be restated using Voigt notation as

$$\mathop{\mathsf{A}}_{K\in\mathcal{T}_h}\Big[\int_K \boldsymbol{v}^T\boldsymbol{B}\;dX+\int_{\Gamma_T}\boldsymbol{v}^T\boldsymbol{t}^N\;dS\Big]$$
$$=\mathop{\mathsf{A}}_{K\in\mathcal{T}_h}\int_K\boldsymbol{v}^T\boldsymbol{B}^{eT}_{\varphi}\mathrm{C}\left(\boldsymbol{B}^e_{\varphi}\boldsymbol{d}^e_n-\boldsymbol{\varepsilon}_0^p-|\Delta\boldsymbol{\varepsilon}^p|\boldsymbol{\nu}\right)\;dX\;.$$

Substituting for $\boldsymbol{v}$ and $\boldsymbol{u}$ in terms of the basis functions, we obtain

$$\underbrace{\mathop{\mathsf{A}}_{K\in\mathcal{T}_h}\int_K\boldsymbol{B}^{eT}_{\varphi}\mathrm{C}\left(\boldsymbol{B}^e_{\varphi}\boldsymbol{d}^e_n-\boldsymbol{\varepsilon}_0^p-|\Delta\boldsymbol{\varepsilon}^p|\boldsymbol{\nu}\right)\;dX}_{\boldsymbol{F}(\boldsymbol{d})}$$
$$-\underbrace{\mathop{\mathsf{A}}_{K\in\mathcal{T}_h}\Big[\int_K\boldsymbol{N}^T\boldsymbol{B}\;dX+\int_{\Gamma_T}\boldsymbol{N}^T\boldsymbol{t}^N\;dS\Big]}_{\boldsymbol{g}}=\boldsymbol{0}\,. \tag{4.57}$$

The system of equations to be solved is hence $\boldsymbol{F}(\boldsymbol{d})-\boldsymbol{g}=\boldsymbol{0}$. A typical step in the Newton–Raphson scheme for the solution of (4.57) at iteration i of time step n reads

$$\boldsymbol{d}^i=\boldsymbol{d}^{i-1}-\underbrace{\left[\frac{\partial\boldsymbol{F}(\boldsymbol{d})^{i-1}}{\partial\boldsymbol{d}}\right]^{-1}}_{\boldsymbol{K}^{(i-1)}}\left(\boldsymbol{F}(\boldsymbol{d}^{i-1})-\boldsymbol{g}\right)\;.$$

Hence, a linearised approximation of $\dfrac{\partial\boldsymbol{F}(\boldsymbol{d})^{i-1}}{\partial\boldsymbol{d}}$ is sought that permits (4.57) to be expressed in the form

$$\left[\mathop{\mathsf{A}}_{K\in\mathcal{T}_h}\int_K\boldsymbol{B}^{eT}_{\varphi}\mathrm{C}^{\star}\,\boldsymbol{B}^e_{\varphi}\;dX\right]\;\delta\boldsymbol{d}-\boldsymbol{F}_{\text{ext}}+\boldsymbol{F}_{\text{int}}=\boldsymbol{0}\,.$$

We now consider the derivation of the algorithmic consistent tangent operator C^{con}.

Expanding $\dfrac{\partial\boldsymbol{F}(\boldsymbol{d})^{i-1}}{\partial\boldsymbol{d}}$ using index notation, we obtain, from (4.57),

$$\begin{aligned}
\frac{\partial F_A}{\partial d_B} &= \mathop{\mathsf{A}}_{K\in\mathcal{T}_h} \int_K B_{\varphi_{pA}} \mathrm{C}_{pq} \frac{\partial}{\partial d_B^e} \Big[B_{\varphi_{qC}} d_C - \varepsilon_{0q}^p - \Delta\gamma \boldsymbol{\nu}_Q \Big] \, dX \\
&= \mathop{\mathsf{A}}_{K\in\mathcal{T}_h} \int_K B_{\varphi_{pA}} \mathrm{C}_{pq} \Big[B_{\varphi_{qB}} - \frac{\partial\,(\Delta\gamma)}{\partial d_B^e} \boldsymbol{\nu}_q - \Delta\gamma \frac{\partial \boldsymbol{\nu}_q}{\partial d_B^e} \Big] \, dX \\
&= \mathop{\mathsf{A}}_{K\in\mathcal{T}_h} \int_K B_{pA}^u \mathrm{C}_{pq} \Big[B_{\varphi_{qB}} - \frac{\partial\,(\Delta\gamma)}{\partial \varepsilon_r} \frac{\partial \varepsilon_r}{\partial d_B} \boldsymbol{\nu}_q - \Delta\gamma \frac{\partial \boldsymbol{\nu}_q}{\partial \varepsilon_r} \frac{\partial \varepsilon_r}{\partial d_B} \Big] \, dX \\
&= \mathop{\mathsf{A}}_{K\in\mathcal{T}_h} \int_K B_{\varphi_{pA}} \mathrm{C}_{pq} \Big[B_{\varphi_{qB}} - \underbrace{\frac{\partial\,(\Delta\gamma)}{\partial \varepsilon_r}}_{(\star)} B_{\varphi_{rB}} \boldsymbol{\nu}_q - \Delta\gamma \underbrace{\frac{\partial \boldsymbol{\nu}_q}{\partial \varepsilon_r}}_{(\star\star)} B_{\varphi_{rB}} \Big] \, dX \,. \qquad (4.58)
\end{aligned}$$

We now seek expressions for $(\star)$ and $(\star\star)$.

The derivative of the normal to the yield function with respect to the total strain, that is $(\star\star)$, is the same for both the classical and gradient problems and is evaluated as

$$\begin{aligned}
\frac{\partial\,(\boldsymbol{\nu}_q)}{\partial \varepsilon_r} &= \frac{\partial}{\partial \varepsilon_r} \left(\frac{\mathrm{dev}[\boldsymbol{\sigma}^\star]_q}{|\boldsymbol{\sigma}^\star|} \right) \\
&= \frac{1}{|\,\mathrm{dev}[\boldsymbol{\varepsilon}] - \boldsymbol{\varepsilon}_0^p|} \left(\mathrm{dev}[I]_{rq} - \boldsymbol{\nu}_r \boldsymbol{\nu}_q \right) , \qquad (4.59)
\end{aligned}$$

where $\mathrm{dev}[\boldsymbol{I}]$ is the matrix representation of the deviatoric identity tensor

$$\mathrm{dev}[\boldsymbol{I}] = \bar{\boldsymbol{I}} - \tfrac{1}{3}\mathbf{1} \otimes \mathbf{1} \quad \text{where } \mathbf{1} = \{1\ 1\ 1\}^T \,.$$

The norm of a quantity expressed in Voigt notation is calculated in such a manner so that it is equivalent to the norm of the related tensorial quantity, that is $\|\boldsymbol{\sigma}\| = \|\boldsymbol{\sigma}\|$.

Classical plasticity

The difference in the derivation of the algorithmic consistent tangent modulus for the case of gradient plasticity lies in the evaluation of $(\star)$. In the classical formulation, the consistency condition is evaluated locally at the level of the quadrature point. Assuming plastic flow at the quadrature point under consideration,

$$
\begin{aligned}
0 &= f(\boldsymbol{\sigma}_{\mathrm{n}}, g_{\mathrm{n}}) \\
&= |\operatorname{dev}[\boldsymbol{\sigma}_{\mathrm{n}}]| - \kappa + g_{\mathrm{n}} \\
&= |\operatorname{dev}[\boldsymbol{\sigma}^{\star}]| - 2\mu\Delta\gamma - \kappa + g_0 - k_2\Delta\gamma \qquad \text{(using (4.50))}\,.
\end{aligned}
$$

Rearranging, we obtain the expression for the increment in $\Delta\gamma$ at the quadrature point as

$$
\Delta\gamma = \frac{f(\boldsymbol{\sigma}^{\star}, g_0)}{(2\mu + k_2)}\,. \tag{4.60}
$$

The partial derivative of $\Delta\gamma$ with respect to the strain for the classical plasticity problem can thus be expressed using index notation as

$$
\begin{aligned}
\frac{\partial\,(\Delta\gamma)}{\partial\varepsilon_r} &= \frac{1}{2\mu + k_2}\frac{\partial\,(f(\operatorname{dev}[\boldsymbol{\sigma}^{\star}], g_0))}{\partial\varepsilon_r} \\
&= \frac{2\mu}{2\mu + k_2}\frac{\operatorname{dev}[I]_{rq}\operatorname{dev}[\boldsymbol{\sigma}^{\star}]_q}{|\operatorname{dev}[\boldsymbol{\sigma}^{\star}]|} \\
&= \frac{2\mu}{2\mu + k_2}\boldsymbol{\nu}_r\,.
\end{aligned} \tag{4.61}
$$

Substitution of (4.59) and (4.61) into (4.58) gives an expression for $\dfrac{\partial \boldsymbol{F}(\boldsymbol{d})^{i-1}}{\partial \boldsymbol{d}}$, and hence for the algorithmic consistent tangent modulus for classical plasticity $\mathrm{C}_{\mathrm{cp}}^{\mathrm{con}}$, viz.

$$
\begin{aligned}
\frac{\partial \boldsymbol{F}(\boldsymbol{d})^{i-1}}{\partial \boldsymbol{d}} &= \mathop{\mathsf{A}}_{K\in\mathcal{T}_h}\int_K \boldsymbol{B}_{\varphi}^{T}\mathrm{C}\Big[\boldsymbol{B}_{\varphi} - \frac{2\mu}{k_2 + 2\mu}\boldsymbol{\nu}(\boldsymbol{B}_{\varphi}^{T}\boldsymbol{\nu})^{T} \\
&\quad - \frac{2\mu\Delta\gamma}{|\boldsymbol{s}^{\star}|}\left(\operatorname{dev}[\boldsymbol{I}]\boldsymbol{B}_{\varphi} - \boldsymbol{m}({\boldsymbol{B}_{\varphi}}^{T}\boldsymbol{m})^{T}\right)\Big]\,dX \\
&= \mathop{\mathsf{A}}_{K\in\mathcal{T}_h}\int_K \boldsymbol{B}_{\varphi}^{T}\underbrace{\left(\mathrm{C} - \frac{2\mu}{k_2 + 2\mu}\mathrm{C}\boldsymbol{\nu}\boldsymbol{\nu}^{T} - \frac{2\mu\Delta\gamma\mathrm{C}}{|\boldsymbol{s}^{\star}|}\left(\operatorname{dev}[\boldsymbol{I}] - \boldsymbol{\nu}\boldsymbol{\nu}^{T}\right)\right)}_{\mathrm{C}_{\mathrm{cp}}^{\mathrm{con}}}\boldsymbol{B}_{\varphi}\,dX\,.
\end{aligned}
$$

Gradient plasticity

The nonlocal expression for $\Delta\gamma$ for the case of gradient plasticity arising from the particular choice of corrector step made here is given in (4.53), from which we obtain

$$\begin{aligned}\Delta\boldsymbol{\gamma} &= [\boldsymbol{K}_\gamma]^{-1}\,\boldsymbol{F}^\gamma \\ &= [\boldsymbol{K}_\gamma]^{-1} \mathop{\mathsf{A}}_{K\in\mathcal{T}_h^\star} \int_K \boldsymbol{N}_\gamma{}^T f\left(\boldsymbol{\sigma}^\star, g_0\right)\, dX\,. \end{aligned} \tag{4.62}$$

The expression for $(\star)$ in (4.58) is obtained by taking derivatives of (4.62) with respect to ε to obtain

$$\begin{aligned}\frac{\partial\Delta\boldsymbol{\gamma}}{\partial\boldsymbol{\varepsilon}} &= [\boldsymbol{K}^\gamma]^{-1} \mathop{\mathsf{A}}_{K\in\mathcal{T}_h^\star} \int_K \boldsymbol{N}_\gamma{}^T \frac{\partial}{\partial\boldsymbol{\varepsilon}} \left(f\left(\boldsymbol{\sigma}^\star, g_0\right)\right)\, dX \\ &= [\boldsymbol{K}^\gamma]^{-1} \mathop{\mathsf{A}}_{K\in\mathcal{T}_h^\star} \int_K \boldsymbol{N}_\gamma{}^T \boldsymbol{\nu}\, dX\ , \quad \text{using (4.59)}\,. \end{aligned} \tag{4.63}$$

Substitution of (4.59) and (4.63) into (4.58) renders an expression for $\dfrac{\partial \boldsymbol{F}(\boldsymbol{d})^{i-1}}{\partial \boldsymbol{d}}$ and hence the algorithmic consistent tangent modulus for gradient plasticity $\mathrm{C}_{\mathrm{gp}}^{\mathrm{con}}$ as

$$\begin{aligned}&\frac{\partial \boldsymbol{F}(\boldsymbol{d})^{i-1}}{\partial \boldsymbol{d}} \\ &= \mathop{\mathsf{A}}_{K\in\mathcal{T}_h} \int_K \boldsymbol{B}_\varphi{}^T \mathrm{C}\Big[\boldsymbol{B}_\varphi - \frac{2\mu}{k_2+2\mu}\boldsymbol{\nu}(\boldsymbol{B}_\varphi{}^T\boldsymbol{\nu})^T \\ &\qquad - \frac{2\mu\Delta\gamma}{|\operatorname{dev}[\boldsymbol{\sigma}^\star]|}\left(\operatorname{dev}[\boldsymbol{I}]\boldsymbol{B}_\varphi - \boldsymbol{\nu}(\boldsymbol{B}_\varphi{}^T\boldsymbol{\nu})^T\right)\Big]\, dX \\ &= \mathop{\mathsf{A}}_{K\in\mathcal{T}_h} \int_K \boldsymbol{B}_\varphi{}^T \underbrace{\left(\mathrm{C} - \frac{2\mu}{k_2+2\boldsymbol{\nu}}\mathrm{C}\boldsymbol{\nu}\boldsymbol{\nu}^T - \frac{2\mu\Delta\gamma\mathrm{C}}{|\operatorname{dev}[\boldsymbol{\sigma}^\star]|}\left(\operatorname{dev}[\boldsymbol{I}] - \boldsymbol{\nu}\boldsymbol{\nu}^T\right)\right)}_{\mathrm{C}_{\mathrm{gp}}^{\mathrm{con}}} \boldsymbol{B}_\varphi\, dX\,. \end{aligned}$$

Remark 4.3. In general, the consistent tangent modulus is nonsymmetric due to the fact that the evolution equation or flow law involves only the deviatoric component of the stress tensor, while the full stress tensor is used in the equilibrium equation. The basis for the construction of the consistent tangent is to include an approximation for the evolution of plastic deformation into the equilibrium statement with the resulting loss of symmetry in the tangent modulus. This loss of symmetry is detrimental to the computational efficiency. Various approaches can be adopted to achieve a symmetric consistent tangent modulus. We adopt the approach implemented in [162, 78] and simply drop the skew part.

5

Numerical examples: small-strain gradient plasticity

The algorithm described in Chapter 4 for the approximation of the small-strain gradient plasticity problem is implemented within a finite element code and used to analyse two illustrative example problems. The finite element code was developed for the purpose of this project using the work of Carstensen and coworkers [7, 9, 40] as a basis. The example problems are chosen to assess the ability of the gradient formulation to overcome the well-documented pathological mesh-dependence associated with classical problems involving a softening material response, and, in addition, to investigate the influence of scale on the solution. Furthermore, a comparison of the efficiency of the consistent tangent and elastic predictor algorithms is presented. A discussion of various features of the discontinuous Galerkin approach to the solution of the corrector step is delayed until Chapter 9 where example problems in finite-deformation gradient plasticity are given.

Various approaches have hitherto been used in the numerical treatment of problems in gradient plasticity based upon a similar model to the one considered here. A distinguishing factor amongst these approaches is the use of either C^1 or C^0 approximations for the interpolation of the internal hardening parameter. The variational approach used to develop the weak form of the yield condition for the model of gradient plasticity considered here, as detailed in Chapter 2, uses an integration by parts procedure to convert the term involving the Laplacian of the internal hardening parameter to a volume integral over the plastic domain and an edge term on the elastic-plastic boundary. The discontinuous Galerkin approximation of the hardening parameter field requires only the approximate solution to be in $L^2(\Omega)$. An alternative

approach is to retain the Laplacian term in the weak form of the yield condition. In this case, C^1 interpolants of the hardening parameter field are required.

Either of the aforementioned approaches could easily be accommodated within the discontinuous Galerkin framework developed here. Indeed, the flexibility of the proposed discontinuous Galerkin formulation to potentially accommodate a variety of models of gradient plasticity is one of the motivations for this work. If required, C^1 continuity could be imposed using the continuous/discontinuous Galerkin approach of Engel et al. [74]. Furthermore, the continuous/discontinuous Galerkin method is an ideal candidate for models of gradient plasticity for which it is essential to impose C^1 continuity on the equivalent plastic strain variable; one such model is that proposed by Mülhaus and Aifantis [136] in which both the Laplacian and the biharmonic of the effective plastic strain enter the yield condition.

Lasry and Belytschko [111] used a C^1 finite element formulation in a gradient theory for one-dimensional rod and spherically symmetric problems, the gradient term serving to regularise the problem and in so doing to overcome problems associated with softening. De Borst and Mülhaus [62] derived a weak form of the gradient plasticity formulation proposed by Mülhaus and Aifantis [136] as well as the resulting finite element framework, and used C^1 continuous interpolants of the hardening parameter to accommodate the higher-order gradient terms. Pamin [145] and de Borst and Pamin [63] solved the gradient enhanced problem proposed in [62] by using both C^1 elements and C^0 elements with a penalty constraint. Related work, also using a conforming approximation, is that of Liebe and Steinmann [115]. De Borst et al. [64] extended their earlier work to include gradient damage within a gradient plasticity formulation. Other contributions concerned with gradient damage include the investigation by Wells et al. [188] in which the discontinuous Galerkin formulation is used to deal with the higher-order continuity requirements that arise. The work of Garikipati [82] explored a variational multiscale approach to a model of gradient plasticity proposed by Fleck and Hutchinson [80]. Other key contributions to the numerical simulation of problems of gradient plasticity include those presented in [58, 57, 114, 177, 18, 178, 195, 116, 5], amongst others.

The finite element code developed here was validated in [153, 124] against a series of benchmark problems in classical plasticity.

5.1 Numerical examples

Conforming quadratic interpolation functions are used to approximate the displacement field and nonconforming linear interpolation functions the isotropic hardening parameter. The domain of the problem is discretised in a manner such that the edges of the quadratic triangular elements are straight in the reference configuration. This is done to allow the same mesh to be used for the interpolation of both the displacement and internal hardening parameter fields.

It should be noted that the analysis presented previously only requires the use of a linear approximant for the displacement and constant for the hardening parameter (see Section 2.2). The particular form of the corrector step employed to solve the fully-discrete problem requires the evaluation of the gradients of γ and hence a linear interpolation of γ is employed. The additive decomposition of the strain would imply that that the strain interpolation should be of the same order as the interpolation of $\gamma = |\Delta \boldsymbol{\varepsilon}^p|$. The displacements should therefore be of one order higher than the strain interpolants and, hence, quadratic. In addition, the choice of quadratic elements potentially circumvents problems associated with the volumetric locking of low-order elements. As mentioned previously, a discontinuous Galerkin approximation of the displacement field could also be used to circumvent locking, see, for example, [190, 180].

The use of high-order elements for the interpolation of the displacement field is not, however, recommended for large deformation problems due to the additional computational expense and their susceptibility to deform excessively when compared to low-order elements. Bilinear Q_1 elements are used when considering finite deformation problems in Part II of this work. The method of enhanced assumed strains [165] is used to circumvent locking.

The additional, higher-order boundary conditions arising due the gradient plasticity formulation are assumed as follows. As in [145, 150] and others, homogeneous

Dirichlet boundary conditions are assumed on the part of $\partial\Omega^p$ internal to Ω while homogeneous Neumann conditions are assumed on $\partial\Omega^p$ when the plastic boundary and the boundary of the domain coincide; that is,

$$\gamma = 0 \quad \text{on } \partial\Omega^p \in \Omega \qquad \text{and} \qquad -\boldsymbol{m}\cdot\boldsymbol{N} = 0 \quad \text{on } \partial\Omega^p \subset \partial\Omega\,.$$

Further discussion on the physical implications of the additional boundary conditions that arise in gradient plasticity formulations can be found in Gurtin [89, 90] and Peerlings [146].

The form of the von Mises yield criterion used in the numerical examples is

$$f(\boldsymbol{\sigma}, g) = |\operatorname{dev}[\boldsymbol{\sigma}]| + \sqrt{\tfrac{2}{3}}\,(\sigma_y - g) \leq 0\ , \tag{5.1}$$

where σ_y is the one-dimensional flow stress. Plane strain conditions are assumed applicable in all examples presented; that is $\boldsymbol{\varepsilon}_{i3} = 0$ $(i = 1, 2, 3)$. In addition, the value of the penalty constant β_2, see (4.52), is specified as 10^{10} for all example problems. The effect of the varying the penalty parameter will be demonstrated in Chapter 9 in the context of the finite-deformation problem.

5.1.1 Shear band formation in a rectangular plate with a small initial imperfection subjected to compressive loading

The example problem initially analysed by Pamin [145], and subsequently in [75, 4, 109], amongst others, is slightly modified here and analysed using the classical and gradient plasticity formulations. The rectangular specimen shown in Fig. 5.1 is subjected to a rate-controlled compressive loading on the upper edge. The lower edge is prevented from displacing vertically but is free to translate horizontally. In order to provide sufficient constraint, the point in the middle of the lower edge is also prevented from moving horizontally. The boundary conditions imposed by Pamin [145] differ in that the left-hand edge is stated to be a symmetry plane, but plots of the displaced configuration appear to contradict this and support the boundary conditions imposed here. In addition, the simulations performed in [4, 5] intend to replicate those performed by Pamin but impose the boundary conditions used here.

A material imperfection is introduced by reducing the yield strength of a 10 mm square region in the lower left corner of the domain. The shear band arising during loading is completely free to follow any path. The area of reduced initial yield strength is relatively small, and hence can be viewed as an imperfection as opposed to an inhomogeneity. The material properties of the domain are listed in Table 5.1.

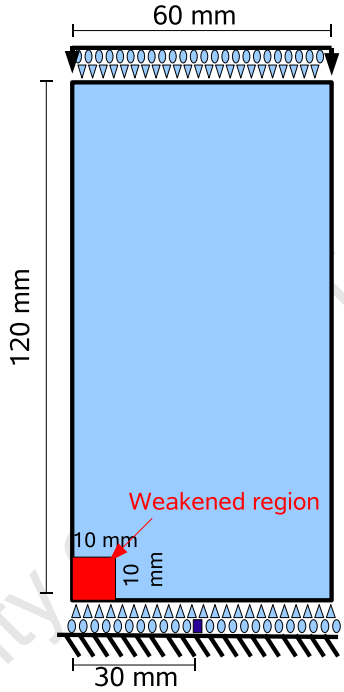

Fig. 5.1. Diagram of the rectangular plate subjected to compressive loading

Table 5.1. Material properties for the problem of a rectangular plate subjected to compressive loading

Young's modulus	$E = 11920$ N/mm^2
Poisson's ratio	$\nu = 0.49$
Yield stress	$\sigma_Y = 100$ N/mm^2
Isotropic hardening constant	$k_2 = -400$ N/mm^2
Gradient hardening constant	$k_3 = 3600$ N

The various meshes investigated are shown in Fig. 5.2. Both structured and unstructured meshes, and structured meshes of varying ratios of the number of horizontal

to vertical elements are investigated to determine the effect of mesh density and mesh orientation on the solution. Solution sensitivity to mesh orientation is another characteristic of pathological mesh-dependence exhibited by classical solutions to softening problems.

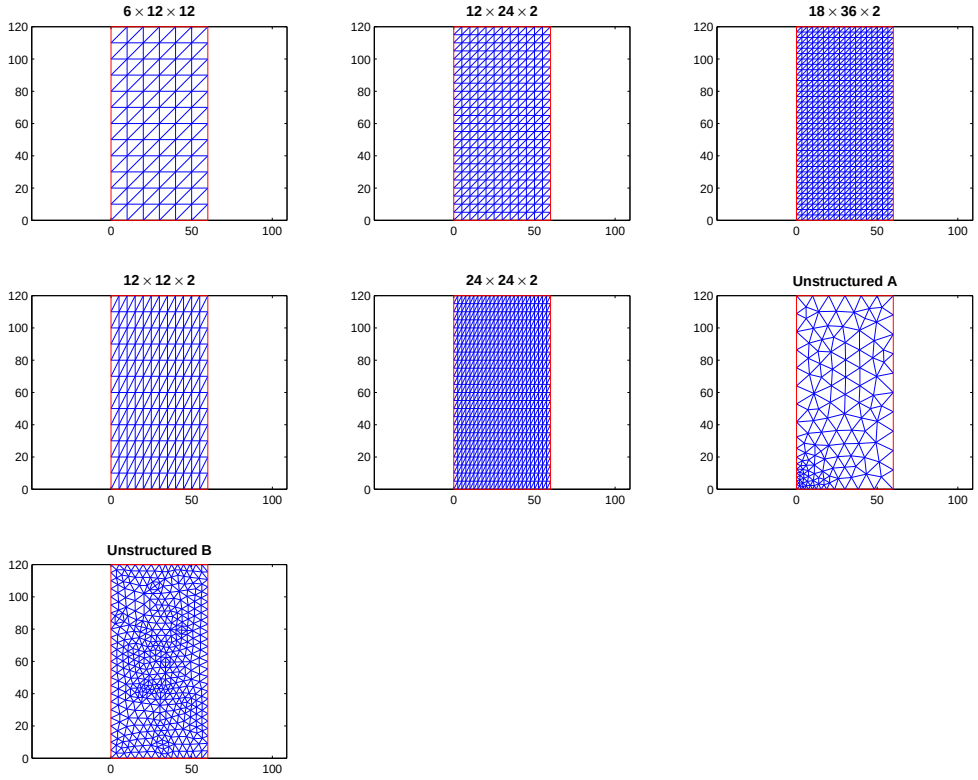

Fig. 5.2. Various discretisations of the rectangular plate using triangular elements

The force on the upper edge of the domain as a function of the imposed displacement for the various configurations analysed is shown in Fig. 5.3. The two solutions obtained using the classical approach demonstrate the widely documented pathological mesh-dependence. Fig. 5.3 clearly shows the ability of the gradient formulation proposed here to predict converging mesh-independent results for the softening problem. The coarser the mesh, the fewer the number of degrees of freedom, and the more rigid the response. The results converge as the number of degrees of freedom in-

creases. In addition, the results predicted using the unstructured mesh coincide with those obtained using the structured meshes upon refinement, once again indicating a mesh-independent solution.

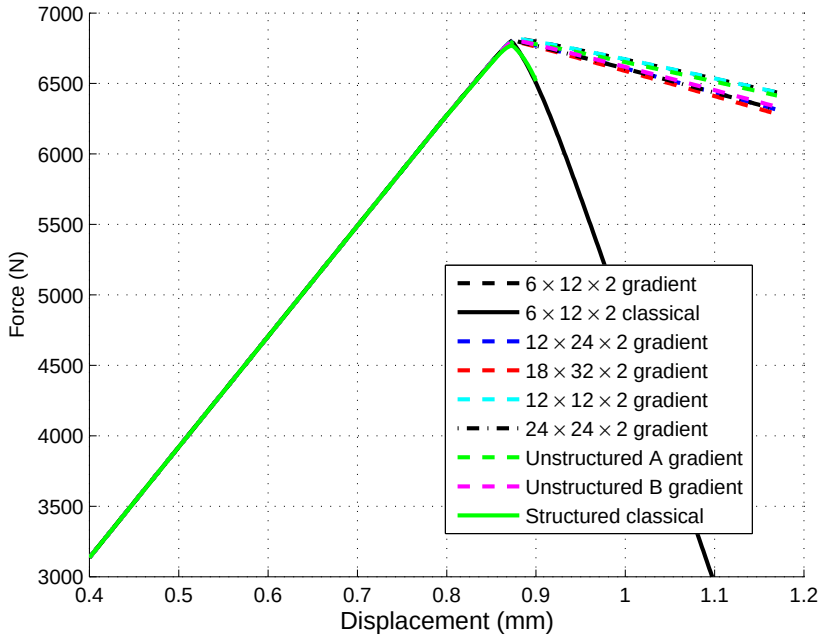

Fig. 5.3. Reaction force versus the prescribed displacement of the top edge of the plate

The extent of the shear band at the end of the imposed loading regime for the various meshes analysed is shown in the plot of the ratio of the von Mises effective stress $\sigma_e := \frac{1}{\sqrt{2}}|\operatorname{dev}[\boldsymbol{\sigma}]|$ to the effective yield stress $\sigma_e^y := \frac{1}{\sqrt{3}}(\sigma_y - g)$ superimposed upon the deformed domain in Fig. 5.4. Figures 5.4(a) – 5.4(c) show the results for the structured meshes with a ratio of one element in the horizontal direction to two in the vertical. It is clear that the shear band converges to a fixed width upon refinement of the regular mesh. That the width of the shear band is governed by the internal length scale $l := \sqrt{\operatorname{abs}[k_3/k_2]}$ will be demonstrated shortly. The shear band localises to the width of a single element for the classical plasticity solution as shown in Fig. 5.4(i). The rest of the domain then unloads elastically and all plastic deformation is concentrated in this narrow band resulting in severe element distortion.

The high degree of element distortion coupled with the rapid loss of residual strength in the shear band are the reasons for the inability of the numerical implementation of the classical solution used here to produce convergent results for more refined meshes.

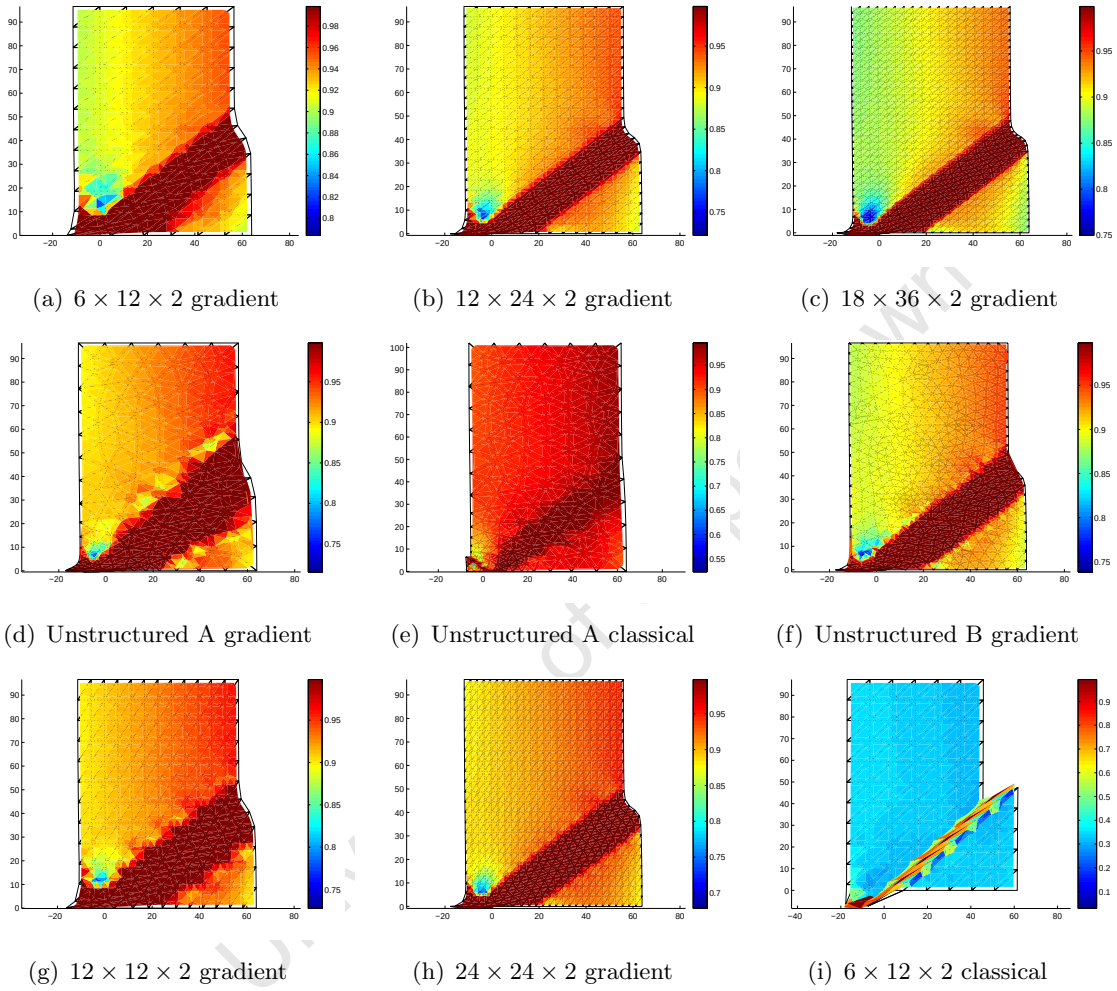

(a) $6 \times 12 \times 2$ gradient (b) $12 \times 24 \times 2$ gradient (c) $18 \times 36 \times 2$ gradient

(d) Unstructured A gradient (e) Unstructured A classical (f) Unstructured B gradient

(g) $12 \times 12 \times 2$ gradient (h) $24 \times 24 \times 2$ gradient (i) $6 \times 12 \times 2$ classical

Fig. 5.4. The deformed domain showing the ratio of the von Mises effective stress to the effective yield stress

Two unstructured meshes, labelled A and B respectively, are analysed. Unstructured mesh A is relatively fine in the vicinity of the imperfection, becoming coarser further away. Unstructured mesh B is uniformly unstructured across the domain. The predicted width of the shear band for mesh A is in good agreement with that predicted by the finest structured mesh shown in Fig. 5.4(c). The agreement becomes

less good as the unstructured mesh becomes coarser. The lack of agreement away from the imperfection is not indicative of pathological mesh-dependence but rather that the unstructured mesh is too coarse. The width of the shear band obtained using unstructured mesh B is in good agreement with that shown in Fig. 5.4(c) for the finest structured mesh analysed.

The solution obtained for the unstructured mesh A using the classical plasticity formulation is different in nature to the gradient and the other classical solutions presented. A small shear band develops in the region containing the imperfection, spreading from the top left corner to the bottom right corner of the region. The shear band then continues across the domain in the same manner as the other examples. A comparison of the position of the active quadrature points superimposed upon the deformed domain, shown in Fig. 5.5, clearly indicates the fundamentally different nature of the solutions. The small shear band in the imperfection results in intense localisation behaviour occurring while other quadrature points in the region unload elastically. As demonstrated by Pamin [145], the choice of a particular solution for softening problems using a gradient plasticity formulation depends on the distribution of imperfections, the presence of symmetry breaking factors (for example, boundary conditions) and the numerical algorithm, but not on the imperfections dimensions. This is not the case for the classical problem where the mesh can dictate the failure mechanism that occurs and hence the solution.

The lack of influence that mesh orientation has on the gradient enhanced solution is shown in Figs 5.4(g) and 5.4(h) where the number of elements in the horizontal and vertical directions are equal. The width and direction of the shear band are in good agreement with the most refined structured and unstructured solutions.

In order to obtain a mesh-independent solution in the softening regime, the width of the shear band should be governed by the internal length scale and not the discretisation. In order to verify this for the gradient formulation, the example problem is analysed using three different internal length scales (3 mm, 2 mm and 1 mm respectively) while keeping the discretisation constant (the $12 \times 24 \times 2$ mesh is used). The predicted relationship between the prescribed displacement of the upper edge and the reaction force acting thereon is shown in Fig. 5.6. It is clear that the internal

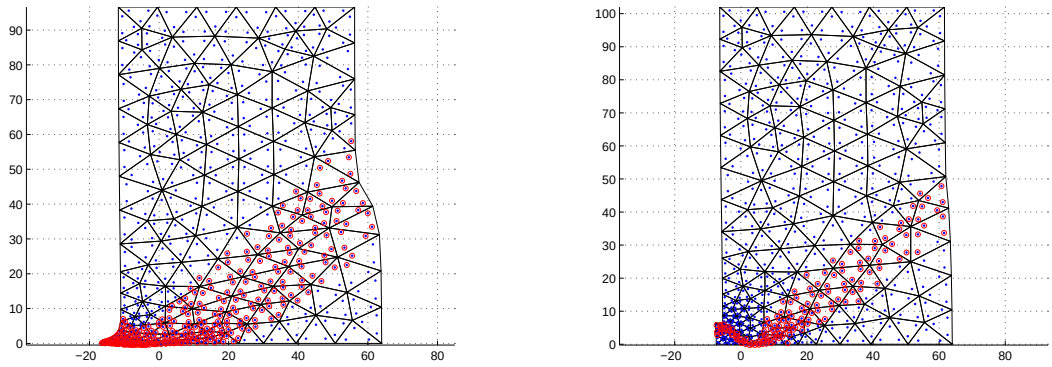

(a) Unstructured gradient

(b) Unstructured classical

Fig. 5.5. The deformed domain with the position of the quadrature points superimposed. Inactive quadrature points are coloured blue and active quadrature points red

length scale dictates the strength of the system, that is, the ability of the domain to withstand the applied loading, with a larger internal length scale resulting in a more resilient structure. The domain becomes weaker as the internal length scale is decreased. Also shown in Fig. 5.6 is a plot of the yield ratio (i.e. σ_e/σ_y^e) superimposed upon the deformed domain for the various length scales. The larger the length scale the thicker the shear band. As the width of the internal length scale decreases, so the results begin to resemble those of the classical solution with intense deformation occurring in a band of diminishing width.

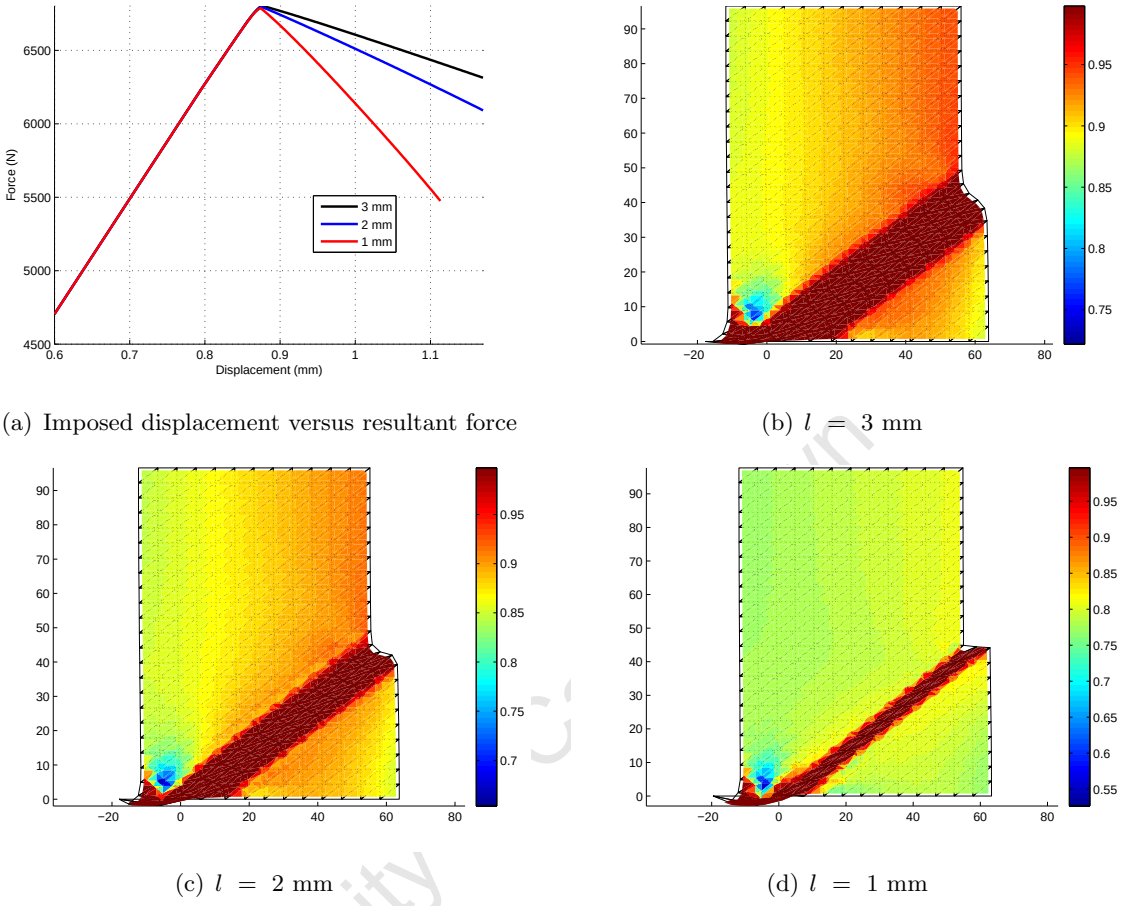

(a) Imposed displacement versus resultant force

(b) $l = 3$ mm

(c) $l = 2$ mm

(d) $l = 1$ mm

Fig. 5.6. The relationship between the prescribed displacement and the resultant force acting on the upper edge, and the deformed domain with the yield ratio superimposed for various internal length scales

5.1.2 Scale effects in microindentation tests on a rectangular specimen

The absence of a length scale in classical continuum mechanics renders the formulation scale-independent. Thus, the resulting classical finite element formulations are also independent of any scale other than that provided by the discretisation itself. Scale-independence is an appropriate assumption when considering a large class of engineering applications at the macroscale. The images shown in Fig. 5.7, adapted from [1], shows the relative scale of various human fabricated and natural objects. The influence of scale when simulating material at the microscale cannot, however, be ignored. For example, microindentation experiments indicate that the microhardness is significantly influenced by the indentation depth (see, for example, [174, 118, 22, 127, 140, 161]), with smaller being stronger. The increased hardening can be explained by noting that the large strain gradients present in small indentations lead to the formation of geometrically necessary dislocations resulting in increased hardening [118, 80]. Statistically stored dislocations arise due to homogenous deformations while geometrically necessary dislocations are related to the curvature of the crystal lattice (or the strain gradient). The concept of statistically stored and geometrically necessary dislocations was originally conceived by Ashby [16] in the early 1970s. The length scale present in gradient plasticity formulations allows the presence of scale effects to be accounted for naturally. This has been demonstrated in various microindentation simulations using gradient enhanced finite element formulations (see, for example, [22, 193, 194, 184], amongst others).

The microindentation of a small specimen of width $2L$ and depth L, shown in Fig. 5.8(a), is analysed here to assess the ability of the gradient formulation to capture size effects. The simulated indentation test is not intended to replicate an actual experiment, but rather to capture the salient features of microindentation. As such, linear isotropic hardening is assumed. In addition, the circular tip indenter of radius $r = 0.025H$ is rigidly attached to the specimen, and moves downwards at a constant rate into the specimen. The indenter is initially embedded within the specimen at a depth of r and the domain assumed stress free. The depth of penetration is measured from this initial embedded depth. The dimensions of the indenter are small compared to the extent of the specimen to minimise edge effects. The material properties of the

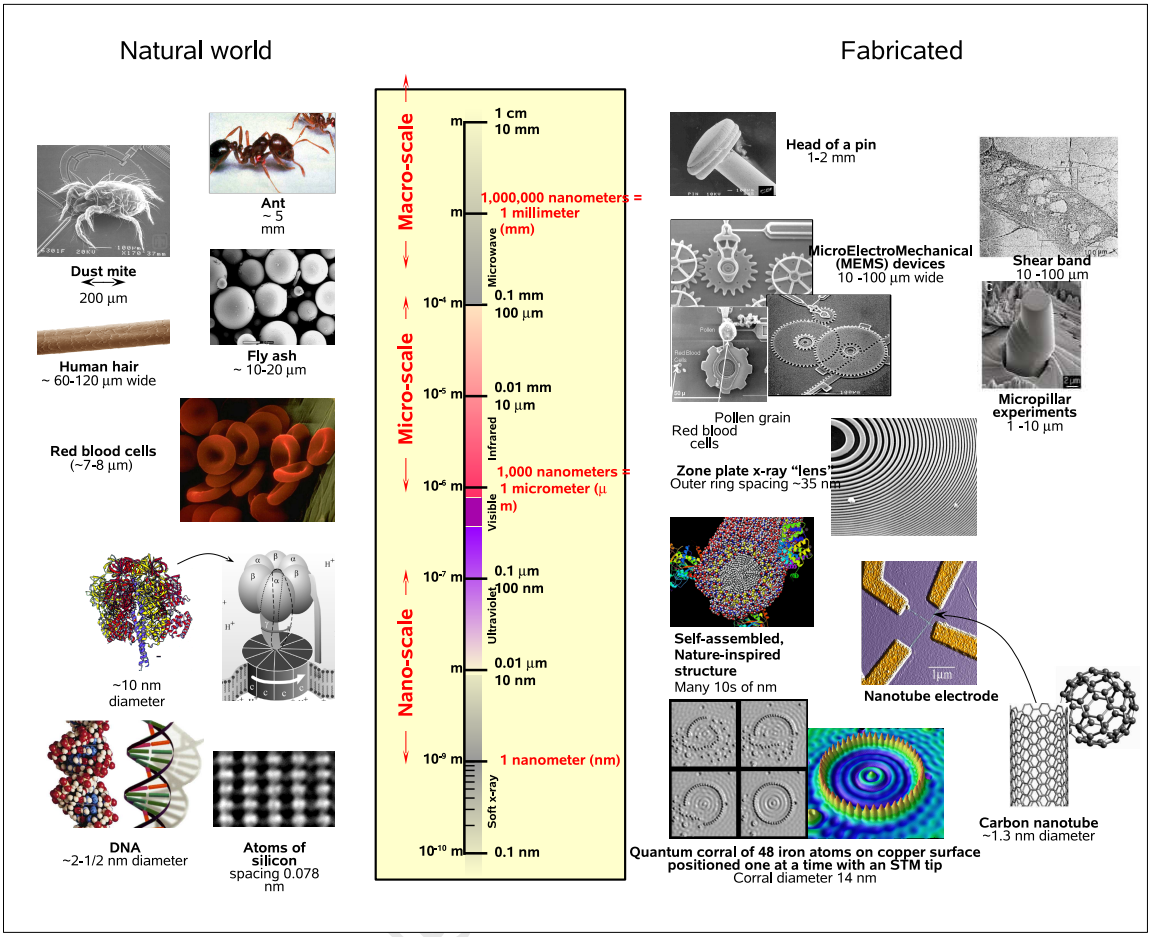

Fig. 5.7. The relative scale of human fabricated and natural objects (from [1])

specimen are listed in Table 5.2. Three different ratios of specimen width to internal length scale are analysed ($L/l = 33.3$, $L/l = 50$ and $L/l = 100$) using the finite element mesh shown in Fig. 5.8(b). The unstructured mesh is more refined in the region close to the indenter tip. Due to the symmetry of the problem, only half of the domain is analysed and the appropriate symmetry boundary conditions imposed. The lower and right boundaries are assumed fixed.

The net force acting on the indenter tip as a function of the ratio of the indentation depth to the specimen depth is shown in Fig. 5.9 for both the gradient and classical plasticity formulations. The gradient results are clearly influenced by the relative scale of the problem, with smaller being stronger. The indentation depth at which plastic

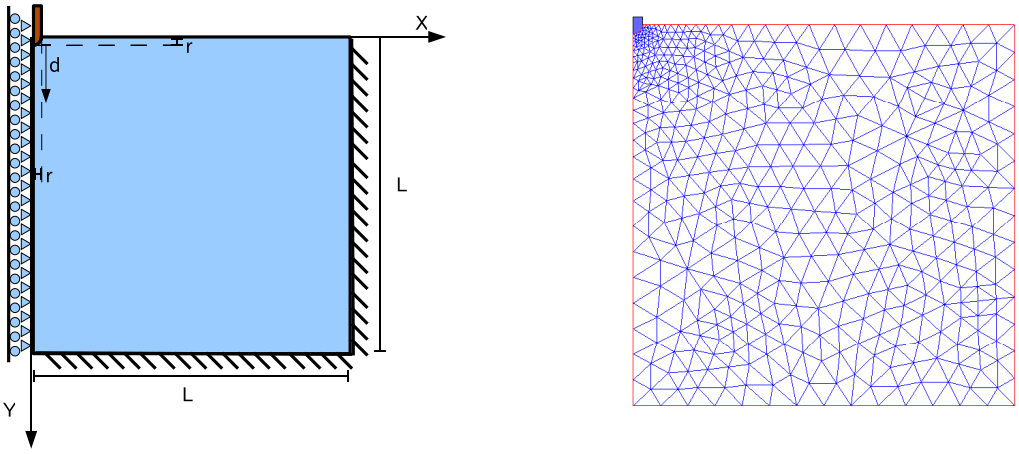

(a) Diagram of the microindentation problem

(b) Finite element mesh

Fig. 5.8. Diagram of the microindentation test and the triangulation of the domain

Table 5.2. Material properties for the microindentation problem

Young's modulus	$E = 11920$ N/mm^2
Poisson's ratio	$\nu = 0.3$
Yield stress	$\sigma_Y = 450$ N/mm^2
Isotropic hardening constant	$k_2 = 458$ N/mm^2

flow is detected is the same for all problems and formulations as indicated in Fig. 5.9. The extent of the active plastic zone predicted for the various ratios of L to l in the gradient formulation and the classical formulation are shown in Fig. 5.10, where the shaded elements contain active quadrature points. The presence of the Laplacian term in the yield function of the gradient formulations allows the active zone to spread further than for the classical formulation at the same indentation depth. The active zone is more extensive for the smaller ratios of L to l (i.e. smaller specimens) and decreases upon increasing specimen size.

The simulated microindentation results demonstrate that the proposed gradient formulation is capable of predicting scale-dependent effects.

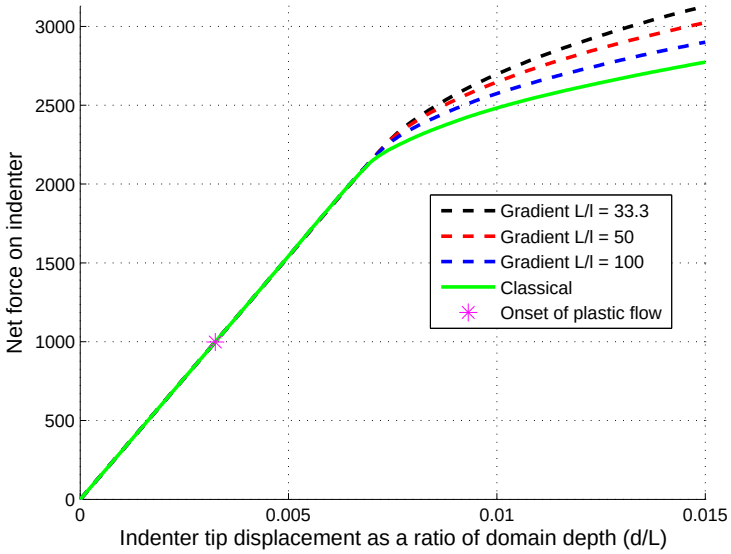

Fig. 5.9. The resulting force acting on the indenter as a function of the ratio of the indentation depth d to the domain length L

5.1.3 Comparison of the performance of the solution algorithm using the consistent tangent and elastic predictors

The motivation for the development of a consistent predictor step incorporating the algorithmic consistent tangent modulus was to reduce the computational expense of the solution procedure. It is well known that for classical finite element problems in plasticity convergence is achieved in far fewer iterations when using the consistent tangent as opposed to the elastic predictor (see, for example, [169, 25, 166]). The number of iterations required to reach convergence should, however, not be the only criterion upon which to judge the performance of the various predictors. The elastic predictor is simple to implement and requires no matrix assembly or inversion operations beyond the pre-processing phase. On the contrary, the consistent tangent formulation imposes a computational overhead on the solution procedure due to the need to reform the consistent tangent operator during each iteration. The primary computational bottleneck, however, in finite element codes is generally the solution of the global problem for the increment in the displacements. Thus, even though there is a computational overhead associated with the construction of the consistent tangent

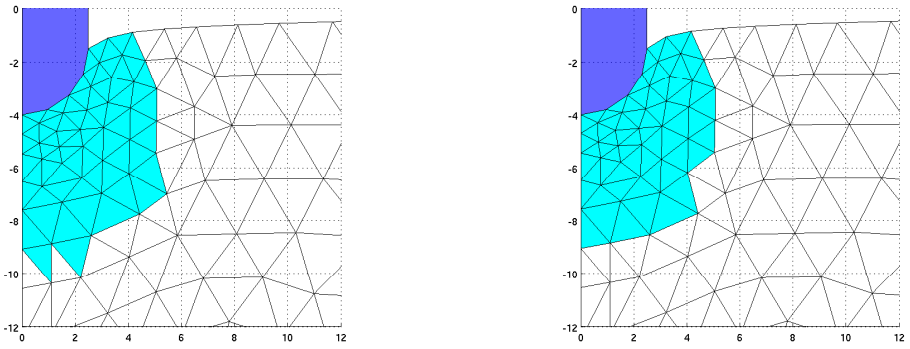

(a) $L/l = 33.3$ (b) $L/l = 50$

(c) $L/l = 100$ (d) *Classical*

Fig. 5.10. Extent of the active plastic zone in the vicinity of the indenter tip. The domain has been scaled by $100/H$ and the elements containing active quadrature points are shaded

operator, this is generally far less than that associated with the solution of the global problem for the displacements. The results presented here compare the two predictors based on the number of iterations required to achieve a certain tolerance.

The performance of the algorithm using two different predictors when approximating a single step of the gradient plasticity problem presented in Section 5.1.1 is shown in Fig. 5.11. The magnitude of the force residual $|\boldsymbol{R}|$ at each increment is shown to indicate the state of convergence. The consistent tangent predictor is far more efficient, in terms of the number of iterations performed to obtain a specified residual norm, than the elastic predictor. The initial poor performance of the consistent tangent predictor is due to the first increment utilising the elastic predictor.

The computational time required to perform the analysis using the elastic predictor was approximately twice as long than when using the consistent tangent predictor. Other factors, such as proportion of the domain undergoing plastic flow, will influence such a comparison but it is clear that the consistent tangent formulation should be preferred to the elastic predictor.

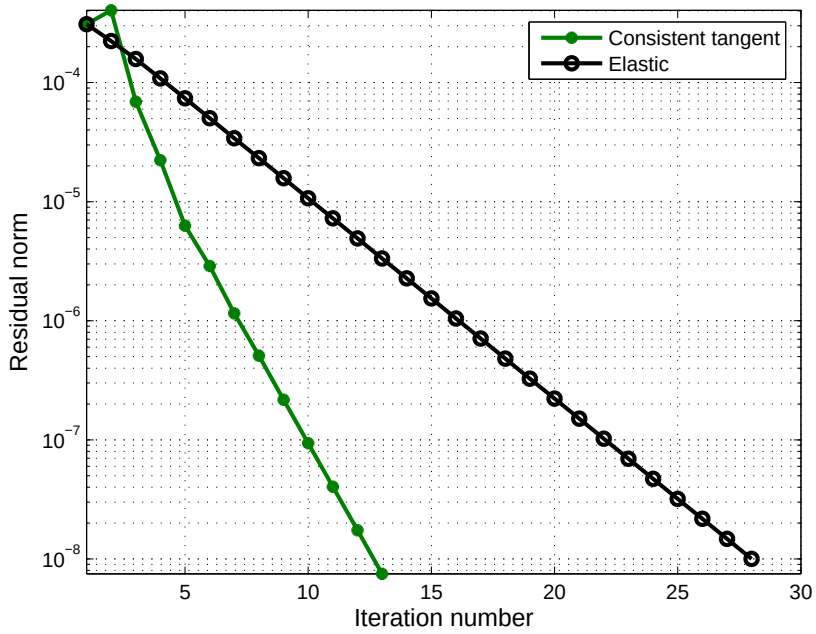

Fig. 5.11. Comparison of the norm of the force residual versus iteration number for the consistent tangent and elastic predictors

Part II

The finite-strain theory

Summary: The finite-strain theory

In Part II the model of gradient plasticity developed in Part I is extended to the finite-strain regime.

A summary of standard results in nonlinear continuum mechanics is presented in Chapter 6. The remainder of the chapter presents the constitutive equations for the elastic response and the plastic constitutive relations. The form of these relations is greatly simplified by choosing an exponential approximation for the evolution of plastic deformation.

The assumption of incompressible plastic deformation causes low-order finite element approximations to exhibit spurious locking behaviour. Low-order elements are, however, attractive as they are more robust and simplify the implementation of the discontinuous Galerkin formulation. Chapter 7 details one potential technique to remedy the shortcomings of low-order elements: the enhanced assumed strain formulation.

The form of the corrector step for the model of gradient plasticity is presented in Chapter 8. The nonlocal expression for the increment in plastic strain is solved using a symmetric interior penalty discontinuous Galerkin formulation. The corrector step at finite strains resembles the small-strain case, thus, only the distinguishing features are discussed. Details of the algorithm are given and the consistent tangent predictor is derived for both the classical and gradient cases.

Features of the algorithm at finite strains are demonstrated using two example problems in Chapter 9.

6

A formulation of elastoplasticity at finite strains

The purpose of this chapter is to present an overview of aspects of nonlinear continuum mechanics and the theory of classical plasticity at finite strains. This background material serves to facilitate the extension of the model of gradient plasticity developed in Part I to the finite-strain regime. In addition, the review introduces the notation adopted. The notation is relatively standard and closely follows that used by Simo [164]. Detailed expositions on nonlinear continuum mechanics can be found in Truesdell and Noll [186], Gurtin [88], Ogden [143] and Ciarlet [52], amongst others. Another excellent concise overview of nonlinear continuum mechanics in the context of the finite element method is given by Belytschko et al. [23].

A review of the theory of nonlinear continuum mechanics is presented in Section 6.1. The formulation of classical plasticity at finite strains is then considered within a hyperelastic multiplicative framework in Section 6.2. Following the seminal work of Simo [163], we adopt an exponential approximation for the evolution of plastic deformation in Section 6.4. This approximation, in combination with the use of a Hencky model for the elastic response, allows features of the infinitesimal theory presented in Part I to be extended in a relatively straightforward manner to the finite-strain regime, thereby facilitating the subsequent development of the gradient model. The extension of the classical small-strain plasticity theory to finite strains using logarithmic strain measures has a considerable history [137, 48, 76, 147, 100, 129, 31, 131]. The simplicity of this model of plasticity has been exploited by Geers [83] as the basis for a nonlocal implicit gradient plasticity formulation at finite strains.

6.1 Overview of nonlinear continuum mechanics

In this section we review several standard results in nonlinear continuum mechanics.

6.1.1 Kinematic results

We denote by $\Omega \subset \mathbb{R}^{n_{\rm dim}}$ the reference placement of a continuum, as shown in Fig. 6.1, with material particles labelled $\boldsymbol{X}$. The boundary of Ω, assumed smooth, is denoted $\partial\Omega$. We denote by the injective, orientation preserving map $\boldsymbol{\varphi} : \Omega \to \mathbb{R}^{n_{\rm dim}}$ a smooth motion of the reference placement. The current placement of the body associated with the motion $\boldsymbol{\varphi}$ is denoted $\mathcal{S} = \boldsymbol{\varphi}(\Omega)$, with material points designated as $\boldsymbol{x} \in \mathcal{S}$.

The deformation gradient, denoted $\boldsymbol{F}$, is defined as the derivative of the motion with respect to the reference configuration; that is,

$$\boldsymbol{F}(\boldsymbol{X}) = \mathrm{GRAD}\, \boldsymbol{\varphi}(\boldsymbol{X}) \ , \tag{6.1}$$

where $\mathrm{GRAD}[(\cdot)] := \partial(\cdot)/\partial\boldsymbol{X}$ is the gradient operator with respect to the reference configuration. We distinguish here between the deformation gradient and the enhanced deformation gradient to be defined in the next chapter. The determinant of the deformation gradient is denoted $j_{xX}(\boldsymbol{X}) := \det[\boldsymbol{F}(\boldsymbol{X})] > 0$. The displacement of a material point relative to the reference configuration is denoted $\boldsymbol{u}(\boldsymbol{X}, t) = \boldsymbol{\varphi}(\boldsymbol{X}, t) - \boldsymbol{X}$. The right and left Cauchy–Green tensors are respectively defined by

$$\boldsymbol{C} = \boldsymbol{F}^T\boldsymbol{F} \qquad \text{and} \qquad \boldsymbol{b} = \boldsymbol{F}\boldsymbol{F}^T \ . \tag{6.2}$$

In index notation these definitions read

$$C_{IJ} = F_{mI}F_{mJ} \qquad \text{and} \qquad b_{ij} = F_{iM}F_{jM} \ ,$$

where lower and upper case Roman indices refer to tensor components defined on the current and reference configurations respectively.

The polar decomposition theorem allows the deformation gradient to be multiplicatively decomposed according to

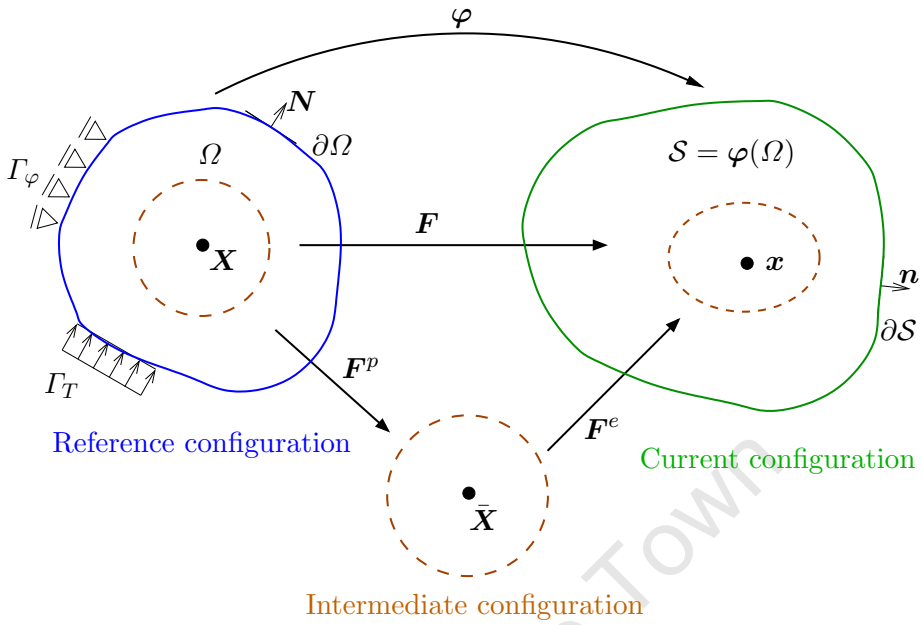

Fig. 6.1. Motion from the reference configuration Ω to the current configuration $\mathcal{S}$

$$\boldsymbol{F} = \tilde{\boldsymbol{R}}\boldsymbol{U} = \tilde{\boldsymbol{V}}\tilde{\boldsymbol{R}}\,, \tag{6.3}$$

where $\tilde{\boldsymbol{R}}$ is a proper orthogonal tensor termed the rotation tensor, and $\boldsymbol{U}$ and $\tilde{\boldsymbol{V}}$ are the right and left stretching tensors respectively. The principal invariants of either $\boldsymbol{C}$ or $\boldsymbol{b}$ are denoted by I_A, $(A = 1, \ldots, n_{\text{dim}})$, and in $\mathbb{R}^3$ are given by

$$I_1 = \text{tr}[\boldsymbol{C}]\,, \qquad I_2 = \tfrac{1}{2}\left(I_1^2 - \text{tr}[\boldsymbol{C}^2]\right)\,, \qquad I_3 = \det[\boldsymbol{C}]\,. \tag{6.4}$$

In subsequent chapters it will prove convenient to make use of various quantities defined relative to the principal bases of the current and reference configurations, termed the Eulerian and Lagrangian axes respectively. For $n_{\text{dim}} = 3$, the triads $\{\boldsymbol{N}^{(1)}, \boldsymbol{N}^{(2)}, \boldsymbol{N}^{(3)}\}$ and $\{\boldsymbol{n}^{(1)}, \boldsymbol{n}^{(2)}, \boldsymbol{n}^{(3)}\}$ denote the principal directions (eigenvectors) of the positive definite tensors $\boldsymbol{C}(\boldsymbol{X})$ and $\boldsymbol{b}(\boldsymbol{x})$ respectively, defined by the eigenvalue problems

$$\boldsymbol{C}\boldsymbol{N}^{(A)} = \lambda_A^2\boldsymbol{N}^{(A)} \qquad \text{and} \qquad \boldsymbol{b}\boldsymbol{n}^{(A)} = \lambda_A^2\boldsymbol{n}^{(A)} \qquad (A = 1, \ldots, n_{\text{dim}})\,, \tag{6.5}$$

where $\lambda_A^2 \geq 0$ are the eigenvalues of either $\boldsymbol{C}$ or $\boldsymbol{b}$.

The right and left Cauchy–Green tensors can thus be expressed in their principal bases as

$$\boldsymbol{C} = \sum_{A=1}^{n_{\text{dim}}} \lambda_A^2 \boldsymbol{N}^{(A)} \otimes \boldsymbol{N}^{(A)} \qquad \text{and} \qquad \boldsymbol{b} = \sum_{A=1}^{n_{\text{dim}}} \lambda_A^2 \boldsymbol{n}^{(A)} \otimes \boldsymbol{n}^{(A)} \,. \tag{6.6}$$

The relationships between $\boldsymbol{C}$ and $\boldsymbol{b}$, and $\boldsymbol{N}^{(A)}$ and $\boldsymbol{n}^{(A)}$, obtained using (6.3) and the definition of the Eulerian and Lagrangian eigenvectors to have unit length, that is $|\boldsymbol{N}^{(A)}| = |\boldsymbol{n}^{(A)}| = 1$, are given by

$$\boldsymbol{b} = \tilde{\boldsymbol{R}} \boldsymbol{C} \tilde{\boldsymbol{R}}^T \qquad \text{and} \qquad \boldsymbol{n}^{(A)} = \tilde{\boldsymbol{R}} \boldsymbol{N}^{(A)} \,.$$

The spectral decompositions of the deformation gradient, the rotation tensor, and the left and right stretching tensors are given by

$$\begin{aligned}
\boldsymbol{F} &= \sum_{A=1}^{n_{\text{dim}}} \lambda_A \boldsymbol{n}^{(A)} \otimes \boldsymbol{N}^{(A)} \,, \\
\tilde{\boldsymbol{R}} &= \sum_{A=1}^{n_{\text{dim}}} \boldsymbol{n}^{(A)} \otimes \boldsymbol{N}^{(A)} \,, \\
\boldsymbol{U} &= \sum_{A=1}^{n_{\text{dim}}} \lambda_A \boldsymbol{N}^{(A)} \otimes \boldsymbol{N}^{(A)} \,, \\
\tilde{\boldsymbol{V}} &= \sum_{A=1}^{n_{\text{dim}}} \lambda_A \boldsymbol{n}^{(A)} \otimes \boldsymbol{n}^{(A)} \,.
\end{aligned}$$

6.1.2 Lagrangian and Eulerian descriptions of motion

The motion of a continuum can be described in either a Lagrangian (material) or an Eulerian (spatial) framework. In the Lagrangian description the coordinates defining the reference placement of the body are taken as independent variables, while in an Eulerian description it is the spatial coordinates that define the current placement that are the independent variables.

The position of the body at any point in time t is denoted $\mathcal{S}_t$. The material velocity $\boldsymbol{V}(\boldsymbol{X}, t)$ is defined as time derivative of the motion; that is, in component form we have

$$V_i(X_I, t) = \frac{\partial \boldsymbol{\varphi}_i(X_I, t)}{\partial t} \, .$$

An Eulerian description of the motion can be obtained from the Lagrangian description by transforming the independent variables from the material coordinates to the spatial coordinates. The spatial velocity field, denoted $\boldsymbol{v}(\boldsymbol{x}, t)$, is obtained from the material velocity field as

$$\begin{aligned} \boldsymbol{V}(\boldsymbol{X}, t) &= \boldsymbol{V}(\boldsymbol{\varphi}^{-1}(\boldsymbol{x}, t), t) \\ &= \boldsymbol{v}(\boldsymbol{x}, t) \, . \end{aligned} \tag{6.7}$$

The spatial velocity field plays an integral role in the forthcoming discussions concerning the motion of an elastoplastic body.

The Lagrangian framework is adopted here, as it is for the vast majority of problems in solid mechanics. Thus, while we make use of spatial variables they can always be expressed in terms of the independent variables defined in terms of the Lagrangian reference configuration and the current time.

The gradient of the material velocity field with respect to the reference configuration is denoted $\text{GRAD}\,[\boldsymbol{V}(\boldsymbol{X}, t)] = \partial \boldsymbol{V} / \partial \boldsymbol{X}$, while the gradient of the spatial velocity field with respect to the current configuration is denoted $\boldsymbol{l} := \nabla \boldsymbol{v}(\boldsymbol{x}, t) = \partial \boldsymbol{v} / \partial \boldsymbol{x}$. The time rate of change of the deformation gradient is thus $\dot{\boldsymbol{F}} = \text{GRAD}[\boldsymbol{V}]$. The relationship between the time rate of change of the deformation gradient and the spatial velocity gradient is therefore

$$\begin{aligned} \dot{\boldsymbol{F}} &= \text{GRAD}[\boldsymbol{V}] \\ &= \text{GRAD}[\boldsymbol{v}] \\ &= (\nabla \boldsymbol{v}) \, \boldsymbol{F} \, . \end{aligned} \tag{6.8}$$

The preceding relationship implies that

$$\boldsymbol{l} = \nabla \boldsymbol{v} = \dot{\boldsymbol{F}} \boldsymbol{F}^{-1} \ . \tag{6.9}$$

The spatial velocity gradient is additively decomposed into a symmetric part and a skew-symmetric part, denoted $\boldsymbol{d}$ and $\hat{\boldsymbol{w}}$ respectively, as follows:

$$\boldsymbol{l} = \underbrace{\tfrac{1}{2}\left(\nabla \boldsymbol{v} + (\nabla \boldsymbol{v})^T\right)}_{\boldsymbol{d}} + \underbrace{\tfrac{1}{2}\left(\nabla \boldsymbol{v} - (\nabla \boldsymbol{v})^T\right)}_{\hat{\boldsymbol{w}}} \ . \tag{6.10}$$

The symmetric tensor $\boldsymbol{d}$ is the rate of deformation tensor, while the skew-symmetric tensor $\hat{\boldsymbol{w}}$ is the spin tensor. The axial vector $\boldsymbol{w}$ associated with the skew-symmetric spin tensor is characterised by the relation

$$\hat{\boldsymbol{w}} \boldsymbol{h} = \boldsymbol{w} \times \boldsymbol{h} \qquad \forall \boldsymbol{h} \in \mathbb{R}^{n_{\text{dim}}} \ .$$

Another strain measure used extensively in nonlinear continuum mechanics is the Green strain tensor, denoted $\boldsymbol{E}$. The Green strain tensor is related to the right Cauchy–Green tensor as

$$\boldsymbol{E} = \tfrac{1}{2}\left(\boldsymbol{C} - \boldsymbol{I}\right) \qquad \text{or} \qquad E_{IJ} = \tfrac{1}{2}\left(C_{IJ} - \delta_{IJ}\right) \ . \tag{6.11}$$

The Green strain tensor can be expressed in terms of the displacement gradient GRAD$[\boldsymbol{u}]$ as

$$E_{IJ} = \frac{1}{2}\left(\frac{\partial u_I}{\partial X_J} + \frac{\partial u_J}{\partial X_I} + \frac{\partial u_M}{\partial X_I}\frac{\partial u_M}{\partial X_J}\right) \ .$$

If the contribution of the final term in the preceeding expression is negligible, due to the displacement gradient being small, we obtain the standard expression for the infinitesimal-strain tensor $\boldsymbol{\varepsilon}$ defined in Chapter 2 as

$$\boldsymbol{\varepsilon}_{IJ} = \frac{1}{2}\left(\frac{\partial u_I}{\partial X_J} + \frac{\partial u_J}{\partial X_I}\right) \ .$$

The relationship between the time rate of change of the right Cauchy–Green tensor and the rate of deformation tensor is found from (6.2) and (6.8), and is given by

$$\dot{\boldsymbol{C}} = 2\boldsymbol{F}^T \boldsymbol{d}\boldsymbol{F} \ . \tag{6.12}$$

6.1.3 Stress measures

The symmetric Cauchy stress tensor, denoted $\boldsymbol{\sigma}$ and defined on the current placement, is the fundamental measure of stress. The Cauchy stress tensor is defined by the relationship

$$\boldsymbol{\sigma}\boldsymbol{n} = \boldsymbol{t}^n \qquad \text{or} \qquad \sigma_{ij} n_j = t_i^n \ ,$$

where $\boldsymbol{n}$ is the outward unit normal vector to an arbitrary surface $\mathit{\Gamma}^n$ at a point $\boldsymbol{x}$ in the current configuration $\mathcal{S}$, and $\boldsymbol{t}^n$ is the traction force per unit area of $\mathit{\Gamma}^n$ as depicted in Fig. 6.2. A more detailed discussion of the Cauchy stress can be found in Malvern [119] and other introductory texts on continuum mechanics. The nonsymmetric nominal stress tensor, denoted $\boldsymbol{P}$, is defined on the reference configuration as

$$\boldsymbol{P}\boldsymbol{N} = \boldsymbol{t}^N \qquad \text{or} \qquad P_{iJ} N_J = t_i^N \ ,$$

where $\boldsymbol{N}$ is the outward unit normal to the arbitrary plane $\mathit{\Gamma}^N$ in the reference configuration, and $\boldsymbol{t}^N$ is the traction expressed as a force per unit area of $\mathit{\Gamma}^N$. The nominal stress tensor is also known as the first Piola–Kirchhoff stress tensor [164]. The traction vectors in the reference and current configurations are related by

$$\boldsymbol{t}^n \mathit{\Gamma}^n = \boldsymbol{t}^N \mathit{\Gamma}^N \ .$$

Nanson's relation [119] gives the surface traction $\boldsymbol{t}^n$ acting on $\mathit{\Gamma}^n$ in the current configuration in terms of the surface traction $\boldsymbol{t}^N$ acting on $\mathit{\Gamma}^N$ in the reference configuration, and is

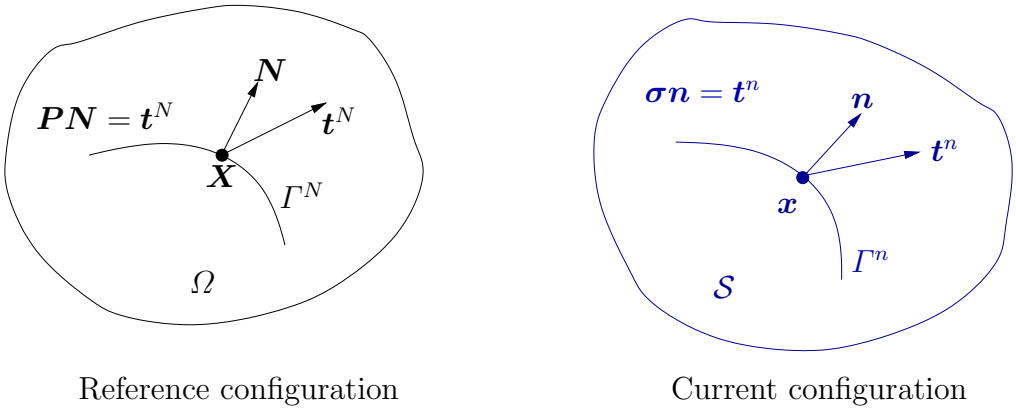

Fig. 6.2. Schematic of the stress measures in the reference and current placement

$$\boldsymbol{n}\Gamma^n = j_{xX}\boldsymbol{F}^{-T}\boldsymbol{N}\Gamma^N \qquad \text{or} \qquad n_i\Gamma^n = j_{xX}F^{-1}_{Ji}N_J\Gamma^N \,.$$

The relationship between the Cauchy and the nominal stress tensors is obtained with the aid of Nanson's relation as

$$\underbrace{j_{xX}\boldsymbol{\sigma}}_{\boldsymbol{\tau}} = \boldsymbol{P}\boldsymbol{F}^T \qquad \text{or} \qquad \underbrace{j_{xX}\sigma_{ij}}_{\tau_{ij}} = P_{iM}F_{jM} \,,$$

where $\boldsymbol{\tau}$ is the symmetric Kirchhoff stress tensor.

The second Piola–Kirchhoff stress tensor $\boldsymbol{S}$ is a symmetric Lagrangian quantity defined by

$$\boldsymbol{S} = \boldsymbol{F}^{-1}\boldsymbol{P} = \boldsymbol{F}^{-1}\boldsymbol{\tau}\boldsymbol{F}^{-T} \qquad \text{or} \qquad S_{IJ} = F^{-1}_{Im}P_{mJ} = F^{-1}_{Im}\tau_{mn}F^{-1}_{Jn} \,.$$

The relationships between the various stress measures are summarised in Table 6.1.

Each stress tensor is conjugate to an associated measure of the deformation rate in the sense that the internal power $\mathcal{P}_{\text{int}}$ can be written in equivalent form as

$$\mathcal{P}_{\text{int}} = \boldsymbol{\tau} : \boldsymbol{d} = \boldsymbol{P} : \dot{\boldsymbol{F}} = \tfrac{1}{2}\boldsymbol{S} : \dot{\boldsymbol{C}} \,,$$

or

$$\mathcal{P}_{\text{int}} = \tau_{ij}d_{ij} = P_{iJ}\dot{F}_{iJ} = \tfrac{1}{2}S_{IJ}\dot{C}_{IJ} \,. \tag{6.13}$$

Table 6.1. Relationships between the various stress measures in index and index-free notation

	Cauchy stress	Nominal stress	2nd Piola–Kirchhoff stress	Kirchhoff stress
	σ_{ij}	P_{iJ}	S_{IJ}	τ_{ij}
$\sigma_{ij} =$	-	$j_{xX}^{-1} P_{iM} F_{jM}$	$j_{xX}^{-1} F_{iJ} S_{JK} F_{jK}$	$j_{xX}^{-1} \tau_{ij}$
$P_{iJ} =$	$j_{xX} \sigma_{im} F_{Jm}^{-1}$	-	$F_{iM} S_{MJ}$	$\tau_{im} F_{Jm}^{-1}$
$S_{IJ} =$	$j_{xX} F_{Im}^{-1} \sigma_{mn} F_{Jn}^{-1}$	$F_{Im}^{-1} P_{mJ}$	-	$F_{Im}^{-1} \tau_{mn} F_{Jn}^{-1}$
$\tau_{ij} =$	$j_{xX} \sigma_{ij}$	$P_{iM} F_{jM}$	$F_{iJ} S_{JK} F_{jK}$	-
	$\boldsymbol{\sigma}$	$\boldsymbol{P}$	$\boldsymbol{S}$	$\boldsymbol{\tau}$
$\boldsymbol{\sigma} =$	-	$j_{xX}^{-1} \boldsymbol{P}\boldsymbol{F}^T$	$j_{xX}^{-1} \boldsymbol{F}\boldsymbol{S}\boldsymbol{F}^T$	$j_{xX}^{-1} \boldsymbol{\tau}$
$\boldsymbol{P} =$	$j_{xX} \boldsymbol{\sigma}\boldsymbol{F}^{-T}$	-	$\boldsymbol{F}\boldsymbol{S}$	$\boldsymbol{\tau}\boldsymbol{F}^{-T}$
$\boldsymbol{S} =$	$j_{xX} \boldsymbol{F}^{-1}\boldsymbol{\sigma}\boldsymbol{F}^{-T}$	$\boldsymbol{F}^{-1}\boldsymbol{P}$	-	$\boldsymbol{F}^{-1}\boldsymbol{\tau}\boldsymbol{F}^{-T}$
$\boldsymbol{\tau} =$	$j_{xX} \boldsymbol{\sigma}$	$\boldsymbol{P}\boldsymbol{F}^{-T}$	$\boldsymbol{F}\boldsymbol{S}\boldsymbol{F}^T$	-

6.1.4 Conservation equations

The strong form of the equations governing the response of a continuum are obtained from fundamental conservation principles. The constitutive relations governing the response of the material to applied loading will be discussed shortly. We consider here, as in Part I, quasi-static problems in which the effect of inertial forces is assumed negligible. In addition we assume, for the sake of simplicity, that body forces can be neglected. These assumptions are not restrictive but are made to emphasise the salient features of the elastoplastic problem at finite strains.

As depicted in Fig. 6.1, the outward unit normal to the boundary of the reference domain $\partial\Omega$ is denoted $\boldsymbol{N}$. Dirichlet and Neumann boundary conditions are prescribed on Γ_φ and Γ_T respectively, in addition $\Gamma_\varphi \cap \Gamma_T = \varnothing$ and $\overline{\Gamma_\varphi \cup \Gamma_T} = \overline{\partial\Omega}$. The nominal prescribed traction on Γ_T is denoted $\boldsymbol{t}^N = \boldsymbol{P}\boldsymbol{N}$.

The strong form of the equilibrium equation reads

$$\mathrm{DIV}[\boldsymbol{P}] = \boldsymbol{0} \qquad \text{or} \qquad \frac{\partial P_{iM}}{\partial X_M} = 0 \ , \tag{6.14}$$

where DIV is the divergence operator in the reference configuration, with Dirichlet and Neumann boundary conditions respectively specified as

$$\begin{aligned} \boldsymbol{\varphi} &= \bar{\boldsymbol{\varphi}} \qquad \text{on } \Gamma_{\varphi} \ , \\ \boldsymbol{t}^N &= \boldsymbol{P}\boldsymbol{N} = \bar{\boldsymbol{t}}^N \qquad \text{on } \Gamma_T \ . \end{aligned}$$

The derivation of the resulting weak form of the equilibrium equation and Neumann boundary conditions, a key step in the development of the finite element problem, will be considered in the next chapter.

6.1.5 Elastic constitutive relations

We consider hyperelastic constitutive relationships only, that is, relationships characterised by a stored energy function $W = \hat{W}(\boldsymbol{X}, \boldsymbol{F}(\boldsymbol{X}, t))$ that acts as a potential function for the stress measure. We assume from the outset that the stored energy function is objective, so that the dependence of the stored energy function on $\boldsymbol{F}$ is via $\boldsymbol{C}$ (see, for example, Gurtin [88]); that is,

$$W = \hat{W}(\boldsymbol{X}, \boldsymbol{F}) = \bar{W}(\boldsymbol{X}, \boldsymbol{C}) \ . \tag{6.15}$$

The stored energy function is said to be objective, or frame invariant, if it is unchanged under an arbitrary rigid body motion $\boldsymbol{Q}$ such that

$$W(\boldsymbol{X}, \boldsymbol{Q}\boldsymbol{F}) = W(\boldsymbol{X}, \boldsymbol{F}) \qquad \forall \boldsymbol{Q} \, .$$

As in the infinitesimal theory presented in Section 2.1.2, the elastic relation can be obtained using classical thermodynamic arguments [55] permitting only nonnegative dissipation, from

$$
\begin{aligned}
0 &\leq \boldsymbol{\tau} : \boldsymbol{d} - \dot{\bar{W}} \\
&\leq \boldsymbol{\tau} : \boldsymbol{d} - \frac{\partial \bar{W}(\boldsymbol{C})}{\partial \boldsymbol{C}} : \dot{\boldsymbol{C}} \\
&\leq \boldsymbol{\tau} : \boldsymbol{d} - \frac{\partial \bar{W}(\boldsymbol{C})}{\partial \boldsymbol{C}} : \left(2\boldsymbol{F}^T \boldsymbol{d}\boldsymbol{F}\right) \\
&\leq \boldsymbol{\tau} : \boldsymbol{d} - 2\boldsymbol{F}\frac{\partial \bar{W}(\boldsymbol{C})}{\partial \boldsymbol{C}}\boldsymbol{F}^T : \boldsymbol{d} \\
&\leq \left(\boldsymbol{\tau} - 2\boldsymbol{F}\frac{\partial \bar{W}(\boldsymbol{C})}{\partial \boldsymbol{C}}\boldsymbol{F}^T\right) : \boldsymbol{d}\,,
\end{aligned}
$$

from which one obtains, using Table 6.1, the elastic constitutive equations in the equivalent forms

$$
\boldsymbol{\tau} = 2\boldsymbol{F}\frac{\partial \bar{W}}{\partial \boldsymbol{C}}\boldsymbol{F}^T\,, \quad \boldsymbol{P} = 2\boldsymbol{F}\frac{\partial \bar{W}}{\partial \boldsymbol{C}}\,, \quad \text{and} \quad \boldsymbol{S} = \frac{\partial \bar{W}}{\partial \boldsymbol{C}}\,. \tag{6.16}
$$

Expressions for the time rate of change of the various stress measures will be required in the subsequent incremental formulation of the plasticity problem. It is convenient at this point to define the Lie derivative of the Kirchhoff stress tensor, denoted $\mathcal{L}_v\boldsymbol{\tau}$, by

$$
\mathcal{L}_v\boldsymbol{\tau} = \boldsymbol{F}\dot{\boldsymbol{S}}\boldsymbol{F}^T = \dot{\boldsymbol{\tau}} - (\nabla \boldsymbol{v})\boldsymbol{\tau} - \boldsymbol{\tau}(\nabla \boldsymbol{v})^T\,. \tag{6.17}
$$

This definition and (6.12) for the time derivative of the right Cauchy–Green tensor allow $\mathcal{L}_v\boldsymbol{\tau}$ to be written as

$$
(\mathcal{L}_v\boldsymbol{\tau})_{ij} = F_{iM}\dot{S}_{MN}F_{jN} = \underbrace{[F_{iM}F_{jN}F_{mP}F_{nQ}\mathrm{C}_{MNPQ}]}_{\mathrm{c}_{ijmn}}\, d_{mn}\,,
$$

where C and c are the material and spatial elasticity tensors respectively, defined by

$$
\mathrm{C}_{IJKL} = 4\frac{\partial^2 \bar{W}}{\partial C_{IJ}\partial C_{KL}} \quad \text{and} \quad \mathrm{c}_{ijkl} = F_{iM}F_{jN}F_{kP}F_{lQ}\mathrm{C}_{MNPQ}\,.
$$

We shall further confine attention to homogeneous isotropic materials, where the stored energy function's dependence on $\boldsymbol{C}$ is via the principal invariants of $\boldsymbol{C}$ defined in (6.4); that is,

$$\bar{W}(\boldsymbol{C}) = \tilde{W}(I_1, I_2, I_3) \ .$$

Equivalently, the stored energy function can be written in terms of the principal stretches of $\boldsymbol{C}$ as

$$\bar{W}(\boldsymbol{C}) = w(\lambda_1, \lambda_2, \lambda_3) \, .$$

The elastic constitutive equation for $\boldsymbol{S}$ given in (6.16) can be restated in terms of the principal stretches as

$$\boldsymbol{S} = 2\frac{\partial \bar{W}(\partial \boldsymbol{C})}{\partial \boldsymbol{C}} = \sum_{A=1}^{3} \left(\frac{1}{\lambda_A}\right) \left(\frac{\partial w(\lambda_1, \lambda_2, \lambda_3)}{\partial \lambda_A}\right) \left(\frac{\partial (\lambda_A^2)}{\partial \boldsymbol{C}}\right) \ . \tag{6.18}$$

This relation implies the spectral decomposition of $\boldsymbol{S}$ as follows:

$$\boldsymbol{S} = \sum_{A=1}^{3} S_A \boldsymbol{N}^{(A)} \otimes \boldsymbol{N}^{(A)} \qquad \text{with} \qquad S_A = \frac{1}{\lambda_A}\frac{\partial w}{\partial \lambda_A} \ .$$

Using the relationships given in Table 6.1 we obtain the expression for the Kirchhoff stress tensor in the principal directions as

$$\boldsymbol{\tau} = \sum_{A=1}^{3} \tau_A \boldsymbol{n}^{(A)} \otimes \boldsymbol{n}^{(A)} \qquad \text{with} \qquad \tau_A = \frac{1}{\lambda_A}\frac{\partial w}{\partial \lambda_A} \ .$$

The material elastic modulus C can be restated in terms of the principal stretches as [see 49]

$$\mathrm{C} = \sum_{A=1}^{3} \sum_{\substack{B=1 \\ B \neq A}}^{3} \frac{S_A - S_B}{\lambda_A^2 - \lambda_B^2} \boldsymbol{N}^{(A)} \otimes \boldsymbol{N}^{(B)} \otimes \left[\boldsymbol{N}^{(A)} \otimes \boldsymbol{N}^{(B)} + \boldsymbol{N}^{(B)} \otimes \boldsymbol{N}^{(A)} \right] + \sum_{A=1}^{3} \sum_{B=1}^{3} \frac{1}{\lambda_A} \frac{\partial}{\partial \lambda_B} \left[\frac{1}{\lambda_A} \frac{\partial w}{\partial \lambda_A} \right] \boldsymbol{N}^{(A)} \otimes \boldsymbol{N}^{(B)} \otimes \boldsymbol{N}^{(B)} \otimes \boldsymbol{N}^{(A)} ,$$

for the case where $\lambda_A \neq \lambda_B$. The case where $\lambda_A = \lambda_B$ will be discussed subsequently when we consider specific elasticity models.

The numerical examples presented in later chapters all concern two-dimensional plane problems. The finite element code has been developed to mimic the underlying mathematical structure and all constitutive relations and stress and strain measures are therefore developed in three space dimensions. Restrictions are then placed on the deformation to impose plane strain or plane stress conditions.

6.2 Multiplicative plasticity at finite strains

The purpose of this section is to discuss the local multiplicative decomposition of the deformation gradient $\boldsymbol{F}$ into an elastic part $\boldsymbol{F}^e$ and a plastic part $\boldsymbol{F}^p$ as

$$\boldsymbol{F}(\boldsymbol{X}, t) = \boldsymbol{F}^e(\boldsymbol{X}, t) \boldsymbol{F}^p(\boldsymbol{X}, t) \ .$$

Figure 6.1 illustrates the multiplicative decomposition. The multiplicative decomposition was first proposed by Lee [112] and further developed in [183, 157, 120, 98, 15].

The basis for a multiplicative decomposition of the deformation gradient is provided by the underlying micromechanical descriptions of single crystal plasticity (see, for example, Havner [99] and Mandel [120]). The decomposition introduces a local, stress-free intermediate configuration with material points labelled $\bar{\boldsymbol{X}}$ as depicted in Fig. 6.1. The components of tensors defined on the intermediate configuration are labelled using lower-case Greek letters. Quantities defined on the intermediate configuration are labelled with an overbar. The tensor $\boldsymbol{F}^p$ can be viewed as an internal variable describing the amount of dislocation flow through the crystal lattice, while $\boldsymbol{F}^e$

describes the elastic lattice deformation. An example of a crystal lattice structure for a face-centred cubic material is shown in Fig. 6.3. The multiplicative decomposition also provides an extremely convenient framework for the numerical implementation within the context of the finite element method.

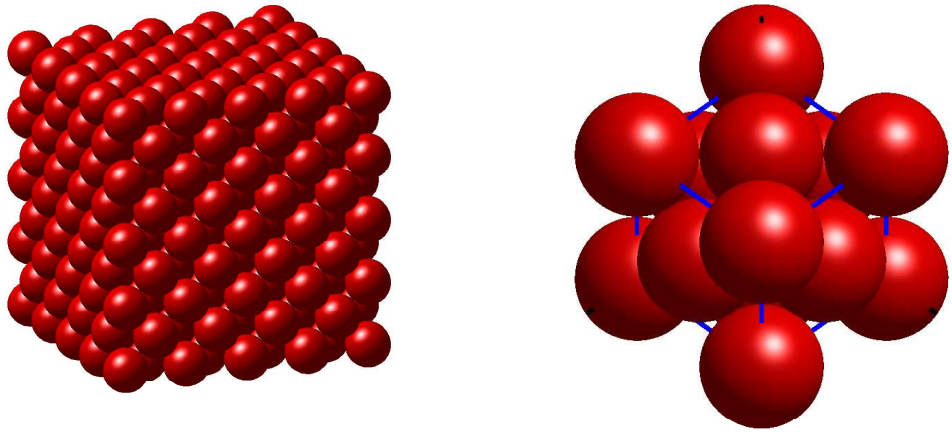

(a) Macrostructure (b) Unit cell

Fig. 6.3. Face-centred cubic crystal lattice

The elastic right and left Cauchy–Green tensors, defined on the intermediate and current configurations respectively, are defined by

$$\bar{\boldsymbol{C}}^e = \boldsymbol{F}^{eT}\boldsymbol{F}^e \qquad \text{or} \qquad \bar{C}^e_{\alpha\beta} = F^e_{m\alpha}F^e_{m\beta} \ , \tag{6.19}$$

$$\boldsymbol{b}^e = \boldsymbol{F}^e\boldsymbol{F}^{eT} \qquad \text{or} \qquad b^e_{ij} = F^e_{i\alpha}F^e_{j\alpha} \ . \tag{6.20}$$

The elastic Green strain tensor in the intermediate configuration is defined by

$$\bar{\boldsymbol{E}}^e = \tfrac{1}{2}\left(\bar{\boldsymbol{C}}^e - \boldsymbol{I}\right) \ .$$

The expression of the spatial velocity gradient $\boldsymbol{l}$ in terms of the deformation gradient in (6.9) motivates the definition of the elastic and plastic velocity gradients, denoted $\bar{\boldsymbol{L}}^p$ and $\boldsymbol{l}^e$ respectively, as

$$\bar{\boldsymbol{L}}^p = \dot{\boldsymbol{F}}^p \boldsymbol{F}^{p-1} \qquad \text{or} \qquad \bar{L}^p_{\alpha\beta} = \dot{F}^p_{\alpha I} F^{p-1}_{I\beta} \ , \tag{6.21}$$

$$\boldsymbol{l}^e = \dot{\boldsymbol{F}}^e \boldsymbol{F}^{e-1} \qquad \text{or} \qquad l^e_{ij} = \dot{F}^e_{i\alpha} F^{e-1}_{\alpha j} \, . \tag{6.22}$$

The multiplicative decomposition of $\boldsymbol{F}$ allows the velocity gradient to be additively decomposed in terms of the elastic component and a plastic component, denoted $\boldsymbol{l}^p$, and expressed in the current configuration as

$$\boldsymbol{l} = \boldsymbol{l}^e + \underbrace{\boldsymbol{F}^e \bar{\boldsymbol{L}}^p \boldsymbol{F}^{e-1}}_{\boldsymbol{l}^p} \qquad \text{or} \qquad l_{ij} = l^e_{ij} + \underbrace{F^e_{i\alpha} \bar{L}^p_{\alpha\beta} F^{e-1}_{\beta j}}_{l^p_{ij}} , \tag{6.23}$$

where $\boldsymbol{l}^p$ is obtained by pushing forward $\bar{\boldsymbol{L}}^p$ from the intermediate configuration by $\boldsymbol{F}^e$. Motivated by the decomposition of the spatial velocity gradient into symmetric and skew-symmetric parts in (6.10), the symmetric and skew-symmetric parts of the elastic and plastic spatial velocity gradients are defined by

$$\boldsymbol{l}^p = \underbrace{\boldsymbol{d}^p}_{\text{sym}[\boldsymbol{l}^p]} + \underbrace{\hat{\boldsymbol{w}}^p}_{\text{skew}[\boldsymbol{l}^p]} \qquad \text{and} \qquad \boldsymbol{l}^e = \underbrace{\boldsymbol{d}^e}_{\text{sym}[\boldsymbol{l}^e]} + \underbrace{\hat{\boldsymbol{w}}^e}_{\text{skew}[\boldsymbol{l}^e]} \ . \tag{6.24}$$

6.3 Elastic response and free energy for hyperelastic multiplicative plasticity

In this section we discuss details of the elastic response and the form of the free energy function for hyperelastic-plastic materials where a multiplicative decomposition of the deformation gradient is assumed. We consider here the case of classical plasticity restricted to linear isotropic hardening.

The free energy function ψ represents the stored energy associated with elastic lattice deformation and is assumed to be additively composed of an elastic part $\bar{W}^e$ and plastic part $\bar{W}^p$. The free energy function is expressed in the intermediate configuration as

$$\psi(\boldsymbol{F}^e, \boldsymbol{\xi}) = \bar{W}^e(\bar{\boldsymbol{C}}^e) + \bar{W}^p(\boldsymbol{\xi}) \ ,$$

where $\boldsymbol{\xi}$ are the set of internal variables associated with hardening due to the evolution of plastic deformation. Objectivity of the free energy implies a local dependence on $\boldsymbol{F}$ via $\bar{\boldsymbol{C}}^e$.

The elastic and plastic constitutive relations are obtained from the dissipation inequality as follows:

$$\begin{aligned} 0 &\leq \boldsymbol{\tau} : \boldsymbol{d} - \dot{\psi} \\ &\leq \boldsymbol{\tau} : (\boldsymbol{d}^e + \boldsymbol{d}^p) - \frac{\partial \bar{W}^e(\bar{\boldsymbol{C}}^e)}{\partial \bar{\boldsymbol{C}}^e} : \dot{\bar{\boldsymbol{C}}}^e - \sum_{\mathrm{A}=1}^{n_{\mathrm{int}}} \frac{\partial \bar{W}^p(\boldsymbol{\xi})}{\partial \boldsymbol{\xi}_{\mathrm{A}}} : \dot{\boldsymbol{\xi}}_{\mathrm{A}} \\ &\leq \left(\boldsymbol{\tau} - 2\boldsymbol{F}^e \frac{\partial \bar{W}^e(\bar{\boldsymbol{C}}^e)}{\partial \bar{\boldsymbol{C}}^e} \boldsymbol{F}^{eT} \right) : \boldsymbol{d}^e + \boldsymbol{\tau} : \boldsymbol{d}^p - \sum_{\mathrm{A}=1}^{n_{\mathrm{int}}} \frac{\partial \bar{W}^p(\boldsymbol{\xi})}{\partial \boldsymbol{\xi}_{\mathrm{A}}} : \dot{\boldsymbol{\xi}}_{\mathrm{A}} \,. \end{aligned}$$

We restrict attention to the case of linear isotropic hardening where $\boldsymbol{\xi} = \xi$ is the isotropic hardening parameter, and set

$$\bar{g} = -\partial \bar{W} / \partial \xi \,.$$

Following standard arguments in constitutive theory, one obtains the elastic relation for the Kirchhoff stress as

$$\boldsymbol{\tau} = 2\boldsymbol{F}^e \frac{\partial \bar{W}^e(\bar{\boldsymbol{C}}^e)}{\partial \bar{\boldsymbol{C}}^e} \boldsymbol{F}^{eT} \,, \tag{6.25}$$

and the reduced dissipation inequality as

$$0 \leq \boldsymbol{\tau} : \boldsymbol{d}^p + \bar{g}\dot{\xi} \,. \tag{6.26}$$

The elastic constitutive relation (6.25) is posed in the current configuration, and can be recast in the intermediate configuration by defining the symmetric second Piola–Kirchhoff stress on the intermediate configuration $\bar{\boldsymbol{S}}$ as the pull-back of the Kirchhoff stress by $\boldsymbol{F}^e$ from the current configuration; that is,

$$\bar{\boldsymbol{S}} = \boldsymbol{F}^{e-1} \boldsymbol{\tau} \boldsymbol{F}^{e-T} \,.$$

Rewriting (6.25) in terms of $\bar{\boldsymbol{S}}$, we obtain the constitutive equation for $\bar{\boldsymbol{S}}$ on the intermediate configuration as

$$\begin{aligned}\bar{\boldsymbol{S}} &= \boldsymbol{F}^{e-1}\boldsymbol{\tau}\boldsymbol{F}^{e-T} \\ &= \boldsymbol{F}^{e-1}\left[2\boldsymbol{F}^{e}\frac{\partial \bar{W}^{e}(\bar{\boldsymbol{C}}^{e})}{\partial \bar{\boldsymbol{C}}^{e}}\boldsymbol{F}^{eT}\right]\boldsymbol{F}^{e-T} \\ &= 2\frac{\partial \bar{W}(\bar{\boldsymbol{C}}^{e})}{\partial \bar{\boldsymbol{C}}^{e}} \ . \end{aligned} \tag{6.27}$$

The reduced dissipation inequality on the intermediate configuration therefore takes the form

$$0 \leq \left[\bar{\boldsymbol{C}}^{e}\bar{\boldsymbol{S}}\right] : \boldsymbol{L}^{p} + \bar{g}\dot{\xi} \ . \tag{6.28}$$

The assumption of a Hencky model for the elastic stored energy function is made here to permit the plastic flow relations to be recast in a form near-identical to those governing the small-strain model discussed in Part I. The elastic stored energy function for the Hencky model is given by

$$\bar{W}^{e}(\boldsymbol{b}^{e}) = \bar{w}^{e}(\varepsilon^{e}_{A}) := \tfrac{1}{2}\Lambda\left(\varepsilon^{e}_{1}+\varepsilon^{e}_{2}+\varepsilon^{e}_{3}\right)^{2} + \mu\left((\varepsilon^{e}_{1})^{2}+(\varepsilon^{e}_{2})^{2}+(\varepsilon^{e}_{3})^{2}\right) \ ,$$

where $\varepsilon^{e}_{A} := \ln[\lambda^{e}_{A}]$ are the principal components of the logarithmic elastic stretches. We also consider a compressible neo-Hookean elastic stored energy function when investigating nonlinear elastic problems in Chapter 7. The elastic stored energy function for the neo-Hookean model takes the form

$$W(\boldsymbol{C}) = \frac{\Lambda}{2}\left(\det[\boldsymbol{F}]-1\right)^{2} + \frac{\mu}{2}\left[\mathrm{tr}[\boldsymbol{C}]-3\right] - \mu\ln\left[\det[F]\right] \ .$$

We restrict our attention henceforth to the Hencky model, unless otherwise stated. The constitutive relation for the components of Kirchhoff stress $\boldsymbol{\tau}$ in the principal directions of $\boldsymbol{b}^{e}$, denoted $\bar{\tau}_{A}$, is

$$\bar{\tau}_A = \Lambda\,(\varepsilon_1^e + \varepsilon_2^e + \varepsilon_3^e) + 2\mu\varepsilon_A^e\ , \qquad A = 1, 2, 3\ . \tag{6.29}$$

Remark 6.1. We note that although $\bar{w}$ is not a polyconvex function of $\boldsymbol{F}$ the Hencky model has been shown to be a good model for all but extreme elastic strains [164]. Polyconvex functions are generalisations of convex functions for functions defined on the space of matrices. While polyconvexity is a weaker property than convexity, it suffices for existence [52] and permits a wide range of realistic materials to be described. For elastoplastic materials undergoing large deformations it is generally the plastic deformation that dominates. The relationship between the lack of polyconvexity of a strain energy function and microstructure formation will be discussed in more detail in Chapter 10.

6.4 Plastic flow relations for classical multiplicative plasticity

The objective of this section is to present the plastic flow relations for classical plasticity where a multiplicative decomposition of the deformation gradient is assumed. The presentation closely follows that in Simo [164].

Classical models of plasticity assumes, pointwise a.e., an elastic domain $\mathcal{E}$ with boundary $\partial\mathcal{E}$, the yield surface, and a generalised normality law for the evolution of plastic deformation. For definiteness $\mathcal{E}$ is defined here by the von Mises condition restricted to linear isotropic hardening wherein plastic flow is incompressible; that is, $\det[\boldsymbol{F}^p] = 1$. The assumption of incompressible plastic flow introduces various complications associated with volumetric locking in the finite element implementation. One potential remedy, the method of enhanced assumed strains [171, 86, 10], will be detailed in the next chapter. The adoption of the von Mises yield criterion results in the admissible generalised stresses becoming the set $(\boldsymbol{\tau}, \bar{g})$ that satisfies

$$f(\boldsymbol{\tau}, \bar{g}) := |\operatorname{dev}[\boldsymbol{\tau}]| - \sqrt{\tfrac{2}{3}}\,(\kappa - \bar{g}) \leq 0\ . \tag{6.30}$$

As in the infinitesimal theory, κ is a constant related to the initial yield stress in uniaxial tension. The assumption of linear isotropic hardening implies that W^p is a quadratic function of ξ of the form

$$W^p = \hat{W}^p(\xi) = \tfrac{1}{2}k_2\xi^2\,,$$

thereby allowing the internal force $\bar{g}$ conjugate to the isotropic hardening parameter ξ to be expressed as

$$\bar{g} = -\frac{\partial W^p}{\partial \xi} = -k_2\xi\ . \tag{6.31}$$

A model of associative plasticity is assumed, so that both the plastic deformation and the internal hardening variable evolve in the normal cone to the yield surface. This corresponds to the assumption of maximum plastic dissipation leading to the set of local plastic evolution equations

$$\boldsymbol{d}^p = \lambda\frac{\partial f(\boldsymbol{\tau},\bar{g})}{\partial \boldsymbol{\tau}}\,, \tag{6.32}$$

$$\dot{\xi} = \lambda\frac{\partial f(\boldsymbol{\tau},\bar{g})}{\partial \bar{g}} = \sqrt{\tfrac{2}{3}}\lambda\,, \tag{6.33}$$

$$\lambda \geq 0, \quad f(\boldsymbol{\tau},\bar{g}) \leq 0, \quad \text{and} \quad \lambda f(\boldsymbol{\tau},\bar{g}) = 0\,, \tag{6.34}$$

where λ is the plastic consistency parameter and (6.34) are the Kuhn–Tucker conditions. As in the infinitesimal theory, the equivalent plastic strain $\gamma(t)$ is related to the plastic consistency parameter by $\dot{\gamma} = \lambda$.

An evolution equation for $\hat{\boldsymbol{w}}^p$ is required to complete the theory. We assume here, for the sake of simplicity, that $\hat{\boldsymbol{w}}^p = \boldsymbol{0}$.

The flow rule as given above is in the standard dual form. The dual form of the flow rule is restated in the equivalent primal form, as done in Chapter 2 for the infinitesimal theory, using the dissipation function D, which is given by

$$\begin{aligned} D(\boldsymbol{d}^p,\dot{\xi}) &= \sup\left[\boldsymbol{\tau} : \boldsymbol{q} + \bar{g}\eta \mid f(\boldsymbol{\tau},\bar{g}) \leq 0\right] \\ &= \begin{cases} \sqrt{\frac{2}{3}}\kappa|\boldsymbol{d}^p| & \text{if } |\boldsymbol{d}^p| \leq \dot{\xi}\,, \\ +\infty & \text{otherwise.} \end{cases} \end{aligned} \tag{6.35}$$

The primal expression of the flow rule is thus

$$(\boldsymbol{\tau}, \bar{g}) \in \partial D(\boldsymbol{d}^p, \dot{\xi})\,, \tag{6.36}$$

or equivalently

$$D(\boldsymbol{q}, \eta) \geq D(\boldsymbol{d}^p, \dot{\xi}) + \boldsymbol{\tau} : (\boldsymbol{q} - \boldsymbol{d}^p) + \bar{g}(\eta - \dot{\xi})\,. \tag{6.37}$$

The primal formulation of classical plasticity at finite deformations was developed by Eve et al. [79].

Remark 6.2. Analysis of the finite-strain plasticity problem is a far more delicate matter than for the infinitesimal theory. The energetic approach pioneered by Mielke [132] appears to be the appropriate framework for such an analysis. We do not attempt to analyse the finite-strain problem in this work.

6.4.1 Time-discrete approximation of the flow law

In this section we discretise the flow law (6.32)–(6.34) in time using a backward-Euler scheme.

We denote an arbitrary function ψ evaluated at time t_{n} as ψ^{n}. Consider a partition of the time interval $[0, T]$ into N subintervals with node points $t_{\mathrm{n}} = nk,\ 0 \leq n \leq N$, where $\Delta t = t_{\mathrm{n}} - t_{\mathrm{n}-1} = T/N$ is the step-size.

The strain driven solution algorithm adopted here for the solution of the coupled elastoplastic problem, and described in the next chapter, allows $\boldsymbol{F}_{\mathrm{n}}$ to be treated as known, but not its decomposition into elastic and plastic parts. The full state of the system is assumed known at the beginning of the current time step n from the equilibrium state at the end of the previous time step n − 1. The increment in a quantity within a time step is defined by

$$\Delta(\cdot) := (\cdot)_{\mathrm{n}} - (\cdot)_{\mathrm{n}-1} = (\cdot)_{\mathrm{n}} - (\cdot)_0\ .$$

Following Simo and Miehe [167] we assume the following exponential approximation for the evolution of $\boldsymbol{F}^p$

$$\boldsymbol{F}^p_{\mathrm{n}} \approx \underbrace{\exp\left[\Delta t \bar{\boldsymbol{L}}^p_{\mathrm{n}}\right]}_{\Delta \boldsymbol{F}^p} \boldsymbol{F}^p_{\mathrm{n-1}} \,. \tag{6.38}$$

The preceeding approximation can be motivated by rewriting (6.21) for $\dot{\boldsymbol{F}}^p$ as

$$\dot{\boldsymbol{F}}^p = \bar{\boldsymbol{L}}^p \boldsymbol{F}^p \,,$$

and recognising that (6.38) would represent the solution to the above were $\bar{\boldsymbol{L}}^p$ constant.

Using the multiplicative decomposition of $\boldsymbol{F}$ we obtain

$$\begin{aligned}
\boldsymbol{F}_{\mathrm{n}} &= \boldsymbol{F}^e_{\mathrm{n}} \boldsymbol{F}^p_{\mathrm{n}} \\
&= \boldsymbol{F}^e_{\mathrm{n}} \exp\left[\Delta t \bar{\boldsymbol{L}}^p_{\mathrm{n}}\right] \boldsymbol{F}^p_{\mathrm{n-1}} \qquad \text{using (6.38)} \\
&= \boldsymbol{F}^e_{\mathrm{n}} \exp\left[\Delta t \bar{\boldsymbol{L}}^p_{\mathrm{n}}\right] \underbrace{\boldsymbol{F}^{e-1}_{\mathrm{n}} \boldsymbol{F}^e_{\mathrm{n}}}_{\boldsymbol{I}} \boldsymbol{F}^p_{\mathrm{n-1}} \\
&= \exp\left[\Delta t \boldsymbol{F}^e_{\mathrm{n}} \bar{\boldsymbol{L}}^p_{\mathrm{n}} \boldsymbol{F}^{e-1}_{\mathrm{n}}\right] \boldsymbol{F}^e_{\mathrm{n}} \boldsymbol{F}^p_{\mathrm{n-1}} \\
&= \exp\left[\Delta t \boldsymbol{l}^p_{\mathrm{n}}\right] \boldsymbol{F}^e_{\mathrm{n}} \boldsymbol{F}^p_{\mathrm{n-1}} \qquad \text{using (6.23)} \,.
\end{aligned}$$

Rearranging, we obtain

$$\boldsymbol{F}^e_{\mathrm{n}} = \exp\left[-\Delta t \boldsymbol{l}^p_{\mathrm{n}}\right] \underbrace{\boldsymbol{F}_{\mathrm{n}} \boldsymbol{F}^{p-1}_{\mathrm{n-1}}}_{\boldsymbol{F}^{e\star}} \,,$$

where $\boldsymbol{F}^{e\star}$ is the trial elastic deformation gradient arising from the assumption that the plastic deformation is "frozen" during the time step. As with the elastic left Cauchy–Green tensor, the trial elastic left Cauchy–Green tensor can be expressed as

$$\begin{aligned}
\boldsymbol{b}^{e\star} &= \boldsymbol{F}^{e\star} \boldsymbol{F}^{e\star T} \\
&= \sum_{A=1}^{3} (\lambda^{e\star}_A)^2 \, \boldsymbol{n}^{\star(A)} \otimes \boldsymbol{n}^{\star(A)} \,,
\end{aligned} \tag{6.39}$$

where $\boldsymbol{n}^{\star(A)}$ $(A = 1, 2, 3)$ are the principal directions of $\boldsymbol{b}^{e\star}$.

Substituting the evolution equation for $\boldsymbol{d}^p$ (6.32) into (6.38) we arrive at the time-discrete expression of the evolution relations in the form

$$\boldsymbol{F}^e_{\mathrm{n}} = \exp\left[\Delta\gamma \frac{\partial f(\boldsymbol{\tau}, \bar{g})}{\partial \boldsymbol{\tau}}\right] \boldsymbol{F}^{e\star}\,, \tag{6.40}$$

$$\xi_{\mathrm{n}+1} = \xi_{\mathrm{n}} + \Delta\gamma \frac{\partial f(\boldsymbol{\tau}, \bar{g})}{\partial \bar{g}}\,, \tag{6.41}$$

$$\Delta\gamma \geq 0, \quad f(\boldsymbol{\tau}, \bar{g}) \leq 0, \quad \text{and} \quad \Delta\gamma f(\boldsymbol{\tau}, \bar{g}) = 0\,. \tag{6.42}$$

The evolution relations in the above form enforce the plastic incompressibility constraint that $\det[\boldsymbol{F}^p] = 1$ [164].

The assumption of an isotropic elastic response implies that the Kirchhoff stress tensor and the elastic left Cauchy–Green tensor are coaxial, that is, their principal directions coincide [164]. Furthermore, the isotropic assumption implies that the elastic logarithmic strain, defined by

$$\boldsymbol{\varepsilon}^e = \tfrac{1}{2}\ln[\boldsymbol{b}^e]\,,$$

is also coaxial to $\boldsymbol{\tau}$, so that

$$\boldsymbol{\varepsilon}^e = \sum_{A=1}^{3} \varepsilon^e_A \boldsymbol{n}^{\star(A)} \otimes \boldsymbol{n}^{\star(A)}\,.$$

Using the definition of the trial elastic left Cauchy–Green tensor (6.39), the algorithmic flow rule (6.40) can be written as

$$\boldsymbol{b}^{e\star} = \exp\left[\Delta\gamma \frac{\partial f(\boldsymbol{\tau}, \bar{g})}{\partial \boldsymbol{\tau}}\right] \boldsymbol{b}^e_{\mathrm{n}} \exp\left[-\Delta\gamma \frac{\partial f(\boldsymbol{\tau}, \bar{g})}{\partial \boldsymbol{\tau}}\right]\,. \tag{6.43}$$

The preceding formulation for the evolution equations yields the following remarkable results [164]:

1. The principal directions $\boldsymbol{n}^A_{\mathrm{n}}$ of the unknown stress $\boldsymbol{\tau}_{\mathrm{n}}$, and the unknown left Cauchy–Green tensor coincide with the known trial principal directions of the trial left Cauchy–Green tensor $\boldsymbol{b}^{e\star}$, that is, $\boldsymbol{n}^{(A)}_{\mathrm{n}} = \boldsymbol{n}^{\star(A)}$.

2. Taking the logarithm of both sides of (6.43), and using the Hencky model and the von Mises yield criterion one obtains the time-discrete approximation of (6.32)–(6.34) as

$$\boldsymbol{\varepsilon}^e_{\mathrm{n}} = \boldsymbol{\varepsilon}^{e\star} - \Delta\gamma \frac{\partial \bar{f}(\bar{\boldsymbol{\tau}}, \bar{g})}{\partial \operatorname{dev}[\bar{\boldsymbol{\tau}}]} = \boldsymbol{\varepsilon}^{e\star} - \Delta\gamma \boldsymbol{\nu} \ , \tag{6.44a}$$

$$\xi_{\mathrm{n}} = \xi_{\mathrm{n}-1} + \Delta\gamma \frac{\partial \bar{f}(\bar{\boldsymbol{\tau}}, \bar{g})}{\partial \bar{g}} = \xi_{\mathrm{n}-1} + \sqrt{\tfrac{2}{3}}\Delta\gamma \ , \tag{6.44b}$$

$$\Delta\gamma \geq 0, \quad \bar{f}(\bar{\boldsymbol{\tau}}_{\mathrm{n}}, \bar{g}_{\mathrm{n}}) \leq 0, \quad \Delta\gamma \bar{f}(\bar{\boldsymbol{\tau}}_{\mathrm{n}}, \bar{g}_{\mathrm{n}}) = 0 \ , \tag{6.44c}$$

where the normal to the yield surface is denoted $\boldsymbol{\nu}$ and the von Mises yield function in the principal directions is denoted $\bar{f}$; that is,

$$\bar{f}(\bar{\boldsymbol{\tau}}, \bar{g}) = |\operatorname{dev}[\bar{\boldsymbol{\tau}}]| - \sqrt{\tfrac{2}{3}}\,(\kappa - \bar{g}) \leq 0 \ , \tag{6.45}$$

$$\boldsymbol{\nu} = \frac{\partial \bar{f}(\bar{\boldsymbol{\tau}}, \bar{g})}{\partial \operatorname{dev}[\bar{\boldsymbol{\tau}}]} = \frac{\operatorname{dev}[\bar{\boldsymbol{\tau}}]}{|\operatorname{dev}[\bar{\boldsymbol{\tau}}]|} = \frac{\operatorname{dev}[\bar{\boldsymbol{\tau}}^\star]}{|\operatorname{dev}[\bar{\boldsymbol{\tau}}^\star]|} \ . \tag{6.46}$$

Remark 6.3. The primary motivation for adopting a flow rule of the form given in (6.44a)–(6.44c) is that it preserves the simplicity of the return mapping algorithms used in the infinitesimal theory. This remarkable feature, first reported in the above form in the pioneering work of Simo [163], allows us to extend the strategy developed in Part I for the case of infinitesimal gradient plasticity to the finite-strain regime in a relatively straightforward manner. Geers [83] has also exploited this feature as a basis for a nonlocal implicit gradient plasticity formulation at finite strains.

7

The method of enhanced assumed strains

The constraint of incompressible plastic deformation renders classical finite element approximations utilising low-order elements susceptible to problems related to volumetric locking (see, for example, Hughes [102] and Belytschko et al. [23] for detailed overviews of locking in the context of linear and nonlinear problems respectively). Furthermore, low-order elements generally perform poorly in problems where the deformation is bending dominated. Low-order elements are preferable, however, as they reduce the computational expense and are more robust for large-deformation problems. In addition, the implementation of the discontinuous Galerkin problem for the model of gradient plasticity considered here, and detailed in Chapter 8, is greatly simplified when using low-order elements.

We choose to address the aforementioned limitations by using the enhanced assumed strain formulation first proposed for nonlinear problems in elasticity and elastoplasticity by Simo and Armero [165] and subsequently extended in [171, 86, 10]. In the enhanced assumed strain formulation the deformation gradient is additively composed of the conventional approximation based on the interpolation of the displacement and an enhanced part; that is,

$$\boldsymbol{F}_h = \underbrace{\mathrm{GRAD}_X[\boldsymbol{\varphi}_h]}_{\text{conventional}} + \underbrace{\tilde{\boldsymbol{F}}_h}_{\text{enhanced}} \quad .$$

The enhanced part $\tilde{\boldsymbol{F}}_h$ is endowed with various properties to circumvent locking whilst still satisfying the incompressibility constraint. The enhanced assumed strain

formulation was originally developed for infinitesimal deformation problems by Simo and Rifai [168].

An additional motivation for selecting the enhanced assumed strain formulation is its improved ability, relative to the widely used Q_1–P_0 formulation (bilinear displacement and constant pressure field interpolations), to sharply discern the extent of a shear band for problems involving a softening material [171]. The ability to predict meaningful mesh-independent solutions for softening problems is one of the key motivations behind the gradient plasticity model examined in this work. Furthermore, pressure-smoothing routines, required to smooth potential pressure oscillations that arise in Q_1–P_0 approximations, are not required.

Discontinuous Galerkin approximations for problems in nonlinear elasticity have been the subject of recent investigations by ten Eyck and Lew [180], ten Eyck et al. [181, 182] and Noels and Radovitzky [141]. Discontinuous Galerkin approximations for the displacement field are an effective approach to overcome problems related to locking that arise in incompressible nonlinear elasticity and plate bending applications [74, 29, 14, 187]. The problem of vanishing compressibility for the infinitesimal theory has been addressed using discontinuous Galerkin methods in [190, 96, 54, 101], amongst others, while ten Eyck and Lew [180] have considered the extension to the nonlinear regime. Furthermore, the analysis of the small-strain gradient plasticity problem using the discontinuous Galerkin method for the approximation of both the displacement and plastic strain fields was presented in Chapter 3.

The weak imposition of interelement continuity in discontinuous Galerkin formulations provides the solution with the additional "flexibility" to overcome locking while still imposing the incompressibility constraint. The weak imposition of interelement continuity may, at first, appear to produce results that seem "incorrect" but, as clearly demonstrated by ten Eyck and Lew [180], the discontinuous Galerkin approximation can be more accurate and less computationally expensive than a conforming approach. Consider, for example, the results in Fig. 7.1 taken from ten Eyck and Lew [180] for the indentation of an incompressible neo-Hookean material. The results on the left, obtained using the discontinuous Galerkin formulation, are as accurate as those on the right obtained using a conforming approach with a finer mesh.

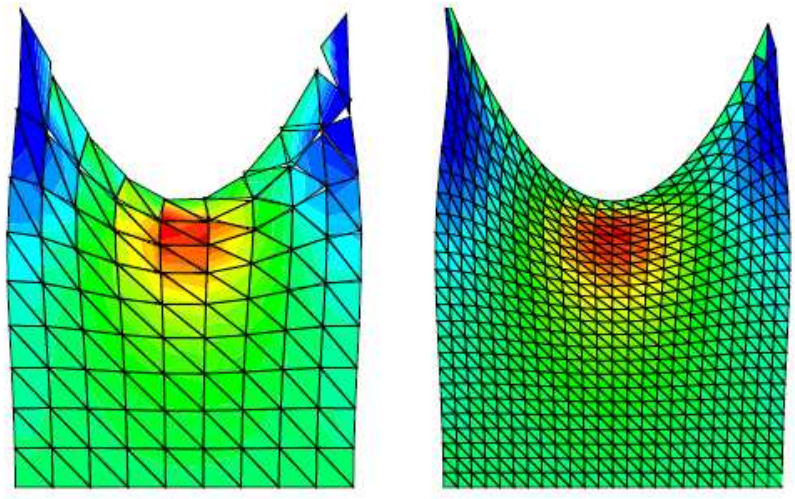

Fig. 7.1. Comparison of a discontinuous Galerkin approximation (left) and a conforming approximation (right) of a problem in incompressible elasticity (from [180])

Discontinuous Galerkin approximations of problems in nonlinear elastodynamics have also been investigated by Noels and Radovitzky [141]. They used a conventional second-order central-difference explicit scheme to perform the temporal integration. In determining the critical time step duration they took into account the discontinuous nature of the displacement approximation. Furthermore, they considered problems involving significant plastic deformation.

The focus of the work here is on a formulation of gradient plasticity that utilises the discontinuous Galerkin approach. We therefore do not use the discontinuous Galerkin method for the displacement field to overcome locking related problems but rather, as mentioned previously, adopt the more widely used method of enhanced assumed strains.

The objective of this chapter is to review the method of enhanced assumed strains for plane problems in nonlinear elasticity. The extension of the formulation to problems in plasticity follows in a straightforward manner due to the strain driven nature of the formulation. The method of enhanced assumed strains is independent of the choice of constitutive model. Indeed, we will use the enhanced assumed strains formulation in conjunction with a model of gradient plasticity in subsequent chapters.

The chapter concludes with several numerical examples that compare the performance of the enhanced assumed strain formulation with other approaches in the literature. While the performance of the enhanced assumed strain formulation is satisfactory, evidence of nonphysical hourglass modes remain for certain problems. These hourglass modes are present in several of the results presented in the literature using alternative formulations, but are yet considered acceptable. There are clearly still open issues in the approximation of nonlinear incompressible media using finite elements (see, for example, the comments in Auricchio et al. [17]).

7.1 An enhanced assumed strain formulation of nonlinear elasticity

The first objective of this section is to present the spatially-discrete nonlinear elasticity problem obtained using the enhanced assumed strain finite element formulation. The second objective is to develop the fully-discrete incremental problem and to give the corresponding matrix expressions.

7.1.1 Semi-discrete problem

Let $\mathcal{T}_h^0 = \{K^0\}$ be a shape-regular subdivision of the reference domain Ω where K^0 are, here, quadrilateral subdomains (finite elements) as shown in Fig. 7.2. We denote by $h_K^0 = \text{diam}[K^0]$ a measure of the element size and by $h = \max\{h_k^0, K^0 \in \mathcal{T}_h^0\}$ a measure of the maximum element size in the discretisation.

Following standard finite element procedure we approximate the displacement field $\boldsymbol{u}$ by a trial function $\boldsymbol{u}_h \in V^h$, where V^h is a finite-dimensional subspace of $V = H^1(\Omega)^2$. Over each element we associate a finite-dimensional function space X with basis functions N_φ^{A}, $(\text{A} = 1, \ldots, n_{\text{node}}^{\text{e}})$ defined on the reference element $\hat{K} \in \square = [-1, -1] \times [1, 1]$. As in the infinitesimal theory, $n_{\text{node}}^{\text{e}}$ denotes the number of displacement nodes per element. For the choice of bilinear elements considered here $n_{\text{node}}^{\text{e}} = 4$.

The interpolation of the reference domain and the approximation of the displacement field over a typical element follow as per conventional Galerkin finite element

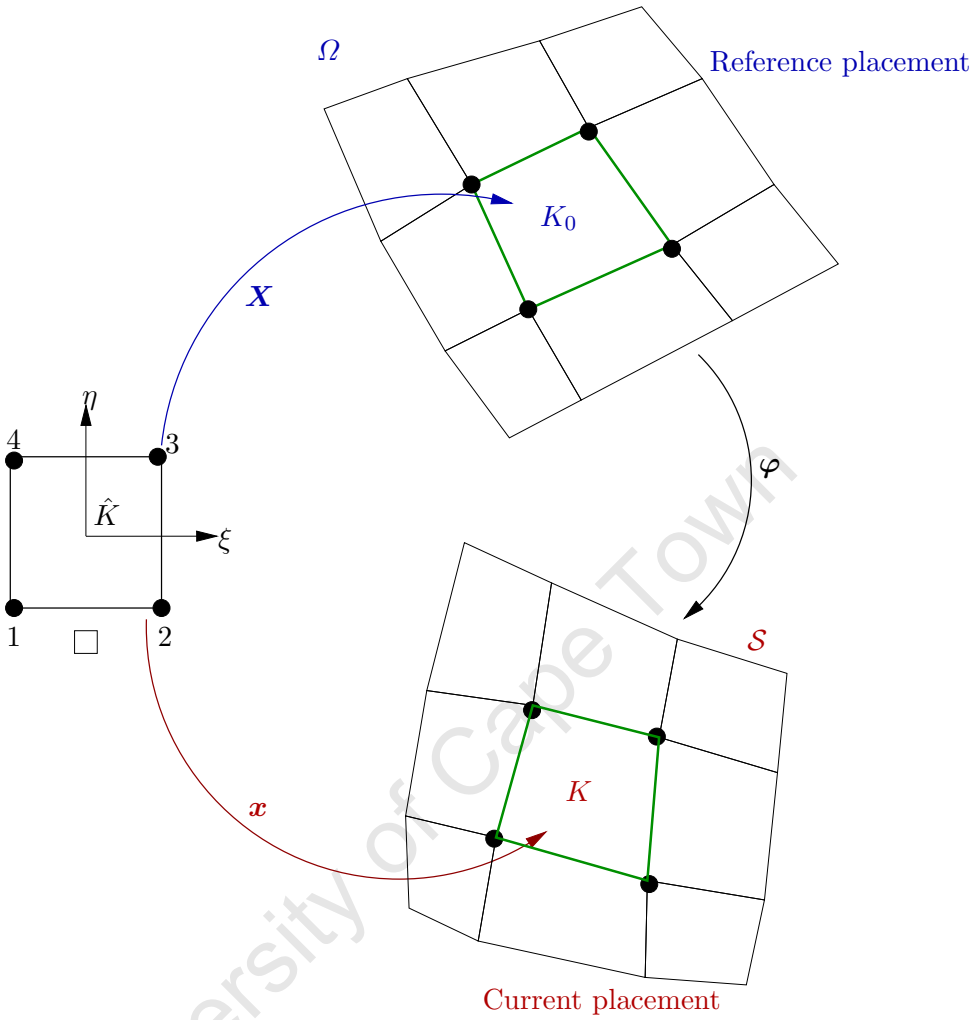

Fig. 7.2. Schematic of the motion and the isoparametric map

procedure based upon the isoparametric concept; that is,

$$\boldsymbol{X} \approx \boldsymbol{X}_h = \sum_{\mathrm{A}=1}^{n^{\mathrm{e}}_{\mathrm{node}}} N^{\mathrm{A}}_{\varphi}(\boldsymbol{\xi}) \boldsymbol{X}^e_{\mathrm{A}} \qquad \text{and} \qquad \boldsymbol{u}_h = \sum_{\mathrm{A}=1}^{n^{\mathrm{e}}_{\mathrm{node}}} N^{\mathrm{A}}_{\varphi}(\boldsymbol{\xi}) \boldsymbol{u}^e_{\mathrm{A}} \ ,$$

where $\boldsymbol{X}_{\mathrm{A}}$ are the reference coordinates of, and $\boldsymbol{u}_{\mathrm{A}}$ the displacement at node A. The points $\boldsymbol{\xi} = (\xi, \eta) \in \square$ are coordinates in the reference element.

The deformation gradient is interpolated across an element from the current nodal positions $\boldsymbol{x}_{\mathrm{A}} := \boldsymbol{X}_{\mathrm{A}} + \boldsymbol{u}_{\mathrm{A}}$ as

$$\mathrm{GRAD}_X[\boldsymbol{\varphi}_e^h] = \sum_{\mathrm{A}=1}^{n_{\mathrm{node}}^{\mathrm{e}}} \boldsymbol{x}_{\mathrm{A}}(t) \otimes \mathrm{GRAD}_X[\boldsymbol{N}_{\varphi}^{\mathrm{A}}] \ . \tag{7.1}$$

The time-independent derivatives of the basis functions N_{φ}^{A} relative to the reference configuration are determined from

$$\mathrm{GRAD}_X[N_{\varphi}^{\mathrm{A}}] = \boldsymbol{J}^{-T}\,\mathrm{GRAD}_{\xi}[N_{\varphi}^{\mathrm{A}}]\,,$$

where

$$\boldsymbol{J}(\boldsymbol{\xi}) := \frac{\partial \boldsymbol{X}_e^h}{\partial \boldsymbol{\xi}}$$

is the Jacobian between the reference configuration and the reference element, with the Jacobian determinant denoted by

$$j = \det[\boldsymbol{J}(\boldsymbol{\xi})] \ .$$

The enforcement of incompressible plastic deformation results in classical finite element approximations using low-order elements being susceptible to problems arising due to volumetric locking. We choose to address this shortcoming by using the enhanced assumed strain formulation [165, 171, 86, 10] in which the deformation gradient is additively composed of the conventional approximation given in (7.1) and an enhanced part; that is,

$$\boldsymbol{F}_h = \underbrace{\mathrm{GRAD}_X[\boldsymbol{\varphi}_h]}_{\text{conventional}} + \underbrace{\tilde{\boldsymbol{F}}_h}_{\text{enhanced}} \ . \tag{7.2}$$

The enhanced deformation gradient will be distinguished henceforth from the conventional deformation gradient by the presence of a super- or subscript h.

The enhanced part of the deformation gradient is constructed on the reference element $\hat{K}$ and denoted $\mathbb{F}$, as depicted in Fig. 7.3 taken from [172]. The enhanced

deformation gradient is then mapped to the current configuration $\mathcal{S} = \boldsymbol{\varphi}(\Omega)$ via the reference configuration Ω. The enhanced deformation is denoted $\tilde{\mathbb{F}}$ in the reference configuration and $\tilde{\boldsymbol{F}}_h$ in the current configuration.

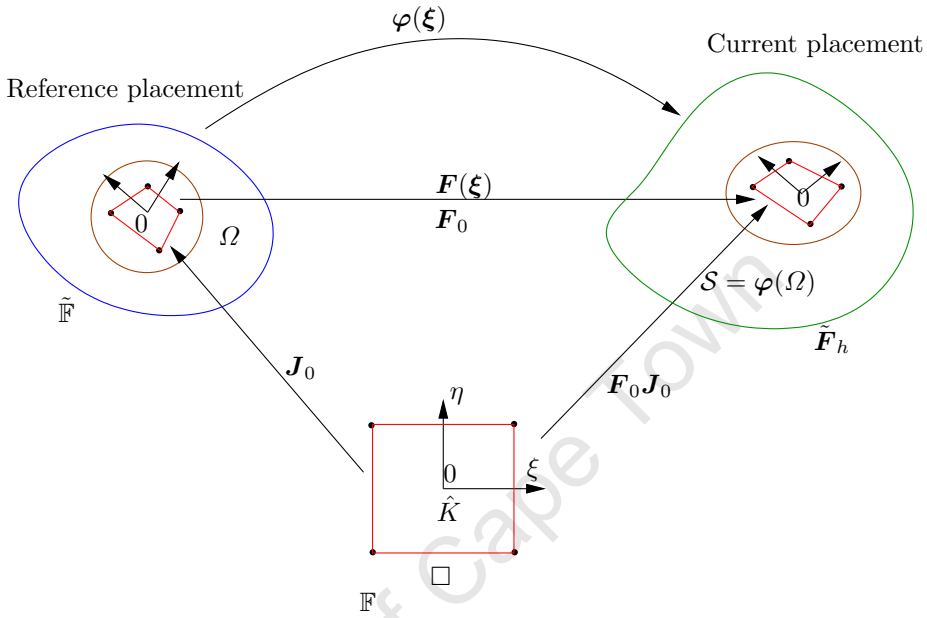

Fig. 7.3. Schematic of the motion in the enhanced assumed strain formulation (from [172])

Constructing $\tilde{\boldsymbol{F}}_h$ on the reference element allows the interpolation to be endowed with various properties critical to the stability and variational consistency of the method (see [165, 171] for further details). The linear map $\mathbb{F}$ is constructed subject to the restriction that is has a zero mean value over the reference element; that is,

$$\int_{\square} \mathbb{F} \, d\xi = \mathbf{0} \, .$$

Several transformations of $\mathbb{F} \in \square$ to $\tilde{\mathbb{F}} \in \Omega$ have been proposed in the literature. The tensorial transformation originally proposed by Simo and Armero [165] takes the form

$$\tilde{\mathbb{F}}(\boldsymbol{\xi}) = \frac{j_0}{j} \boldsymbol{J}_0 \mathbb{F} \boldsymbol{J}_0^{-1} \, , \tag{7.3}$$

where

$$\boldsymbol{J}_0 = \boldsymbol{J}(\boldsymbol{\xi} = \boldsymbol{0}) \qquad \text{and} \quad j_0 = \det[\boldsymbol{J}_0] \; . \tag{7.4}$$

This transformation is motivated by the incompatible modes element proposed by Taylor et al. [179]. A transformation subsequently proposed by Korelc and Wriggers [110] and Glaser and Armero [86] takes the form

$$\tilde{\mathbb{F}}(\boldsymbol{\xi}) = \frac{j_0}{j} \boldsymbol{J}_0^{-T} \mathbb{F} \boldsymbol{J}_0^{-1} \; . \tag{7.5}$$

Both transformations possess the property

$$\int_{K_0} \tilde{\mathbb{F}}_e(\boldsymbol{\xi}) \; dX = \boldsymbol{0} \, . \tag{7.6}$$

The space of enhanced deformation gradients is thus fully specified once the map $\tilde{\mathbb{F}}$ is defined. The enhanced interpolations are approximated from the scalar nodal values of the enhanced variables $\mathit{\Gamma}_{\mathrm{A}}$ according to

$$\mathbb{F} = \sum_{\mathrm{A}=1}^{n_{\mathrm{enh}}} \mathbb{F}^{\mathrm{A}}(\boldsymbol{\xi}) \mathit{\Gamma}_{\mathrm{A}} \, , \tag{7.7}$$

where n_{enh} denotes the number of enhanced variables. Four choices for $\mathbb{F}$ investigated in [165, 171, 86, 10] are

$$\mathbb{F} = \Gamma_1 \begin{bmatrix} \xi & 0 \\ 0 & 0 \end{bmatrix} + \Gamma_2 \begin{bmatrix} 0 & 0 \\ \xi & 0 \end{bmatrix} + \Gamma_3 \begin{bmatrix} 0 & \eta \\ 0 & 0 \end{bmatrix} + \Gamma_4 \begin{bmatrix} 0 & 0 \\ 0 & \eta \end{bmatrix} \qquad [165, 171] \ , \tag{7.8a}$$

$$\mathbb{F} = \Gamma_1 \begin{bmatrix} \xi & 0 \\ 0 & 0 \end{bmatrix} + \Gamma_2 \begin{bmatrix} 0 & \xi \\ \xi & 0 \end{bmatrix} + \Gamma_3 \begin{bmatrix} 0 & \eta \\ \eta & 0 \end{bmatrix} + \Gamma_4 \begin{bmatrix} 0 & 0 \\ 0 & \eta \end{bmatrix} \qquad [86] \ , \tag{7.8b}$$

$$\mathbb{F} = \Gamma_1 \begin{bmatrix} \xi & 0 \\ 0 & 0 \end{bmatrix} + \Gamma_2 \begin{bmatrix} 0 & \xi \\ 0 & 0 \end{bmatrix} + \Gamma_3 \begin{bmatrix} 0 & 0 \\ \eta & 0 \end{bmatrix} + \Gamma_4 \begin{bmatrix} 0 & 0 \\ 0 & \eta \end{bmatrix} \qquad [86] \ , \tag{7.8c}$$

$$\mathbb{F} = \Gamma_1 \begin{bmatrix} 0 & 0 \\ \xi & 0 \end{bmatrix} + \Gamma_2 \begin{bmatrix} 0 & \eta \\ 0 & 0 \end{bmatrix} \qquad [10] \ . \tag{7.8d}$$

It should be emphasised that the nodal values of the enhanced parameters are internal to the element; that is, interelement continuity of Γ is not required.

The mapping $\tilde{\mathbb{F}}$ is transformed to the current configuration using the formula

$$\tilde{\boldsymbol{F}}_h = \boldsymbol{F}_0^h \tilde{\mathbb{F}} \qquad \text{where} \qquad \boldsymbol{F}_0^h = \mathrm{GRAD}_X[\boldsymbol{\varphi}_h]|_{\boldsymbol{\xi}=\boldsymbol{0}} \, . \tag{7.9}$$

The use of $\boldsymbol{F}_0^h$ in the mapping ensures that the formulation is frame-invariant. In addition $\tilde{\boldsymbol{F}}_h$ has a zero mean over an element.

The structure of $\tilde{\boldsymbol{F}}_h$ chosen here is based on the recommendations made in Glaser and Armero [86]; that is, the form of $\mathbb{F}$ is given by (7.8c) and the transformation $\tilde{\mathbb{F}}(\boldsymbol{\xi})$ by (7.5), thereby introducing an additional four internal degrees of freedom per element. These additional degrees of freedom are condensed out at element level as they are not subject to interelement continuity constraints.

Following Simo et al. [171], the variational equations governing the quasi-static enhanced finite element formulation are

$$\int_\Omega \boldsymbol{P}_h : \mathrm{GRAD}[\delta\boldsymbol{\varphi}_h] \, dX = \int_{\Gamma_T} \boldsymbol{t}^N \cdot \delta\boldsymbol{\varphi}_h \, dS \quad \forall \delta\boldsymbol{\varphi}_h \in V^h \ , \tag{7.10a}$$

$$-\int_\Omega \boldsymbol{P}_h : \delta\tilde{\boldsymbol{F}}_h \, dX = 0 \quad \forall \delta\tilde{\boldsymbol{F}}_h \in M^h \ , \tag{7.10b}$$

where $\delta\boldsymbol{\varphi}_h$ are material test functions, and M^h the space of admissible enhanced deformation gradients $\delta\tilde{\boldsymbol{F}}_h$ defined precisely in [165, 171]. Equation (7.10a) results from

the conservation of linear momentum while (7.10b) enforces orthogonality between the enhanced variables and the stress.

The most efficient numerical realisation of the enhanced assumed strain method is obtained by restating the weak form of the governing equations (7.10a)–(7.10b) in terms of variables defined on the current configuration as follows:

$$\int_{\Omega} \boldsymbol{\tau}_h(\boldsymbol{F}_h) : \tilde{\nabla}(\delta\boldsymbol{\varphi}_h)\ dX = \int_{\Gamma_T} \boldsymbol{t}^n \cdot \delta\boldsymbol{\varphi}_h\ dS\,, \tag{7.11a}$$

$$\int_{\Omega} \boldsymbol{\tau}_h(\boldsymbol{F}_h) : \mathrm{sym}[\tilde{\nabla}(\delta\boldsymbol{\varphi}_h)]\ dX = 0\,, \tag{7.11b}$$

where

$$\tilde{\nabla}(\delta\boldsymbol{\varphi}_h) := \mathrm{GRAD}_X[\delta\boldsymbol{\varphi}_h]\boldsymbol{F}_h^{-1}\,.$$

The constitutive models presented in Chapter 6 can be used without modification by simply using the enhanced assumed strain definition of the deformation gradient. The super- or subscript h will be omitted subsequently from all symbols other than $\boldsymbol{F}_h$, where convenient, to simplify the notation.

7.1.2 Linearised semi-discrete problem

The linearisation of the weak form of the governing equations (7.11a)–(7.11b) is a key step in the development of the incremental finite element problem. The linearisation procedure is presented in detail in [86, 10]; thus, only certain key aspects are discussed here. We shall adopt Voigt notation, as in Chapter 4, to express second- and fourth-order tensors as vectors and matrices respectively. Variables expressed using Voigt notation are distinguished using upright font.

The Kirchhoff stress tensor $\boldsymbol{\tau} = \boldsymbol{P}\boldsymbol{F}_h^T$ is expressed using Voigt notation as

$$\boldsymbol{\tau} := [\tau_{11}\ \tau_{22}\ \tau_{12}]^T\,.$$

Furthermore, we define the various material and spatial gradients of the basis function N^{A} associated with node A as follows:

$$
\begin{aligned}
&\mathrm{GRAD}_X[N^{\mathrm{A}}] = \boldsymbol{J}^{-T}\,\mathrm{GRAD}_{\boldsymbol{\xi}}[N^{\mathrm{A}}]\,,\\
&\mathrm{GRAD}_0[N^{\mathrm{A}}] = \boldsymbol{J}_0^{-T}\,\mathrm{GRAD}_{\boldsymbol{\xi}}[N^{\mathrm{A}}(\boldsymbol{\xi}=\mathbf{0})]\,,\\
&\nabla_0[N^{\mathrm{A}}] = \boldsymbol{F}_{h0}^{-T}\,\mathrm{GRAD}_0[N^{\mathrm{A}}]\,,\\
&\overline{\mathrm{GRAD}_X}[N^{\mathrm{A}}] = \mathrm{GRAD}_X[N^{\mathrm{A}}] + \tilde{\mathbb{F}}^T\,\mathrm{GRAD}_0[N^{\mathrm{A}}]\,,\\
&\bar{\nabla}[N^{\mathrm{A}}] = \boldsymbol{F}_h^{-T}\overline{\mathrm{GRAD}_X}[N^{\mathrm{A}}]\,.
\end{aligned}
$$

Substituting the finite element approximations into the weak form of the governing equations produces the following two spatially discrete residual equations

$$
\begin{aligned}
\boldsymbol{R} &= \boldsymbol{f}_{\mathrm{ext}} - \boldsymbol{f}_{\mathrm{int}}\\
&= \boldsymbol{f}_{\mathrm{ext}} - \mathop{\mathsf{A}}_{e}\int_K \tilde{\boldsymbol{b}}^T\boldsymbol{\tau}\,dX = \mathbf{0} \qquad (7.12)\\
\boldsymbol{r}^e_{\mathrm{enh}} &= -\int_K \boldsymbol{g}^T\boldsymbol{\tau}\,dX = \mathbf{0}\,,\quad e=1,2,\ldots,n_{el}\,, \qquad (7.13)
\end{aligned}
$$

where $\boldsymbol{R}$ is the residual vector associated with (7.11a), $\boldsymbol{r}^e_{\mathrm{enh}}$ is the residual vector associated with (7.11b) at the element level, and $\boldsymbol{f}_{\mathrm{ext}}$ is the external force vector due to the applied tractions and body forces. The linearised strain operator $\mathfrak{b}$ is defined by

$$
\mathfrak{b} = \left[\mathfrak{b}^1\ldots\mathfrak{b}^{n_{node}}\right],\quad \text{where}\quad \mathfrak{b}^{\mathrm{A}} = \begin{bmatrix} N^{\mathrm{A}}_{\bar{1}} & 0\\ 0 & N^{\mathrm{A}}_{\bar{2}}\\ N^{\mathrm{A}}_{\bar{2}} & N^{\mathrm{A}}_{\bar{1}}\end{bmatrix},
$$

where

$$
[N^{\mathrm{A}}_{\bar{1}}\ N^{\mathrm{A}}_{\bar{2}}] = \bar{\nabla}N^{\mathrm{A}}\,.
$$

The linearised enhanced strain operator $\boldsymbol{g}$ is defined by

$$
\boldsymbol{g} = \left[\boldsymbol{g}^1\ldots\boldsymbol{g}^{n_{enh}}\right],\quad \text{where}\quad \boldsymbol{g}^{\mathrm{I}} = \begin{bmatrix} G^{\mathrm{I}}_{11}\\ G^{\mathrm{I}}_{22}\\ G^{\mathrm{I}}_{12}+G^{\mathrm{I}}_{21}\end{bmatrix},
$$

where

$$\mathbb{G} = \begin{bmatrix} G^{\mathrm{I}}_{11} & G^{\mathrm{I}}_{12} \\ G^{\mathrm{I}}_{21} & G^{\mathrm{I}}_{22} \end{bmatrix} := \boldsymbol{F}_0 \tilde{\mathbb{F}}^{\mathrm{I}} \boldsymbol{F}_h^{-1} ,$$

and $\mathbb{F}^{\mathrm{I}}$ is defined in (7.7).

The time domain under consideration $[0, T]$ is divided into N time steps of duration $\Delta t = T/N$. The complete system state is assumed known at the beginning of time step n from the converged conditions at the end of time step n − 1.

Consider a typical bilinear element K. The nodal displacement vector is denoted $\boldsymbol{d}^e = \left[\boldsymbol{d}_1^T \; \boldsymbol{d}_2^T \; \boldsymbol{d}_3^T \; \boldsymbol{d}_4^T\right]^T$ and the vector of enhanced variables at the element level is denoted $\boldsymbol{\Gamma}^e = [\Gamma_1 \; \Gamma_2 \; \Gamma_3 \; \Gamma_4]^T$. Linearisation of the system of governing equations (7.11a)–(7.11b) about the current time step produces the following set of matrix equations for the global incremental quantities $\Delta\boldsymbol{d}$ and $\Delta\boldsymbol{\Gamma}$

$$\begin{bmatrix} \boldsymbol{K}_{11} & \boldsymbol{K}_{12} \\ \boldsymbol{K}_{21} & \boldsymbol{K}_{22} \end{bmatrix} \begin{Bmatrix} \Delta\boldsymbol{d} \\ \Delta\boldsymbol{\Gamma} \end{Bmatrix} = \begin{Bmatrix} \boldsymbol{R} \\ \boldsymbol{r}_{\mathrm{enh}} \end{Bmatrix} .$$

The tangent matrix $\boldsymbol{K}$ is additively composed of material and geometric parts, due to the material and geometric nonlinearities inherent in the model; that is,

$$[\boldsymbol{K}] = \begin{bmatrix} \boldsymbol{K}_{11} & \boldsymbol{K}_{12} \\ \boldsymbol{K}_{21} & \boldsymbol{k}_{22} \end{bmatrix} = \underbrace{\begin{bmatrix} \boldsymbol{K}_{m,11} & \boldsymbol{K}_{m,12} \\ \boldsymbol{K}_{m,21} & \boldsymbol{K}_{m,22} \end{bmatrix}}_{\text{material}} + \underbrace{\begin{bmatrix} \boldsymbol{K}_{g,11} & \boldsymbol{K}_{g,12} \\ \boldsymbol{K}_{g,21} & \boldsymbol{K}_{g,22} \end{bmatrix}}_{\text{geometric}} ,$$

where $\boldsymbol{K}$ is assembled from the individual element contributions $\boldsymbol{k}^e$ as $\boldsymbol{K} = \mathop{\mathsf{A}}_{e} \boldsymbol{k}^e$. The contributions to $\boldsymbol{k}$ at the element level are

$$\boldsymbol{k} = \begin{bmatrix} \boldsymbol{k}_{11} & \boldsymbol{k}_{12} \\ \boldsymbol{k}_{21} & \boldsymbol{k}_{22} \end{bmatrix} = \underbrace{\begin{bmatrix} \boldsymbol{k}_{m,11} & \boldsymbol{k}_{m,12} \\ \boldsymbol{k}_{m,21} & \boldsymbol{k}_{m,22} \end{bmatrix}}_{\text{material}} + \underbrace{\begin{bmatrix} \boldsymbol{k}_{g,11} & \boldsymbol{k}_{g,12} \\ \boldsymbol{k}_{g,21} & \boldsymbol{k}_{g,22} \end{bmatrix}}_{\text{geometric}}$$

where

$$\boldsymbol{k}_{m,11} = \int_K \mathfrak{b}^{\mathrm{A}T} \boldsymbol{c} \mathfrak{b}^{\mathrm{B}T}\, dX \quad \text{for A, B} = 1, \ldots, n_{n_{nodes}}$$
$$\boldsymbol{k}_{m,22} = \int_K \boldsymbol{g}^{\mathrm{I}T} \boldsymbol{c} \boldsymbol{g}^{\mathrm{J}T}\, dX \quad \text{for I, J} = 1, \ldots, n_{n_{enh}}$$
$$\boldsymbol{k}_{m,12} = \int_K \mathfrak{b}^{\mathrm{A}T} \boldsymbol{c} \boldsymbol{g}^{\mathrm{J}T}\, dX \quad \text{for A} = 1, \ldots, n_{n_{nodes}} \text{ and J} = 1, \ldots, n_{n_{enh}}$$
$$\boldsymbol{k}_{g,11} = \int_K \mathbb{G}^{\mathrm{A}} \boldsymbol{\tau} : \mathbb{G}^{\mathrm{B}}\, dX \quad \text{for A, B} = 1, \ldots, n_{n_{nodes}}$$
$$\boldsymbol{k}_{g,22} = \int_K \mathbb{G}^{\mathrm{I}} \boldsymbol{\tau} : \mathbb{G}^{\mathrm{J}}\, dX \quad \text{for I, J} = 1, \ldots, n_{n_{enh}}$$
$$\boldsymbol{k}_{g,12} = \int_K \left[\mathbb{G}^{\mathrm{J}} \boldsymbol{\tau} \overline{\nabla} N^{\mathrm{A}} + \boldsymbol{\tau} \mathbb{G}^{\mathrm{J}T} \nabla_0 N^{\mathrm{A}} \right] dX$$
$$\text{for A} = 1, \ldots, n_{n_{nodes}} \text{ and J} = 1, \ldots, n_{n_{enh}},$$

and where $\boldsymbol{c}$ denotes the spatial tangent modulus.

The enhanced parameters are defined locally at the element level. Static condensation of the enhanced parameters leads to the reduced system

$$\boldsymbol{K}^{\star} \Delta \boldsymbol{d} = \boldsymbol{R}^{\star} \tag{7.14}$$

for the increment in the nodal displacements at the structural level, where

$$\boldsymbol{K}^{\star} = \mathop{\mathsf{A}}_{e} \boldsymbol{k}_e^{\star} = \mathop{\mathsf{A}}_{e} \left[\boldsymbol{k}_{11}^e - \boldsymbol{k}_{12}^e \left[\boldsymbol{k}_{22}^e \right]^{-1} \boldsymbol{k}_{21}^e \right], \tag{7.15}$$
$$\boldsymbol{R}^{\star} = \boldsymbol{R} - \mathop{\mathsf{A}}_{e} \left[\boldsymbol{k}_{12}^e \left[\boldsymbol{k}_{22}^e \right]^{-1} \boldsymbol{r}_{\mathrm{enh}} \right], \tag{7.16}$$

and where $\boldsymbol{k}_{21}^e = \boldsymbol{k}_{12}^{e\,T}$. The increment in the enhanced parameters at the element level can be recovered from the increment in nodal displacements as

$$\Delta \boldsymbol{\Gamma}^e = \left[\boldsymbol{k}_{22}^e \right]^{-1} \left(\boldsymbol{r}_{\mathrm{enh}} - \boldsymbol{k}_{21}^{e(k)} \Delta \boldsymbol{d}^e \right).$$

The reduced system of governing equations are solved iteratively using a predictor–corrector scheme in order to determine the increment in the displacement field that

arises due to the increment in loading taking into account the constitutive relations governing the material response.

7.2 Numerical examples

The enhanced assumed strain formulation is implemented within the finite element code developed for this work. The implementation of the enhanced assumed strain method is validated by comparing the results obtained for a series of benchmark problems with those in the published literature. A compressible neo-Hookean constitutive model is considered, with Λ and μ given as 4×10^5 and 80.19 respectively. This choice of Lamé moduli renders the material quasi-incompressible. Details of the neo-Hookean model were presented in Section 6.1.5. Plane strain conditions are assumed appropriate; volumetric locking does not occur in plane stress problems due to the ability of the material to deform in the out-of-plane direction and thereby satisfy the incompressibility constraint without locking.

7.2.1 Upsetting problem

The simulated upsetting of a unit block, the geometry of which is shown in Fig. 7.4, is studied in Wriggers and Hueck [191]. A rigid frictionless platen displaces the upper-edge of the domain downwards to produce a final upsetting of 30 % of the initial domain height. The lower-edge of the block is fully constrained. A relatively coarse uniform 10×10 finite element mesh is used to allow for direct comparisons with the results presented by Wriggers and Hueck.

The force acting on the platen versus the imposed displacement for a variety of different element formulations is shown in Fig. 7.5(a) taken from [191]. The response of the conventional bilinear Q_1 element clearly exhibits an overly stiff response indicative of volumetric locking. The widely used Q_1–P_0 formulation, the incompatible modes formulation $QM6$ developed by Taylor et al. [179] and the $QS6$ element developed by Wriggers and Hueck [191] all demonstrate the correct locking-free response. The force versus displacement history obtained here using the enhanced assumed strain formulation is shown in Fig. 7.5(b). The results are near-identical to those reported in

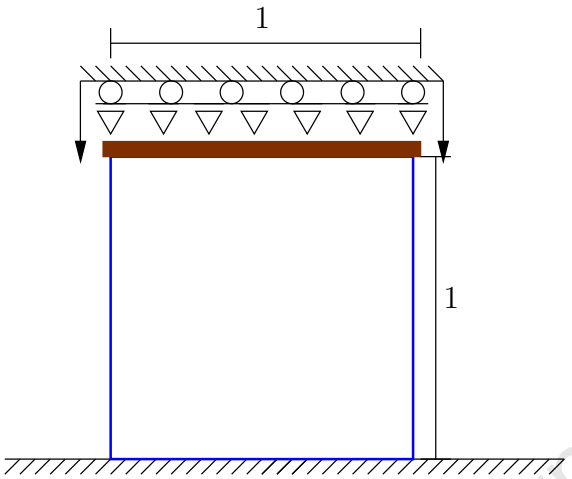

Fig. 7.4. Diagram of the upsetting problem

[191] thereby demonstrating the effectiveness of the method to overcome volumetric locking and partially validating the implementation within the finite element code.

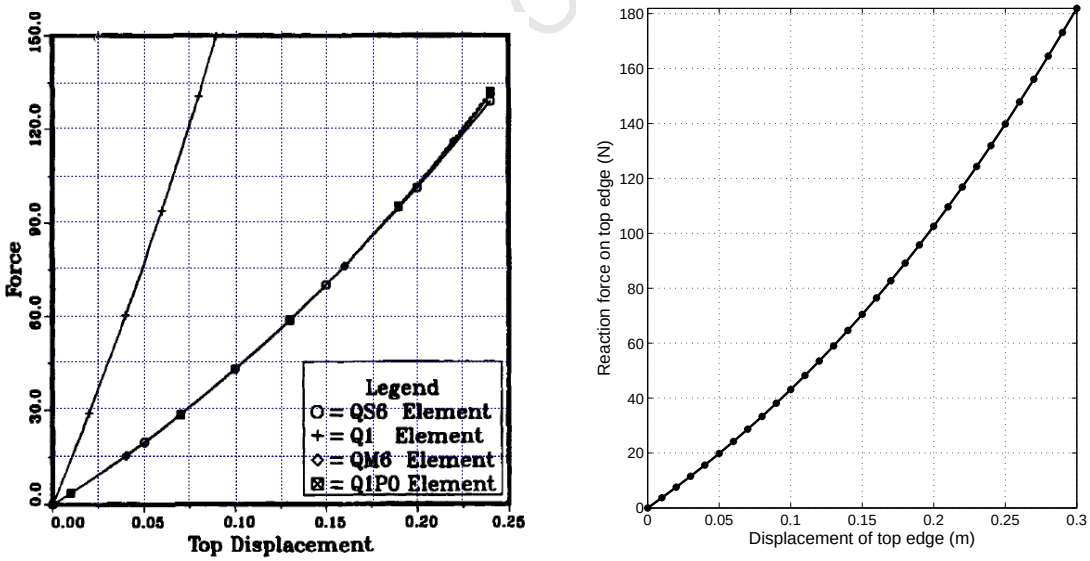

(a) Wriggers and Hueck [191]

(b) Enhanced assumed strain formulation

Fig. 7.5. Relationship between the force on the platen and the imposed displacement for a variety of different formulations reported in the literature and the method of enhanced assumed strains

The final deformed block configuration obtained using the enhanced assumed strain formulation and that obtained by Wriggers and Hueck [191] using the $QS6$ element are shown in Figs 7.6(a) and 7.6(b). The results are identical. The final deformed configuration suggests that some hourglassing is still present in the elements that contain as their boundaries the lower edge of the domain where the displacement is fully constrained. The additional displacement constraints arising from the Dirichlet boundary conditions appear to make it impossible for these elements to satisfy the incompressibility constraint without undergoing some hourglassing.

Both simulations use a 5-point quadrature rule proposed by Simo et al. [171]. The 5-point quadrature rule significantly reduces the computational expense of the formulation relative to a 9-point (3×3) rule without sacrificing accuracy. The final deformed configuration obtained using a 3×3 rule, shown in Fig. 7.6(d), is identical to that obtained using the 5-point rule. A 2×2 quadrature rule is insufficient to properly integrate the bilinear forms arising in the enhanced assumed formulation as indicated by the presence of the hourglass modes in Fig. 7.6(c). Wriggers and Hueck obtained the identical erroneous results using a 2×2 quadrature rule. The extent of the hourglassing is no longer restricted to the region near the lower boundary as it was when using the 5-point and 3×3 quadrature rules; the hourglassing effects all elements in the domain.

The values of the enhanced variables Γ_{A} ($\mathrm{A} = 1, \ldots, 4$) superimposed upon the deformed domain are shown in Fig. 7.7. As expected, the magnitude of the enhanced variables is greater in those elements on the lower outer edge that undergo a significant distortion. These results are purely illustrative as the enhanced variables are defined on the reference element $\hat{K}$ and the orientation of the elements in the current configuration is not necessarily the same for all elements. The aim here is to indicate the regions in which the enhanced parameters are activated and their relative magnitudes.

The enhancement results in the determinant of enhanced deformation gradient $\boldsymbol{F}_h$ remaining close to unity even in the highly distorted elements, as shown in Fig. 7.8(a). The variation in the conventional deformation gradient $\det[\mathrm{GRAD}_X\, \boldsymbol{\varphi}]$ across the deformed configuration is shown in Fig. 7.8(b). The elements on the lower left- and

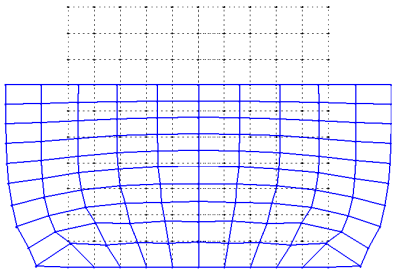

(a) Enhanced assumed strain formulation with a 5-point quadrature rule

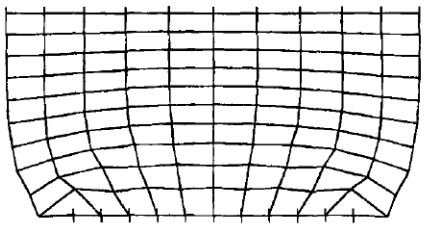

(b) Wriggers and Hueck [191] formulation with a 5-point quadrature rule rule

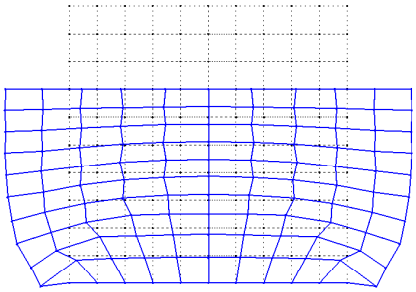

(c) Enhanced assumed strain formulation with a 2 × 2 quadrature rule

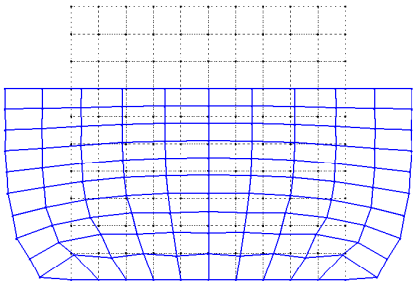

(d) Enhanced assumed strain formulation with a 3 × 3 quadrature rule

Fig. 7.6. Final deformed block configuration after an upsetting of 30 % obtained using three different quadrature rules

right-hand side of the domain have distorted to such a degree that the determinant of the conventional deformation gradient is approaching zero.

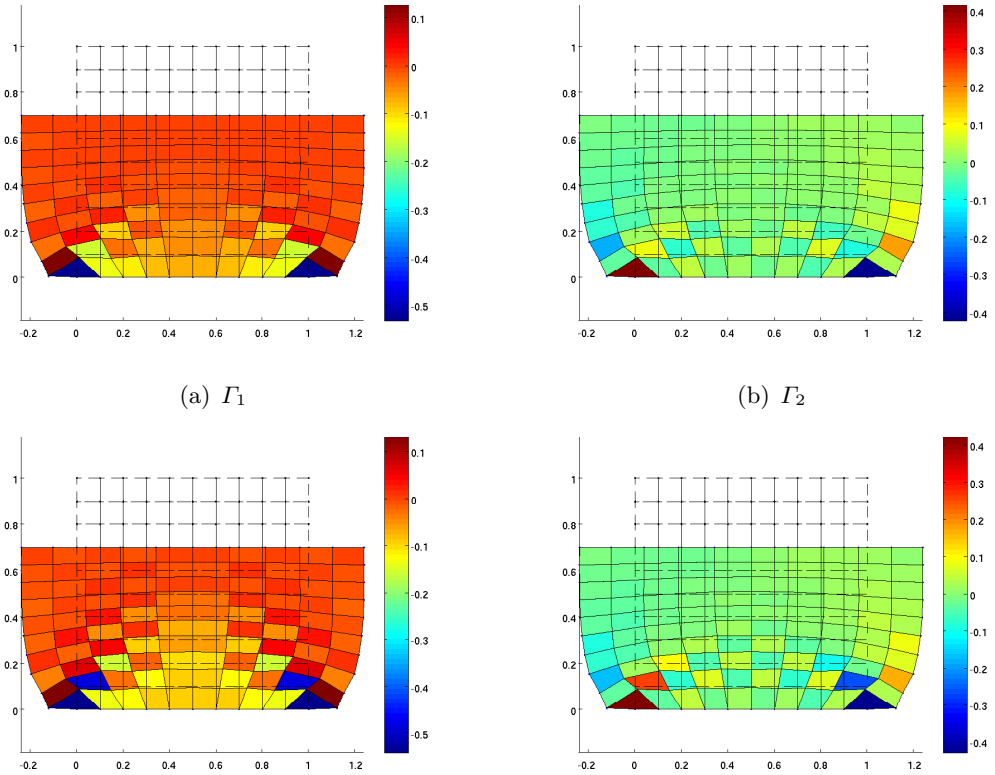

(a) Γ_1 (b) Γ_2

(c) Γ_3 (d) Γ_4

Fig. 7.7. Value of the enhanced variables $\{\Gamma_1,\ \Gamma_2,\ \Gamma_3,\ \Gamma_4\}$ superimposed upon the deformed domain

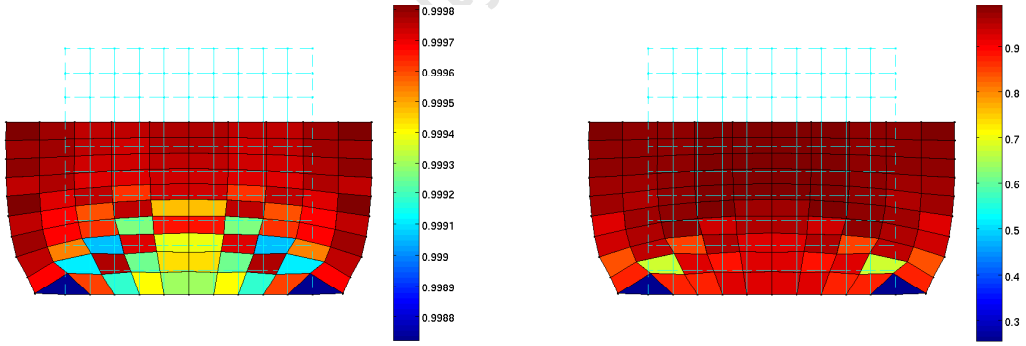

(a) $\det[\boldsymbol{F}_h]$ (b) $\det[\mathrm{GRAD}_X\,\boldsymbol{\varphi}]$

Fig. 7.8. Variation in the minimum value of the determinant of the enhanced and conventional components of the deformation gradient across the deformed domain of the block

7.2.2 Cook's membrane problem

Consider the tapered cantilever fully fixed on the left edge and subjected to a shearing load $F = 100$ on the right edge, as shown in Fig. 7.9. The linear elastic version of this problem is frequently referred to as the "Cook's membrane problem", and is used to ascertain the performance of an element under bending-dominated deformation. The nonlinear elastic version of the problem for quasi-incompressible material has been used as a benchmark problem in [165, 191, 86] amongst others. The vertical displacement of the upper right vertex of the cantilever is used to assess the bending performance of the formulation in the quasi-incompressible regime. The load is applied here in 100 equal intervals.

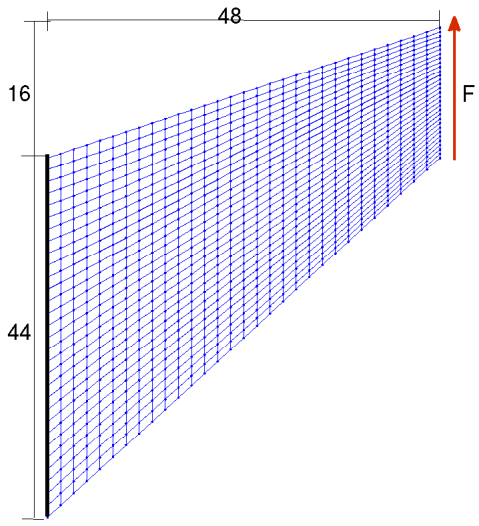

Fig. 7.9. Geometry of the Cook's membrane problem

Figure 7.10 shows the relationship between the tip deflection and the number of elements per side (a measure of the mesh size). The poor performance of the conventional bilinear Q_1 element in bending-dominated problems is responsible for the extremely slow convergence rate seen in Fig. 7.10(a) taken from [191]. The rapid convergence of the $QS6$ element, developed by Wriggers and Hueck [191], is also shown.

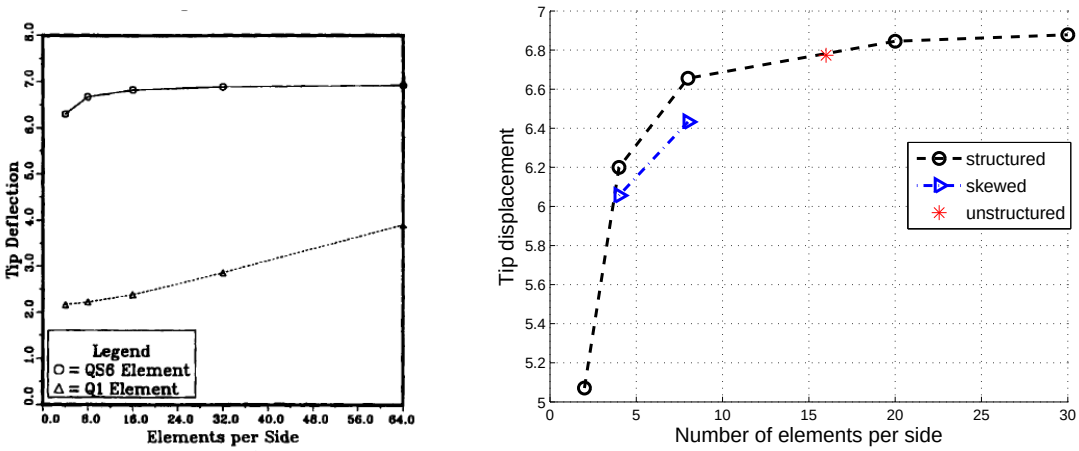

(a) Tip deflection versus the number of elements per side (from [191])

(b) Tip deflection versus the number of elements per side obtained using the enhanced assumed strain formulation

Fig. 7.10. Relationship between the tip deflection and the mesh resolution for the Cook's membrane problem

The performance of the enhanced assumed strain formulation for both regular, skewed and unstructured discretisations of the domain is shown in Fig. 7.10(b). The number of elements per side in the case of the unstructured mesh is obtained by taking the square root of the total number of elements. The rapid rate of convergence obtained using the regular discretisation is near-identical to that reported in [191] for the $QS6$ element. The rate of convergence obtained using the skewed mesh is slower than that obtained using the structured mesh.

The final deformed configuration of the cantilever obtained using the enhanced assumed strain formulation with a variety of structured, unstructured and skewed meshes is shown in Fig. 7.11. The final tip deflections are given in Table 7.1. It is clear that the enhanced assumed strain formulation performs well in bending-dominated problems, even when using unstructured meshes.

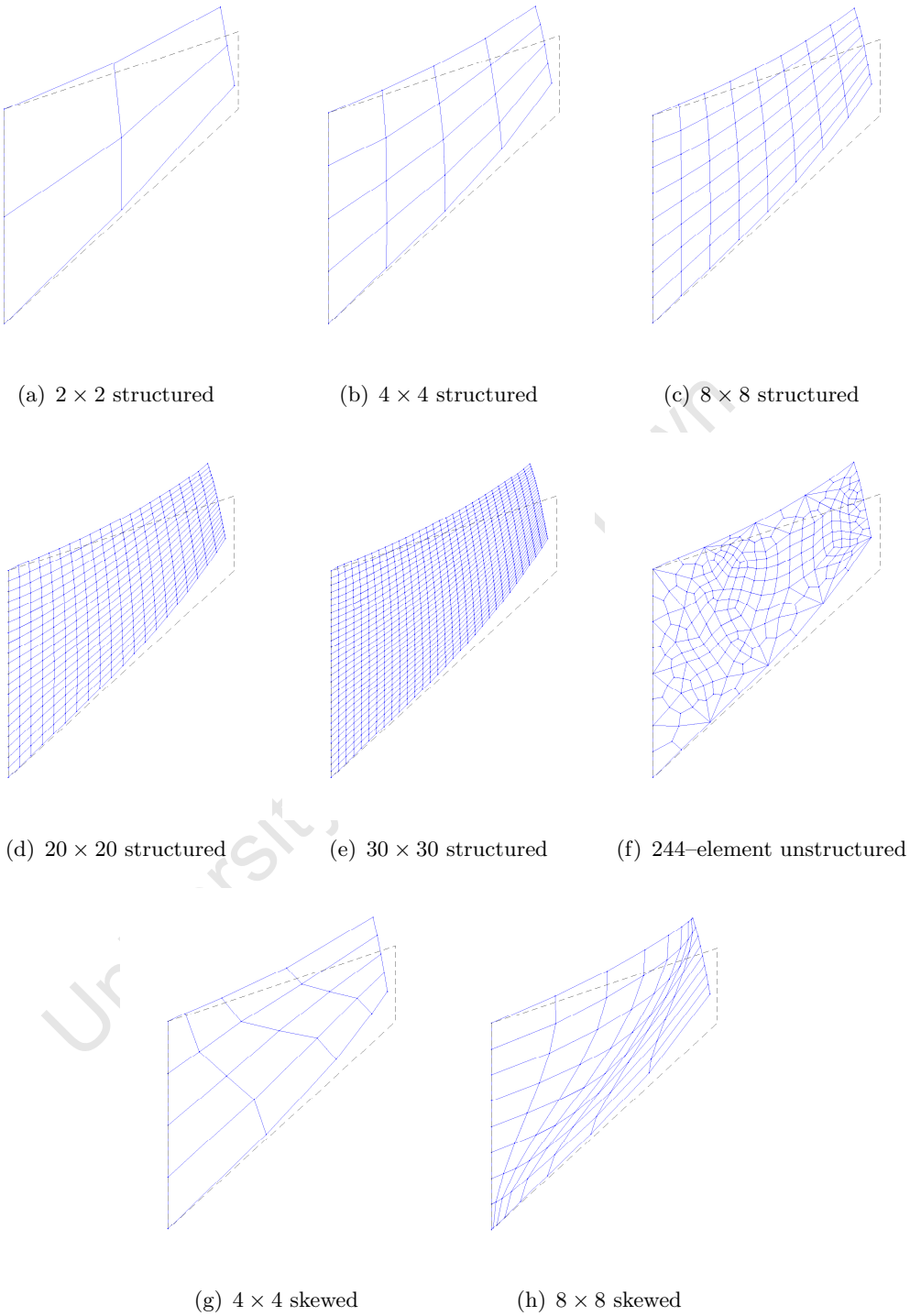

(a) 2×2 structured (b) 4×4 structured (c) 8×8 structured

(d) 20×20 structured (e) 30×30 structured (f) 244–element unstructured

(g) 4×4 skewed (h) 8×8 skewed

Fig. 7.11. Initial (dashed black line) and deformed (solid blue line) configurations for the various structured, unstructured and skewed discretisations of the Cook's membrane problem

Table 7.1. Vertical tip displacement of the cantilever obtained using various triangulations

Mesh	Vertical tip displacement
2×2 structured	5.0709
4×4 structured	6.1996
8×8 structured	6.6558
20×20 structured	6.8451
30×30 structured	6.8783
4×4 skewed	6.0560
8×8 skewed	6.4327
244–element unstructured	6.7732

7.2.3 Indentation problem

The indentation problem consists of a rubber block of rectangular cross-section indented by a frictionless rigid indenter also of rectangular cross-section as shown in Fig. 7.12. This example was considered by Crisfield et al. [60] to investigate a range of low-order element formulations for finite-strain problems under high compressive strains. The problem has subsequently been used as a benchmark by Kasper and Taylor [108] and de Souza Neto et al. [65], amongst others.

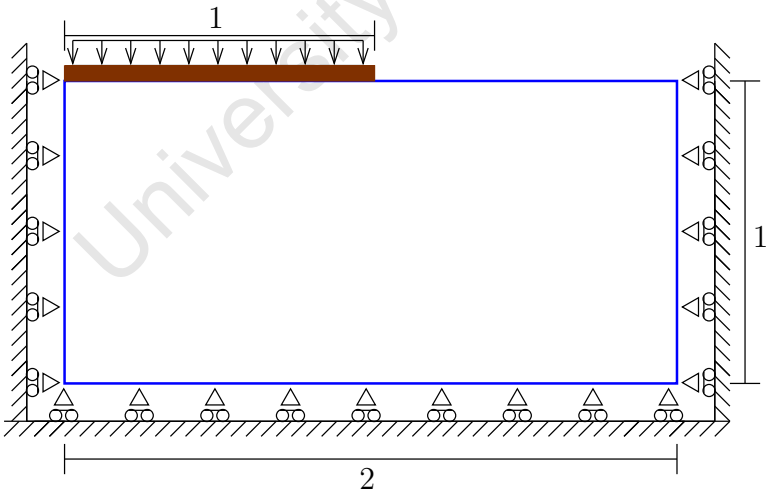

Fig. 7.12. Diagram of the indentation test

The problem is analysed using the original enhanced assumed strain formulation proposed by Simo et al. [171] as well as the modified formulation proposed by Glaser and Armero [86] as used in the previous examples. The results obtained are compared with those in the published literature in Fig. 7.13.

The problem was analysed by de Souza Neto et al. [65] using an extension of their F-bar formulation, while Kasper and Taylor [108] used a mixed–enhanced formulation. The results obtained by de Souza Neto et al. on a coarse 8×4 mesh are reproduced in Fig. 7.13(e). The total indentation is 25 % of the domain height. Kasper and Taylor analysed the problem using a more refined 20×10 mesh with the final configuration after a 25 % indentation reproduced in Fig. 7.13(f). The results given in the two aforementioned publications demonstrate significantly different behaviour. These different results can be reproduced using the enhanced assumed strain formulation by making different choices for the form of the enhanced field.

The results obtained using the enhanced assumed strain formulation proposed by Simo et al. [171] are shown in Fig. 7.13(a). The final deformed configuration is very similar to that obtained by de Souza Neto et al. with what appear to be hourglass modes present. The results obtained using the original enhanced assumed strain formulation on the 20×10 mesh are given in Fig. 7.13(b). The simulation could not proceed beyond the 12.75 % indentation indicated due to excessive element distortion in the central region below the indenter. The results obtained here using the modified enhanced assumed strain formulation proposed in [86] are shown in Figs. 7.13(c) and 7.13(d). The results are very similar in nature to those of Kasper and Taylor presented in Fig. 7.13(f).

Remark 7.1. The findings presented here emphasise the need for well-constructed benchmark tests for the validation of methods to circumvent locking. There appear to be inconsistencies in what constitutes a successful benchmark validation for relatively simple problems involving quasi-incompressible materials at finite strains. A more detailed investigation of the factors contributing to these inconsistencies is recommended. As mentioned in the introduction to this chapter, there are clearly still open issues in the approximation of nonlinear incompressible media using finite elements [17].

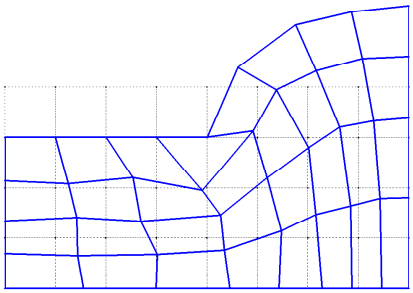

(a) 8×4 Simo et al. formulation

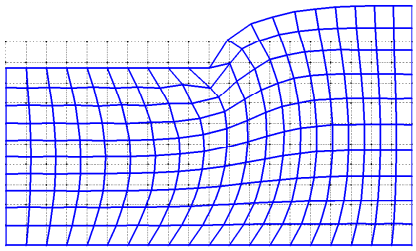

(b) 20×10 Simo and Armero formulation 12.75% indentation

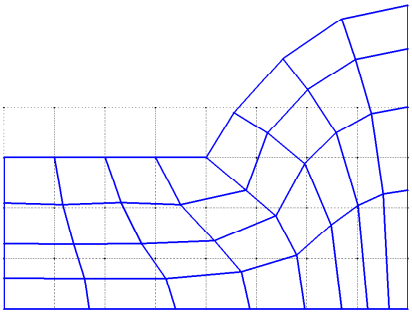

(c) 8×4 enhanced assumed strain Glaser and Armero formulation

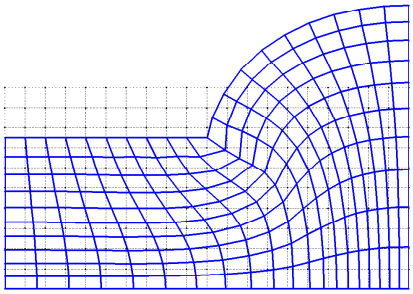

(d) 20×10 Glaser and Armero formulation

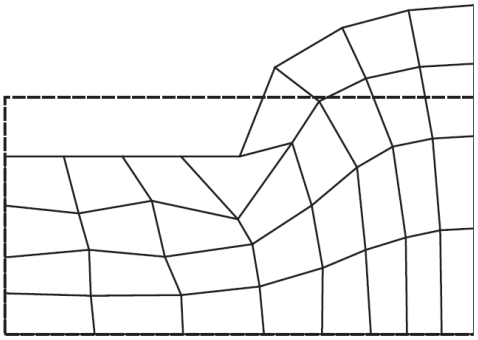

(e) 8×4 F-bar formulation [65]

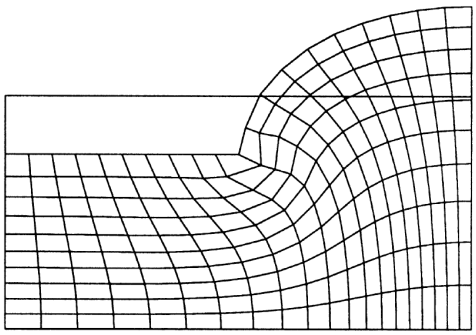

(f) 20×10 mixed–enhanced formulation [108]

Fig. 7.13. Initial and deformed domain after an indentation of 25 %, unless otherwise stated, obtained using the original and modified enhanced assumed strain formulation as well as results from the published literature

8

A discontinuous Galerkin formulation of gradient plasticity at finite strains

A predictor–corrector solution strategy has been adopted here to solve the gradient elastoplasticity problem at finite strains. The approximation of the incremental form of the equilibrium equation using an enhanced assumed strain formulation, as presented in the previous chapter, constitutes the predictor step of the algorithm. The outcome of the predictor step is an approximation of the deformation field. The form of the corrector step varies according to the constitutive model adopted. The objective this chapter is to present details of the corrector step for the model of gradient plasticity considered here at finite strains.

The corrector step for the model of gradient plasticity involves the solution of the discretised weak form of the plastic flow law using a discontinuous Galerkin finite element formulation. We therefore do not assume continuity of the effective plastic strain field but impose this in a weak sense where needed. The key steps involved in this procedure and the motivation for the selection of a discontinuous Galerkin formulation have been presented in Part I and in particular, in Chapter 4, where the algorithm for the small-strain case was described in detail. Furthermore, the assumption of an exponential approximation for the evolution of plastic flow (as detailed in Chapter 6) renders the corrector step near-identical to the small-strain problem. Indeed, this was the motivation for selecting the exponential approximation proposed by Simo [163]. The focus of the current chapter is, therefore, on features of the corrector step particular to the finite-strain problem.

The gradient plasticity model analysed here has been extended to the finite-strain regime by various researchers (see, for example, [113, 134, 150, 116] amongst others).

Li and Cescotto [113] considered a conforming approximation in which the Laplacian term in the yield criterion was interpolated locally from neighbouring quadrature points. A mixed finite element formulation was adopted and low-order Q_1 elements used in combination with a reduced quadrature scheme to circumvent volumetric locking. Details of the consistent tangent predictor are given. The approach of Ramaswamya and Aravas [150] also makes use of an exponential approximation for the evolution of plastic deformation. A conforming C^0 finite element approximation is adopted for the interpolation of the effective plastic strain. Mikkelsen [134] considers both a C^0 and a C^1 formulation and presents a series of examples in two and three dimensions that demonstrate the effectiveness of the approach in circumventing the various pathologies associated with locking. The approach of Liebe et al. [116], an extension their previous work for small strains [115], bears various similarities to the formulation presented here. They present the constitutive equations in a thermodynamically consistent manner. The nonlocal algorithmic consistency condition is solved using a conforming formulation within a standard finite element framework. Furthermore, a series of numerical examples demonstrate the effectiveness of their strategy.

The structure of this chapter is as follows. A thermodynamically consistent formulation of the constitutive equations is given in Section 8.1. The formulation exploits the dissipation inequality to derive the constitutive relations and define the various conjugate quantities. The nature of the additional boundary conditions that arise due to the model of gradient plasticity is made clear and their treatment discussed. A brief overview of the discontinuous Galerkin approach is then given in Section 8.2. The chapter concludes with details of the algorithm and, in particular, the derivation of the consistent tangent predictor, an essential component of an efficient numerical implementation.

8.1 Constitutive relations and the flow law

As with the classical problem of finite plasticity discussed in Chapter 6, the response of the system is characterised by a free energy function W additively composed of

an elastic part $\bar{W}^e$ and a plastic part $\bar{W}^p$. The free energy function is extended to the gradient regime by including in $\bar{W}^p$ an additional quadratic term involving the gradient of the equivalent plastic strain; that is,

$$W = \bar{W}\left(\boldsymbol{F}^e, \xi, \nabla\xi\right) = \bar{W}^e(\bar{\boldsymbol{C}}^e) + \underbrace{\tfrac{1}{2}k_2\xi^2 + \tfrac{1}{2}k_3|\nabla\xi|^2}_{\bar{W}^p(\xi,\nabla\xi)},$$

where, as in the infinitesimal formulation, $k_3 > 0$ is the gradient hardening constant. The classical plasticity formulation is recovered by setting $k_3 = 0$.

Following the same classical thermodynamic arguments [55] exploited previously, the dissipation inequality is used to derive consistently the constitutive relations and the quantity conjugate to the gradient of the internal hardening parameter rate as follows:

$$\begin{aligned}
0 &\leq \boldsymbol{\tau} : \boldsymbol{d} - \dot{W} \\
&\leq \boldsymbol{\tau} : (\boldsymbol{d}^e + \boldsymbol{d}^p) - 2\boldsymbol{F}^e\left[\frac{\partial\bar{W}^e(\bar{\boldsymbol{C}}^e)}{\partial\bar{\boldsymbol{C}}^e}\right]\boldsymbol{F}^{eT} : \boldsymbol{d}^e - \frac{\partial\bar{W}^p(\xi,\nabla\xi)}{\partial\xi}\dot{\xi} \\
&\qquad - \frac{\partial\bar{W}^p(\xi,\nabla\xi)}{\partial\nabla\xi}\cdot\nabla\dot{\xi} \\
&\leq \boldsymbol{\tau} : (\boldsymbol{d}^e + \boldsymbol{d}^p) - 2\boldsymbol{F}^e\left[\frac{\partial\bar{W}^e(\bar{\boldsymbol{C}}^e)}{\partial\bar{\boldsymbol{C}}^e}\right]\boldsymbol{F}^{eT} : \boldsymbol{d}^e + \bar{g}\dot{\xi} + \boldsymbol{m}\cdot\nabla\dot{\xi}\,.
\end{aligned} \tag{8.1}$$

Here $\bar{\boldsymbol{C}}^e = \boldsymbol{F}^{eT}\boldsymbol{F}^e$ is the elastic left Cauchy–Green tensor defined in (6.19), and, as with the classical problem, $\bar{g} := -\partial W/\partial\xi$, and $\boldsymbol{m} := -\partial W/\partial\nabla\xi$. From the dissipation inequality (8.1) we obtain, as before, the elastic relation for the Kirchhoff stress $\boldsymbol{\tau}$ as

$$\boldsymbol{\tau} = 2\boldsymbol{F}^e\frac{\partial\bar{W}^e(\bar{\boldsymbol{C}}^e)}{\partial\bar{\boldsymbol{C}}^e}\boldsymbol{F}^{eT}\,, \tag{8.2}$$

and, hence, the reduced dissipation inequality in the form

$$\boldsymbol{\tau} : \boldsymbol{d}^p + \bar{g}\dot{\xi} + \boldsymbol{m}\cdot\nabla\dot{\xi} \geq 0\,. \tag{8.3}$$

The gradient plasticity model considered here assumes, pointwise, an elastic domain $\mathcal{E}$ with boundary $\partial\mathcal{E}$, the yield surface, and a generalised normality law. For definiteness $\mathcal{E}$ is assumed here to be defined by the von Mises condition restricted to linear isotropic hardening and extended to the gradient regime. The region of admissible generalised stresses is defined as the set $(\boldsymbol{\tau}, g)$ that satisfies

$$f(\boldsymbol{\tau}, g) := |\operatorname{dev}[\boldsymbol{\tau}]| - \sqrt{\tfrac{2}{3}}(\kappa - \underbrace{(\bar{g} - \operatorname{div}[\boldsymbol{m}])}_{g}) \leq 0\,, \tag{8.4}$$

where $g := \bar{g} - \operatorname{div}[\boldsymbol{m}]$.

The plastic deformation evolution expressions for classical plasticity were presented in both their primal and dual forms in Section 6.4. Following the approach adopted in Chapter 2 for the small-strain problem, the primal statement of the flow rule for the case of gradient plasticity reads

$$\begin{aligned} &\boldsymbol{\tau} \in \partial D(\boldsymbol{d}^p, \dot{\xi}) \\ &\qquad \Updownarrow \\ &D(\boldsymbol{q}, \eta) \geq D(\boldsymbol{d}^p, \dot{\xi}) + \boldsymbol{\tau} : (\boldsymbol{q} - \boldsymbol{d}^p) + g(\eta - \dot{\xi})\,. \end{aligned} \tag{8.5}$$

Homogeneous boundary conditions on the internal hardening parameter are considered in the form

$$\xi = 0 \text{ on } \partial\mathcal{S}_H \qquad \text{and} \qquad -\boldsymbol{m}\cdot\boldsymbol{n} = k_3 \frac{\partial \xi}{\partial \boldsymbol{n}} = 0 \text{ on } \partial\mathcal{S}_F\,,$$

where $\partial\mathcal{S}_H$ and $\partial\mathcal{S}_F$ are complementary subsets of $\partial\mathcal{S}$. The motivation for imposing the additional boundary conditions on the boundary of the domain is discussed further in the next section on the solution algorithm.

As in the small-strain case, the appropriate integral expression of the flow law is obtained by integrating (8.5) over the current domain, substituting for g, integrating by parts, and, finally, applying the additional boundary conditions to obtain

$$\int_{\mathcal{S}} D(\boldsymbol{q},\eta)\; dx \geq \int_{\mathcal{S}} D(\boldsymbol{d}^p,\dot{\xi})\; dx + \int_{\mathcal{S}} \boldsymbol{\tau} : (\boldsymbol{q}-\boldsymbol{d}^p)\; dx + \int_{\mathcal{S}} \bar{g}(\eta-\dot{\xi})\; dx + \int_{\mathcal{S}} \boldsymbol{m}\cdot\nabla[\eta-\dot{\xi}]\; dx\,. \tag{8.6}$$

The preceeding weak form of the flow rule forms the basis for the discontinuous Galerkin formulation of gradient plasticity at finite strains.

8.2 A discontinuous Galerkin formulation

The corrector step for the solution of the incremental change in the internal hardening parameter is performed here by solving the incremental form of the nonlocal plastic flow law (8.6) using a discontinuous Galerkin finite element formulation. Interelement continuity of the internal hardening parameter is therefore not assumed but is imposed in a weak sense. We present in this section various features of the discontinuous Galerkin formulation of the corrector step for the finite-strain problem.

It is worth recalling that we have chosen to use low-order bilinear Q_1 elements and an enhanced assumed strain formulation to interpolate the displacement field in the predictor step, so that the edges of the elements are straight lines. An alternative strategy using standard biquadratic Q_2 elements to interpolate the displacement was explored initially but the resulting discontinuous Galerkin problem is complicated by the presence of curved element edges. It would appear that most discontinuous Galerkin formulations of nonlinear problems in elasticity use low-order elements with straight edges (see, for example, [180, 141, 181, 182]).

We denote by $\mathcal{P}_k(K)$ the space of polynomials of degree at most $k \geq 0$ on K. Let $\mathcal{T}_h = \{K\}$ be a shape-regular subdivision of the current domain $\mathcal{S}$ as depicted in Fig. 8.1 where, here, K are quadrilaterals. As indicated in the figure, interelement continuity of the internal hardening parameter field is not assumed.

We consider here the subdivision of the current configuration as this is the placement in which the nonlocal expression of the flow rule is most appropriately defined. In the nonlocal implicit gradient framework proposed by Geers [83] it is also the current configuration that is used. The choice of either the material or spatial setting

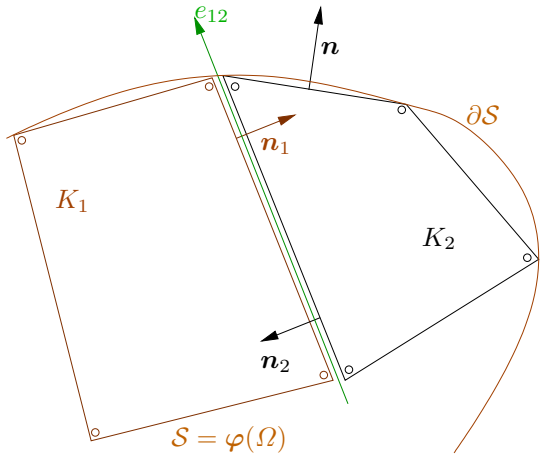

Fig. 8.1. Schematic of the subdivision of the current configuration $\mathcal{S}$ into nonconforming bilinear quadrilateral elements

has been investigated in the context of quasi-brittle damage by Steinmann [173], and in the context of softening problems in the finite deformation regime by Geers [83]. The conclusions of these analyses appear to be that there is little difference between the spatial and material settings. Modification of the approach adopted here to the reference configuration would be trivial.

Let $\mathcal{E}_h = \{e\}$ denote the set of the edges of $\mathcal{T}_h$, and $\mathcal{E}_h^{\text{int}} = \mathcal{E}_h \setminus \partial\mathcal{S}$ the set of interior edges. We associate with each edge e of an element K_i the outward unit normal vector $\boldsymbol{n}_i$. For an edge that lies on the boundary $\partial\mathcal{S}$ of the domain, $\boldsymbol{n}_i$ is defined to be the outward normal to $\partial\mathcal{S}$.

The jumps and averages, denoted $[\![\cdot]\!]$ and $\{\!\{\cdot\}\!\}$ respectively, of $\eta \in L^2(\mathcal{E}_h)$, $\boldsymbol{v} \in L^2(\mathcal{E})^2$ and $\boldsymbol{v} \in L^2(\mathcal{E})^{2\times 2}$ across an interior edge e_{12} common to elements K_1 and K_2 are defined in a near-identical manner to that in Chapter 3 as follows:

$$\begin{aligned}
[\![\eta]\!] &= \eta_1\boldsymbol{n}_1 + \eta_2\boldsymbol{n}_2 \;, & \{\!\{\eta\}\!\} &= \tfrac{1}{2}(\eta_1 + \eta_2) \;, \\
[\![\boldsymbol{v}]\!] &= \boldsymbol{v}_1 \otimes \boldsymbol{n}_1 + \boldsymbol{v}_2 \otimes \boldsymbol{n}_2 \;, & \{\!\{\boldsymbol{v}\}\!\} &= \tfrac{1}{2}(\boldsymbol{v}_1 + \boldsymbol{v}_2) \;, \\
[\![\boldsymbol{\tau}]\!] &= \boldsymbol{\tau}_1\boldsymbol{n}_1 + \boldsymbol{\tau}_2\boldsymbol{n}_2 \;, & \{\!\{\boldsymbol{\tau}\}\!\} &= \tfrac{1}{2}(\boldsymbol{\tau}_1 + \boldsymbol{\tau}_2) \;.
\end{aligned} \tag{8.7}$$

If e is an edge of element K_1 that lies on $\partial\mathcal{S}$, then the jumps and averages are defined by

$$
\begin{aligned}
[\![\eta]\!] &= \eta_1 \boldsymbol{n}_1 \ , & \{\!\{\eta\}\!\} &= \eta_1 \ , \\
[\![\boldsymbol{v}]\!] &= \boldsymbol{v}_1 \otimes \boldsymbol{n}_1 \ , & \{\!\{\boldsymbol{v}\}\!\} &= \boldsymbol{v}_1 \ , \\
[\![\boldsymbol{\tau}]\!] &= \boldsymbol{\tau}_1 \boldsymbol{n}_1 \ , & \{\!\{\boldsymbol{\tau}\}\!\} &= \boldsymbol{\tau}_1 \ .
\end{aligned} \tag{8.8}
$$

8.2.1 Fully-discrete symmetric interior penalty discontinuous Galerkin formulation

Consider a partition of the time interval $[0, T]$ into N subintervals with nodal points $t_n = nk,\ 0 \leq n \leq N$, where $\Delta t = t_{\mathrm{n}} - t_{\mathrm{n}-1} = T/N$ is the step-size. Following the approach detailed in Chapter 3 for the small-strain problem, we obtain the nonlocal expression of the discrete consistency condition for $\Delta\gamma$ from the linearised, symmetric interior penalty discontinuous Galerkin formulation of (8.6) as

$$
\begin{aligned}
&\int_{\mathcal{T}} \left(\left(\left(2\mu + \tfrac{2}{3} k_2 \right) \Delta\gamma \right) \varrho + \tfrac{2}{3} k_3 \nabla \left[\Delta\gamma \right] \cdot \nabla \varrho \right) \, dx + \int_{\mathcal{E}_h} \frac{k_2 \beta}{h_e} [\![\Delta\gamma]\!] \cdot [\![\varrho]\!] \, ds \\
&\quad - \int_{\mathcal{E}_h} \tfrac{2}{3} k_3 \left([\![\varrho]\!] \cdot \{\!\{\nabla[\Delta\gamma]\}\!\} + \{\!\{\nabla \varrho\}\!\} \cdot [\![\Delta\gamma]\!] \right) \, ds \\
&\quad = \int_{\mathcal{T}} \bar{f}(\bar{\boldsymbol{\tau}}^\star, g_0) \varrho \, dx \, .
\end{aligned} \tag{8.9}
$$

The additional boundary conditions arising due the model of gradient plasticity considered are assumed to be homogeneous and are applied on the external boundary of the current domain, i.e. $-\boldsymbol{m} \cdot \boldsymbol{n} = 0$ on $\partial \mathcal{S}_F$. This parallels the approach adopted by Meftah et al. [128], Mikkelsen [134] and Neff et al. [138]. The partition of the domain into active and plastic subsets is achieved, as in the small-strain case, by a local evaluation of the von Mises yield criterion at the level of the quadrature point. The value of the trial yield function $f^\star$ is set to zero for inactive quadrature points. The numerical results presented in Chapter 9 indicate that this approach effectively imposes a homogeneous Dirichlet condition on the internal elastoplastic boundary. One reason for the change in methodology is an attempt to eliminate the computational expense associated with explicitly tracking the elastoplastic boundary and applying boundary conditions upon it. The approach adopted here simplifies the problem as the moving elastoplastic interface need not be tracked explicitly. However, potentially, this

approach significantly increases the size of the problem. Initial numerical results indicate little difference in the solution but further work is indeed needed. Furthermore, the choice of a more efficient programming environment (the high-level programming environment Matlab [105] is used here) and parallel implementation should alleviate the computational overhead. This recommendation is explored in more detail in Chapter 10.

While the choice of appropriate boundary conditions for the internal hardening parameter field should generally be motivated by physical considerations, the emphasis in this work is to demonstrate the salient features of the gradient plasticity formulation. We remark however that any choice of boundary condition could, in theory, be implemented. Further discussion on the physical implications of the additional boundary conditions that arise in gradient plasticity formulations can be found in Gurtin [89, 90] and Peerlings [146], amongst others.

The approximation of the displacement and hardening parameter fields using finite element interpolation functions follows as per Sections 7.1.1 and 4.3.1. Substitution of these approximations into the incremental discontinuous Galerkin problem (8.9) yields the matrix problem for the nonconforming nodal values of the increment in the hardening parameter, denoted $\Delta\boldsymbol{\gamma}$, as:

$$\boldsymbol{K}^{\gamma}\Delta\boldsymbol{\gamma} = \boldsymbol{F}^{\gamma}\,. \tag{8.10}$$

8.3 Implementation of the predictor–corrector solution procedure

As in the infinitesimal problem, a predictor–corrector solution algorithm is used to solve the gradient plasticity problem for the increment in displacement and internal hardening parameter during a time step of duration $\Delta t = t_{\mathrm{n}} - t_{\mathrm{n-1}} = t_{\mathrm{n}} - t_0$. The predictor–corrector algorithm is described in Alg. 8.1. Due to the near-identical structure of the finite- and small-strain plastic evolution relations, and the desire to avoid unnecessary repetition, we choose to omit a detailed discussion of the finite-strain algorithm. Rather, a discussion of the key distinguishing features is presented.

In particular, we derive the algorithmic consistent tangent for the classical and gradient formulations. The predictor step, that is, the solution of the enhanced equilibrium equations, has been discussed in detail in Chapter 7 and example problems presented.

8.3.1 Derivation of the algorithmic tangent modulus for classical and gradient plasticity

The convergence rate and stability of the predictor–corrector algorithm is governed by the form of the predictor step. As demonstrated using numerical examples in Chapter 5 for the small-strain problem and schematically in Chapter 6 the use of a consistently derived predictor is optimal from the perspective of numerical efficiency. We derive here the consistent algorithmic tangent predictor for the classical and gradient plasticity problems. The classical derivation closely follows that in Simo [164].

The algorithmic incremental constitutive relationship arising in the predictor step takes the form

$$\mathcal{L}_{\Delta \boldsymbol{u}} \boldsymbol{\tau} = \bar{\boldsymbol{c}} \left[\nabla [\Delta \boldsymbol{u}] \right] \ ,$$

where $\mathcal{L}_{\Delta \boldsymbol{u}} \boldsymbol{\tau}$ is the incremental form of Lie derivative of the Kirchhoff stress tensor (see (6.17)), and $\bar{\boldsymbol{c}}$ the algorithmic tangent modulus. In order to preserve the quadratic rate of convergence associated with a typical Newton–Raphson solution scheme for the fully-discrete problem of finite plasticity one needs to formulate the algorithmic tangent modulus in a manner that is consistent with the corrector step. The consistently derived tangent modulus is denoted $\bar{\boldsymbol{c}}^{\text{con}}$. The derivation of the algorithmic consistent tangent modulus for the problem of finite-strain classical plasticity based on the logarithmic hyperelastic–plastic model is near-identical to the infinitesimal case, as demonstrated by Simo [163].

The algorithmic elastic constitutive relationship in the principal directions $\boldsymbol{n}^{\star}$ of the trial elastic left Cauchy–Green tensor $\boldsymbol{b}^{e\star}$, see (6.39) in Section 6.4.1, takes the form

Algorithm 8.1 Algorithm for the finite element method approximation of the gradient enhanced discontinuous Galerkin plasticity problem at iteration i of time step n assuming linear isotropic hardening

Initial conditions
if i == 0 **then**
  Record $\boldsymbol{A}_0^p := [\boldsymbol{C}^p]^{-1} = \boldsymbol{F}_h^{-1}\boldsymbol{b}^e\boldsymbol{F}_h^{-T}$ and g_0
  Set each quadrature point as inactive. $\bar{\mathrm{c}}^{ep} \leftarrow \bar{\mathrm{c}}$ and $\Delta\gamma = 0$
  Determine nodal force contributions arising from applied tractions
end if
Predictor step
Assemble effective global stiffness matrix $\tilde{\boldsymbol{K}}^{(\mathrm{i})}$ and effective residual force vector from element contributions
Impose Dirichlet boundary conditions
Solve effective system for increment in nodal displacement vector $\delta\boldsymbol{d}$ and update $\boldsymbol{d}^{\mathrm{i}}$
for each element e **do**
  Determine the increment in the enhanced variables $\Delta\Gamma^e$ and update Γ_e^{i}
  for each quadrature point **do**
    Determine the deformation gradient $\boldsymbol{F}_h^{\mathrm{i}}$
    Determine $\boldsymbol{b}^{e\star} = \left(\boldsymbol{F}_h^{\mathrm{i}}\boldsymbol{A}_{\mathrm{n}}^p{\boldsymbol{F}_h^{\mathrm{i}}}^T\right)$
    Perform spectral decomposition of $\boldsymbol{b}^{e\star}$ and determine the principal trial stresses $\boldsymbol{\tau}^\star$
    Determine trial yield state $\bar{f}(\boldsymbol{\tau}^\star, g_{\mathrm{n}})$
    if $\bar{f}(\boldsymbol{\tau}^\star, g_0) < 0$ **then**
      Quadrature point inactive $\boldsymbol{\tau} = \boldsymbol{\tau}^\star$
      Update stress state in global axes and determine $\bar{\mathrm{c}}^{ep}$
    end if
  end for
end for
Corrector step
Solve discontinuous Galerkin problem (8.10) for $\Delta\boldsymbol{\gamma}$
for each quadrature point **do**
  Calculate $\nabla^2[\Delta\gamma]$ and update g
  if current quadrature point is active **then**
    Update γ and determine new stress state
    Determine $\bar{\mathrm{c}}^{ep}$ using (8.14)
  end if
end for
Check global convergence. If not converged, return to the predictor step and increment i

$$\begin{aligned}\bar{\boldsymbol{\tau}} &= \bar{\boldsymbol{c}}\boldsymbol{\varepsilon}^e \\ &= \bar{\boldsymbol{c}}\,(\boldsymbol{\varepsilon} - \boldsymbol{\varepsilon}^p) \\ &= \underbrace{\bar{\boldsymbol{c}}\boldsymbol{\varepsilon}}_{\bar{\boldsymbol{\tau}}^\star} - 2\mu\Delta\gamma\boldsymbol{\nu} \qquad \text{using (6.44a) in Section 6.4.1 ,}\end{aligned} \tag{8.11}$$

where the 3×3 matrix expression of $\bar{\boldsymbol{c}}$ is given by

$$\bar{\mathrm{c}} = \left(\Lambda + \tfrac{2}{3}\mu\right)\bar{\mathbf{1}} \otimes \bar{\mathbf{1}} + 2\mu\,\underbrace{\left(\bar{\boldsymbol{I}} - \tfrac{1}{3}\bar{\mathbf{1}} \otimes \bar{\mathbf{1}}\right)}_{\bar{\boldsymbol{I}}^{\mathrm{d}}} ,$$

and where $\mathbf{1} := \{1, 1, 1\}^T$ and $\bar{\boldsymbol{I}}^{\mathrm{d}}$ is the deviatoric identity matrix. We denote by $\bar{\mathrm{c}}^{ep}$ the 3×3 matrix obtained from the elastic constitutive relationship given in (8.11); that is,

$$\begin{aligned}\bar{\mathrm{c}}^{ep} &= \frac{\partial \bar{\boldsymbol{\tau}}}{\partial \boldsymbol{\varepsilon}^{e\star}} \\ &= \frac{\partial\left(\bar{\boldsymbol{c}}\boldsymbol{\varepsilon} - 2\mu\Delta\gamma\boldsymbol{\nu}\right)}{\partial \boldsymbol{\varepsilon}^{e\star}} \\ &= \bar{\mathrm{c}} - 2\mu\boldsymbol{\nu}^\star \otimes \underbrace{\left(\frac{\partial \Delta\gamma}{\partial \boldsymbol{\varepsilon}^{e\star}}\right)}_{(\bigstar)} - 2\mu\Delta\gamma\underbrace{\left(\frac{\partial \boldsymbol{\nu}^\star}{\partial \boldsymbol{\varepsilon}^{e\star}}\right)}_{(\bigstar\bigstar)} .\end{aligned} \tag{8.12}$$

The term $(\bigstar\bigstar)$ is the same for both the classical and gradient plasticity formulations; that is,

$$\begin{aligned}\frac{\partial \boldsymbol{\nu}^\star}{\partial \boldsymbol{\varepsilon}^{e\star}} &= \frac{\partial\left(\boldsymbol{\nu}^\star\right)}{\partial\left(\operatorname{dev}[\boldsymbol{\tau}^\star]\right)} \frac{\partial\left(\operatorname{dev}[\boldsymbol{\tau}^\star]\right)}{\partial\left(\boldsymbol{\varepsilon}^{e\star}\right)} \\ &= \frac{2\mu}{|\operatorname{dev}[\boldsymbol{\tau}^\star]|}\left(\bar{\boldsymbol{I}}^d - \boldsymbol{\nu}^\star \otimes \boldsymbol{\nu}^\star\right) .\end{aligned} \tag{8.13}$$

The term $(\bigstar)$, however, depends on the form of the corrector step which differs for classical and gradient plasticity. Details will be presented shortly. Once expressions for $(\bigstar)$ and $(\bigstar\bigstar)$ have been obtained the algorithmic incremental tangent modulus utilised in the predictor step can be expressed in the global system as (see Simo [164] for further details):

$$\boldsymbol{c}^{ep} = \sum_{A=1}^{3}\sum_{B=1}^{3}\left(\bar{\mathrm{c}}^{ep}_{AB}\boldsymbol{n}^{\star(A)}\otimes\boldsymbol{n}^{\star(A)}\otimes\boldsymbol{n}^{\star(B)}\otimes\boldsymbol{n}^{\star(B)}\right) + \bar{\boldsymbol{g}}^{\star}\ , \tag{8.14}$$

where the nonzero components $\bar{g}^{\star}_{IJKL}$ of the fourth-order tensor $\bar{\boldsymbol{g}}^{\star}$ relative to the basis $\{\boldsymbol{n}^{\star(A)}\}$ are defined by

$$\begin{aligned}
\bar{g}^{\star}_{IIII} &= -2\tau_I \qquad \text{for } I,J=1,2,3\,,\\
\bar{g}^{\star}_{IJIJ} = \bar{g}^{\star}_{IJJI} &= \frac{\tau_I\left(\lambda^{e\star}_J\right)^2 - \tau_J\left(\lambda^{e\star}_I\right)^2}{\left(\lambda^{e\star}_I\right)^2 - \left(\lambda^{e\star}_J\right)^2} \quad \text{for } I,J=1,2,3 \text{ and } I\neq J\ .
\end{aligned}$$

For the case where $\lambda^{e\star}_I = \lambda^{e\star}_J$ we use the relations given in Chadwick and Ogden [49, 50] and numerically exploited in Duffett and Reddy [71]; that is,

$$\bar{g}^{\star}_{IJIJ} = -\tau_I + \frac{\lambda^e_I}{2}\left(\frac{\partial\tau_I}{\partial\lambda_I} - \frac{\partial\tau_J}{\partial\lambda_J}\right) \quad \text{for } I=J\ .$$

Classical plasticity

In the classical formulation of plasticity, the consistency condition is evaluated locally at the level of the quadrature point to determine the increment in the internal hardening parameter. Assuming plastic flow at the quadrature point under consideration,

$$\begin{aligned}
0 &= \bar{f}(\bar{\boldsymbol{\tau}}_{\mathrm{n}}, \bar{g}_{\mathrm{n}})\\
&= |\operatorname{dev}[\bar{\boldsymbol{\tau}}_{\mathrm{n}}]| - \sqrt{\tfrac{2}{3}}\,(\kappa - \bar{g}_{\mathrm{n}})\\
&= |\operatorname{dev}[\boldsymbol{\tau}^{\star}]| - 2\mu\Delta\gamma - \sqrt{\tfrac{2}{3}}\left(\kappa - \bar{g}_0 + \sqrt{\tfrac{2}{3}}k_2\Delta\gamma\right)\ .
\end{aligned}$$

Rearranging, we obtain the classical consistency condition in the principal directions as

$$\Delta\gamma = \frac{\bar{f}(\bar{\boldsymbol{\tau}}^{\star}, \bar{g}_0)}{2\mu + (2/3)\,k_2}\ .$$

The partial derivative of $\Delta\gamma$ with respect to the trial elastic strain $\boldsymbol{\varepsilon}^{e\star}$, term (★) in (8.12), is thus

$$\frac{\partial\,(\Delta\gamma)}{\partial\boldsymbol{\varepsilon}^{e\star}} = \left(\frac{1}{2\mu + (2/3)\,k_2}\right)\frac{\partial\left(\bar{f}(\bar{\boldsymbol{\tau}}^{\star},\bar{g}_0)\right)}{\partial\boldsymbol{\varepsilon}^{e\star}} = \frac{2\mu}{2\mu + (2/3)\,k_2}\boldsymbol{\nu}^{\star}\,. \tag{8.15}$$

Substituting (8.13) and (8.15) into (8.12) we obtain the expression for the consistent algorithmic tangent modulus in the principal directions for classical plasticity, denoted $\bar{\mathrm{c}}^{\mathrm{con}}_{\mathrm{cp}}$, as

$$\bar{\mathrm{c}}^{\mathrm{con}}_{\mathrm{cp}} = \left[\bar{\mathrm{c}} - \frac{4\mu^2}{2\mu + (2/3)\,k_1}\boldsymbol{\nu}^{\star}\otimes\boldsymbol{\nu}^{\star} - \frac{4\mu^2\Delta\gamma}{|\,\mathrm{dev}[\boldsymbol{\tau}^{\star}]|}\left(\bar{\boldsymbol{I}}^{\mathrm{d}} - \boldsymbol{\nu}^{\star}\otimes\boldsymbol{\nu}^{\star}\right)\right]\,.$$

Gradient plasticity

The matrix expression of the discontinuous Galerkin problem for the nodal increments $\Delta\boldsymbol{\gamma}$ given in (8.10) can be rewritten as

$$\Delta\boldsymbol{\gamma} = [\boldsymbol{K}^{\gamma}]^{-1}\,\boldsymbol{F}^{\gamma} = [\boldsymbol{K}^{\gamma}]^{-1}\,\mathop{\mathsf{A}}_{K\in\mathcal{T}_h}\int_K N_{\gamma}^{T}\,\bar{f}(\boldsymbol{\tau}^{\star},g_0)\;dx \tag{8.16}$$

The expression for the term (★) in (8.12) is obtained by taking the derivative of (8.16) with respect to $\boldsymbol{\varepsilon}^{e\star}$ to obtain

$$\frac{\partial\Delta\boldsymbol{\gamma}}{\partial\boldsymbol{\varepsilon}^{e\star}} = [\boldsymbol{K}^{\gamma}]^{-1}\,\mathop{\mathsf{A}}_{K\in\mathcal{T}_h}\int_K N_{\gamma}^{T}\frac{\partial}{\partial\boldsymbol{\varepsilon}^{e\star}}\bar{f}(\boldsymbol{\tau}^{\star},g_0)\;dx = [\boldsymbol{K}^{\gamma}]^{-1}\,\mathop{\mathsf{A}}_{K\in\mathcal{T}_h}\int_K N_{\gamma}^{T}\boldsymbol{\nu}^{\star}\;dx\,. \tag{8.17}$$

The value of $\partial\Delta\boldsymbol{\gamma}/\partial\boldsymbol{\varepsilon}^{e\star}$ is extrapolated from the nodal values to the quadrature points and denoted there as $\partial\Delta\boldsymbol{\gamma}/\partial\boldsymbol{\varepsilon}^{e\star}|_{\boldsymbol{\xi}}$. Substitution of (8.17) into (8.12) renders the consistent algebraic tangent modulus for gradient plasticity at a quadrature point as

$$\bar{\mathrm{c}}^{\mathrm{con}}_{\mathrm{gp}} = \left[\bar{\mathrm{c}} - 2\mu\boldsymbol{\nu}^{\star}\otimes\left(\frac{\partial\Delta\gamma}{\partial\varepsilon^{e\star}}|_{\bar{\boldsymbol{\xi}}}\right) - \frac{4\mu^2\Delta\gamma}{|\,\mathrm{dev}[\boldsymbol{\tau}^{\star}]|}\left(\bar{\boldsymbol{I}}^{d} - \boldsymbol{\nu}^{\star}\otimes\boldsymbol{\nu}^{\star}\right)\right]\,.$$

9

Numerical examples: finite-strain gradient plasticity

The software realisation of the finite-strain discontinuous Galerkin formulation of gradient plasticity is used to simulate the response of two example problems. These problems demonstrate various features of the gradient plasticity formulation.

The first problem, a rectangular plate with a small initial imperfection subjected to compressive loading where the material undergoes softening, is chosen to assess the ability of the gradient plasticity formulation to overcome the pathological mesh-dependence associated with classical problems involving softening, that is, when $k_2 < 0$. The problem has been investigated by several other researchers including [145, 75, 4, 109, 68] and is near-identical to that presented in Section 5.1.1 under the assumption of infinitesimal deformation. We circumvent problems associated with the loss of residual strength at a material point by considering a relatively small deformation for this example problem. In addition, the influence of the internal length scale on the response of the system is demonstrated. The influence of the penalty parameter in the discontinuous Galerkin formulation on the solution is also shown. As the interelement continuity of the internal hardening parameter is imposed more poorly, so the solution resembles the classical one. This suggests various interesting features of a discontinuous Galerkin formulation in which moving interfaces and varying degrees of nonlocality could readily be accommodated. Indeed, the potential flexibility of the discontinuous Galerkin method to accommodate a wide variety of problem types within a familiar Galerkin finite element framework is one of the reasons for its widespread adoption (see, for example, the scope of work presented in the volume [12]).

The second example problem concerns the indentation of a specimen where the material undergoes a hardening response. The objective of this example problem is to assess the behaviour of the gradient formulation for a system experiencing significant deformation, especially in the region surrounding the indenter.

Plane strain conditions are assumed applicable, so that $F^h_{i3} = 1,\ i = 1, 2, 3$. Additionally, there is a need to introduce a remedy, here in the form of the enhanced assumed strain formulation, to circumvent volumetric locking which does not arise in the case of plane stress.

Conforming enhanced assumed bilinear elements are used to interpolate the displacement field while nonconforming discontinuous bilinear elements are used to interpolate the equivalent plastic strain field. The value of the penalty parameter β_2 is set to the value of the Young's modulus of the material, unless otherwise indicated. The five-point quadrature rule described in Chapter 7 is used to numerically integrate volume contributions while edge contributions are evaluated using a two-point rule.

9.1 Rectangular plate with a small initial imperfection subjected to compressive loading

The plane rectangular plate with a small initial imperfection subjected to compressive loading is shown in Fig. 9.1. The lower edge of the plate is prevented from displacing vertically and, in addition, the lower left-hand corner of the plate is prevented from displacing in the horizontal direction. The material properties of the plate are listed in Table 9.1. The formation of the shear band is induced via the introduction of a 10 mm square region in the lower left-hand corner of the plate in which the yield strength is reduced by 10 % relative to the rest of the domain. Three regularly refined and one skewed discretisation of the domain are considered.

The pathological localisation of the shear band to the scale of the discretisation (that is, the mesh size) for the classical problem is evident in Fig. 9.2. Figures 9.2(a)–9.2(c) indicate the active quadrature points superimposed upon the undeformed domain while Figs 9.2(d)–9.2(f) show the deformed domain superimposed upon the initial. The width of the shear band is clearly governed by the element size. The final

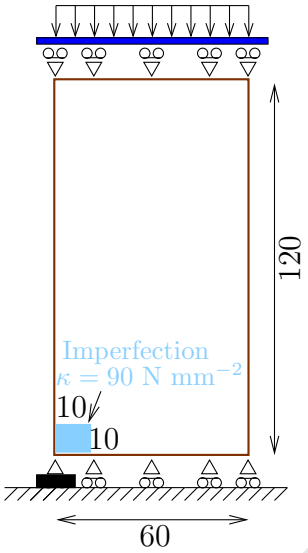

Fig. 9.1. Diagram of the rectangular plate subjected to compressive loading

Table 9.1. Material properties for the problem of a rectangular plate subjected to compressive loading

Young's modulus	$E = 11920$ N mm^{-2}
Poisson's ratio	$\nu = 0.49$
Yield stress	$\kappa = 100$ N mm^{-2}
Isotropic hardening constant	$k_2 = -400$ N mm^{-2}
Gradient hardening constant	$k_3 = 3600$ N

deformed configuration of the plate is also dependent upon the discretisation; as the element size is reduced so the plastic deformation localises to a narrower band resulting in significant element distortion within this region. The relationship between the resulting force and the applied displacement on the upper edge of the plate, shown in Fig. 9.3, illustrates once again the mesh-dependent response. The post-peak response of the force displacement curve is governed by the discretisation: the finer the mesh, the greater the rate at which the material loses residual strength.

The ability of the gradient plasticity formulation to produce solutions independent of the mesh for softening problems is shown in Fig. 9.4. As the mesh resolution is increased so the width of the shear band converges to a constant value determined by the internal length scale. The final deformed configurations obtained using the various discretisations are shown in Figs 9.4(e)–9.4(g). It is evident that the patho-

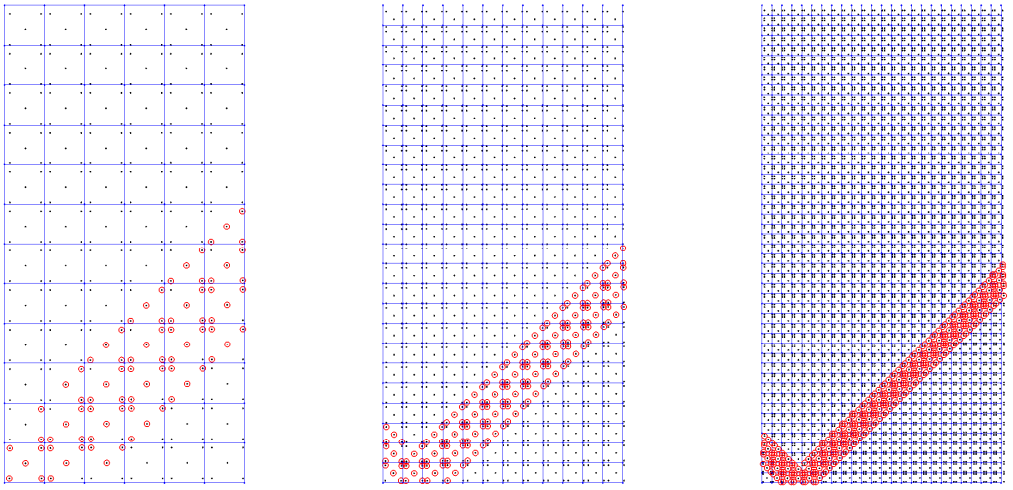

(a) 6×12 (b) 12×24 (c) 24×48

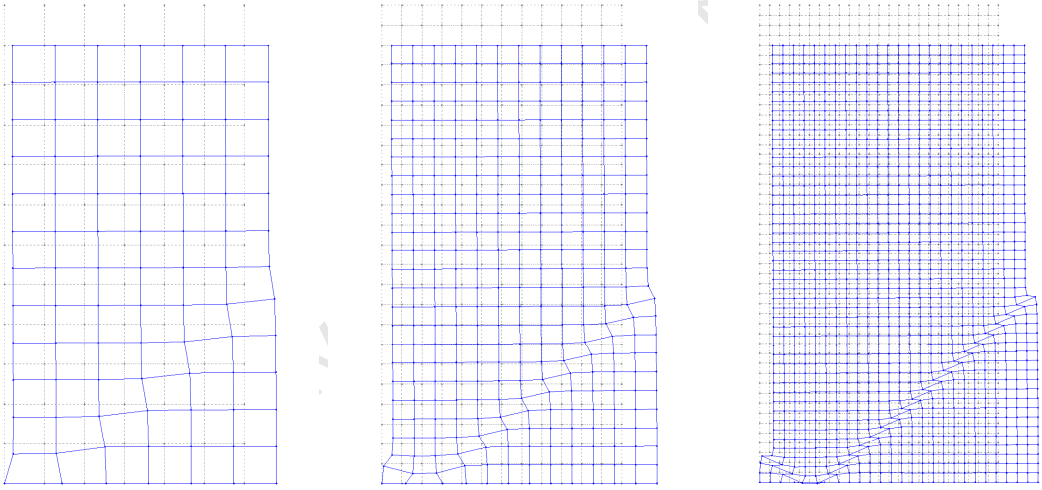

(d) 6×12 (e) 12×24 (f) 24×48

Fig. 9.2. The position of the active quadrature points, denoted by open red circles, superimposed upon the undeformed mesh (a)–(c) and the deformed mesh superimposed upon the undeformed mesh (d)–(f) for the various discretisations investigated using the classical plasticity formulation

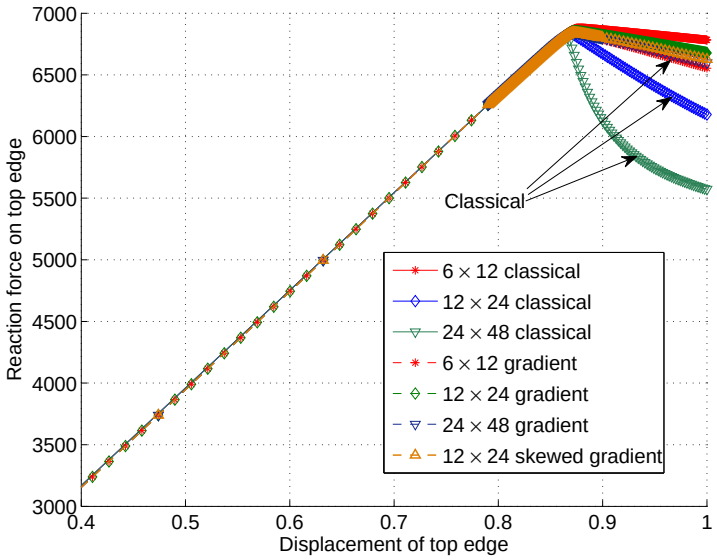

Fig. 9.3. Comparison of the applied force versus the resulting displacement for both the classical and gradient plasticity formulations

logical localisation demonstrated by the classical formulation has been overcome. The final deformed configurations are extremely similar to one another with any minor differences attributable to the improved solution resolution obtained upon mesh refinement.

Solution sensitivity to mesh orientation is another characteristic of the pathological mesh-dependence exhibited by classical solutions to softening problems. The results obtained using the skewed mesh, shown in Figs 9.4(d) and 9.4(h), coincide with those obtained using the structured meshes upon refinement, once again indicating a mesh-independent solution.

The derivation of the consistent tangent modulus in Section 8.3.1 was motivated by the improved performance of the predictor–corrector solution algorithm relative to the elastic predictor. The performance of the consistent tangent and elastic predictors for the gradient plasticity problem are compared in Fig. 9.5 where the norm of the force residual is given at each increment within a typical time step. As expected, the consistent tangent predictor converges more rapidly than the elastic predictor; the elastic predictor requires approximately twice the number of iterations to reach

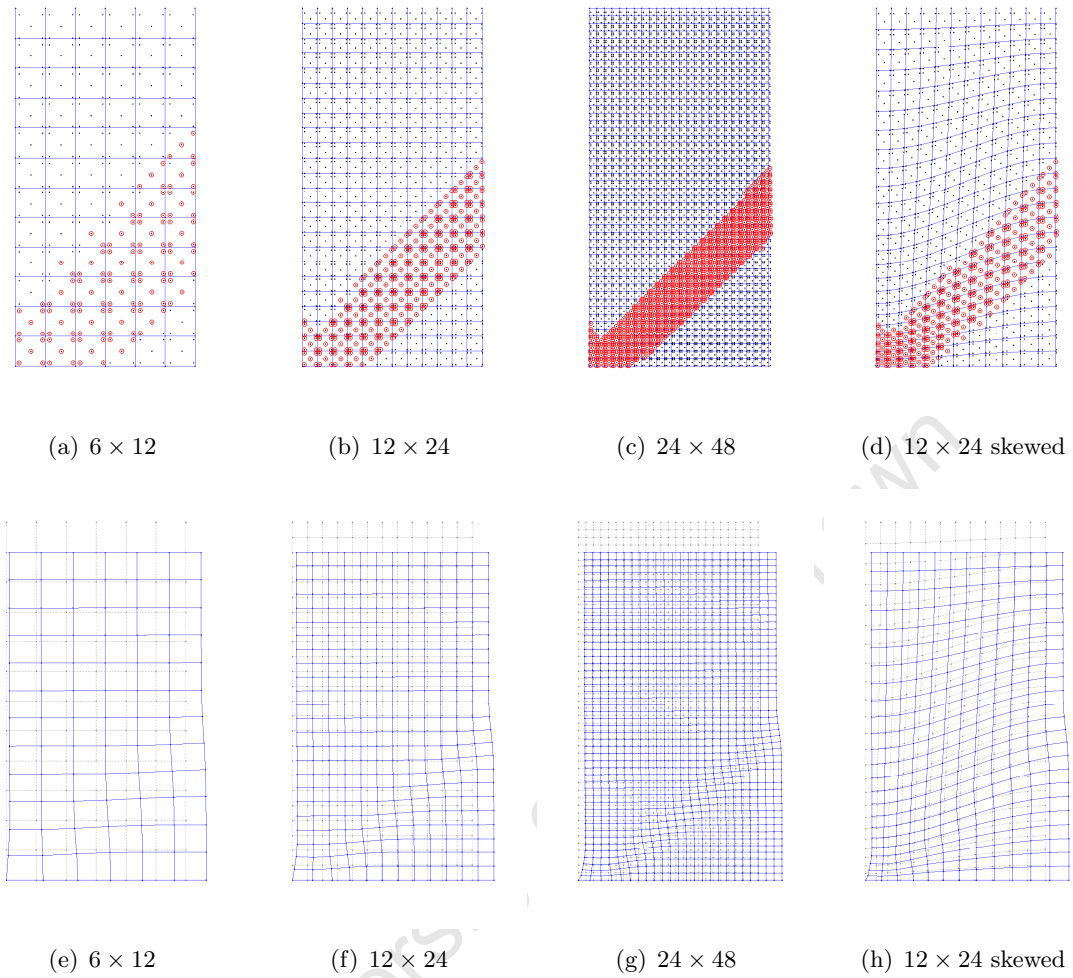

(a) 6×12 (b) 12×24 (c) 24×48 (d) 12×24 skewed

(e) 6×12 (f) 12×24 (g) 24×48 (h) 12×24 skewed

Fig. 9.4. The position of the active quadrature points, denoted by open red circles, superimposed upon the undeformed mesh (a)–(d) and the deformed mesh superimposed upon the undeformed mesh (e)–(h) for the various discretisations investigated using the gradient plasticity formulation

the same level of convergence. There is, however, additional computational overhead associated with the construction of the consistent tangent modulus for each iteration. The additional expense per iteration is, however, minor relative to the improved overall efficiency of the consistent tangent formulation.

The influence of the penalty parameter β_2 on the variation of $\Delta\gamma$ predicted within a typical time step during the deformation process is depicted in Fig. 9.6. As shown in Fig. 9.6(a), the use of a sufficiently high value for β_2 clearly enforces the continuity of

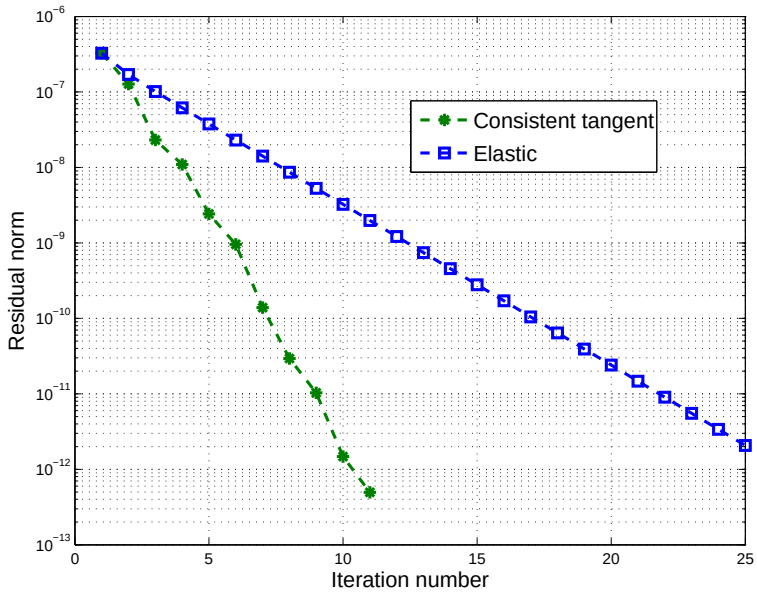

Fig. 9.5. Comparison of the norm of the force residual versus iteration number during a typical time step for both the consistent tangent and elastic predictors

the approximation field sufficiently well. The use of a relatively small value of 10 for the penalty parameter allows discernable discontinuities to develop in the approximation field, as shown in Fig. 9.6(b). As the penalty parameter is reduced further, so the distribution of $\Delta\gamma$ resembles that obtained using the classical plasticity formulation. The effectiveness of the formulation to distinguish the active and inactive regions is clear, with the value of $\Delta\gamma$ being zero outside of the active zone containing elements with active quadrature points.

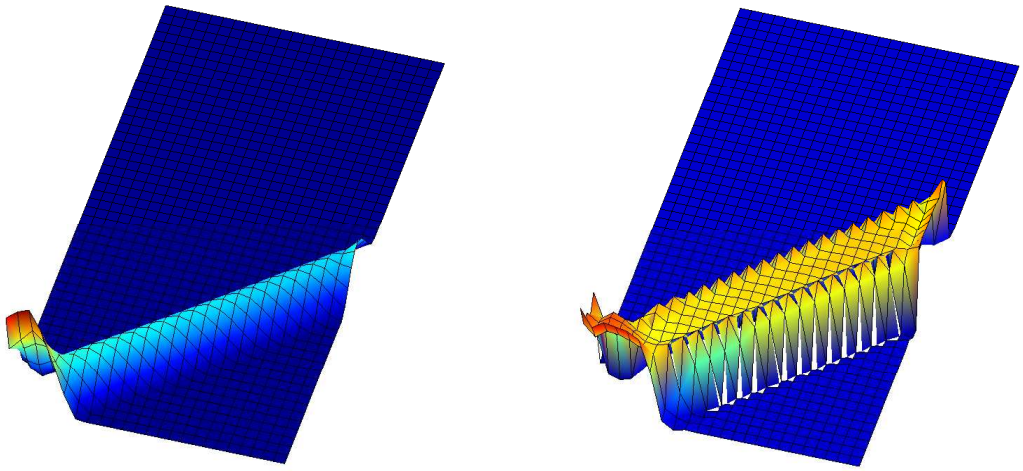

(a) $\beta_2 = 11920$ (b) $\beta_2 = 10$

Fig. 9.6. The variation in $\Delta\gamma$ across the plate obtained using the gradient plasticity formulation with both a high (a) and a low (b) value for the penalty parameter β_2

9.2 Indentation of a rectangular specimen

Half of the rectangular domain subjected to loading via a frictionless rigid indenter is shown in Fig. 9.7(a). The domain is composed of a hardening elastoplastic material with properties listed in Table 9.2. The indenter moves downwards at a constant rate into the specimen resulting in significant deformation. The final indentation depth is 8% of the initial specimen height. Due to the symmetry of the problem, only half of the domain is analysed and the appropriate boundary conditions imposed, as indicated in Fig. 9.7. The discretisation of the resulting square domain is shown in Fig. 9.7(b).

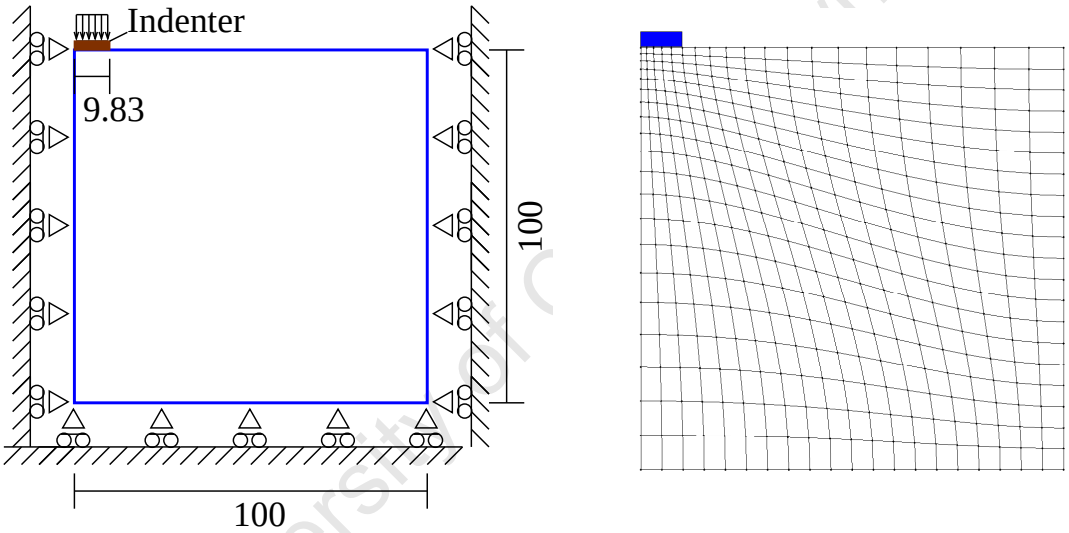

Fig. 9.7. Diagram of (a) the domain of the indentation test and (b) its finite element discretisation

Table 9.2. Material properties for the problem of a rectangular domain loaded via a rigid indenter

Young's modulus	$E = 11920$ N mm^{-2}
Poisson's ratio	$\nu = 0.3$
Yield stress	$\kappa = 100$ N mm^{-2}
Isotropic hardening constant	$k_2 = 400$ N mm^{-2}

The results predicted using the classical plasticity formulation at various stages of the deformation process are shown on the right-hand side of Fig. 9.8. The results obtained using the gradient plasticity formulation with an internal length scale of 2.83 mm are mirrored around the symmetry axis for the purpose of direct comparison with the classical formulation and indicated on the left-hand side of Fig. 9.8. Details of the gradient formulation will be given shortly. The positions of the quadrature points are shown and the subset of those quadrature points that are active indicated.

Consider firstly the deformation history arising from the classical plasticity formulation. Plastic flow is initiated in the vicinity of the outer edge of the indenter at a very early stage in the deformation process. The plastic region grows into a "bulb" surrounding an elastic wedge as indicated in the plot of the deformed domain after a total indentation, denoted d, of 0.5 mm in Fig. 9.8(a). The extent of the plastic zone after an indentation of 4 mm is shown in Fig. 9.8(b). The plastic zone has extended downwards and outwards and the elastic wedge is no longer present. The plastic zone has reached the lower and far upper boundaries of the domain after an indentation of 8 mm, as shown in Fig. 9.8(c). Two distinct inactive zones separated by active plastic regions are now present.

The relationship between the resulting force on the indenter and the imposed displacement is shown in Fig. 9.9. Also indicated are the positions in the indentation history corresponding to the deformation states shown in Figs 9.8(a)–9.8(c).

The evolution of the plastic deformation for the gradient problem is similar to the classical problem. The extent of the plastic domain at identical points in the deformation history is greater due to the nonlocal gradient effects. This is indicated in Fig. 9.8 by distinguishing the active quadrature points in the gradient solution that are not active in the classical solution from the remaining active quadrature points in the gradient solution. The extent of the plastic zone after an indentation of 8 mm, presented in Fig. 9.8(c), shows the plastic domain extending to the far lower corner of the domain. The classical solution reaches a similar state as the indentation proceeds beyond 8 mm.

The influence of the internal length scale on the relationship between the resulting force on the indenter and the imposed displacement is shown in Fig. 9.9. The gradient

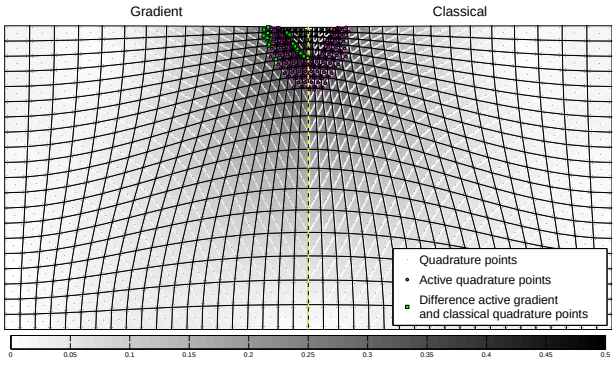

(a) $d = 0.5$ mm

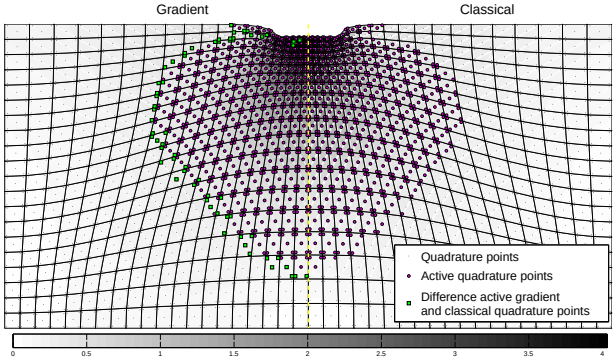

(b) $d = 4$ mm

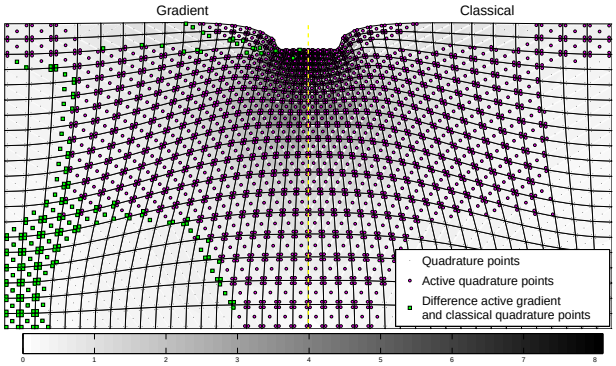

(c) $d = 8$ mm

Fig. 9.8. Comparison of the deformation of the indented domain obtained using the gradient (left) and classical (right) plasticity formulations. The magnitude of the displacement field is superimposed upon the deformed mesh and the position and plastic state of the quadrature points indicated

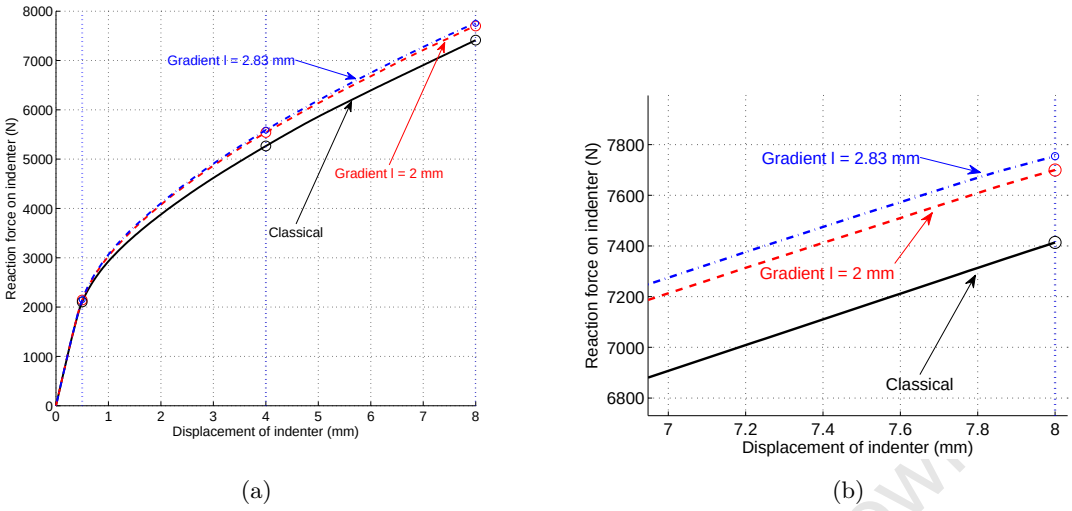

Fig. 9.9. Relationship between the resulting force on the indenter and the imposed displacement for the classical problem and the gradient problem using two different internal length scales

results are clearly influenced by the relative scale of the problem, that is the ratio of the internal length scale to a characteristic dimension of the domain. The material offers increased resistance to deformation with increasing internal length scale.

The variation in $\Delta\gamma$ at an indentation depth of 7 mm for the gradient problem is shown in Fig. 9.10. As in the previous example problem, it is evident that the discontinuous Galerkin formulation weakly imposes the interelement continuity of $\Delta\gamma$ sufficiently well.

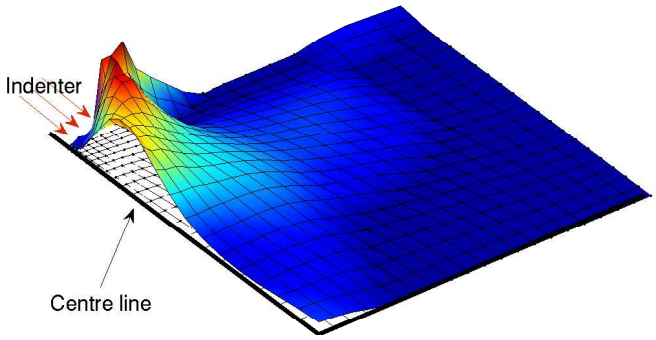

Fig. 9.10. Variation in $\Delta\gamma$ superimposed upon the reference domain at an indentation depth of 7 mm

10

Conclusions and recommendations for future work

A novel application of the discontinuous Galerkin finite element method to problems in classical and gradient plasticity has been presented. The model of gradient plasticity investigated, due to Dillon and Kratochvil [66], Aifantis [2] and Coleman and Hodgdon [56], is based on the assumption of a von Mises yield function in which dependence is on both the isotropic hardening parameter and its Laplacian. A careful analysis of the underlying mathematical structure and the predictor–corrector solution algorithms, required for the numerical realisation of the formulation within a finite element code, was performed in the context of the infinitesimal-deformation problem. The extension of the infinitesimal formulation to the finite-deformation regime followed; emphasis was placed on retaining the key features of the small-strain formulation. Various properties of the formulation were elucidated using representative numerical examples.

The major contributions and findings of this work include the analysis of the well-posedness and convergence of discontinuous Galerkin approximations for problems in both classical and gradient elastoplasticity subject to the infinitesimal-strain assumption. The analysis considered a discontinuous Galerkin approximation of both the displacement and equivalent plastic strain fields. Error estimates that mimic those obtained for classical plasticity within a conventional Galerkin formulation have been derived for the semi- and fully-discrete approximations. The ability of the gradient model to accommodate softening is clear from the analysis.

Predictor–corrector solution algorithms for the fully-discrete problem were developed and their convergence properties studied, initially in abstract form and subsequently specialised to various predictors. The convergence study did not assume

symmetry of the underlying bilinear form, thereby accommodating a broad range of nonsymmetric discontinuous Galerkin formulations. The form of the consistent tangent predictor, essential for the efficient numerical implementation, has been derived, and its connection to the discontinuous Galerkin problem for the hardening parameter made clear.

Finally, a number of numerical examples served to demonstrate the properties of the algorithm as well as a range of features such as those associated with softening and size dependence. As would be expected from the analysis, the pathological features that arise in classical finite element formulations of problems with softening are absent.

The extension of the model of gradient plasticity to the finite-strain regime was the focus of the second part of this work. Attention was paid to developing a framework that contained the key features of the infinitesimal problem; by adopting a logarithmic hyperelastic–plastic model, the plastic flow relations take a form near-identical to the small-strain problem. The enhanced assumed strain formulation allowed locking-free low-order elements to be used to approximate the displacement field in what is essentially the predictor step of the solution procedure. The use of low-order elements simplified the formulation of the nonlocal corrector step for the gradient plasticity problem, solved here, as in the small-strain case, using a discontinuous Galerkin finite element formulation to interpolate the internal hardening parameter.

Finally, two numerical examples served to demonstrate various properties of the algorithm as well as a range of features associated with softening media and the effect of the internal length scale on large deformation hardening problems. As would be expected from the application of the formulation to small-strain problems, the pathological features that arise in classical finite element formulations of problems with softening are absent. In addition, for the hardening problem, increasing the ratio of the internal length scale to the characteristic dimension of the domain increases the apparent strength of the material. The effect of varying the penalty parameter associated with the discontinuous Galerkin interpolation was demonstrated.

The primal formulation of the plasticity problem has been exploited extensively here, in particular for the analysis of the classical and gradient formulations and the

solution algorithms for the small-strain problem; a task for which it is particularly well suited. The equivalence of the primal and more widely adopted dual formulation was demonstrated and exploited in the implementation of the solution algorithm. A flexible object-based finite element code, developed for this project, provided the basis for the numerical investigations.

The primary benefit of adopting a discontinuous Galerkin formulation for models of gradient plasticity is that it offers the additional flexibility to handle the higher-order terms that arise within a consistent finite element formulation. Continuity of the internal hardening parameter field is not assumed but imposed consistently in a weak sense. Indeed, the solution algorithms developed here are, in general, direct extensions of those for classical plasticity.

There remain a number of avenues which require further exploration and study. First among these would be the analysis of more computationally challenging plane problems, that is, problems with greater levels of mesh refinement. The second would be the extension of the present work to three space dimensions, the framework for which has already been laid in much of the work reported here. The programming environment used here to implement the finite element formulation is a major obstacle to overcoming the aforementioned challenges. The object-oriented C++ finite element library deal.ii [20, 19] has been identified as one of several possible environments that will facilitate the simulation of more complex problems. Indeed, initial investigations of the extension of the work reported here to models of rate-independent single crystal plasticity in three space dimensions have demonstrated the effectiveness of deal.ii.

A related issue is the design of efficient large-scale discontinuous Galerkin finite element programming methodologies to truly assess the computational efficiency of the method relative to a conforming approximation. The finite element library deal.ii contains optimised tools for discontinuous Galerkin finite-element-based approximations. Furthermore, the conforming gradient plasticity model developed by Liebe and Steinmann [115], which bears many similarities to the model presented here, and the finite-strain crystal plasticity formulation of Schmidt-Baldassari [160] have been implemented using deal.ii by Young [192].

The extension of the current work to account for dynamic effects is another recommended extension. The algorithms developed by Simo [163, 164] for classical dynamic elastoplasticity would provide the foundation for such an extension. The recent work of Noels and Radovitzky [141] documenting an explicit discontinuous Galerkin formulation for nonlinear elastodynamics would also be of considerable value.

The technique adopted here to identify the elastoplastic boundary and the choice of the additional boundary conditions that arise in the gradient formulation are relatively conventional. The correct choice of boundary conditions should be motivated by both mircomechanical considerations and the nature of the gradient plasticity model, as shown, for example, in the recent work of Peerlings [146]. Motivated by the application of Nitsche's method [139] to evolving interface problems (see, for example, [69] and references therein), it is proposed that the discontinuous Galerkin formulation be used to discern more accurately the elastoplastic boundary within an element. The weak enforcement of interelement continuity in the discontinuous Galerkin approximation could also allow for the more straightforward application of a range of boundary conditions. Furthermore, discontinuous Galerkin time integration schemes appear to be ideally suited to evolving interface problems, as demonstrated by Alberty and Carstensen [6].

Further questions worth addressing include the extension of the work reported here to other models of strain gradient plasticity. For example, the class of problems that involve the Burgers vector, or the curl of plastic deformation, represents a group that is worth studying computationally (see, for example, Gurtin and Anand [92, 91] and Liebe et al. [116]). To this end, progress has already been made. The work of Reddy et al. [154] casts the model of Gurtin and Anand [91] into the same convex analytic framework exploited here and, thus, provides a useful starting point for considering such an extension. The recent work of Ebobisse et al. [73] extends the aforementioned investigation by Reddy et al. [154] by using the energetic approach proposed by Mielke [132]. The energetic approach to problems in plasticity possesses many similarities to the time-discrete expression of the primal formulation used extensively in this work. Related works using the energetic approach include that of Dal Maso et al. [61] on

models of classical plasticity with softening and of Giacomini and Lussardi [85] on the model of gradient plasticity due to Gurtin and Anand [91].

An alternative, widely-adopted gradient plasticity model also worth investigating is that proposed by Fleck and Hutchinson [81] that involves more than one length scale. The Fleck and Hutchinson theory as it stands cannot, however, be cast into a convex analytic framework (see the comment by Gudmundson [87] after (27)), unlike the Aifantis [2] and the Gurtin and Anand [92] models. A generalisation of the Aifantis model to incorporate multiple length scales could, in principle, be developed, starting from scratch.

A further recommended extension of the work presented here is the application of the convex analytic framework arising from the primal formulation and the discontinuous Galerkin method to models of single crystal gradient plasticity, such as those proposed by Gurtin [89, 90] and Geers et al. [84]. In single crystals exhibiting geometrical softening or latent hardening effects, the stored-energy function is not quasiconvex and possesses wells corresponding to single-slip deformations, thus favouring the formation of microstructure consisting locally of single slip [144]. Indeed, it appears that any time-evolving nonlinear material in finite geometry and a natural time-discretisation contradicts the assumption of quasiconvexity of the energy density [21]. The problem of finite classical elastoplasticity clearly falls into this category.

There is currently a significant amount of research into the solution of problems involving microstructure, but many unresolved issues and opportunities remain. The approach of Mielke [133] involves a relaxation of the variational incremental problem, and uses Young measures to describe the microscopic distribution of internal variables and the quasiconvexification of the elastic stored-energy density with respect to the deformation gradient. Importantly, a length scale is not introduced into the formulation. Carstensen and coworkers have also made significant contributions to the mathematical analysis and numerical approximation of problems involving microstructure using various approaches [33, 41, 38, 43, 42, 35, 45, 39, 21, 36, 46]. One approach adopted to quasiconvexify the stored-energy density is to introduce a stabilisation term of the same nature as the gradient term in the stored-energy function for

the model of gradient plasticity considered here. Ortiz and Repetto [144] approximate a quasiconvex stored-energy function using a series of pseudoelastic energy densities. Furthermore, they also propose what is essentially a nonlocal gradient crystal plasticity model that bears similarities to that proposed by Gurtin [89, 90]. It is suggested that the framework developed for the model of gradient plasticity investigated here could find application in the analysis and solution of problems in single crystal plasticity and related issues concerning the formation of microstructure.

A further related possible extension of the work presented here is to the multiscale framework. Multiscale modelling aims to eliminate empiricism and uncertainty from material models by systematically identifying the rate-controlling mechanisms at all scales and the fundamental laws that govern those mechanisms and, by bridging of the relevant space and time length scales, a mathematically rigorous determination of laws of effective or macroscopic behaviour [59]. The work of Garikipati [82] explored a variational multiscale approach to a model of gradient plasticity proposed by Fleck and Hutchinson [80]. The recent work of Conti et al. [59] establishes the link between multiscale methods and the enhanced strain formulation in the context of single crystal plasticity. The formation of microstructure in single crystals and texture in polycrystals, for example, can be captured within a multiscale framework (see, for example, [130, 59]).

A further area of suggested investigation is the use of multiscale methods to reduce the computational expense of discontinuous Galerkin formulations to that of a conforming approximation using the methodology proposed by Hughes et al. [103].

In conclusion, many challenges remain for the accurate and efficient simulation of materials exhibiting scale-dependent behaviour. The analysis and algorithms presented in this work for a relatively simple model of gradient plasticity within the framework of continuum plasticity provides a solid basis for an extension to various challenging problems associated with microstructure formation in the context of finite deformations, crystal plasticity, multiscale problems, and the design of efficient and robust discontinuous Galerkin procedures.

References

[1] http://www.er.doe.gov/bes/scale_of_things.html.

[2] E. C. Aifantis. On the microstructural origin of certain inelastic models. *Transactions of ASME Journal of Engineering Materials and Technology*, 106:326–330, 1984.

[3] E. C. Aifantis. The physics of plastic deformation. *International Journal of Plasticity*, 3:211–247, 1987.

[4] R. K. A. Al-Rub. *Material Length Scales in Gradient-Dependent Plasticity / Damage and Size Effects: Theory and Computation*. PhD thesis, Louisiana State University and Agricultural and Mechanical College, 2004.

[5] R. K. A. Al-Rub and G. Z. Voyiadjis. A direct finite element implementation of the gradient dependent theory. *International Journal for Numerical Methods in Engineering*, 63:603–629, 2005.

[6] J. Alberty and C. Carstensen. Discontinuous Galerkin time discretization in elastoplasticity: Motivation, numerical algorithms, and applications. *Computer Methods in Applied Mechanics and Engineering*, 191:4949–4968, 2002.

[7] J. Alberty, C. Carstensen, and S. A. Funken. Remarks around 50 lines of Matlab: short finite element implementation. *Numerical Algorithms*, 20:117–137, 1999.

[8] J. Alberty, C. Carstensen, and D. Zarrabi. Adaptive numerical analysis in primal elastoplasticity with hardening. *Computer Methods in Applied Mechanics and Engineering*, 171:175–204, 1999.

[9] J. Alberty, C. Carstensen, S. A. Funken, and R. Klose. Matlab implementation of the finite element method in elasticity. *Computing*, 69(3):239–263, 2002.

[10] F. Armero. On the locking and stability of finite elements in finite deformation plane strain problems. *Computers and Structures*, 75:261–290, 2000.

[11] D. N. Arnold. An interior penalty finite element method with discontinuous elements. *SIAM Journal on Numerical Analysis*, 19:742–760, 1982.

[12] D. N. Arnold, F. Brezzi, B. Cockburn, and L. Donatella Marini. Discontinuous Galerkin methods for elliptic problems. In B. Cockburn, G. E. Karniadakis, and C.-W. Shu, editors, *Discontinuous Galerkin Methods: Theory, Computation and Applications*, volume 11, pages 89–101. Springer–Verlag, New York, 2000.

[13] D. N. Arnold, F. Brezzi, B. Cockburn, and L. Donatella Marini. Unified analysis of discontinuous Galerkin methods for elliptic problems. *Society for Industrial and Applied Mathematics Journal of Numerical Analysis*, 39(5):1749–1779, 2002.

[14] D. N. Arnold, F. Brezzi, R. S. Falk, and L. Donatella Marini. Locking-free Reissner-Mindlin elements without reduced integration. *Computer Methods in Applied Mechanics and Engineering*, 196:3660–3671, 2007.

[15] R. J. Asaro and J. R. Rice. Strain localization in ductile single crystals. *Journal of the Mechanics and Physics of Solids*, 25:309–338, 1977.

[16] M. F. Ashby. The deformation of plastically non-homogeneous alloys. *Philosophical Magazine*, 21:399–424, 1970.

[17] F. Auricchio, L. Beirão da Veiga, C. Lovadina, and A. Reali. A stability study of some mixed finite elements for large deformation elasticity problems. *Computer Methods in Applied Mechanics and Engineering*, 194:1075–1092, 2005.

[18] D. J. Bammann, D. Mosher, D. A. Hughes, N. R. Moody, and P. R. Dawson. Using spatial gradients to model localization phenomena. Technical report, Sandia National Laboratories, 1999.

[19] W. Bangerth, R. Hartmann, and G. Kanschat. `deal.II` *Differential Equations Analysis Library, Technical Reference*. URL `http://www.dealii.org`.

[20] W. Bangerth, R. Hartmann, and G. Kanschat. deal.ii — a general purpose object oriented finite element library. *ACM Transactions on Mathematical Software*, 33(4):24, 2007.

[21] S. Bartels, C. Carstensen, K. Hackl, and U. Hoppe. Effective relaxation for microstructure simulations: algorithms and applications. *Computer Methods in Applied Mechanics and Engineering*, 193:5143–5175, 2004.

[22] M. R. Begley and J. W. Hutchinson. The mechanics of size-dependent indentation. *Journal of the Mechanics and Physics of Solids*, 46(10):2049–2068, 1998.

[23] T. Belytschko, W. K. Liu, and B. Moran. *Nonlinear Finite Elements for Continua and Structures*. Wiley, New York, 2000.

[24] M. Bernacki, L. Fezoui, S. Lanteri, and S. Piperno. Parallel discontinuous Galerkin unstructured mesh solvers for the calculation of three-dimensional wave propagation problems. *Applied Mathematical Modelling*, 30(8):744–763, 2006.

[25] W. W. Bird. *Formulations for the Incremental Elastic-Plastic Analysis and the Consolidation of Porous Media*. PhD thesis, University of Cape Town, 1987.

[26] W. W. Bird and J. B. Martin. A secant approximation for holonomic elastic-plastic incremental analysis with a von Mises yield condition. *Engineering Computations*, 3:192–201, 1986.

[27] W. W. Bird and J. B. Martin. Consistent predictors and the solution of the piecewise holonomic incremental problem in elasto-plasticity. *Engineering Structures*, 12:9–14, January 1990.

[28] P. Bochev, T. J. R. Hughes, and G. Scovazzi. A multiscale Discontinuous Galerkin method. In I. Lirkov, S. Margenov, and J. Wasniewski, editors, *Large-Scale Scientific Computing: 5th International Conference*, Lecture Notes in Computer Science, Bulgaria, 2005. Springer.

[29] F. Brezzi and L. Donatella Marini. A nonconforming element for the Reissner–Mindlin plate. *Computers and Structures*, 81:515–522, 2003.

[30] F. Brezzi, B. Cockburn, L. Donatella Marini, and E. Suli. Stabilization mechanisms in discontinuous Galerkin finite element methods. *Computer Methods in Applied Mechanics and Engineering*, 195:3293–3310, 2006.

[31] O. T. Bruhns, H. Xiao, and A. Meyers. Self-consistent Eulerian rate type elasto-plasticity models based upon the logarithmic stress rate. *International Journal of Plasticity*, 15:479–520, 1999.

[32] S. Caddemi and J. B. Martin. Convergence of the Newton–Raphson algorithm in elastic–plastic incremental analysis. *International Journal for Numerical Methods in Engineering*, 31(1):177–191, 1990.

[33] C. Carstensen. Numerical analysis of nonconvex minimization problems allowing microstructures. *ZAMM - Journal of Applied Mathematics and Mechanics*, 76 (2):497–498, 1996.

[34] C. Carstensen. Numerical analysis of the primal problem of elastoplasticity with hardening. *Numerische Mathematik*, 82(4):577–597, 1999.

[35] C. Carstensen. Numerical analysis of microstructure. In J. F. Blowey, J. P. Coleman, and A. W. Craig, editors, *Theory And Numerics of Differential Equations*, Universitext, pages 59–126, Berlin, 2001. Springer-Verlag.

[36] C. Carstensen. Ten remarks on nonconvex minimisation for phase transition simulations. *Computer Methods in Applied Mechanics and Engineering*, 194: 169–193, 2005.

[37] C. Carstensen and J. Alberty. Numerical analysis of time-depending primal elastoplasticity with hardening. *SIAM Journal on Numerical Analysis*, 37(4): 1271–1294, 2000.

[38] C. Carstensen and K. Hackl. On microstructures occuring in a model of finite-strain elastoplasticity involving a single slip-system. *ZAMM - Journal of Applied Mathematics and Mechanics*, 80(2):421–422, 2000.

[39] C. Carstensen and K. Jochimsen. Adaptive finite element methods for microstructures? Numerical experiments for a 2-well benchmark. *Computing*, 71: 175–204, 2003.

[40] C. Carstensen and R. Klose. Elastoviscoplastic finite element analysis in 100 lines of Matlab. *Journal of Numerical Mathematics*, 10(3):157–192, 2002.

[41] C. Carstensen and P. Plecháč. Numerical solution of the scalar double-well problem allowing microstructure. *Mathematics of Computation*, 66(219):997–1026, 1997.

[42] C. Carstensen and T. Roubíček. Numerical approximation of Young measures in non-convex variational problems. *Journal of Numerical Mathematics*, 84(3): 395–415, 2000.

[43] C. Carstensen, P. Plecháč, and S. Bartels. Finite element computation of macroscopic quantities in nonconvex minimisation problems and applications in materials science. In A.-M. Sändig, W. Schiehlen, and W. L. Wendland, editors, *Multifield Problems. State of the Art*, pages 69–79, Berlin, 2000. Springer.

[44] C. Carstensen, D. Zarrabi, and J. Alberty. Numerical analysis of primal elastoplasticity with hardening. *ZAMM - Journal of Applied Mathematics and Mechanics*, 80(3):831–832, 2000.

[45] C. Carstensen, A. Mielke, and K. Hackl. Nonconvex potentials and microstructures in finite-strain plasticity. *The Royal Society of London. Philosophical Transactions. Series A. Mathematical, Physical and Engineering Sciences*, 458 (2018):299–317, 2002.

[46] C. Carstensen, S. Bartels, K. Hackl, A. Orlando, R. H. W. Hoppe, and S. Conti. Relaxation and the computation of effective energies and microstructures in solid mechanics. In A. Mielke, editor, *Analysis, Modeling and Simulation of Multiscale Problems*, pages 197–224, Berlin, 2006. Springer-Verlag.

[47] C. Carstensen, J. Valdman, and A. Orlando. A convergent adaptive finite element method for the primal problem of elastoplasticity. *International Journal for Numerical Methods in Engineering*, 67(13):1851–1887, 2006.

[48] J. Casey and P. M. Naghdi. On the nonequivalence of stress space and strain space formulations of plasticity theory. *Journal of Applied Mechanics*, 50:350–354, 1983.

[49] P. Chadwick and R. W. Ogden. On the definition of elastic moduli. *Archive for Rational Mechanics and Analysis*, 44:41–53, 1971.

[50] P. Chadwick and R. W. Ogden. A theorem of tensor calculus and its application to isotropic elasticity. *Archive for Rational Mechanics and Analysis*, 44:54–68, 1971.

[51] P. G. Ciarlet. *The Finite Element Method for Elliptic Problems*. North-Holland, Amsterdam, 1978.

[52] P. G. Ciarlet. *Mathematical Elasticity. Volume I: Three-Dimensional Elasticity*. North-Holland Publishing Company, Amsterdam, 1988.

[53] B. Cockburn, G. E. Karniadakis, and C.-W. Shu, editors. *Discontinuous Galerkin Methods: Theory, Computation and Applications*, volume 11 of *Lecture Notes in Computational Science and Engineering*. Springer, New York, 2000.

[54] B. Cockburn, D. Schötzau, and J. Wang. Discontinuous Galerkin methods for incompressible elastic materials. *Computer Methods in Applied Mechanics and Engineering*, 195:3184–3204, 2006.

[55] B. D. Coleman and M. Gurtin. Thermodynamics with internal variables. *Journal of Chemistry and Physics*, 47:597–613, 1967.

[56] B. D. Coleman and M. L. Hodgdon. On shear bands in ductile materials. *Archive for Rational Mechanics and Analysis*, 90:219–247, 1985.

[57] C. Comi and A. Corigliano. On uniqueness of the dynamic finite-step problem in gradient-dependent softening plasticity. *International Journal of Solids and Structures*, 33(26):3881–3902, 1996.

[58] C. Comi and U. Perego. A generalized variable formulation for gradient dependent softening plasticity. *International Journal for Numerical Methods in Engineering*, 39:3731–3755, 1996.

[59] S. Conti, P. Hauret, and M. Ortiz. Concurrent multiscale computing of deformation microstructure by relaxation and local enrichment with application to single-crystal plasticity. *Multiscale Modeling and Simulation*, 6(1):135–157, 2007.

[60] M. A. Crisfield, G. F. Moita, G. Jelenić, and L. P. R. Lyons. Enhanced lower-order element formulations for large strains. In D. R. J. Owen and E. Oñate, editors, *Computational Plasticity IV Proceedings*, 1995.

[61] G. Dal Maso, A. DeSimone, M. G. Mora, and M. Morini. Globally stable quasistatic evolution in plasticity with softening. *Networks and Heterogeneous Media*, 3(3):567–614, 2008.

[62] R. de Borst and H.-B. Mülhaus. Gradient-dependent plasticity: formulation and algorithmic aspects. *International Journal for Numerical Methods in Engineering*, 35:521–539, 1992.

[63] R. de Borst and J. Pamin. Some novel developments in finite element procedures for gradient-dependent plasticity. *International Journal for Numerical Methods in Engineering*, 39:2477–2505, 1996.

[64] R. de Borst, J. Pamin, and M. G. D. Geers. On coupled gradient-dependent plasticity and damage theories with a view to localization analysis. *European Journal of Mechanics and Solids*, 18:939–962, 1999.

[65] E. A. de Souza Neto, F. M. Andrade Pires, and D. R. J. Owen. F-bar-based linear triangles and tetrahedra for finite strain analysis of nearly incompressible solids. Part I: formulation and benchmarking. *International Journal for Numerical Methods in Engineering*, 62:353–383, 2005.

[66] O. W. Dillon and J. Kratochvil. A strain gradient theory of plasticity. *International Journal of Solids and Structures*, 6(12):1513–1533, 1970.

[67] J. K. Djoko, F. Ebobisse, A. T. McBride, and B. D. Reddy. A discontinuous Galerkin formulation for classical and gradient plasticity – Part 1: Formulation and analysis. *Computer Methods in Applied Mechanics and Engineering*, 196: 3881–3897, 2007.

[68] J. K. Djoko, F. Ebobisse, A. T. McBride, and B. D. Reddy. A discontinuous Galerkin formulation for classical and gradient plasticity. Part 2: Algorithms and numerical analysis. *Computer Methods in Applied Mechanics and Engineering*, 197:1–21, 2007.

[69] J. E. Dolbow and L. P. Franca. Residual-free bubbles for embedded Dirichlet problems. *Computer Methods in Applied Mechanics and Engineering*, 2008. doi: 10.1016/j.cma.2008.02.033. In press.

[70] A. V. C. Duarte, F. A Rochinha, and E. G. D. do Carmo. Discontinuous finite element formulations applied to cracked elastic domains. *Computer Methods in Applied Mechanics and Engineering*, 185:21–36, 2000.

[71] G. A. Duffett and B. D. Reddy. The solution of multi-parameter systems of equations with application to problems in nonlinear elasticity. *Computer Methods in Applied Mechanics and Engineering*, 59(2):179–213, 1986.

[72] N. T. Dung and G. N. Wells. Geometrically nonlinear formulation for thin shells without rotation degrees of freedom. *Computer Methods in Applied Mechanics*

and Engineering, 197:2778–2788, 2008.

[73] F. Ebobisse, A. T. McBride, and B. D. Reddy. On the mathematical formulations of a model of strain gradient plasticity. In B. D. Reddy, editor, *IUTAM Symposium on Theoretical, Modelling and Computational Aspects of Inelastic Media*. Springer, In press.

[74] G. Engel, K. Garikipati, T. J. R. Hughes, M. G. Larson, L. Mazzei, and R. L. Taylor. Continuous/discontinuous finite element approximations of fourth-order elliptic problems in structural and continuum mechanics with applications to thin beams and plates, and strain gradient elasticity. *Computer Methods in Applied Mechanics and Engineering*, 191:3669–3750, 2002.

[75] R. A. B. Engelen, M. G. D. Geers, and F. P. T. Baaijens. Nonlocal implicit gradient-enhanced elasto-plasticity for the modelling of softening behaviour. *International Journal of Plasticity*, 19:403–433, 2003.

[76] A. L. Eterović and K.-J. Bathe. A hyperelastic-based large strain elasto-plastic constitutive formulation with combined isotropic-kinematic hardening using the logarithmic stress and strain measure. *International Journal for Numerical Methods in Engineering*, 30:1099–1114, 1990.

[77] L. C. Evans and R. F. Gariepy. *Measure Theory and Fine Properties of Functions*. CRC Press, Boca Raton, 1992.

[78] R. A. Eve. *Theoretical and Numerical Aspects of Problems in Finite Strain Plasticity*. PhD thesis, University of Cape Town, 1992.

[79] R. A. Eve, T. Gültop, and B. D. Reddy. An internal variable finite strain theory of plasticity. *Quarterly of Applied Mathematics*, 48:625–644, 1990.

[80] N. A. Fleck and J. W. Hutchinson. Strain gradient plasticity. *Advances in Applied Mechanics*, 33:295–361, 1997.

[81] N. A. Fleck and J. W. Hutchinson. A reformulation of strain gradient plasticity. *Journal of the Mechanics and Physics of Solids*, 49:2245–2271, 2001.

[82] K. Garikipati. Variational multiscale methods to embed the macromechanical continuum formulation with fine-scale gradient theories. *International Journal for Numerical Methods in Engineering*, 57:1283–1298, 2003.

[83] M. G. D. Geers. Finite strain logarithmic hyperelasto-plasticity with softening: a strongly non-local implicit gradient framework. *Computer Methods in Applied Mechanics and Engineering*, 193:3377–3401, 2004.

[84] M. G. D. Geers, W. A. M. Brekelmans, and P. J. M. Janssen. Size effects in miniaturized polycrystalline fcc samples: Strengthening versus weakening. *International Journal of Solids and Structures*, 43:7304–7321, 2006.

[85] A. Giacomini and L. Lussardi. Quasistatic evolution for a model in strain gradient plasticity. *SIAM Journal on Numerical Analysis*, 2007. Accepted paper.

[86] S. Glaser and F. Armero. On the formulation of enhanced strain finite elements in finite deformations. *Engineering Computations*, 14(7):759–791, 1997.

[87] P. Gudmundson. A unified treatment of strain gradient plasticity. *Journal of the Mechanics and Physics of Solids*, 52:1379–1406, 2004.

[88] M. E. Gurtin. *An Introduction to Continuum Mechanics*. Academic Press, Orlando, 1981.

[89] M. E. Gurtin. On the plasticity of single crystals: free energy, microforces, plastic strain gradients. *Journal of the Mechanics and Physics of Solids*, 48: 989–1036, 2000.

[90] M. E. Gurtin. A gradient theory of single-crystal viscoplasticty that accounts for geometrically necessary dislocations. *Journal of the Mechanics and Physics of Solids*, 50:5–32, 2002.

[91] M. E. Gurtin and L. Anand. A theory of strain gradient plasticity for isotropic, plastically irrotational materials. Part II: Finite deformations. *International Journal of Plasticity*, 21:2297–2318, 2005.

[92] M. E. Gurtin and L. Anand. A theory of strain gradient plasticity for isotropic, plastically irrotational materials. Part I: Small deformations. *Journal of the Mechanics and Physics of Solids*, 53:1624–1649, 2005.

[93] W. Han and B. D. Reddy. Computational plasticity: the variational basis and numerical analysis. *Computational Mechanics Advances*, 2(4):283–400, 1995.

[94] W. Han and B. D. Reddy. *Plasticity: Mathematical Theory and Numerical Analysis*. Springer, New York, 1999.

[95] W. Han, B. D. Reddy, and G. C. Schroeder. Qualitative and numerical analysis of quasistatic problems in elastoplasticity. *SIAM Journal on Numerical Analysis*, 34:143–177, 1997.

[96] P. Hansbo and M. G. Larson. Discontinuous Galerkin methods for incompressible and nearly incompressible elasticity by Nitsche's method. *Computer Methods in Applied Mechanics and Engineering*, 191:1895–1908, 2002.

[97] P. Hansbo and M. G. Larson. Discontinuous Galerkin and the Crouzeix-Raviart element: Application to elasticity. *Mathematical Modeling and Numerical Analysis*, 37:63–72, 2003.

[98] K. S. Havner. On the mechanics of crystalline solids. *Journal of the Mechanics and Physics of Solids*, 21(6):383–394, 1973.

[99] K. S. Havner. The theory of finite plastic deformation of crystalline solids. In H. G Hopkins and M. J. Swell, editors, *Mehcanics of Solids, the Rodney Hill 60th Anniversary Volume*, pages 265–302. Pergamon Press, 1982.

[100] K. Heiduschke. The logarithmic strain space description. *International Journal of Solids and Structures*, 32(8/9):1047–1062, 1995.

[101] P. Houston, D. Schötzau, and T. P. Wihler. An hp-adaptive mixed discontinuous Galerkin FEM for nearly incompressible linear elasticity. *Computer Methods in Applied Mechanics and Engineering*, 195:3224–3246, 2006.

[102] T. J. R. Hughes. *The Finite Element Method. Linear Static and Dynamic Finite Element Analysis*. Prentice–Hall, Englewood Cliffs, N. J., 1987.

[103] T. J. R. Hughes, G. Scovazzi, P. B. Bochev, and A. Buffa. A multiscale discontinuous Galerkin method with the computational structure of a continuous Galerkin method. *Computer Methods in Applied Mechanics and Engineering*, 195:2761–2787, 2006.

[104] A. Idesman, R. Niekamp, and E. Stein. Continuous and discontinuous Galerkin methods with finite elements in space and time for parallel computing of viscoelastic deformation. *Computer Methods in Applied Mechanics and Engineering*, 190:1049–1063, 2000.

[105] The Mathworks Inc. Matlab r2007a.

[106] H. Ji and J. E. Dolbow. On strategies for enforcing interfacial constraints and evaluating jump conditions with the extended finite element method. *International Journal for Numerical Methods in Engineering*, 61:2508–2535, 2004.

[107] H. Ji, H. Mourad, E. Fried, and J. Dolbow. Kinetics of thermally induced swelling of hydrogels. *International Journal of Solids and Structures*, 43:1878–1907, 2006.

[108] E. P. Kasper and R. L. Taylor. A mixed-enhanced strain method Part II: Geometrically nonlinear problems. *Computers and Structures*, 75:251–260, 2000.

[109] A. R. Khoei, A. R. Tabarraie, and S. A. Gharehbaghi. H-adaptive mesh refinement for shear band localization in elasto-plasticity Cosserat continuum. *Communications in Nonlinear Science and Numerical Simulation*, 10:253–286, 2005.

[110] J. Korelc and P. Wriggers. Consistent gradient formulation for a stable enhanced strain method for large deformations. *Engineering Computations*, 13(1):103–123, 1996.

[111] D. Lasry and T. Belytschko. Localization limiters in transient problems. *International Journal of Solids and Structures*, 24(24):581–597, 1998.

[112] E. H. Lee. Elastic–plastic deformation at finite strain. *Journal of Applied Mechanics*, 36:1–6, 1969.

[113] X. Li and S. Cescotto. Finite element method for gradient plasticity at large strains. *International Journal for Numerical Methods in Engineering*, 39:619–633, 1996.

[114] X. Li and S. Cescotto. A mixed element method in gradient plasticity for pressure dependent materials and modelling of strain localization. *Computer Methods in Applied Mechanics and Engineering*, 144:287–305, 1997.

[115] T. Liebe and P. Steinmann. Theory and numerics of a thermodynamically consistent framework for geometrically linear gradient plasticity. *International Journal for Numerical Methods in Engineering*, 51:1437–1467, 2001.

[116] T. Liebe, A. Menzel, and P. Steinmann. Theory and numerics of geometrically non-linear gradient plasticity. *International Journal of Engineering Science*, 41: 1603–1629, 2003.

[117] J. Lubliner. On the thermodynamic foundations of non-linear solid mechanics. *International Journal of Non-Linear Mechanics*, 7(3):237–254, 1972.

[118] Q. Ma and D. R. Clarke. Size dependent hardness of silver single crystals. *Journal of Materials Research*, 10:853–863, April 1995.

[119] L. E. Malvern. *Introduction to the Mechanics of a Continuous Medium*. Prentice–Hall, Upper Saddle River, N. J., 1969.

[120] J. Mandel. *Plasticité Classique et Viscoplasticité*. Springer–Verlag, Berlin, 1972.

[121] J. B. Martin. An internal variable approach to the formulation of the finite element problems in plasticity. In J. Hult and J. Lemaitre, editors, *IUTAM Symposium on Physical Non-Linearities in Structural Analysis*. Springer–Verlag, 1980.

[122] J. B. Martin and S. Caddemi. Sufficient conditions for convergence of the Newton–Raphson iterative algorithm in incremental elastic–plastic analysis. *European Journal of Mechanics and Solids*, 13(3):351–365, 1994.

[123] J. B. Martin and A. Nappi. An internal variable formulation for perfectly plastic and linear hardening relations in plasticity. *European Journal of Mechanics and Solids*, 9(2):107–131, 1990.

[124] A. T. McBride and B. D. Reddy. Primal plasticity within a discontinuous Galerkin framework. Part 2: numerics and comparison with standard formulations. In T. M. Harms, editor, *Proceedings of the Fifth South African Conference on Computational and Applied Mechanics (SACAM)*, pages 311–320, Cape Town, 2006.

[125] A. T. McBride and B. D. Reddy. Some aspects of a Discontinuous Galerkin formulation for gradient plasticity at finite strains. In B. D. Reddy, editor, *IUTAM Symposium on Theoretical, Modelling and Computational Aspects of Inelastic Media*. Springer, In press.

[126] A. T. McBride and B. D. Reddy. A discontinuous Galerkin formulation for gradient plasticity at finite strains. *Computer Methods in Applied Mechanics and Engineering*, In press.

[127] K. W. McElhaney, J. J. Vlassak, and W. D. Nix. Determination of indenter tip geometry and indentation contact area for depth-sensing indentation experiments. *Journal of Materials Research*, 13:1300–1306, 1998.

[128] F. Meftah, G. Pijaudier-Cabot, and J. M. Reynouard. A C^0 finite element in gradient plasticity for localised failure modes analysis. In S. Idelsohn, E. Oñate, and E. Dvorkin, editors, *Computational Mechanics: New Trends and Application: Proceedings of the* 4^{th} *World Congress on Computational Mechanics*, Barcelona, 1998. CINME.

[129] G. Meschke and W. N. Liu. A re-formulation of the exponential algorithm for finite strain plasticity in terms of Cauchy stresses. *Computer Methods in Applied Mechanics and Engineering*, 173:197–187, 1999.

[130] C. Miehe, J. Schröder, and J. Schotte. Computational homogenization analysis in finite plasticity. Simulation of texture development in polycrystalline materials. *Computer Methods in Applied Mechanics and Engineering*, 171:387–418, 1999.

[131] C. Miehe, N. Apel, and M. Lambrecht. Anisotropic additive plasticity in the logarithmic strain space: modular kinematic formulation and implementation based on incremental minimization principles for standard materials. *Computer Methods in Applied Mechanics and Engineering*, 191:5383–5425, 2002.

[132] A. Mielke. Energetic formulation of multiplicative elasto-plasticity using dissipation distances. *Continuum Mechanics and Thermodynamics*, 15(4):351–382, 2003.

[133] A. Mielke. Deriving new evolution equations for microstructures via relaxation of variational incremental problems. *Computer Methods in Applied Mechanics and Engineering*, 193:5095–5127, 2004.

[134] L. P. Mikkelsen. Post-necking behaviour modelled by a gradient dependent plasticity theory. *International Journal of Solids and Structures*, 34(35–36): 4531–4546, 1997.

[135] L. Molari, G. N. Wells, K. Garikipati, and F. Ubertini. A discontinuous Galerkin method for strain gradient-dependent damage: Study of interpolations and convergence. *Computer Methods in Applied Mechanics and Engineering*, 195(13-16):1480–1498, 2006.

[136] H.-B. Mülhaus and E. C. Aifantis. A variational principle for gradient plasticity. *International Journal of Solids and Structures*, 28(7):845–857, 1991.

[137] P. M. Naghdi and J. A. Trapp. The significance of formulating plasticity theory with reference to loading surfaces in strain space. *International Journal of Engineering Science*, 13:785–797, 1975.

[138] P. Neff, A. Sydow, and C. Wieners. Numerical approximation of incremental infinitesimal gradient plasticity. 2008. IWRMM-preprint.

[139] J. A. Nitsche. Über ein Variationspringzip zur Lösung von Dirichlet-Problemen bei Verwendung von Teilräumen, die keinen Randbedingungen unterworfen sind. *Abh. Math. Sem. Univ. Hamburg*, 36:9–15, 1971.

[140] W. D. Nix and H. Gao. Indentation size effects in crystalline materials: a law for strain gradient plasticity. *Journal of the Mechanics and Physics of Solids*, 46(3):411–425, 1998.

[141] L. Noels and R. Radovitzky. An explicit discontinuous Galerkin method for non-linear solid dynamics: Formulation, parallel implementation and scalability properties. *International Journal for Numerical Methods in Engineering*, 74(9): 1393–1420, 2008.

[142] L. Noels and R. Radovitzky. A new discontinuous Galerkin method for Kirchhoff–Love shells. *Computer Methods in Applied Mechanics and Engineering*, 197:2901–2929, 2008.

[143] R. W. Ogden. *Nonlinear Elastic Deformations*. Ellis Horwood Ltd., West Susex, England, 1982.

[144] M. Ortiz and E. A. Repetto. Nonconvex energy minimization and dislocation structures in ductile single crystals. *Journal of the Mechanics and Physics of Solids*, 47:397–462, 1999.

[145] J. Pamin. *Gradient-Dependent Plasticity in Numerical Simulation of Localization Phenomena*. PhD thesis, Delft University of Technology, 1994.

[146] R. H. J. Peerlings. On the role of moving elastic–plastic boundaries in strain gradient plasticity. *Modelling and Simulation in Materials Science and Engineering*, 15:S109–S120, 2007.

[147] D. Perić, D. R. J. Owen, and M. E. Honnor. A model for finite strain elasto-plasticity based on logarithmic strains: Computational issues. *Computer Methods in Applied Mechanics and Engineering*, 94(1):35–61, January 1992.

[148] C. Polizzotto and G. Borino. A thermodynamic based formulation of gradient dependent plasticity. *European Journal of Mechanics and Solids*, 17:741–761, 1998.

[149] W. H. Press, S. A. Teukolsky, W. T. Vetterling, and B. P. Flannery. *Numerical Recipes in C++ The Art of Scientific Computing*. Cambridge University Press, Cambridge, 2002.

[150] S. Ramaswamya and N. Aravas. Finite element implementation of gradient plasticity models. Part I: Gradient-dependent yield functions. *Computer Methods in Applied Mechanics and Engineering*, 163:11–32, 1998.

[151] B. D. Reddy. Existence of solutions to a quasistatic problem in elastoplasticity. In C. Bandle, J. Bemelmans, M. Chipot, M. Grüter, and J. Saint Jean Paulin, editors, *Progress in Partial Differential Equations: Calculus of Variations, Applications*, number 267 in Pitman Research Notes in Mathematics Series, pages 299–311. Longman Scientific & Technical, 1992.

[152] B. D. Reddy. *Introductory Functional Analysis*. Springer, New York, 1997.

[153] B. D. Reddy and A. T. McBride. Primal plasticity within a discontinuous Galerkin framework. Part 1: basic formulation. In T. M. Harms, editor, *Proceedings of the Fifth South African Conference on Computational and Applied Mechanics (SACAM)*, pages 300–310, Cape Town, 2006.

[154] B. D. Reddy, F. Ebobisse, and A. T. McBride. Well-posedness of a model of strain gradient plasticity for plastically irrotational materials. *International Journal of Plasticity*, 24(1):55–73, 2008.

[155] L. J. Rencontrè, W. W. Bird, and J. B. Martin. Internal variable formulation of a backward difference corrector algorithm for piecewise linear yield surfaces. *Meccanica*, 27:13–24, 1992.

[156] S. Repin. Errors of finite element methods for perfectly elasto-plastic problems. *Mathematical Models and Methods in Applied Sciences*, 6:587–604, 1996.

[157] J. R. Rice. Inelastic constitutive relations for solids: An internal-variable theory and its application to metal plasticity. *Journal of the Mechanics and Physics of Solids*, 19(6):433–455, 1971.

[158] B. Rivière and V. Girault. Discontinuous finite element methods for incompressible flows on subdomains with non-matching interfaces. *Computer Methods in Applied Mechanics and Engineering*, 195:3274–3292, 2006.

[159] B. Rivière and M. F. Wheeler. Optimal error estimates for discontinuous Galerkin methods applied to linear elasticity problems. Technical Report 00-30, Texas Institute for Computational and Applied Mathematics, 2000.

[160] M. Schmidt-Baldassari. Numerical concepts for rate-independent single crystal plasticity. *Computer Methods in Applied Mechanics and Engineering*, 192:1261–1280, 2003.

[161] J. Y. Shu and N. A. Fleck. The prediction of size effect in micro-indentation. *International Journal of Solids and Structures*, 35(13):1363–1383, 1998.

[162] J. C. Simo. A framework for finite strain elastoplasticity based on maximum plastic dissipation and the multiplicative decomposition. Part II: Computational aspects. *Computer Methods in Applied Mechanics and Engineering*, 68(1):1–31, 1988.

[163] J. C. Simo. Algorithms for static and dynamic multiplicative plasticity that preserve the classical return mapping schemes of the infinitesimal theory. *Computer Methods in Applied Mechanics and Engineering*, 99(1):61–112, 1992.

[164] J. C. Simo. Topics on the numerical analysis and simulation of plasticity. In P. G. Ciarlet and J. L. Lions, editors, *Handbook of Numerical Analysis*, volume VI of *Handbook of numerical analysis*, pages 183–499. North-Holland, Amsterdam, 1998.

[165] J. C. Simo and F. Armero. Geometrically non-linear enhanced strain mixed methods and the method of incompatible modes. *International Journal for Numerical Methods in Engineering*, 33:1413–1449, 1992.

[166] J. C. Simo and T. J. R. Hughes. *Computational Inelasticity*. Springer–Verlag, New York, 1998.

[167] J. C. Simo and C. Miehe. Associative coupled thermoplasticity at finite strains: Formulation, numerical analysis and implementation. *Computer Methods in Applied Mechanics and Engineering*, 98(1):41–104, 1992.

[168] J. C. Simo and M. S. Rifai. A class of mixed assumed strain methods and the method of incompatible modes. *International Journal for Numerical Methods in Engineering*, 29:1595–1638, 1990.

[169] J. C. Simo and R. L. Taylor. Consistent tangent operators for rate independent elasto-plasticity. *Computer Methods in Applied Mechanics and Engineering*, 48: 101–118, 1985.

[170] J. C. Simo, J. G. Kennedy, and S. Govindjee. Non-smooth multisurface plasticity and viscoplasticity. Loading/unloading conditions and numerical algorithms. *International Journal for Numerical Methods in Engineering*, 26:2161–2185, 1988.

[171] J. C. Simo, F. Armero, and R. L. Taylor. Improved versions of assumed enhanced strain tri-linear elements for 3d finite deformation problems. *Computer Methods in Applied Mechanics and Engineering*, 110:359–386, 1993.

[172] J. C. Simo, J. Oliver, and F. Amero. An analysis of strong discontinuities induced by strain softening in rate-independent inelastic solids. *Computational Mechanics*, 12:277–296, 1993.

[173] P. Steinmann. Formulation and computation of geometrically non-linear gradient damage. *International Journal for Numerical Methods in Engineering*, 46 (5):757–779, 1999.

[174] M. A. Stelmashenso, M. G. Walls, L. M. Brown, and Y. V. Miman. Microindentation on W and Mo oriented single crystals: An SEM study. *Acta Materialia*, 41:2855–2865, 1993.

[175] G. Strang and G. J. Fix. *An Analysis of the Finite Element Method*. Prentice–Hall, Englewood Cliffs, N. J., 1973.

[176] T. Svedberg and K. Runesson. A thermodynamically consistent theory of gradient-regularized plasticity coupled to damage. *International Journal of Plasticity*, 13(6-7):669–696, 1997.

[177] T. Svedberg and K. Runesson. An algorithm for gradient-regularized plasticity coupled to damage based on a dual mixed FE-formulation. *Computer Methods in Applied Mechanics and Engineering*, 161:49–65, 1998.

[178] T. Svedberg and K. Runesson. An adaptive finite element algorithm for gradient theory of plasticity coupling to damage. *International Journal of Solids and*

Structures, 37(6-7):7481–7499, 2000.

[179] R. L. Taylor, P. J. Beresford, and E. L. Wilson. A non-conforming element for stress analysis. *International Journal for Numerical Methods in Engineering*, 10:1211–1219, 1976.

[180] A. ten Eyck and A. Lew. Discontinuous Galerkin methods for nonlinear elasticity. *International Journal for Numerical Methods in Engineering*, 67:1204–1243, 2006.

[181] A. ten Eyck, F. Celiker, and A. Lew. Adaptive stabilization of discontinuous Galerkin methods for nonlinear elasticity: Motivation, formulation and numerical examples. *Computer Methods in Applied Mechanics and Engineering*, In press, 2008. doi: 10.1016/j.cma.2008.02.020.

[182] A. ten Eyck, F. Celiker, and A. Lew. Adaptive stabilization of discontinuous Galerkin methods for nonlinear elasticity: Analytical estimates. *Computer Methods in Applied Mechanics and Engineering*, In press, 2008. doi: 10.1016/j.cma.2008.02.022.

[183] C. Teodosiu. A dynamic theory of dislocations and its applications to the theory of elastic–plastic continuum. In J. A. Simmons, R. de Witt, and R. Bullough, editors, *Fundamental Aspects of Dislocation Theory*, volume 2, pages 837–876, Washington, 1969. National Bureau of Standards Special Publication.

[184] K. K. Thoa, S. Swaddiwudhipong, J. Hua, and Z. S. Liu. Numerical simulation of indentation with size effect. *Materials Science and Engineering*, A(421):268–275, 2006.

[185] A. Toselli and O. Widlund. *Domain Decomposition Methods – Algorithms and Theory*. Springer, 2005.

[186] C. Truesdell and W. Noll. *The Non-Linear Field Theories of Mechanics*. Springer, New York, 3rd edition, 2004.

[187] G. N. Wells and N. Tien Dung. A C^0 discontinuous Galerkin formulation for Kirchhoff plates. *Computer Methods in Applied Mechanics and Engineering*, 196:3370–3380, 2007.

[188] G. N. Wells, K. Garikipati, and L. Molari. A discontinuous Galerkin formulation for a strain gradient-dependent damage model. *Computer Methods in Applied*

Mechanics and Engineering, 193:3633–3645, 2004.

[189] G. N. Wells, E. Kuhl, and K. Garikipati. A discontinuous Galerkin method for the Cahn–Hilliard equation. *Journal of Computational Physics*, 218:860–877, 2006.

[190] T. P. Wihler. *Discontinuous Galerkin FEM for Elliptic Problems in Polygonal Domains*. PhD thesis, Swiss Federal Institute of Technology, Zurich, 2002.

[191] P. Wriggers and U. Hueck. A formulation of the QS6 element for large elastic deformations. *International Journal for Numerical Methods in Engineering*, 39: 1437–1454, 1996.

[192] R. Young. Computational tools for the modeling of crystalline materials. Technical report, Industrial Research Limited, June 2005.

[193] H. Yuan and J. Chen. Analysis of size effects based on a symmetric lower-order gradient plasticity model. *Computational Materials Science*, 19:143–157, 2000.

[194] H. Yuang and J. Chen. Identification of the intrinsic material length in gradient plasticity theory from micro-indentation tests. *International Journal of Solids and Structures*, 38:8171–8187, 2001.

[195] A. Zervos, P. Papanastasiou, and I. Vardoulakis. Modeling of localisation and scale effect in thick-walled cylinders with gradient elastoplasticity. *International Journal of Solids and Structures*, 38:5081–5095, 2001.

[196] O. C. Zienkiewicz. *The Finite Element Method*. Butterworth–Heinemann, Oxford, 5th edition, 2000.